Structural and Quantitative Proteomic Analyses of Argonaute2-containing Ribonucleoprotein Complexes

Anne Frohn

aus

Düsseldorf

2011

Summary

Argonaute (AGO) proteins are the key components of small RNA-mediated regulatory pathways. They bind small regulatory RNAs, for example microRNAs (miRNAs) generated by the ribonuclease Dicer, and assemble with several other factors into ribonucleoprotein (RNP) complexes. These AGO-containing RNP complexes are guided to target RNAs in a sequence specific manner by their bound small RNAs and regulate transcription, translation and messenger RNA (mRNA) stability.

To gain a better understanding of the mechanisms of miRNA-mediated regulation, it is important to characterize the underlying structural features. Therefore, it was aimed to determine the structures of the human AGO2-Dicer complex, as well as of the methylosome, an AGO-modifying complex, by electron microscopy.

The accessory factors involved in the regulation of the activity and the assembly of AGO-containing RNPs have been only partly defined so far. Therefore, quantitative proteomic studies were carried out to identify the proteins interacting with murine AGO2. For this purpose, the protein composition of AGO2-containing RNPs isolated from mouse embryonic fibroblasts (MEFs) by using a novel antibody specific for mouse AGO2 was analyzed. In contradiction to the current opinion that AGO2 and Dicer form a stable complex, the proteomic analysis of the endogenous AGO2-complexes suggested that Dicer may not stably associate with AGO2 under basal cellular conditions. Furthermore, the influence of miRNAs on the protein composition of AGO-containing RNPs was analyzed. For this purpose, RNPs containing tagged AGO2 were isolated from wild type and MEFs devoid of mature miRNAs due to a Dicer depletion. The comparison between the protein compositions revealed that several proteins specifically interacted with AGO2 only in the presence or absence of miRNAs, whereas other proteins associated with AGO2 under both conditions. Opposing the current general assumption that AGO2 complexes only associate with mRNAs when guided by miRNAs, it could be demonstrated that AGO2-containing RNPs stably associated with large RNAs in a miRNA-independent manner and that large RNA binding strongly influenced the protein composition of the complex. The data was combined into an interaction network presenting an overview of AGO2-associated proteins as well as the RNA requirements of the interactions, thereby providing a detailed basis for further analyses of AGO2 function and regulation.

Contents

1 Introduction

1.1 RNA Interference

Non-coding RNAs play an important role in various cellular processes such as transcription, splicing, transposon control and translation. The first inhibitory function of RNAs was observed in plants in 1990 when Napoli *et al.* introduced transgenes into petunia to enhance flower coloring. Instead of an enhanced pigment synthesis, they observed repression of both the transgene and the homologous endogenous sequence [233]. This nucleotide sequence-specific gene silencing phenomenon, referred to as post transcriptional gene silencing, was subsequently shown to be involved in viral defense in plants [47, 190]. A comparable mechanism called quelling was soon after established in the fungus *Neurospora crassa* [279]. Developmental studies in *Caenorhabditis elegans* revealed that this pathway of posttranscriptional regulation is conserved in eukaryotes [176, 350]. The underlying molecular mechanism, termed RNA interference (RNAi), was discovered in 1998 when long double stranded (ds) RNAs were identified as the trigger of this type of post transcriptional gene silencing in *C. elegans* [83]. Subsequent studies revealed that the long dsRNAs are processed into short fragments by the ribonuclease Dicer [22, 106, 116, 133, 180]. These so called small interfering RNAs (siRNAs) are incorporated into a protein of the AGO family and guide the sequence specific degradation of target mRNAs [118, 119, 214, 229, 362]. RNA interference was soon established as a general regulatory mechanism conserved between species, including fruit flies, plants, planaria, hydra, zebrafish and mammals [2, 16, 155, 200, 250, 346, 348].

Over the last years, RNAi has developed into a powerful tool to repress specific genes experimentally and it is widely applied for the characterization of protein functions. The employment of long dsRNAs as silencing triggers in the mammalian system proved to be inapplicable because their transfection resulted in cell death [308]. However, efficient RNAi can be triggered in mammalian cells by transfection of 21 nucleotides (nt) long siRNA duplexes [66]. RNAi also has great potential for medical therapy but despite several promising results [253, 307, 367], the outcome of these efforts is hard to predict.

1

Besides siRNAs, several classes of endogenous small regulatory RNAs have been identified in plants, worms, flies and mammals (reviewed in [96]). These small RNAs regulate gene expression by various, not yet fully elucidated mechanisms at the transcriptional and postranscriptional level.

1.2 Classes and Biogenesis of Small RNAs

Many species of small RNAs have emerged over the last decade and are categorized into the three main classes of siRNAs, miRNAs and PIWI-interacting RNAs (piRNAs) (for review see Ref. [96]). These RNA species differ in their biogenesis, expression profiles, RNA target nature and the mechanism of target regulation. They have in common that they all bind to an effector protein, a member of the AGO protein family, and guide the effector to the target RNA by base pairing. Small regulatory RNAs are only known in eukaryotes, but AGO proteins are also present in some bacteria and archaeal species. The most broadly distributed classes of small regulatory RNAs are siRNAs and miRNAs. They are generated from long dsRNA precursors by cleavage through the ribonuclease Dicer and associate with an AGO protein and auxiliary proteins to form the RNA-induced silencing complex (RISC) that mediates target regulation. The expression of the third well studied class of small regulatory RNAs, the piRNAs, is restricted to the germline. PiRNAs are produced from single stranded RNA precursors in a Dicer-independent fashion and bind to a protein of the P-element induced wimpy testis (PIWI)-clade of Argonaute proteins ([36, 96, 161], see Section 1.5)

1.2.1 Biogenesis of Small Interfering RNAs

Small interfering RNAs derive from long, linear and perfectly base-paired dsRNAs (Figure 1.2.1). These precursor RNAs can be taken up from the environment or can be experimentally introduced into the cytoplasm. Originally, siRNAs were observed in plants as a response to transgene- or virus induced post transcriptional gene silencing [116]. The long dsRNA precursor is cleaved into 21 nt long ds-siRNAs by the RNase III type ribonuclease Dicer ([22], see Section "Dicer" on page 7 for a detailed description). The RNA duplexes produced by Dicer processing have 5' phosphates and 3' hydroxyl groups and a two nucleotides 3' overhang [66, 67]. In *Drosophila melanogaster*, siRNAs are methylated at the 3' end [128]. The ds-siRNA is loaded into an AGO protein by the RISC loading complex composed of Dicer and an RNA binding protein (RBP) cofactor (TRBP in mammals, R2D2 in flies). One of the siRNA strands, the so called guide strand, stays incorporated into the AGO protein and guides target recognition, whereas
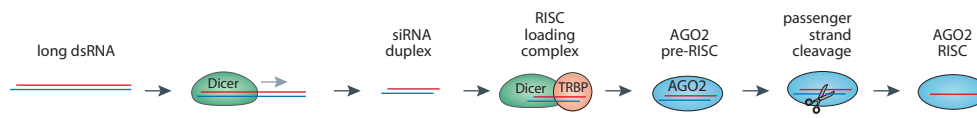
Figure 1.2.1: SiRNA biogenesis in mammals. SiRNA duplexes are generated through cleavage of long dsRNA precursors by the endonuclease Dicer and are loaded into AGO2. The passenger strand is cleaved and discarded whereas the guide strand stays incorporated and directs target cleavage (Figure adapted from [96]).

the other strand, the passenger strand, is discarded (see Section "RISC loading and Maturation" on page 11 for more details). Besides the siRNAs originating from exogenous sources (exogenous siRNAs (exo-siRNAs)) several genomic loci have been identified as sources for endogenous siRNAs (endo-siRNAs) in plants, *C. elegans*, flies and mammals [36, 96]. Unlike exo-siRNAs, endo-siRNAs have an obligate nuclear phase and derive, among others, from transposons or other repetitive elements, convergent mRNA transcripts and hairpin RNAs (hpRNAs). With the exception of *C. elegans*, the biogenesis of endo-siRNAs is also Dicer-dependent [36, 96].

RNAi is a very potent mechanism as a low number of dsRNA molecules can trigger a strong response. In nematodes and plants, the initial RNAi triggers can induce the synthesis of secondary siRNAs through the action of RNA-dependent RNA polymerases (RdRPs) [51, 230, 249, 301]. A consequence of the siRNA amplification through RdRPs is referred to as transitive RNAi. This term describes the appearance of secondary siRNAs with target mRNA sequences not corresponding to the sequence of the initial trigger siRNA, which can lead to the silencing of multiple transcripts with conserved sequences [301, 302, 329]. RdRP-dependent siRNA amplification and transitive RNAi have not been described in vertebrates and mammals so far [36, 96]. In nematodes and plants, silencing can spread from its initiation site throughout the whole organism, a process know as systemic silencing [83, 126, 251, 335]. Systemic silencing involves the movement of mobile RNAs between adjacent cells and between organs and tissues and it has been suggested to be a signaling mechanism associated with postranslational regulation as well as epigenetic modifications (reviewed in [222]).

1.2.2 Biogenesis of MicroRNAs

MicroRNAs are endogenous small RNAs that are encoded by a diverse set of genes. A few miRNAs are encoded in a separate transcription unit but most miRNAs are present as clusters (Figure 1.2.2A). In many cases, miRNAs are encoded in introns of protein

A Biogenesis of canonical miRNA

miRNA gene
→ Pol II

Transcription

pri-miRNA

Drosha

m⁷G —— AAAAA

DGCR8
(Pasha in flies)

Cropping

pre-miRNA

Exportin 5–RanGTP

Export

Nucleus

Cytoplasm

Dicer
(Dicer1 in flies)

AGO1-4
(AGO1 in flies)

TRBP or PACT
(LOQS in flies)

Dicing

TRBP or PACT
(LOQS in flies)

Dicer
(Dicer1 in flies)

AGO1-4
(AGO1 in flies)

Loading

AGO1-4
(AGO1 in flies)

miRNA

B Canonical intronic miRNA

Microprocessor
(Drosha-DGCR8)

Pol II

Commitment
complex

DNA

Cropping

pre-miRNA

Pol II

Spliceosome

Dicing

Splicing

Mature miRNA

Mature miRNA

C Non-canonical small RNA (mirtron)

pre-miRNA   Spliceosome

Splicing

Mature mRNA

Branched pre-mirtron
(excised intron)

Debranching

or

Trimming

pre-miRNA

Dicing

Mature miRNA

Figure 1.2.2: MicroRNA biogenesis. A) Canonical pathway from non-coding RNA transcripts, B) Biogenesis of miRNAs from introns of protein coding transcripts, C) Drosha-independent miRNA biogenesis pathway of mirtrons (Figure adapted from [161]).

coding transcripts (Figure 1.2.2B) [36]. Precursor transcripts, termed primary miRNAs (pri-miRNAs), are transcribed by RNA polymerase II or III and transcripts are capped and polyadenylated [29, 179]. In the canonical biogenesis pathway (Figure 1.2.2A), the

stem-loop structured pri-miRNA transcripts are trimmed to the mature miRNA by two sequential processing steps. The first processing step is carried out in the nucleus by the Microprocessor complex consisting of the RNase Drosha in association with an RBP cofactor (DGCR8 in mammals and Pasha in flies) [54, 103, 120, 172, 177]. Drosha cleavage produces 60-79 nt long hairpin structured precursor miRNAs (pre-miRNAs) [177] that are subsequently exported into the cytoplasm by Exportin 5 [25, 202, 358]. The second processing step is carried out in the cytoplasm by Dicer and its cofactors TRBP and/or PACT (Dicer-1 and Loquacious in *Drosophila*) [43, 90, 178, 285]. By excision of the terminal loop, Dicer produces 22 nt long miRNA duplexes [22]. In the duplex, the strands are termed miRNA and miRNA* and correspond to the guide and passenger strand of an siRNA. The miRNA strand is then incorporated into an AGO protein, except for rare cases in which the miRNA* is incorporated [247], and form the core of the so called micro-ribonuleoprotein (miRNP) or microRNA-induced silencing complex (miRISC). MiRNAs then guide their effector complex to the target mRNAs for posttranscriptional repression [36, 80].

An alternative, Drosha independent miRNA biogenesis pathway involves the pre-mRNA splicing machinery (Figure 1.2.2C). So called mirtrons are spliced out from RNA transcripts and form hairpin structures that mimic pre-miRNAs and are exported from the nucleus and further processed by Dicer [241, 281]. MicroRNAs can also derive from other non-coding small RNAs, for example small nucleolar RNAs (snoRNAs) or tRNAs [13, 68]. Recently, a Dicer-independent miRNA biogenesis pathway has been described for the murine miRNA 451. This miRNA is processed by Drosha, but its maturation does not require Dicer but instead depends upon cleavage of the miRNA precursor by AGO2 [40, 45].

MicroRNAs exhibit specific expression patterns [170]. This requires a tight regulation of the miRNA biogenesis process, yet only two regulation mechanisms have been described so far: the transcription of miRNA encoding genes can be controlled by a double-negative feedback loop [186, 295] or the processing of the pri-miRNA through the Microprocessor complex can be regulated by RBPs [52, 109].

1.2.3 Interactions of Small Interfering RNAs and MicroRNAs to Target RNAs

SiRNAs show perfect complementarity to their target mRNAs and induce cleavage of the target through the endonuclease activity of the AGO protein. In contrast, animal miRNAs exhibit only partial complementarity to their target mRNAs (Figure 1.2.3) and do not induce target mRNA cleavage but influence translational repression and
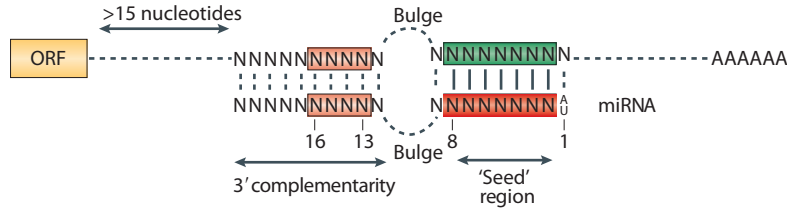
Figure 1.2.3: Principles of miRNA to target mRNA interaction. MiRNAs show a preference for an uridine or an adenine at the 5' end and only a perfect complementarity of the 5' nucleotides 2-8, the so called "seed region", is required for target recognition. A complementarity of the 3' nucleotides stabilizes the interaction with the target RNA. Mismatches or bulges in the central region prevent an siRNA-like endonucleolytic cleavage of the target RNA (Figure adapted from [82]).

degradation of the target. MiRNAs show a preference for an uridine or an adenine at the 5' end [82, 85] and only a perfect complementarity of the 5' nucleotides 2-8, referred to as the "seed sequence", is necessary for their function [185, 270]. Mismatches or bulges in the central region (nucleotides 10-12) prevent an siRNA-like endonucleolytic cleavage of the target RNA. A complementarity of the 3' nucleotides is of minor importance but stabilizes the interaction [80, 82]. Since full complementarity is not required for target recognition, a single miRNA can control a large number of mRNAs. This displays a high regulatory potential, but makes prediction of target mRNAs very difficult [18].

Usually, miRNA-binding sites are located in 3' untranslated regions (UTRs) of the mRNA target and are present in multiple copies [63, 107]. These clusters of multiple miRNA-binding sites have a cooperative effect and increase efficiency [58, 105]. MiRNA-binding sites are frequently located near AU-rich regions, close to the open reading frame (ORF) or to the 3' end of the 3' UTR [105, 234, 270]. These factors reduce the structure of the mRNA and enhance accessibility of the miRNA-binding sites [82]. In animals, miRNAs can also target binding sites in the 5' UTR or coding regions of mRNAs and exert regulatory effects similar to those binding in the 3' UTRs [62, 166, 204, 369]. RNAi and miRNA-mediated repression are not strictly separated pathways. If a miRNA is fully complementary to the target RNA, it can induce cleavage and siRNAs with imperfect matching can influence translational repression and degradation of the target in a miRNA-like fashion [53, 57, 357]. This interplay between the pathways offers additional regulatory possibilities but causes problems when using siRNAs as a scientific tool. Imperfect binding of the guide strand to unidentified targets leads to a miRNA-like regulation of these targets. These regulatory effects, the so called off-target effects, often overlap with the intended siRNA function and impair the use of RNAi for the definition of gene function [139].

1.3 Key Proteins in Small RNA-Mediated Functions

1.3.1 Drosha

Drosha is the catalytically active component of the Microprocessor complex and is responsible for pri-miRNA processing ([177], see Section 1.2.2). The protein is a member of the RNase III family and localizes to the nucleus. Drosha contains an N-terminal proline-rich region and an arginine- and serine-rich region, followed by two RNase III domains and a double stranded RNA binding domain (dsRBD). Pri-miRNA cleavage by Drosha produces 60-79 nt long hairpin structured pre-miRNAs with 2' nt long overhangs at the 3' end by excising the stem-loop structure from the pri-miRNA transcript [177]. Correct processing depends on the stem-loop structure of the pri-miRNA, which is normally a 33 nt long imperfectly base paired stem with a terminal loop and flanking segments [18]. For effective and precise cleavage, Drosha requires its associated cofactor DGCR8/Pasha [54, 103]. The cofactor serves as a molecular ruler that binds the pri-miRNA hairpin and positions Drosha to cleave the stem exactly 11 bp away from the junction between the stem and the flanking single stranded regions [121].

1.3.2 Dicer

Dicer is a dsRNA specific nuclease of the RNase III family. It cleaves dsRNAs into small duplexes with lengths between 21-25 nt and was identified as the key enzyme for si- and miRNA biogenesis [22]. Mammals and nematodes have only one Dicer protein, whereas *Drosphila* has two and *Arabidopsis thaliana* expresses four different Dicer enzymes. If existent, multiple Dicers have specialized functions, for example in flies, Dicer-1 is involved in miRNA biogenesis and Dicer-2 is required for siRNA production [180, 321].

The typical domain structure of Dicer enzymes from human and *Giardia intestinalis* is depicted in Figure 1.3.1A. In human Dicer, an amino terminal DEXD/H ATPase domain is followed by a DUF283, a PIWI-Argonaute-Zwille (PAZ) domain, two tandem RNase III domains and a dsRBD near the C-terminus. The spatial arrangement of the domains confers the ability of Dicer to produce dsRNAs with a specific length. PAZ domains bind 3' ends of single stranded (ss) RNAs [191, 305, 354] and the Dicer PAZ domain specifically binds duplex RNAs with 2 nt 3' overhangs [209]. In *G. intestinalis* Dicer, the two RNase III domains are arranged in a way that they form an intramolecular dimer closely resembling the homodimeric structure of prokaryotic RNase III and the distance between the two active sites matches the width of the major groove of an RNA helix. The duplex RNA with its 3' nucleotide bound in the PAZ domain extents approximately two helical turns on the protein surface until it reaches the active sites of
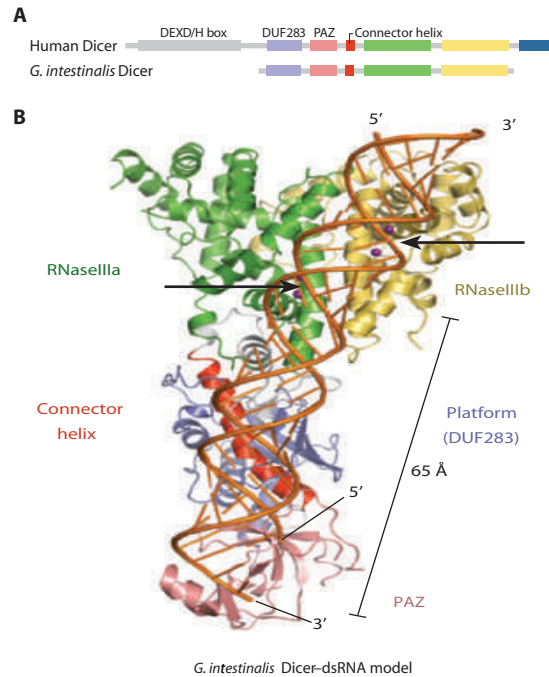
Figure 1.3.1: Domain organization of Dicer family proteins and structure of *Giardia intestinalis* Dicer. A) Schematic presentation of the domain organization of Dicer family enzymes. B) Crystal structure of *G. intestinalis* Dicer with a model of a bound dsRNA substrate. Black arrows indicate cleavage sites (Figure adapted from [145]).

the RNase III domains. This distance corresponds to the length of a 25 nt RNA duplex. Each of the RNAse III domains cleaves one strand, leading to staggered cleavage yielding new 2 nt 3' overhangs with 5' monophosphates [210]. Therefore, the distance between the PAZ domain and the processing center functions as an internal molecular ruler that determines the length of the small RNA product starting from the 3' end of the RNA substrate ([209, 210], see Figure 1.3.1B). A recent study revealed that human Dicer anchors the 5' phosphate in a basic binding pocket in addition to binding of the 3' end in the PAZ domain. This 5' end anchoring facilitates the precise cleavage of 3' modified pre-miRNAs and seems to also be critical for precise and efficient generation of canonical miRNAs [256].

Less detail is known about the functions of the dsRBD and DEXD/H ATPase domains. The dsRBD undergoes conformational changes upon RNA cleavage [59]. DsRBD mutants show reduced cleavage activity, yet target binding is unaffected [205], suggesting that this domain might be involved in target cleavage. Functions of the DEXD/H ATPase domain vary between Dicer enyzymes. *D. melanogaster* Dicer-2 and the *C. elegans* Dicer protein Dcr-1 are ATP-dependent [205, 239], while human Dicer is ATP-independent and the ATPase domain actually has an autoinhibitory effect [205]. Thus, the domain function among the distinct Dicers remains generally unknown.

Dicer enzymes rely on different cofactors for the processing of different small RNA classes [50], for example in flies binds Dicer-2 to R2D2 [197, 198] and Dicer-1 to Loquacious

[90, 285]. The sole Dicer in human associates with two dsRBD cofactors, TRBP and PACT [43, 167, 178]. This association with dsRBDs is not necessary for processing activity but is involved in RISC loading and guide strand selection ([198, 320], see Sections "RISC Loading and Maturation" on page 11 and "Small RNA Sorting" on page 12).

1.3.3 The Argonaute Proteins

Argonaute proteins are the central component of RISC and a common feature of all small RNA-mediated silencing pathways. SiRNA-induced silencing of target mRNAs is achieved through endonucleolytic cleavage of perfectly complementary target mRNAs by an AGO protein, a process referred to as slicing. The AGO family is divided into three clades: the AGO, the PIWI and the nematode specific WAGO clade. Except for *Schizosaccharomyces pombe*, most species contain multiple AGO genes, for example five in *D. melanogaster*, ten in plants and 27 in *C. elegans*. Humans have eight AGO genes. Four of them belong to the AGO clade (AGO 1-4) and are ubiquitously expressed. HILI, HIWI, HIWI2 and HIWI 3 (MILI, MIWI and MIWI2 in mouse) are members of the PIWI-clade. PIWI-proteins are only expressed in the germ line and bind specifically to piRNAs (see Section 1.5). In plants, worms and flies, the functional specialization of different AGO proteins is well described. For human the deep sequencing of small RNAs associated with the four AGO proteins revealed little differences, so the functional specialization in mammals remains unclear [36].

Structure

Argonaute proteins consist of four domains, the N-terminal, the PAZ, the middle (MID) and a PIWI domain (Figure 1.3.2A). Crystal structures of bacterial AGO proteins revealed a bilobal architecture wherein the MID and PIWI domains form one and the N- and PAZ domain the other lobe [145]. The PIWI domain adopts a fold similar to RNase H [257, 306, 361] and confers the slicer activity to RISC. AGO cleaves the target RNA at the phosphodiester bond between the nucleotides that are paired with nucleotides ten and eleven of the guide strand (counting from the 5' end of the siRNA) [66, 67] and generates 5' products with a free 3' hydroxyl group and a 3' product that carries a 5' phosphate group [194, 215].

A conserved Asp-Asp-His motif and divalent cations are required for this catalytic activity in AGO proteins [194, 276]. Strikingly, among the four human AGO proteins, only AGO2 has slicer activity [194, 220]. AGO1 and 4 have altered sequences at the catalytic site and although AGO3 contains an Asp-Asp-His motif it does not display slicer

Figure 1.3.2: Domain architecture and structure of *Thermus thermophilus* Argonaute. A) Schematic presentation of the four domains of Argonaute proteins. B) Crystal structure of *T. thermophilus* AGO bound to a 21 nt guide DNA strand (red) and a 20 nt target RNA (blue) with mismatches at nucleotides 10-11. Backbone phosphorus atoms are depicted in yellow (Figure B adapted from [344]).
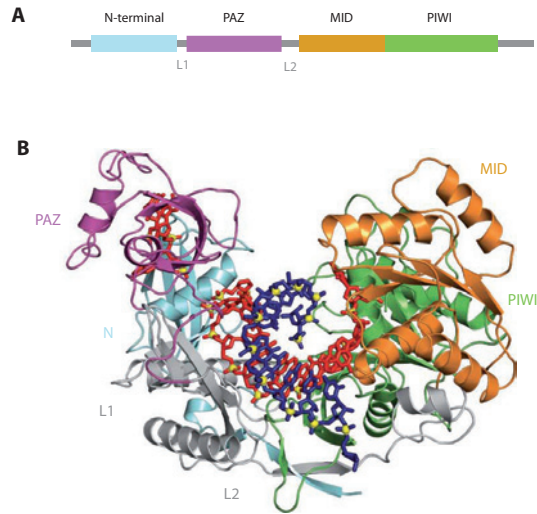
activity [194, 220]. In *D. melanogaster*, both AGO proteins, AGO1 and 2, feature the Asp-Asp-His motif and are both capable of slicing. AGO2 cleaves targets efficiently but AGO1 has a lower turnover rate because of slower target release [89]. These observations and the fact that the population of small RNAs associated with human AGO1-4 show only little differences are indications that slicer activity is not only determined by the catalytic residues but by other internal or external factors [145].

The 3' end of the guide strand RNA is inserted into a hydrophobic pocket in the PAZ domain of the AGO protein [191, 305, 354]. This pocket is lined with aromatic residues and the position of the terminal nucleotide is fixed by stacking against the aromatic ring of a conserved phenylalanine residue [206]. In AGO proteins, the 5' nt of the guide strand does not base pair with the target RNA but is bound in a pocket at the interface between the MID and PIWI domains via an interaction of the phosphate group to a magnesium ion [27, 56, 207, 258]. Analyses of the crystal structure of the human AGO2-MID domain revealed that adenosine monophosphate or uridine monophosphate bound in the 5' binding pocket stack against a tyrosine in the binding pocket and make contact with the so called nucleotide specificity loop of the MID domain. This loop discriminates against the binding of cytidine monophosphate and guanosine monophosphate and provides an explanation for the preference for adenine and uridine at the 5' position of the miRNA guide strand [85]. Interestingly, the MID-PIWI domain interface of eukaryotic AGO was reported to feature a second ligand binding pocket. The function of the second ligand is so far unknown, but it is suggested to have an allosteric effect and to possibly bind to the m^7GpppN group at the 5' end, the so called 5' cap, of the mRNA during miRNA-mediated repression [27, 56].

Crystal structures of *Archaeoglobus fulgidus* PIWI-RNA complex [207, 258] and *T. themophilus* Argonaute with a DNA guide strand [345] revealed that the guide-target duplex is stretched over a basic channel on the surface of the MID and PIWI domains. Modeling of the guide-strand-target duplex places the phosphate bond of the target mRNA into the catalytic site, which explains why specific cleavage occurs only at this fixed distance [207]. RNA-protein interactions are dominated by sequence-unspecific interactions between positively charged amino acid residues on the protein surface with the sugar phosphate backbone of the RNA. The bases of the seed region of the miRNA are exposed and stacked in a helical conformation that allows for base pairing with the target [345]. A structure of *T. thermophilus* Argonaute with a DNA guide strand paired to a target RNA [344] (Figure 1.3.2B) shows that the bases of the seed region engage in Watson-Crick base pairing with the target RNA in an A-form helical conformation. To accommodate the helical structure, pronounced conformational changes, mainly rotation of the N- and PAZ domain, are required [344]. The MID-PIWI lobe of an eukaryotic AGO protein conserves the domain orientation compared to prokaryotic AGOs, though it differs in the position of some residues at the MID-PIWI interface. These residues were previously thought to participate in regulation of guide strand binding but appear to be buried in the eukaryotic structure [26].

RISC Loading and Maturation

Single stranded siRNAs can be directly loaded onto AGO but siRNA and miRNA duplexes generated by Dicer depend on RISC assembly pathways [276]. One strand of the duplex, the guide strand/miRNA stays bound to the AGO protein, whereas the other strand, the passenger strand/miRNA* is removed. The identity of the guide and passenger strand is determined by the thermodynamic stability of the 5' end. According to this asymmetry rule, the strand with the thermodynamically less stable end is preferentially retained [156, 294]. The relative thermodynamic stabilities are sensed by either Dicer itself or by a Dicer cofactor [197, 198, 237]. In *D. melanogaster*, the siRNA duplex is bound by Dicer-2 in association with its cofactor R2D2 [197, 198]. Together with other unknown protein factors a RISC loading complex (RLC) is formed that is transformed into a pre-RISC by the addition of AGO2 [160]. The slicer activity of AGO2 cleaves the passenger strand in an ATP-independent manner [184, 217, 225, 271] and discarding of the passenger strand leads to formation of the mature holo-RISC [36, 303]. In humans, Dicer, TRPB and AGO2 form the RISC loading complex [102, 212]. This complex is capable of dsRNA binding, dicing, AGO2 loading and passenger strand removal leading to active RISC formation [208]. The presence of a dsRNA trigger or other cofactors is

not required for RLC formation and activity [208]. Dicer itself is not essential for RISC loading in the murine system, as shown by the fact that Dicer-deficient cells are still capable of siRNA-induced gene silencing [232].

Of the four human AGO proteins, only AGO2 has slicer activity but the other AGO proteins are nevertheless loaded with ss-siRNAs [194, 221]. Despite the fact that miRNA duplexes contain central mismatches that prevent cleavage of the passenger strand, ss-miRNAs are bound into all AGO proteins [12]. Therefore, RISC maturation can also occur in a slicer-independent mechanism that involves unwinding of the RNA duplex. In contrast to passenger strand degradation, the loading of the small RNA duplex into RISC is an ATP-dependent process [151, 239, 263, 360]. Structural studies predict that RNA double helices are too bulky to easily fit into AGO and that conformational changes are necessary to allow the binding of the small RNA duplex [207, 258, 341]. AGO proteins interact with the chaperones HSP90 and HSP70 and a current model proposes that the chaperone machinery uses ATP to mediate conformational changes of the AGO protein which facilitate the loading of the small RNA [134, 138, 148, 226]. In the open conformation, AGO is expected to be under structural tension and the release of this tension is thought to drive unwinding of the miRNA-miRNA* duplex [151].

Other factors of the RISC machinery are also involved in RISC loading and maturation, for example the putative RNA helicase Armitage (MOV10 in human), which associates with AGO and is required for RISC maturation in flies and human [221, 320]. Another human helicase, RNA helicase A/DDX9, is involved in guide strand incorporation [278]. Furthermore, in flies and mammals the endoribonuclease C3PO has been reported to activate RISC by removing passenger strand cleavage products [199, 356].

Small RNA Sorting

For accurate RISC function, it is crucial that the correct small RNA is bound into the corresponding AGO protein. In plants, small RNA association with the correct AGO protein depends on the identity and modifications of the 5' nucleotide [303]. *D. melanogaster* pre-miRNAs are processed by Dicer-1 in complex with the dsRBP Loquacious, whereas siRNAs are generated by the Dicer-2-R2D2 heterodimer. Whether a small RNA produced by Dicer-1 is loaded into AGO1 for translational repression or into AGO2 for target degradation is regulated by the Dicer-2-R2D2 complex and depends on the structure of the small RNA duplex [89, 319]. R2D2 has a binding preference for highly paired duplexes and thereby promotes the binding of perfectly matched siRNAs to AGO2. Small RNA duplexes with central bulges are poorly bound by R2D2 and thus routed to AGO1. Perfectly base paired miRNA-miRNA* duplexes also enter AGO1, indicating

that the AGO1 loading pathway is also selective and not a default pathway for small RNAs rejected by AGO2 [152, 303].

Localization

Argonaute proteins are predominantly localized in the cytoplasm [182]. A fraction is concentrated in distinct cytoplasmic granules known as mRNA processing bodies (P-bodies) [196, 298]. AGO also localizes to multivesicular bodies (MVBs) and, upon cellular stresses, to stress granules (SGs). Localization of AGO in the nucleus has also been reported [277, 282, 349].

P-bodies are cytoplasmic granules that function in storage and degradation of mRNAs [70]. They are also referred to as GW-bodies as the GW182 protein (see Section 1.3.4) is an integral component of P-bodies. AGO localizes to P-bodies in a predominantly miRNA-independent manner and localization relies on direct interactions with P-body components instead [19, 317, 359]. P-bodies are enriched in translationally repressed mRNAs and proteins involved in 5'-3' mRNA degradation such as the exonuclease XRN1, the deadenylation complex including CAF1, CCR4 and NOT and the decapping enzymes DCP1 and DCP2 [70]. In addition, nonsense-mediated mRNA decay (NMD) also takes place in P-bodies [325]. Ribosomal proteins, the majority of translation initiation factors and the 3'-5' mRNA degradation machinery are absent from P-bodies [5, 300, 315]. P-bodies are highly dynamic structures [71, 187] and the depletion of GW182 or other miRNA pathway proteins disrupts visible P-body formation [259, 355]. It seems as if the disruption of P-bodies does not affect miRNA-mediated repression and it is suggested that this process starts in the cytosol and that translationally repressed mRNAs are consecutively transported to P-bodies for storage or degradation [71, 359]. Therefore, P-body formation is assumed to be a consequence of and not a prerequisite for miRNA-mediated repression [71]. Although mRNAs are necessary for P-body formation [70], repression and storage of mRNAs in P-bodies are reversible processes since repressed mRNAs can be released from storage upon cellular signals and translation resumes [23, 31].

Stress granules are sites where non-translating mRNAs accumulate when cells experience stresses such as heat shock, osmotic or oxidative stress or when translation initiation is specifically inhibited. They contain small ribosomal subunits, early translation initiation factors and several RBPs, among them poly(A)-binding protein, cytoplasmic (PABPC), RCK, XRN, HuR and FXR1 [3]. P-bodies and SGs are known to be dynamically associated with each other and share several protein components [154]. AGO2 localizes to stress granules in a miRNA-dependent way [182] and its recruitment to SGs as well as

to P-bodies is regulated by HSP90 [255].

AGO proteins also associate with cellular membranes and multivesicular bodies [97, 311]. MVBs are specialized late endosomal compartments with a characteristic multivesicular morphology that colocalize with P-bodies and contribute to miRNA function and miRISC turnover in mammals and flies [97, 181]. Some miRNAs and GW182, but not AGO, are secreted from MVBs in exosome-like vesicles, a mechanism that might represent a measure to control RISC activity by eliminating components from the cell or a way of miRNA-dependent cellular communication [330].

Post-Translational Modifications

Besides the nature of the small RNA and the protein composition of the RISC the activity of AGO proteins is also influenced by post-translational modifications. Qi *et al.* [269] reported that hydroxylation of human AGO2 at Pro_{700} is important for AGO2 stability. The mouse E3 ubiquitin ligase mLin41 mediates ubiquitinylation of AGO2, thereby regulating AGO2 turnover [283]. Phosphorylation of Ser_{387} is related to P-body localization of AGO [364] and phosphorylation of Tyr_{529} in the 5' binding pocket of the MID domain interferes with small RNA binding and AGO loading [284].

1.3.4 The GW182 Protein Family

GW182 was originally cloned from human cells and termed GW182 because of the presence of glycine-tryptophan repeat (GW-repeat) motifs and its molecular weight. The protein localizes to distinct cytoplasmic foci, the so called GW-bodies, which turned out to coincide with P-bodies [77, 78]. In human and *D. melanogaster*, the GW182 proteins associate with AGO proteins and are essential for miRNA-mediated gene silencing [195, 221, 273]. Insects express a single GW182 ortholog, whereas in the mammalian system the GW182 protein family consists of the three paralogs trinucleotide repeat containing 6 (TNRC6)A, TNRC6B and TNRC6C [19]. GW182 proteins contain several N-terminal GW-repeats, an ubiquitin associated (UBA) domain and a glutamine (Q)-rich domain (see Figure 1.3.3). The latter has been implicated in P-body localization [19, 76], yet it is dispensable for the silencing activity since P-body localization and silencing are not correlated [72]. The so called MID domain of the proteins consists three domains (M1, poly(A)-binding protein-interacting motif 2 (PAM2) and M2) and is followed by an RNA recognition motif (RRM) domain and a C-terminal domain (Figure 1.3.3) [324]. An interaction of the TNRC6 N-terminal GW-repeats with the AGO PIWI domain is necessary for AGO function in translation inhibition and deadenylation [73, 195]. Only a minimal fragment of two tandem GW-motifs, termed the AGO-hook,
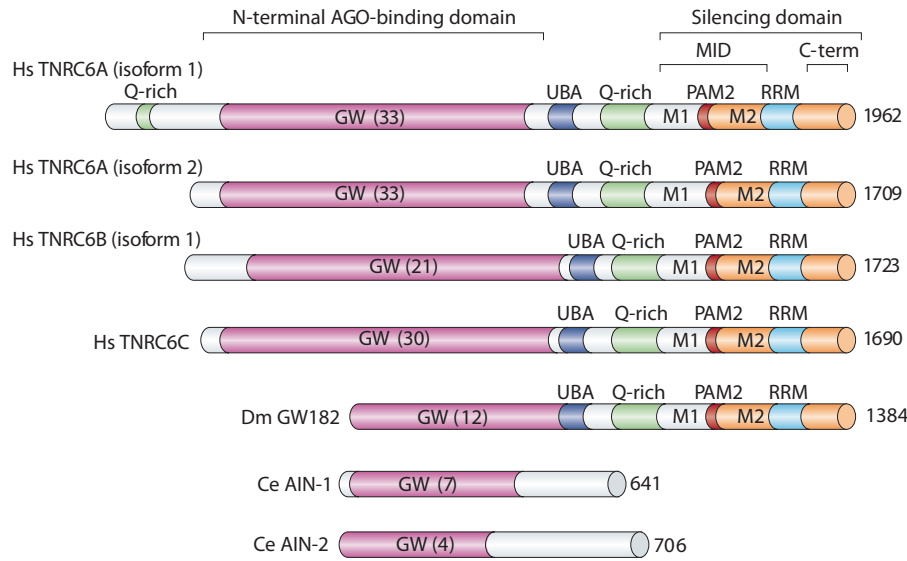
Figure 1.3.3: Domain Organization of GW182 Proteins. For the human TNRC6 proteins only selected isoforms are shown. Hs, *Homo sapiens*; Dm, *Drosophila melanogaster*; Ce, *Caenorhabditis elegans* (Figure adapted from [324]).

is sufficient for mediation of this interaction [188, 313, 317]. The MID and C-terminal domains of TNRC6 proteins together are called the bipartite silencing domain and have autonomous silencing activity [72, 174, 368].

Recently, it emerged that the TNRC6 proteins also function as poly(A)-binding protein interacting proteins (PAIPs). This interaction is mediated by binding of the PAM2 motif to the *mademoiselle* (Mlle) domain of the poly(A)-binding protein protein (PABP) [79, 131, 146, 168] and indirect binding of the M2 and C-terminal domains to the RRMs in PABPC1 [146, 363]. PABP binds the poly-(A) tails of mRNAs and is involved in the deadenylation of mRNAs by its role in the recruitment of deadenylation factors (reviewed in [80]) and in translation initiation through its interaction with the translation initiation factor eIF4G (reviewed in [140]). Therefore, the GW proteins present a link between PABP and miRNA-mediated deadenylation. Besides the molecular binding mechanism, this finding is supported by the observation that the depletion of PABP abolishes miRNA-mediated deadenylation and that overexpression of PABP or a PAM2 peptide suppresses miRNA-mediated silencing [79, 146, 339, 363]. In addition, the GW182-proteins are likely to interfere with PABP function in translation and mRNA stabilization, either by competing with eIF4G for PABP binding or by acting as a binding platform for other proteins involved in miRNA-mediated silencing [79, 324, 363].

1.4 Mechanisms of Small RNA Functions

1.4.1 Poststranscriptional Silencing by Short Interfering RNAs

Short interfering RNA guide strands direct RISCs to perfectly complementary target RNAs, which are then cleaved by the slicer activity of the AGO protein. The cleaved target dissociates and is further degraded by cellular exonucleases or oligouridylated at the 3' terminus and thereby targeted for decapping and 5'-3' degradation [246, 299]. Target dissociation frees the RISC and allows for multiple rounds of target cleavage. Highly purified RISCs fail to release the cleaved target RNA, suggesting that this process depends on accessory factors [36, 89, 276]. Target cleavage is suppressed by mismatches between target and siRNA and no target cleavage occurs despite perfect base pairing if an siRNA is bound in an endonucleolytically inactive AGO protein. In those cases, the siRNA mediates posttranscriptional silencing of the target RNA in a manner similar to miRNA-mediated translational repression [36].

1.4.2 MicroRNA-Mediated Translational Repression

The repressive effect on translation is a well accepted miRNA function. In eukaryotes, the process of translation is divided into three steps: initiation, elongation and termination. At the initiation step, the ribosomal subunits assemble at the start codon of the mRNA to form the 80S ribosome complex. The recruitment of the ribosome to the mRNA is facilitated by the 5' cap of the mRNA. During this cap-dependent translation initiation, the mRNA is first bound by eIF4A, a helicase which is thought to unwind the mRNA, followed by binding of the 5' cap by eIF4E. The protein eIF4G binds to eIF4A and eIF4E and functions as a scaffold for other proteins. The 3' poly(A)-tail of the mRNA is bound by PABP, which in turn interacts with eIF4G. This interaction leads to circularization of the mRNA and an enhanced rate of translation initiation. The circularized mRNA is bound by the ribosomal 43S pre-initiation complex that scans the mRNA for the start codon. After initiation codon recognition, the so called 48S initiation complex is formed. This complex is then joined by the 60S subunit, the 80S ribosome is formed and translation begins. During the second step of translation, the elongation step, the peptide chain is synthesized. The final termination step involves release of the newly synthesized protein and dissociation of the ribosomal proteins from the mRNA [80, 140].

There is an ongoing debate about the mechanisms that might be employed by miRNAs to repress translation (Figure 1.4.1). Several studies provide evidence that miRNA-mediated translational repression takes place at the translation initiation step. One indication for a repression at translation initiation is the observation that miRNA-repressed target mRNAs shift to lighter, non-translating fractions in polysome gradients [23, 265]. A possible explanation for this observation is that the miRNA interferes with binding of eIF4E to the 5' cap [130]. This explanation is supported by the observation that mRNAs without functional 5' caps are not affected by miRNA-mediated repression [130, 137, 216, 265, 316, 338, 340]. An alternative mechanism is that AGO binds directly to the 5' cap structure and thereby prevents binding of eIF4E. The MID domain of AGO has limited sequence homology to eIF4E and two aromatic residues in this se-
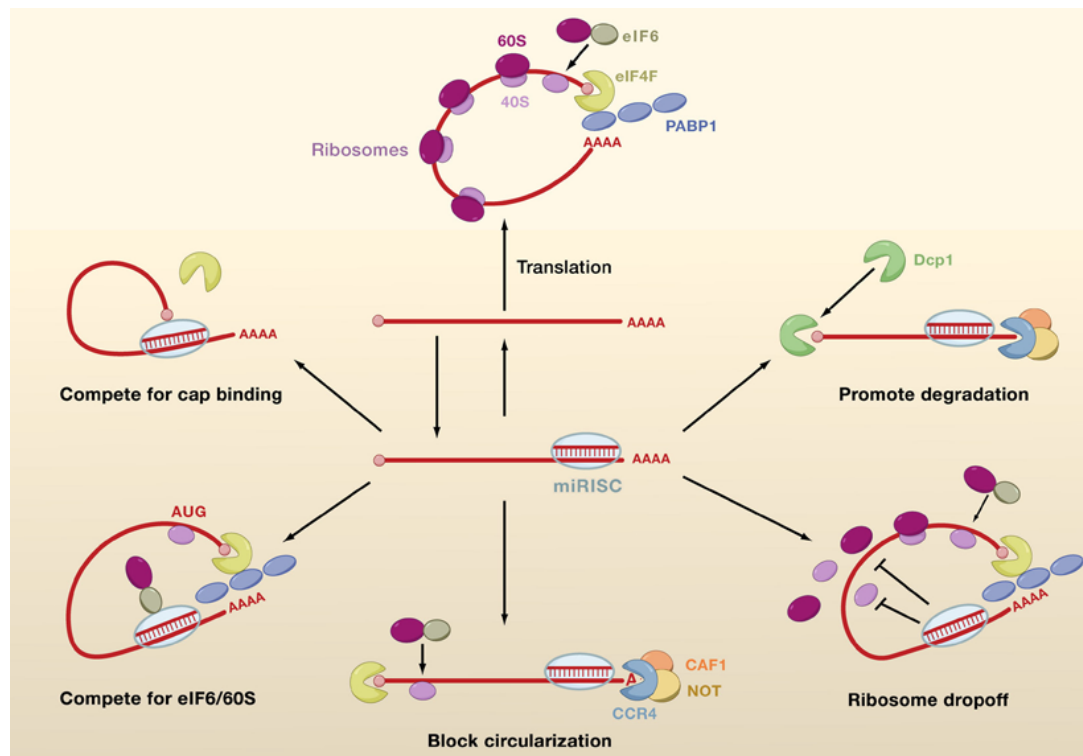
Figure 1.4.1: Possible mechanisms of miRNA-mediated translational repression. Translation could be repressed at the initiation step by competing for cap binding (upper left) or ribosome recruitment (lower left). MicroRNA-induced deadenylation of the target mRNA could block circularization and thereby prevent translation initiation (bottom). At post-initiation translation steps, miRNAs could induce ribosome drop off (lower right). Alternatively, miRNAs can promote mRNA deadenylation followed by decapping and degradation (upper right) (Figure taken from [36]).

quence are required for translational repression [163]. This mechanism was supported by the observation that the addition of the recombinant cap-binding complex eIF4F rescues mRNAs from miRNA-mediated repression [216]. Later studies questioned this proposed mechanism. No structural similarities between AGO2 and eIF4E were observed [162] and the aromatic residues required for translational repression were shown to be unrelated to cap binding but to be required for the association of GW182 and AGO [73]. In addition, it was shown that the interaction between the AGO2 MID domain and the cap-structure is not specific but is based on the general nucleotide binding ability of the MID domain instead [84]. An impaired joining of the 60S subunit and formation of the 80S subunit could also be the mechanism underlying miRNA-mediated translational repression [316, 341]. This theory is supported by the fact that eIF6, a factor preventing premature joining of the 60S subunit to the 40S subunit, associates with human RISC [42].

It has also been suggested that miRNA-mediated translational repression takes place during translation elongation since repressed miRNA target mRNAs were found in the same polysome gradient fractions as actively translating polysomes [213, 243, 295]. Furthermore, cap-independent, internal ribosome entry site (IRES)-driven translation is also inhibited by miRNAs [204, 262]. In another model, miRNA-mediated translational repression is mediated by the cotranslational degradation of nascent polypeptide chain [238, 243, 262]. This model is highly improbable. Polypeptides that are targeted to the endoplasmatic reticulum (ER) should not be accessible for degradation but a number of ER proteins are regulated by miRNAs [265, 297]. Moreover, protease inhibitors have no effect on miRNA-mediated repression [238, 262, 265].

Translation inhibition could also happen at the step of translation termination. Petersen *et al.* proposed a model in which repression is due to premature termination and ribosome drop off [262].

1.4.3 Modulation of MicroRNA-Mediated Translational Regulation by RNA Binding Proteins

MiRNA-mediated translational repression is regulated by RBPs. Some proteins activate miRNA-mediated translational repression, for example the TRIM-NHL family proteins. The murine TRIM-NHL protein TRIM32 binds to AGO1 and activates the miRNA let-7a [291]. In *C. elegans*, the TRIM-NHL protein NHL-2 associates with miRISC components and enhances the posttranscriptional repression of several miRNA targets [117]. The relieve of miRNA-mediated repression through RBPs also takes place. DND1 can bind miRNA target sites and thereby prevents miRNA binding in human and zebrafish [153].

Another example is the relieve of miR-134-mediated translational repression of LIMK1 upon extracellular stimuli [290]. The modulation of miRNA repression is important for developmental processes, e.g. the miR-430-based regulation of Nanos and TDRD7 is suppressed by an unknown factor in the germline, but not in somatic cells of zebrafish [224]. Some RBPs, such as HuR, show different regulatory functions depending on cellular conditions, their RNA and protein cofactors and their target RNA. For example, miRNA let-7 and HuR protein regulate the expression of cMyc by an interdependent mechanism. HuR binds to the 3'UTR in close proximity to the let-7 binding site and recruits let-7 loaded RISC, which represses mRNA translation [159]. In cooperation with its protein cofactor AUF, HuR destabilizes p16 mRNA by recruiting RISC to the 3' UTR [39]. On the other hand, HuR rescues CAT1 mRNA from translational repression through miR-122 under stress conditions, most likely by interfering with miRNA association to the target RNA [23].

Taken together, these examples of RBP function highlight the importance of the protein composition of a messenger-ribonucleoprotein (mRNP) for miRNA-guided gene silencing and support the idea that RBPs and miRNAs regulate their respective activity by competing or complementing their binding to the target RNAs [94].

1.4.4 MicroRNA-Mediated Deadenylation and Destabilization

Initial studies suggested that the mRNA stability is not affected by miRNA-mediated repression but recent findings demonstrate that mRNA destabilization is the predominant mode of regulation by miRNAs in mammalian cells ([111, 124, 132], Figure 1.4.2). A large fraction of down-regulation after miRNA transfection is accounted for by mRNA degradation ([15, 189, 353]. An example for this mechanism is the miRNA-controlled destruction of transiently required transcripts and maternal mRNAs during development and cell differentiation [99, 352]. On the other hand, a set of enodgenous miRNA targets are only translationally repressed but not degraded [19, 75, 297].

Recently several quantitative proteomic studies addressed the effect of miRNAs on proteome level. Selbach *et al.* [297] observed that miRNA targeted mRNAs are only regulated at the translation level at early time points after miRNA transfection but that protein and mRNA levels correlate strongly at a later time point [297]. A study by Baek *et al.* shows that modestly repressed targets are translationally repressed, whereas strong miRNA regulated repression was based on mRNA destabilization [14].

In general, messenger RNA decay starts with the removal of the poly(A)-tail through the CCR4-NOT deadenylation complex. The deadenylated mRNAs are then either degraded in 3'-5' direction by the exosome or the 5' cap is removed by the DCP1-DCP2 decap-

ping complex. Decapped mRNAs are subsequently degraded in 5'-3' direction by the exonuclease XRN1 [80, 324]. Deadenylation is a widespread effect of miRNA-mediated regulation [74, 99, 338, 353]. It is mediated by the CCR4-NOT1 complex [19, 74, 264] and requires a GW182 protein, CAF1 and PABP [73, 79]. It is possible that the TNRC6-PABP interaction (see Section 1.3.4) places the poly(A)-tail in close proximity to the miRISC associated deadenylation complex [79].
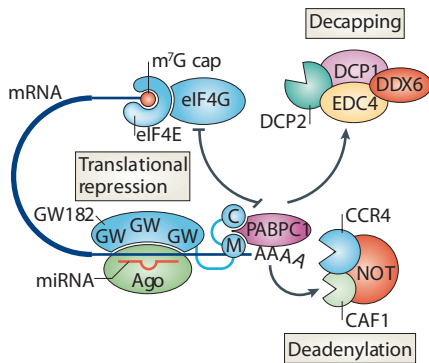
Figure 1.4.2: MicroRNA-mediated mRNA degradation. (Figure taken from [324]).

MicroRNA-mediated deadenylation precedes decapping of target mRNAs through the DCP2 complex containing the decapping activators DCP1, Ge-1 and RCK/DDX6 in flies [75, 273, 359]. The interaction between the decapping complex and repressed mRNAs has been suggested to be mediated by UPF1 [143], a helicase involved in NMD that associates with DCP1, DCP2 and AGO2 [127, 203]. MiRNA-mediated deadenylation is independent of the translation status of the target mRNA. The process is not blocked by translation inhibitors [79, 338] and poorly translated transcripts are deadenylated in a miRNA dependent manner [74, 353]. MicroRNA targets with defective cap structures are also deadenylated [224, 338]. It is not clear whether additional mechanisms besides deadenylation repress translation of polyadenylated miRNA targets. Additionally, it appears as if deadenylation contributes to, but it is not absolutely required for the establishment of silencing of polyadenylated mRNAs [132].

AU-rich elements (AREs) are regulatory signals located in the 3' UTR of mRNAs. They have been shown to influence translation and to decrease the stability of the mRNA [337]. This involvement of AREs in mRNA decay is termed ARE-mediated mRNA decay (AMD) [17] and growing evidence suggests that AMD is connected to miRNA mediated gene silencing [17, 337]. Both processes involve the same effectors of degradation and are localized to P-bodies and stress granules [86, 182, 196, 309]. Several studies have reported miRNA targeting of AREs [23, 39, 159] and Jing *et al.* [147] showed that RISC components and miR-16 are required for AMD of TNFα mRNA.

1.4.5 MicroRNA-Mediated Translation Activation

MicroRNAs generally function as translation repressors but in some cases miRNAs mediate activation of translation. In human cells, miR-369-3-directed association of FXR1 and AGO2 to the ARE of TNFα mRNA during cell cycle arrest leads to translational activation [331, 332]. Other well studied miRNAs, including let-7, also induce translation upregulation of mRNA targets during cell cycle arrest but repress translation in proliferating cells [332]. Translational activation also occurs with miRNAs binding in the 5' UTR. Translational repression of ribosomal protein mRNAs during amino acid starvation is alleviated by miRNA binding in the 5' UTR [369] and the translation of viral mRNAs is stimulated by miRNAs [125, 149]. Nevertheless, miRNA-mediated translation activation seems a rare mechanism which applies only under certain cellular conditions and further investigations are necessary to clarify the relevance of this miRNA function. Furthermore, miRNAs can function as decoys by blocking RBP mediated translational repression [65]. For example, the translation of CEBPA mRNA is inhibited by binding of hnRNP E2 to a regulatory sequence in the 5' UTR. The sequence of the miR-328 is similar to the sequence of the hnRNPE2 binding site on the mRNA. MiR-328 is thereby able to bind into the mRNA binding site of hnRNPE2. This association prevents the binding of hnRNPE2 to the CEBPA mRNA and translational repression is relieved. It is striking that the miR-328-hnRNPE2 interaction is AGO independent [65].

1.4.6 Small RNA-Mediated Transcriptional Gene Silencing

Small RNA-mediated gene silencing pathways are not restricted to the level of mRNA translation and stability, but they also act at transcriptional and chromatin levels. First evidence for small RNA-mediated transcriptional gene silencing was discovered in plants. Here, viral RNAs or small RNAs derived from transgenes guide the methylation of homologous DNA sequences [223, 347]. Methylation of these homologous DNA sequences is Dicer and AGO dependent [123, 366]. It is also linked to histone H3 lysine 9 methylation, a classical mark of transcriptionally inactive chromatin [193]. In *S. pombe*, small RNAs guide histone methylation through the AGO1-containing RNA-induced transcriptional silencing (RITS) complex [333, 336]. The RITS complex associates with nascent transcripts via siRNA-RNA base pairing and recruits the RNA-directed RNA polymerase complex (RDRC) and the Clr4 methylase complex, resulting in dsRNA synthesis, siRNA production, H3K9 methylation and chromatin compaction [192, 227, 228, 310]. In mammals, siRNAs can direct histone methylation in an AGO1- and AGO2-dependent mechanism [141, 158]. On the one hand, human miRNAs directed against promotors facilitate transcriptional silencing [157]. On the other hand, it was found that promotor targeting

RNAs are involved in transcription activation [142, 293]. This evidence and the nuclear localization of AGO proteins [349] suggest that small RNA-directed transcriptional gene silencing pathways are conserved, but the endogenous mechanism by which this is achieved in mammals remains for the most part unknown [69, 227].

1.5 The PIWI Subfamily of Argonaute Proteins and PIWI-interacting RNAs

1.5.1 PIWI-interacting RNA Biogenesis

PIWI-interacting RNAs are the third well studied class of small RNAs. These endogenous small RNAs are 24-29 nt long and are germ-line specific [8, 9]. They associate with AGO proteins of the PIWI-clade in fly, mouse and zebrafish [7, 100, 129, 286]. Although a subset of fly piRNAs is involved in silencing protein encoding genes [236], piRNAs are mainly involved in silencing of mobile genetic elements [11, 35]. In flies and mammals, piRNAs are 2'-O-methylated at the 3' end, but the biological significance of this modification remains to be elucidated [128, 165, 240, 287, 327].

In *D. melanogaster*, piRNAs derive from piRNA clusters. Their sequences correspond to retrotransposons and intergenic repetitive elements and are enriched in species that are antisense to transposons [286, 327]. Distinct piRNA species associate with each PIWI-protein. AUB- and PIWI-associated piRNAs arise from antisense transcripts and show a preference for uridine at the 5' end. AGO3, however, associates with piRNAs derived from sense transcripts with a preference for an adenine at nucleotide 10 but no 5' end bias [7, 32, 110]. Since PIWI proteins have slicer activity [236, 286] and piRNA biogenesis is Dicer independent [327], the current "ping-pong" model for piRNA biogenesis involves the PIWI proteins themselves [7, 32, 110]. Antisense piRNAs bound into AUB and PIWI guide the cleavage of the sense transcript, thereby generating the 5' end of a sense piRNA. The newly generated sense piRNA associates with AGO3, which subsequently cleaves an antisense transcript and generates the 5' end of an antisense piRNA. This piRNA then again binds to PIWI or AUB and induces the next sense transcript cleavage. The factors facilitating the generation of piRNA 3' ends have not been identified so far. PiRNAs and at least AUB are maternally inherited and initiate the amplification of piRNAs through the "ping-pong" cycle [32, 33, 236]. Several other factors besides the PIWI proteins are involved in piRNA biogenesis [159]. Some piRNAs are only found in PIWI and are not produced by the ping-pong cycle but via a separate pathway known as the primary processing pathway [11]. Ongoing discussions concern the role of piRNAs in somatic cells and a possible interplay between piRNAs and endo-siRNAs as both small RNA species

repress transposons. Endo-siRNAs might provide rapid response to new transposons in the germ line and piRNAs, on the other hand, can provide robust and permanent control of transposons [82].

Mammalian piRNAs have been shown to mediate transcriptional silencing of their target genes by DNA methylation [10, 11, 35, 169]. Two classes of piRNAs have been described in mammals. Murine pre-pachytene piRNAs are expressed before meiosis, derive from repeat and transposon rich clusters and interact with MILI and MIWI2. Pachythene piRNAs associate with MILI and MIWI and their sequences give no indications for possible targets [159, 211]. The biogenesis of pre-pachytene piRNAs has been suggested to occur through the ping-pong cycle, whereas pachythene piRNAs are likely to be generated by primary processing pathways [10].

1.5.2 Regulation of PIWI Protein Interactions by Arginine Methylation

PIWI proteins in mammals, fly and *Xenopus laevi* contain symmetrical dimethly arginines (sDMA). Such arginine methylations modulate protein-protein interactions and thereby regulate the biological activity of proteins [219, 304]. DMA modifications of PIWI proteins are carried out by the protein methyltransferase 5 (PRMT5) [164]. PRMT5 is a type II protein arginine methyltransferase that produces symmetric dimethylarginines [30, 267, 275]. It localizes predominantly to the cytoplasma and methylates, amongst others, myelin basic protein [267], histones [314] and the Sm proteins [87, 218]. By methylation of target proteins, PRMT5 influences various cellular processes such as U snRNP assembly [87, 218], cell cyle progression [122], pluripotency of ES cells [314] and tumor growth [268]. PRMT5 associates with its co-factors MEP50 (also known as WDR77) and different adaptor proteins for substrate recognition into a complex referred to as the methylosome [87, 88, 108, 261].

First evidence of sDMA modification of PIWI proteins were reported for MILI and MIWI in mice but they are also present in *Drosophila* and *Xenopus*. So far there are no indications that the ubiquitously expressed AGO proteins are also methylated [304]. In *Drosophila*, sDMAs were only mapped in AGO3 and AUB [235]. Mapping of methylated arginines in murine PIWI proteins in mouse testes revealed several mono- and/or dimethylated sites and all detected dimethylations were symmetric [41, 274, 328]. The different studies show a discrepancy for the methylation status of PIWI proteins, which indicates a dynamic regulation of the methylation status [304].

Symmetrical DMA modifications do not influence the association of PIWI proteins with piRNAs [274] or the protein stability but affect transposon silencing [164] and subcellular localization [235]. The methylosome complex associates with all three murine PIWI pro-

teins in mouse testes [328] as well as in *Drosphila* [6] and the sDMA modification of the PIWI proteins is required for their interaction with Tudor domain containing (TDRD) family proteins in mouse and flies [41, 235, 274, 328, 343]. These sDMA mediated associations between PIWI and TDRD proteins have been identified as a factor regulating piRNA production and PIWI-protein to piRNA association [304].

1.6 Quantitative Proteomics

The mechanism of small RNA-mediated gene regulation is one of the examples for the substantial influence of the protein complex composition on the function of an individual protein. Although all small regulatory RNAs are bound into AGO proteins, the ensuing activity of AGO is not only defined by the nature of the bound small RNA but is significantly influenced by the other protein components in the RISC (see Section 1.4.3). The protein composition of RISC is in turn dependent on the whole proteome of the cell, which again varies between cell types and undergoes major changes upon external stimulation. It is hence of great interest for the understanding of AGO function to unravel the influence of the cellular proteome and to define the interplay between AGO and its specific interaction partners under varying cellular conditions. Over the last decade, mass-spectrometry (MS)-based proteomics has developed into a powerful method for the global measurement of proteins. The development of high resolution instruments and sophisticated data analysis tools greatly improved data reliability and facilitates the identification of thousands of proteins from a complex mixture. MS can be applied to identify the relative or absolute amount of proteins in a sample, for example the abundance of proteins in a cell. Unlike mRNA microarrays or deep sequencing methods, expression proteomics take posttranscriptional and translational expression regulation into account and give detailed information about the protein composition of a cell in a certain state. In combination with quantitative techniques, MS based proteomics can be applied to compare the protein composition of different samples or to monitor dynamic changes [49, 98]. MS itself is not quantitative but two methods, the label free and isotope labeling approaches, add a quantitative dimension to MS. Label free quantitation approaches such as spectral counting [194] and the exponentially modified protein abundance index [135] are based on the fact that abundant proteins produce more MS/MS spectra than low abundant proteins and provide a good estimation of relative abundances. The drawback of label free quantitation is that samples to be compared have to be measured separately, which introduces experimental variability [64].

Stable isotope labeling approaches introduce 'heavy' stable isotopes such as ^{13}C or ^{15}N into the sample. Heavy isotope labeled peptides are chemically equivalent to unlabeled

'light' peptides and differ only in their mass. Peptides with both labels behave identically in biochemical purification and fractionation procedures and thus enter the mass spectrometer simultaneously. In the full MS scan, two precursor masses are detected that represent the two peptide species. The ratio of the signal intensity of the peaks corresponds to the relative abundance of the proteins in the input samples and allows an accurate quantification [98].

Isotope-based quantitative proteomics relies on two different approaches to introduce isotope labeling. In chemical labeling approaches such as isotope-coded affinity tag (ICAT) [113] and isobaric tags for relative and absolute quantitation (iTRAQ) [280] the reactive groups of peptides are used to couple them to an isotope containing tag. These methods can be applied to all sample types including fixed tissues. Its disadvantages are the labeling efficiency and experimental variability caused by the necessity to handle samples seperately. In metabolic labeling strategies, the heavy isotopes are introduced through the growth medium or food by replacing essential amino acids with heavy labeled counterparts, a method known as stable isotope labeling by amino acids in cell culture (SILAC) ([244], Figure 1.6.1).
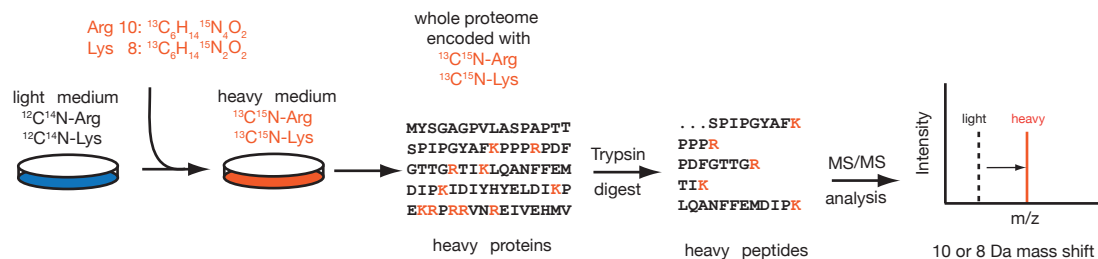
Figure 1.6.1: Stable isotope labeling by amino acids in cell culture (SILAC). Cells grown in medium with normal amino acids ("light", depicted in blue) are transferred to medium containing arginine and lysine labeled with the stable isotopes ^{13}C and ^{15}N ("heavy", depicted in red). Protein turnover during growth leads to metabolic incorporation of the heavy amino acids into the whole proteome. Digestion of the proteins with trypsin results in peptides with either a ^{13}C-^{15}N-arginine or a ^{13}C-^{15}N-lysine at the C-terminus. The presence of the heavy amino acid leads to a residue specific mass shift of 10 or 8 Da for arginine or lysine, respectively, compared to the light peptide (Figure adapted from [245]).

The most commonly used amino acids for metabolic labeling are arginine and lysine. During growth, the protein turnover leads to metabolic incorporation of the heavy amino acids into the whole proteome. The great advantage of metabolic labeling compared to chemical methods is that the isotopic label is introduced before protein purification,

Figure 1.6.2: SILAC based expression proteomics. Cells in two different states can be labeled with light or heavy amino acids. The samples are then mixed in a 1:1 ratio and analyzed together. For every peptide common for both states two isotope clusters, a so-called SILAC pair can be detected in the mass spectrum. The mass difference between the SILAC pair corresponds to the mass difference between the heavy and light amino acids. A ratio can be assigned to every detected peptide pair. This ratio correlates to the relative abundance of the protein in the two samples and indicates if a protein is unchanged, or up- or down regulated in the different states (Figure adapted from [64]).

leading to a significant reduction of errors caused by sample handling. SILAC-based quantitative proteomics can be applied to compare whole proteome changes between different cellular states, for example upon stimulation [24] or between protein isoforms ([322], Figure 1.6.2). Pulsed SILAC has been established as a technique for the monitoring of dynamic changes [292] and this method has been successfully used to identify miRNA targets [14, 297].

Protein-protein interactions and the underlying dynamics are of great importance for the understanding of cellular processes. Different approaches such as the yeast two-hybrid system [81] have been established for the identification of protein-protein interactions. Great advances in the field of interaction proteomics came from the combination of affinity purification and mass spectrometry (AP-MS). In this set-up, isolation of multiprotein complexes by affinity purification is followed by the identification of complex components by MS. A great advantage of AP-MS is that it does not require pre-existing knowledge of the protein complex to be analyzed. Another advantages of this approach is that, unlike yeast two-hybrid screens that rely on expression and interaction of proteins in the yeast nucleus, proteins are isolated from near physiological conditions and post-translational modifications that are crucial for organization and activity of a protein complex are not perturbed [98].

With the increasing sensitivity of modern mass spectrometers it is difficult to differentiate background binders and contaminants from true interactors [1]. Immunoprecipitations do not only contain the target protein itself and its specific interaction partners but con-
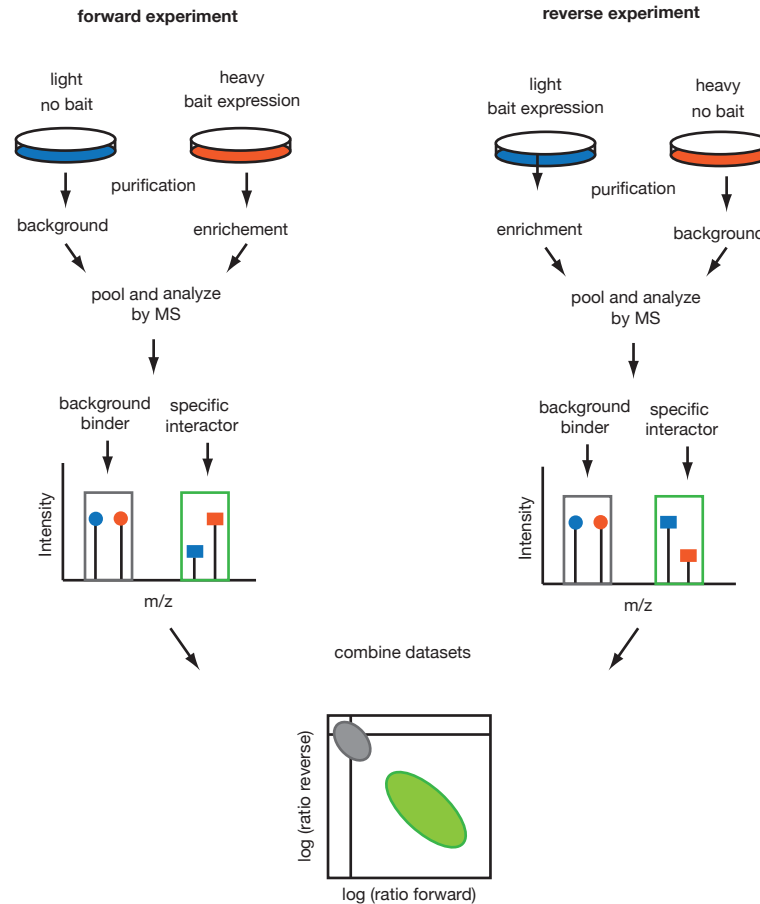
Figure 1.6.3: SILAC-based interaction proteomics. In order to identify its interactors, the protein of interest ("bait") is purified from heavy labeled cells while a light labeled cell line without the bait is used for the background control (forward experiment, left panel). The two samples are combined after the enrichment and further processed and analyzed together. The experiment is repeated with a label switch (reverse experiment, right panel). Both datasets are combined and the ratios from the two experiments are plotted against each other on a logarithmic scale. Specific interactors appear as outliers in the lower right quadrant (high ratios, green sphere) while background binders cluster around zero (ratios 1:1, grey sphere) (Figure adapted from [64]).

tain additional proteins non-specifically binding to the beads or the antibodies. Proteins with cross-reactivity to the antibody are also detected. Applying a stringent purification procedure, such as tandem affinity purification, can reduce the background binding. However, it harbors the risk of loosing weak interactors and requires high amounts of input sample. Quantitative proteomic approaches present a solution for these problems [272]. These methods allow the direct distinction between background binders and true

interaction partners based on the direct quantification between sample and control and thus facilitate the high confidence identification of interaction partners from low stringency and single step purifications [334]. In SILAC-based interaction proteomics the protein of interest, the "bait" protein, is isolated from heavy labeled cells while a light labeled cell line without the bait is used as background control. The ratios between the SILAC pairs clearly distinguish specific interactors from background binders and contaminants (Figure 1.6.3).

For the high confidence identification of interaction partners of endogenous proteins, aquantitative immunoprecipitation combined with knockdown (QUICK) approach can be used [296]. In this approach, the abundance of the protein of interest is reduced in one of the SILAC labeled cell populations by RNAi. In affinity purifications followed by MS analysis, the proteins of interest and its specific interaction partners show peptide ratios whereas unspecific background binders show no ratio difference. Thereby the two groups are easily distinguishable from each other. QUICK also harbors the advantage that proteins cross-reacting with the antibody appear as background binders. The abundance of the cross reactant is not affected by the knockdown, so equal amounts of both SILAC states are bound by the antibody and no ratio differences are observed.

1.7 Aim of the Thesis

Argonaute proteins are the key components of small RNA-mediated regulatory pathways. They bind small regulatory RNAs and assemble with several other protein factors into RNP complexes. The role of the small regulatory RNA bound into AGO is to guide the RNP to a target RNA in a sequence specific manner. Depending on the nature of the bound small regulatory RNA and on the protein composition of the RNPs, AGO exerts various regulatory functions such as the regulation of transcription, translation and mRNA decay.

To better understand the mechanisms of miRNA mediated regulation, it is necessary to characterize the underlying structural features. One of the aims of this work was to gather structural insights into RISC architecture by determining the structure of a minimal RISC by electron microscopy. For this purpose, a purification strategy for the isolation of a complex consisting of AGO2 and Dicer from cultured human cells had to be established. In addition, the reconstruction of the structure of the methylosome core complex, a protein complex involved in the post-translational modification of germ line specific AGO proteins, was attempted.

So far, the identities of the accessory protein factors regulating the assembly and function of AGO2-containing RNPs have been addressed by several semiquantitative proteomic screens [127, 171, 220] but none of these studies allowed a direct comparison between AGO2-containing RNPs under different cellular conditions. Therefore, it was aimed to conduct a SILAC-based quantitative proteomic screen of murine AGO2-containing RNP complexes in the absence or presence of mature miRNAs, allowing the definition and comparison of the protein composition of the complexes under these two conditions. For the studies on endogenous protein complexes, a highly specific antibody is a prerequisite. Therefore, we aimed to establish an antibody highly specific for mouse AGO2 to be used for the purification of endogenous AGO2-containing RNP complexes. As the quality of affinity purifications of endogenous protein complexes are highly dependent on the performance of the antibody, it was also an aim to establish MEF cell lines stably overexpressing FLAG/HA-tagged AGO2 and to perform proteomic screens of AGO2-containing RNPs isolated by this tag-based purification system.

2 Results

2.1 Structural Analysis of the AGO2 Complex I by Electron Microscopy

The majority of structural insights on Argonaute and Dicer have come from crystallization studies of full length prokaryotic homologues or from individual domains of the eukaryotic proteins (see Section 1.3.3). These crystal structures reveal detailed information about the individual proteins but they do not give insights into the architecture of RISC. The AGO2 complex I described by Höck *et al.* has an approximate size of 232 kDa and sediments at 11 S in sucrose gradients. It exhibits RISC and Dicer activity and the components are associated in an RNA-independent manner [127]. Therefore, the AGO2 complex I was assumed to correspond to the RISC-loading complex. We established a strategy to purify the AGO2 complex I from human cells and aimed to determine the structure of the complex by electron microscopy (EM).

Our attempts to purify endogenous complexes were abandoned after initial experiments (data not shown). When endogenous complexes were purified from cultured human cells, the yield of the purification was very low so that the amount of protein after the last purification step was not high enough to reach the concentration required for grid preparation. Since we were mainly limited by the amount of input sample, we increased the amount of input protein by simultaneous overexpression of FLAG/HA-tagged AGO2 (F/H-AGO2) and cMyc-tagged Dicer in HEK 293T cells. AGO2-containing complexes were separated by density centrifugation as described ([127], Figure 2.1.1A). Gradient fractions containing the AGO2 complex I were combined and F/H-AGO2 was immunoprecipitated with FLAG-antibody coupled agarose beads. AGO2-containing complexes were eluted from the antibody with competing peptide and further purified in a GraFix gradient [150]. The GraFix sample preparation method applies a glycerol gradient with an increasing concentration of a chemical fixation reagent. During the centrifugation, protein complexes are separated by the density gradient and simultaneously chemically fixed. The fixation stabilizes the complexes, thereby leading to an increased homogeneity and reduced aggregation and degradation of the sample [150]. In the glycerol gradient used for the GraFix, AGO2 was distributed over fractions 7-23 and
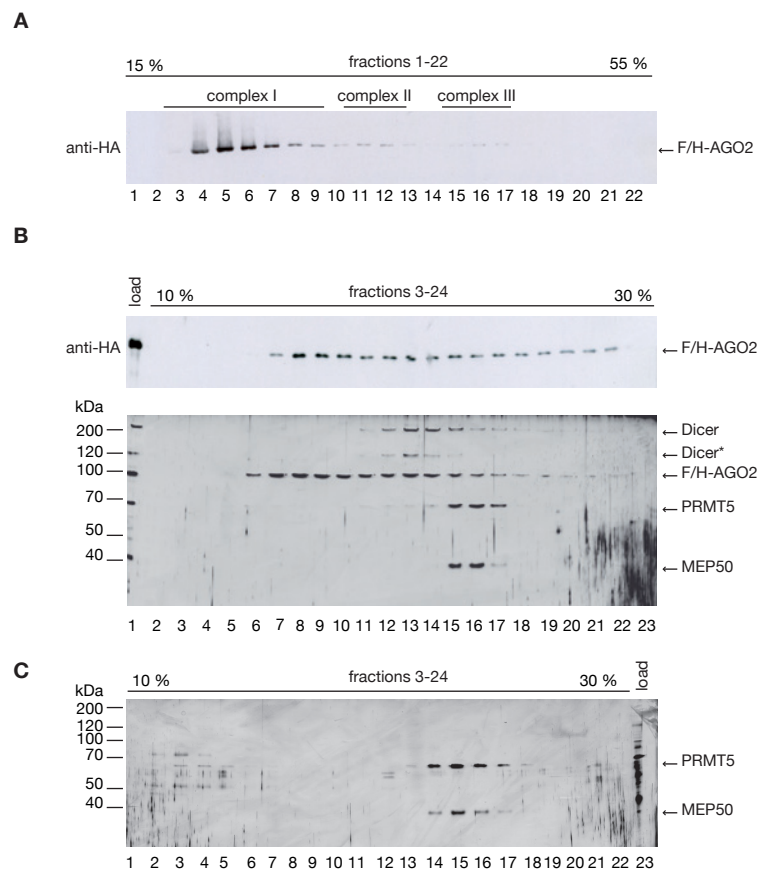
Figure 2.1.1: Purification of the AGO2 complex I from HEK293T cells in a Tris-based buffer system. A) Lysate from HEK293T cells transiently transfected with F/H-AGO2 and cMyc-Dicer was separated by density centrifugation in a 15-55% sucrose gradient. The individual fractions were analyzed by Western blotting against F/H-AGO2. B) F/H-AGO2-containing protein complexes were immunoprecipitated from the combined fractions 3-8 with FLAG-agarose. Bound protein was eluted with 3x FLAG peptide and separated by density centrifugation in a 10-30% glycerol gradient. The distribution of F/H-AGO2 in the individual fractions was analyzed by Western blot (upper panel) and silver stain (lower panel). Protein bands were cut out and identified by mass spectrometry. Asterisks indicate protein degradation products. C) Protein complexes were purified from untransfected HEK293T cells as described in A and B and were analyzed by silver staining.

we visually distinguished three different protein complexes based on the protein band pattern (Figure 2.1.1B). The individual proteins were identified by mass spectrometry. Fractions 7-12 (corresponding to lanes 6-11 in Figure 2.1.1B) contained free AGO2 only. In fractions 13-15, we saw clear bands for AGO2, full length Dicer and a Dicer degradation product. The protein band running at a size of 70 kDa was identified as the protein methyltransferase 5. PRMT5 and its interaction partner MEP50 were highly abundant

in fractions 16-19 together with the proteins found in fractions 13-15. The third reported methylosome component pICln [87, 108, 261] was not detected. Fractions 19 and higher contained only AGO2 and full length Dicer in low amounts.

PRMT5 and MEP50 have been identified in FLAG-purifications of AGO2 complexes previously [221] and it is known that the PIWI proteins are substrates for the methylase activity of PRMT5 [164]. It might be possible that AGO2 is also a substrate for methylation and is therefore found in a stable complex with PRMT5. In order to demonstrate that the methylosome components associate specifically with the AGO2 complex I, we performed protein purification from untransfected HEK cells to define contaminating proteins in our sample (Figure 2.1.1C). To our surprise, we obtained the PRMT5-MEP50 complex in fractions 16-19 with high purity. This implies that the methylosome components do not specifically interact with the AGO2 complex I, but that their presence in the sample is based on a non-specific association with the FLAG-antibody or the agarose matrix.

It was our hope that the two unrelated complexes differ so significantly in their shape or size that they can be clearly distinguished from each other. Therefore, we negatively stained the particles in glutaraldehyde fixed fractions 17 and 20 from purifications from untransfected HEK293T cells and from HEK293T cells transiently transfected with F/H-AGO2 and cMyc-Dicer and compared the particles visible in the electron micrographs (Figure 2.1.2). In fraction 17, which contains a mixture of the PRMT5-MEP50 and the AGO2 complex I or the PRMT5-MEP50 complex alone, we saw predominantly distinct particles and only little aggregation in both samples. For the PRMT5-MEP50 complex, we observe a specific circular shape for a set of particles. A few particles with this distinct shape were also visible in the mixed sample, but otherwise particles in both samples looked very similar. Therefore, we were not able to distinguish the two complexes from each other based on their shape and size in the electron micrograph of this fraction. The methylosome sample contained almost no proteins in fraction 20. In the AGO2 complex I purification, this fraction should therefore contain the AGO2-Dicer complex only. We see an increased aggregation in this fraction compared to fraction 17. No ring shaped particles were observed in this sample but single particles were heterogenous and had a bigger size and aberrant shapes. Since the complexes in fraction 20 migrated further into the gradient they are expected to have a slightly higher mass than the complexes in the previous fractions. This mass shift might be caused by aggregation, which would explain size and heterogeneity of the particles. Because of this heterogeneity the particles of the AGO2 complex I in fraction 20 were also not suitable for single particle reconstruction. Consequently, it was necessary to further refine the purification strategy.
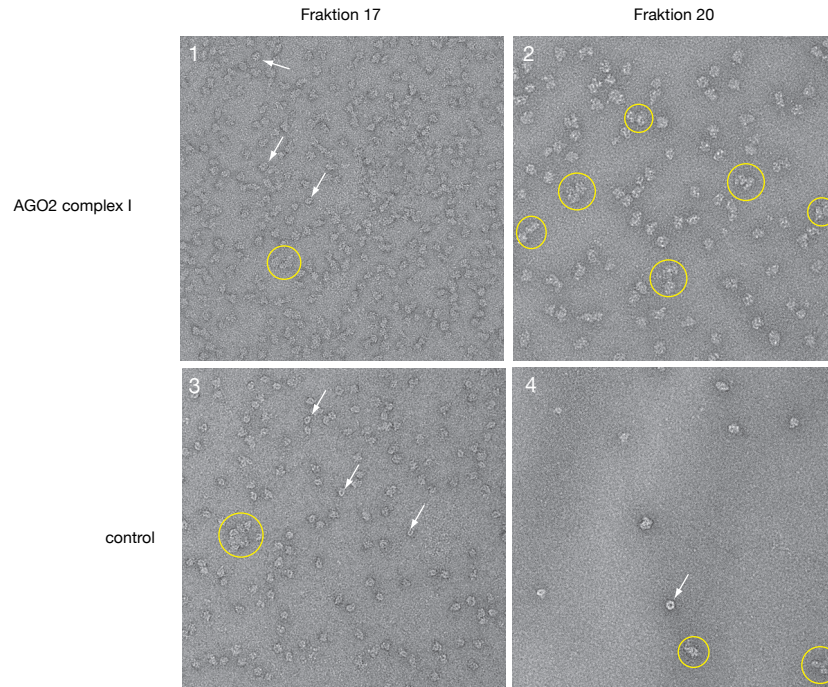
Figure 2.1.2: Representative electron micrographs of cross-linked, negatively stained AGO2 complex I and PRMT5-MEP50 complex particles. Protein complexes were purified from HEK293T cells transiently transfected with F/H-AGO2 and cMyc-Dicer (panels 1-2) or untransfected cells (panels 3-4). GraFix fractions 17 (panels 1 and 3) or 20 (panels 2 and 4) were negatively stained and examined by EM. Yellow circles highlight aggregates and arrows point at particles with a distinct circular shape.

We solved the problem of the PRMT5-MEP50 contamination by performing the purification in a different buffer system. All steps remained the same except that Tris was exchanged for HEPES as buffer substance. As seen in Figure 2.1.3, the PRMT5-MEP50 contamination was eliminated and we obtained only AGO2 and Dicer. Several attempts to reduce the Dicer degradation were unsuccessful (data not shown). The specific degradation product with a size of 130 kDa was identified as the N-terminal part of Dicer (Stephanie Schell, personal communication) and this fragment was also observed in other purifications of Dicer protein [102].

Electron micrographs of negatively stained AGO2 complex I from this purification revealed a very low number of heterogenous particles (Figure 2.1.4). To increase the concentration, the purification procedure was refined by introducing several elution steps
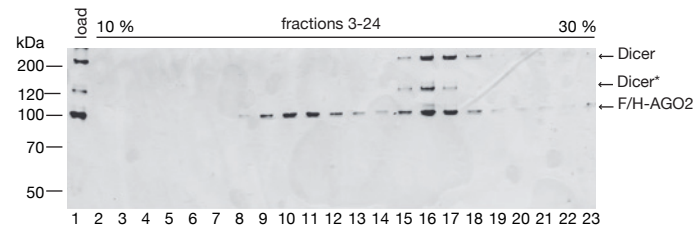
Figure 2.1.3: Purification of the AGO2 complex I from HEK293T cells in a HEPES-based buffer system. The AGO2 complex I was isolated in a HEPES-based buffer system following the same purification procedure as described in Figure 2.1.1. Individual fractions of the glycerol gradient were analyzed by SDS-PAGE and silver stain.

and an enrichment step (data not shown). These efforts proved to be futile as the protein amount on the grid increased only very slightly and the heterogeneity of particles remained. The sample quality could not be increased to the standard necessary for determination of a high-resolution structure and with the publication of the low resolution EM structure of an *in vitro* reconstituted human RISC loading complex by Wang *et al.* in 2009 [342] the project was discontinued.
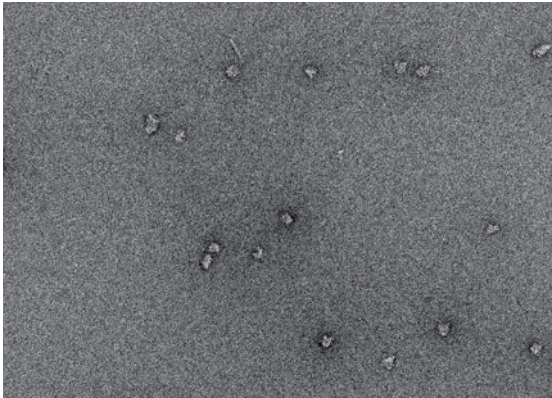
Figure 2.1.4: Micrograph of the formaldehyde fixed, negatively stained AGO2 complex I. AGO2 complex I was isolated from HEK293T cells in a HEPES-based buffer system and fixed in a GraFix gradient before negative stain and analysis by EM.

2.2 Structural Analysis of the PRMT5-MEP50 Complex by Electron Microscopy

PRMT5 is a type II protein arginine methyltransferase that produces symmetric dimethylarginines [275]. Among its substrates are the Sm proteins [87, 218] and the PIWI proteins of mouse, fly and *X. laevi* [164, 235, 326]. We have discovered a way to purify endogenous PRMT5 in complex with its cofactor MEP50 from human cells (Figure 2.1.1C).
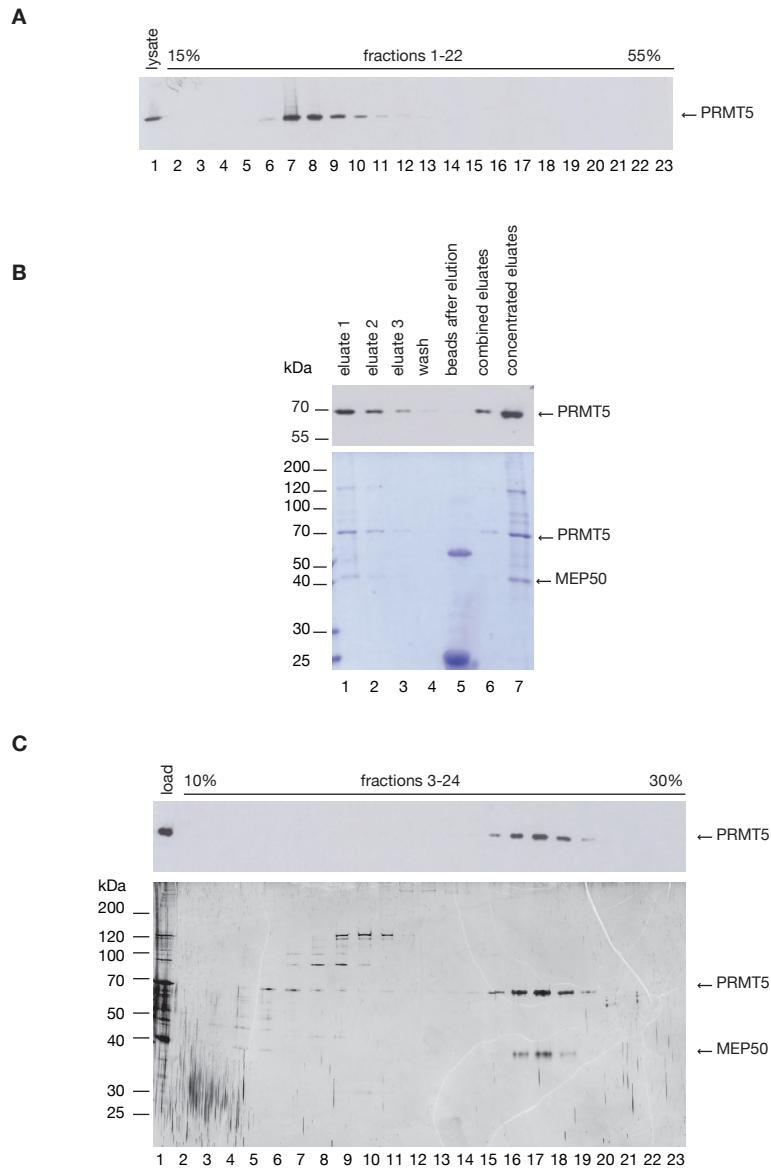
Figure 2.2.1: Purification of the PRMT5-MEP50 complex from HEK293T cells.
A) Lysate from HEK293T cells was separated by density centrifugation in a sucrose gradient and analyzed for PRMT5 by Western blot. B) PRMT5-MEP50 compleses were immunoprecipitated from the combined fractions 4-9 with FLAG-agarose and eluted from the beads with 3x FLAG peptide. Bound protein was eluted in three steps. Eluates were combined and concentrated before loading on a glycerol gradient. The elution procedure was analyzed by Western blot against PRMT5 (upper panel) and Coomassie stain (lower panel). C) The eluted proteins were separated by density centrifugation in a 10-30% glycerol gradient. Individual fractions were analyzed by Western blot against PRMT5 (upper panel) and silver stain (lower panel)

Although the affinity of the FLAG-antibody for the PRMT5-MEP50 complex is assumed to be unspecific, it was still strong enough to allow an efficient purification. This purified PRMT5 complex could be used to determine its structure and to study the methylation of human PIWI proteins. We improved the described purification strategy by adding several elution and an enrichment step and obtained a PRMT5-MEP50 complex that appears highly pure in a silver stain (Figure 2.2.1). Electron micrographs of the glutaraldehyde fixed, negatively stained complex (Figure 2.2.2) revealed a strong heterogeneity of the particles. As expected, we observed the previously described ring shaped particles. We saw additional particles that cannot be side views of the ring shaped particles because of their size, which was a clear indication that we had at least two different particle populations in the sample. PRMT5 forms homo-multimers under cellular conditions [275], so it is quite possible that the sample contained different complexes with varying multimers. In addition to particle heterogeneity, we had a low amount of particles on the grids and sometimes observed non-uniform staining of the particles.

Figure 2.2.2: Micrograph of the formaldehyde fixed, negatively stained PRMT5-MEP50 complex PRMT5-MEP50 complexes were isolated from HEK293T cells in a Tris-based buffer system and fixed in a GraFix gradient before negative stain and analysis by EM.

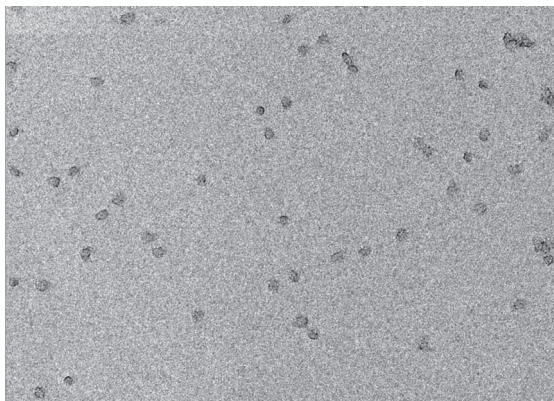Particles were picked automatically and particles with positive staining or a flat appearance as well as particles not discernible from background were sorted out manually. The remaining 1700 particles were used for the generation of class averages. In the class averages we see the typical ring shaped structure and additional particles of bigger size without any distinguishable features. To separate the different particles, we used three representative class averages of different sizes to subclassify the particles according to their size and generated new class averages for the three groups (Figure 2.2.3, groups A-C). Group A contains the 300 biggest particles without any distinct structural features. 490 particles with the distinct circular shape were sorted into group B. Group C consists of 747 particles. These particles are smaller than the ones in group B but also
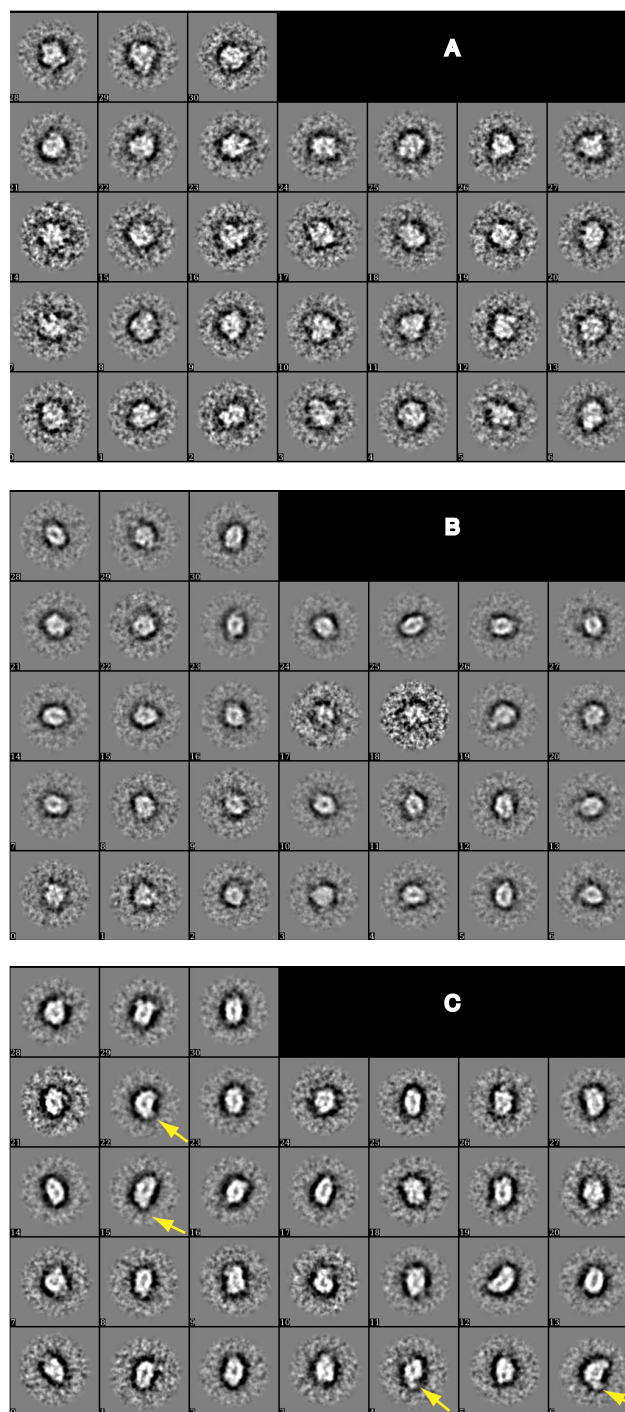
Figure 2.2.3: Class averages of the PRMT5-MEP50 complex. The particles were separated into three groups (A-C) according to their size and 30 class averages per set were generated from 300 (A), 490 (B) and 747 (C) particles. Arrows indicate additional densities on the circular structure of the particles.

show the distinctive circular shape without (boxes 2, 13 and 23) or with an additional density (boxes 4, 6, 15 and 22) (Figure 2.2.3). Initial models were generated from the class averages and we tried to refine the model by fifty rounds of refinement by projection matching as shown in Figure 2.2.4A for the group of the smallest particles (group C). Although some structural features such as an internal cavity and the previously mentioned additional density seemed to become slightly more distinct, other densities grew and disappeared between the refinement rounds. If a model converges into a three dimensional map, the structural differences between the models of two consecutive refinement rounds are very little and the curves in the Fourier Shell Correlation (FSC) plot (Figure 2.2.4B) representing these structural variations show very similar shapes. In our case, the curves in the plot did not overlap and thereby indicated strong differences between the models generated by each refinement round. An analysis of the Euler angles describing the orientation of the particles revealed two problems (Figure 2.2.4C). First, we did not see an isotropic angular distribution. This indicates a strong preferential orientation of the particles on the grid, meaning that particles did not lie on the grid in all possible orientations but tended to lie in a few preferred orientations. Thereby, the possible views of the complex are not equally represented in our data, which makes the reconstruction of a three dimensional structure difficult. Second, the class averages of the particles assigned to a specific orientation often did not match to the corresponding projections. During projection matching, the refinement method used for the reconstruction, projections of different orientations are computed from the initial model. The images of the particles are compared to the projections and are assigned to the projection they match best. Next, a refined map is computed and the generation of projection and assignment of images is repeated. The wrong assignment of the images to projections in the refinement of the PRMT5-MEP50 complex are an indication that some of the particles are lacking sufficient structural details required for an assignment to a certain projection during the refinement process. When we tried a similar 3D reconstruction with the particles from the groups with higher particle sizes (groups A an B) the refinements also did not converge (data not shown).

Taken together, these results show that with the present sample quality it is not possible to reconstruct a three dimensional model. The project to gain structural insights on the endogenous PRMT5-MEP50 complex was abandoned at this point but a second attempt with an *in vitro* reconstituted complex has already been initiated (Nicholas Putz, personal communication).

A

B

C
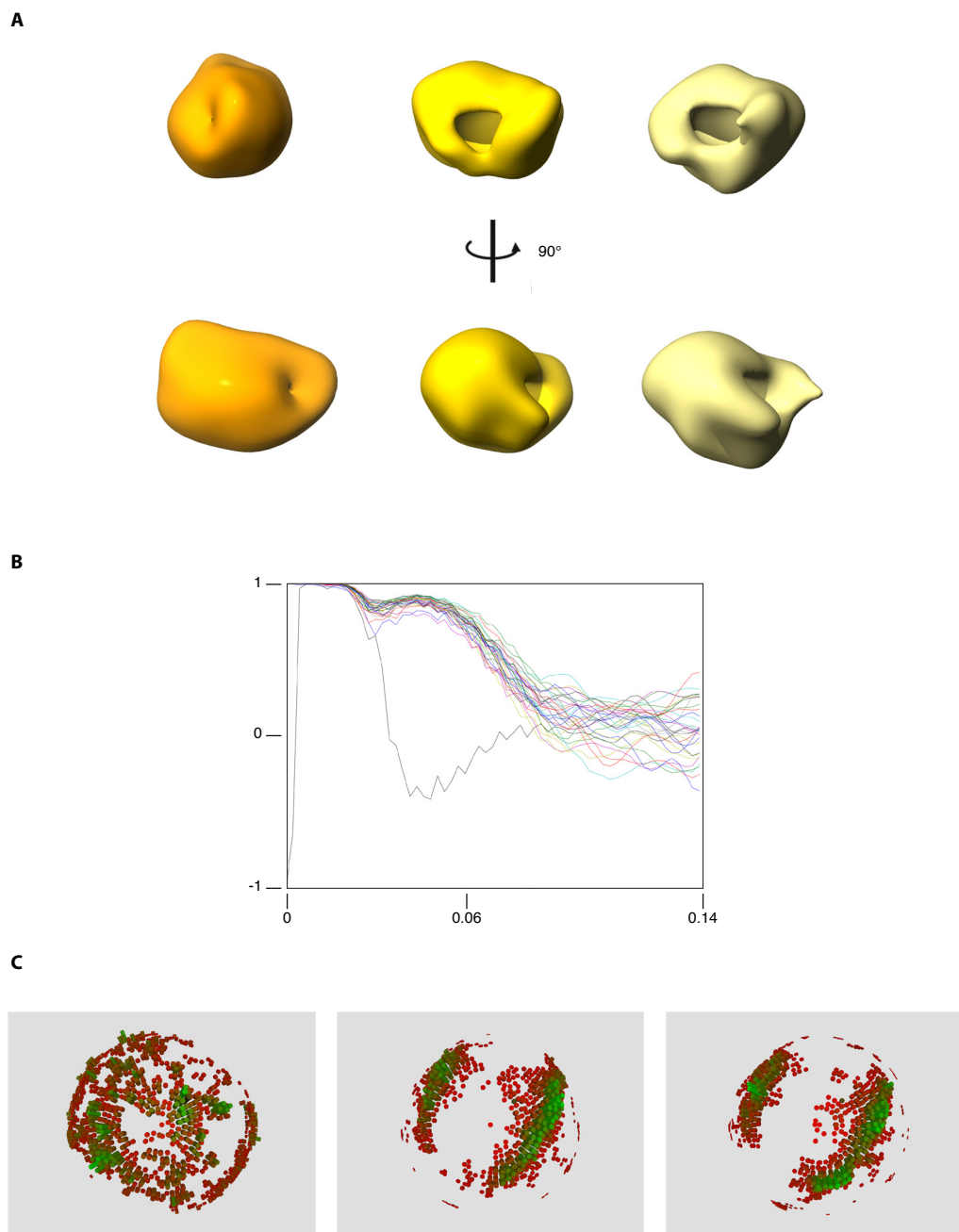
Figure 2.2.4: Three dimensional reconstruction of the group C particles. A) Initial model (left) and refined models after 30 (middle) and 50 (right) rounds of refinement are shown in different orientations. B) Fourier Shell Correlation plot comparing individual models between refinement rounds. C) Spheres showing the assigned Euler angles for the initial (left) and refined models after 30 (middle) and 50 (right) rounds of refinement. Height and color of the cylinders correspond to the number of particles assigned to each projection. Red indicate low numbers and green corresponds to high numbers.

2.3 Generation and Characterization of the Monoclonal Mouse AGO2 Specific Antibody anti-AGO2(6F4)

Many of the studies on AGO complexes have been conducted with overexpressed, tagged proteins due to the lack of highly specific and potent monoclonal antibodies against the different AGO proteins. With the establishment of antibodies specific to human AGO 1-4 [20, 282, 349] it became possible to study the functions of endogenous AGO complexes in human. However, antibodies against mouse AGO proteins were not available. Since we aimed to analyze the function of endogenous RISCs in the murine system, we established a monoclonal antibody specific for mouse AGO2.

A peptide spanning residues 13-26 of mouse AGO2, a region that is not conserved within the mouse AGO proteins (Figure 2.3.1), was injected into rats for monoclonal antibody production. The hybridoma clone 6F4 reacted strongly in the initial peptide coated ELISA screen (data not shown) and was further analyzed by Western blotting (Figure 2.3.2A). Whole cell lysate from murine N2A cells and murine F/H-AGO2 purified from HEK 293 cells were probed with the anti-AGO2(6F4) antibody. A signal at the expected size of approximately 100 kDa was detected in both samples. This result indicated that the antibody recognizes tagged and most likely endogenous AGO2. We next tested if the anti-AGO2(6F4) immunoprecipitates endogenous AGO2 (Figure 2.3.2B). The antibody was coupled to protein G sepharose beads and incubated with whole cell lysate from N2A cells. Beads without antibody served as a control. The samples were analyzed by Western blotting using the anti-AGO2(6F4). Signals were detected in the lysate and supernatants of the immunoprecipitations (IPs). The signal in the IP with the anti-AGO2(6F4) antibody was significantly enhanced, whereas no signal was observed in the IP without antibody. Taken together, these findings indicate that the anti-AGO2(6F4) immunoprecipitated AGO2.

```
mmuAgo2   NP_694818.3   1   MYSGAPGVLASPAPTTSPIPGYAFKPPPRP   30

mmuAgo1   NP_700456.1   1   MEAGPSGAAAGAYLPPLQQVFQAPRRPGIG   30
mmuAgo3   NP_700451.1   1   MEIGSAGPIGAQPLFIVPRRPGYGTMGKPI   30
mmuAgo4   NP_694817.2   1   MEALGPGPPASLLFQPPRRPGPGTVGKPIR   30

hsaAgo2   NP_036286.2   1   MYSGAGPALAPPAPPPPIQGYAFKPPPRPD   30
```

Figure 2.3.1: Amino acid alignment of the N-termini of mouse AGO 1-4 and human AGO2. The peptide used for immunization and amino acid residues conserved between the AGO proteins are depicted in red. mmu, *Mus musculus*; hsa, *Homo sapiens*.
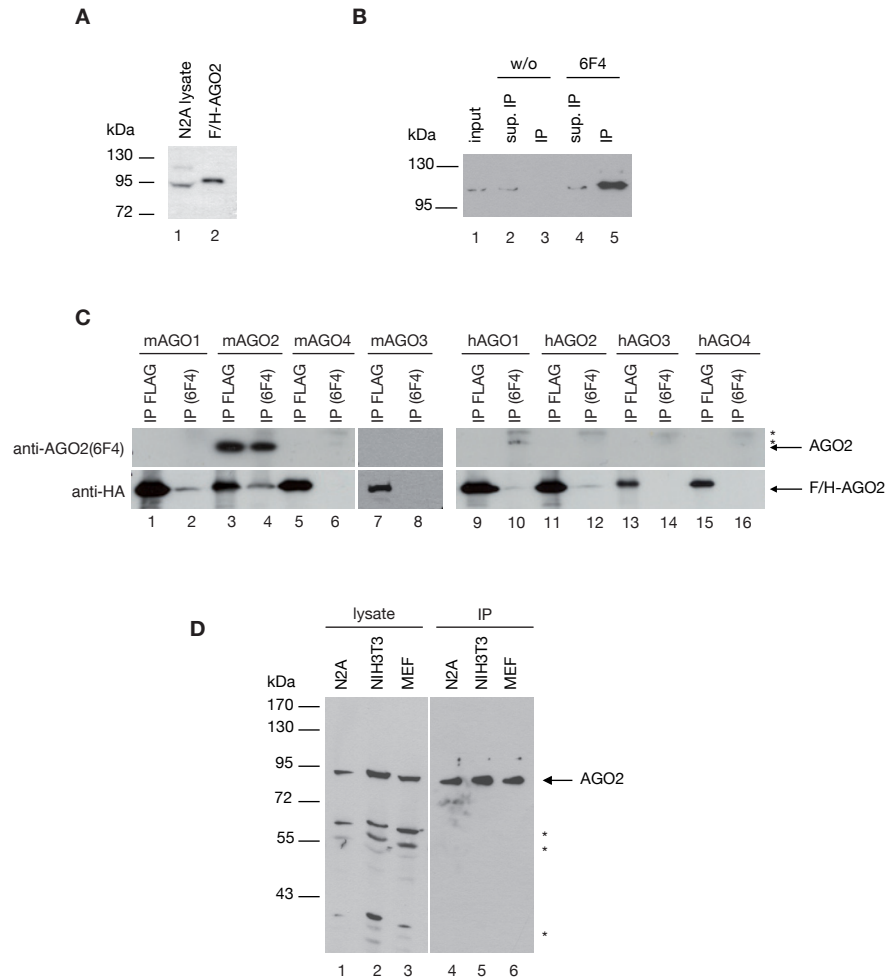
Figure 2.3.2: Specificity of the anti-AGO2(6F4) in Western blot and immunoprecip-itation. A) To test the Western blot specificity, 30 µg whole cell lysate from N2A cells (lane 1) and purified F/H-AGO2 (lane 2) were probed with the anti-AGO(6F4) diluted 1:5000. B) Im-munoprecipitations were performed from N2A whole cell lysate with the anti-AGO2(6F4) (lanes 4-5) or beads without antibody (w/o, lanes 2-3). 0,2% input (lane 1), 0,2% supernatants after IP (lanes 2 and 4) and the 4% of the IPs (lanes 3 and 5) were analyzed by Western blot with anti-AGO2(6F4). C) F/H-tagged mouse AGO 1-4 (mAGO1-4, lanes 1-8) and human AGO 1-4 (hAGO-1-4, lanes 9-16) were overexpressed in HEK293T and immunoprecipitated with FLAG antibody (odd-numbered lanes) or the anti-AGO2(6F4) antibody (even numbered lanes). Pro-teins were detected with anti-AGO2(6F4) (upper panel) or anti-HA (lower panel). D) For the detection of endogenous AGO2 in different cell lines, whole cell lysates (30 µg, lanes 1-3) and IPs with anti-AGO2(6F4) (lanes 4-6) from N2A, NIH 3T3 and a MEF cell line were analyzed with the anti-AGO2(6F4) by Western blotting.

In order to assess the specificity of the antibody for mouse AGO2, we overexpressed F/H-tagged mouse and human AGO1-4 in HEK293T cells and immunoprecipitated proteins either with anti-AGO2(6F4) or FLAG antibody (Figure 2.3.2C). Proteins were detected with the anti-AGO2(6F4) or an antibody against the HA-tag. We observed strong signals for all AGO proteins in the FLAG-IPs with the HA-antibody but the anti-AGO2(6F4) detected only mouse AGO2.

This verifies that the antibody specifically recognizes mouse AGO2 in Western blot analysis. The anti-AGO2(6F4) efficiently immunoprecipitated F/H-tagged AGO2 but shows a cross reactivity with mouse AGO1 and a weak cross reactivity with human AGO1 and AGO2 (Figure 2.3.2C, lower panel). Mass spectrometry analysis of murine proteins immunoprecipitated with anti-AGO2(6F4) confirmed this cross reactivity with mouse AGO1 and revealed additional cross reactivities, including an affinity for AGO3 (see Figure 2.3.6 and Section 2.4).

We next tested the ability of the antibody to detect endogenous AGO2 in whole cell lysates from different mouse cell lines (Figure 2.3.2D) and observed strong signals at the expected size in all cell lines. Several signals with lower molecular weights (65, 55 and 30 kDa) were also visible. Since these signals disappeared in the immunoprecipitations they were classified as background signals and not analyzed further. The anti-AGO2(6F4) also specifically immunoprecipitated and detected rat AGO2 (Andrea Rinck, personal communication).

Bound AGO2 protein can be eluted from the antibody matrix by addition of a peptide encompassing the antibody epitope (Figure 2.3.3A). AGO2 was immunoprecipitated with anti-AGO2(6F4) and incubated with the peptide used for immunization. A significant amount of AGO2 was eluted from the antibody matrix but the bigger part remained bound to the antibody. To increase elution efficiency, the concentration of the competing peptide was varied but the efficiency of the elution was not influenced by the peptide concentration (Figure 2.3.3B). However, it was significantly improved by performing multiple elution steps (Figure 2.3.3C). The highest elution efficiency was reached with eluting three times for 30 minutes. No protein was eluted when the competing peptide was omitted from the reaction, a clear indication that AGO2 binding by the antibody is strong and stable over time. The elution efficiency could be further increased by raising the pH to 8.0 (Figure 2.3.3D). By using the commercially available antibody anti-AGO2(C34C6) for the detection of AGO2 in the eluates (Figure 2.3.3C and D), we validated the identity of the precipitated protein as AGO2 again. In summary, the experiments showed that bound AGO2 protein can be efficiently eluted from the anti-AGO2(6F4) with a competing peptide.
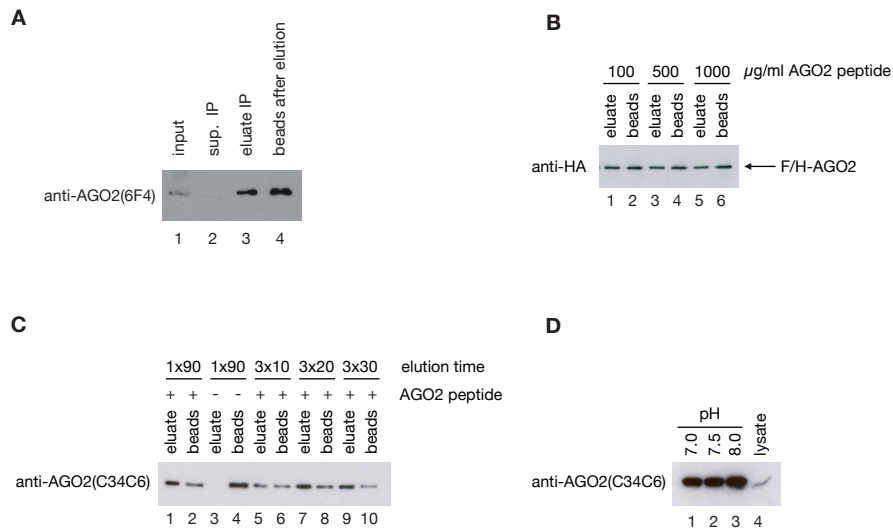
Figure 2.3.3: Isolation of native RISC by peptide elution. A) AGO2 was immunoprecipitated with anti-AGO2(6F4) from Hepa 1-6 whole cell lysate and eluted with 1 mg/ml competing peptide. Equal amounts of input (lane 1), supernatant after the IP (lane 2), eluate (lane 3) and beads after elution were analyzed for AGO2 by Western blot with anti-AGO2(6F4). B) F/H-tagged mouse AGO2 was overexpressed in HEK293T cells and immunoprecipitated with anti-AGO2(6F4). Bound protein was eluted with 100 (lanes 1-2), 500 (lanes 3-4) or 1000 (lane 5-6) µg/ml peptide for 90 min. Eluates and beads after elution were analyzed by Western blot with an antibody against the HA-tag. C) AGO2-containing complexes were immunoprecipitated with anti-AGO2(6F4) from wild type MEF whole cell lysate and eluted without (lanes 3-4) or with 500 µg/ml peptide once for 90 min (lanes 1-2) or three times for 10 (lanes 5-6), 20 (lane 7-8) or 30 (lanes 9-10) min. AGO2 amounts in eluates and beads after elution were detected by Western blotting with the commercially available anti-AGO2(C34C6) antibody. D) AGO2 containing protein complexes were immunoprecipitated with anti-AGO2(6F4) from wild type MEF whole cell lysate and eluted with 500 µg/ml peptide for 90 min at pH 7.0 (lane 1), 7.5 (lane 2) or 8.0 (lane 3). Input sample was loaded in lane 4. Samples were analyzed by Western blotting with anti-AGO2(C34C6).

Small RNAs bound to AGO proteins are essential for RISC function and of high interest for functional studies. Therefore, we analyzed if the anti-AGO2(6F4) coimmunoprecipitates miRNAs. RNAs were extracted from lysates and AGO2 immunoprecipitations and were analyzed by Northern blotting using probes against miR-19b and miR-21 (Figure 2.3.4). We analyzed different cell lines including Dicer wild type MEFs (Dicer wt) and Hepa 1-6 cells. As controls we used Dicer-depleted MEFs (Dicer ko) [101] and an AGO2-depleted MEF cell line (AGO2 ko) [55]. The Dicer-depleted MEFs should not contain mature miRNAs and therefore serve as negative control. The AGO2-depleted MEFs contained mature miRNAs but because of the loss of AGO2 these should not be

immunoprecipitated by the anti-AGO2(6F4). As expected, miRNAs were detected in the lysates from all cell lines except the Dicer-depleted MEFs. An interesting observation is that the abundance of miRNAs is significantly reduced in the AGO2-depleted MEFs. In the IPs, both miRNAs were strongly enriched in the wild type MEFs and Hepa 1-6 cells but not in the AGO2-depleted cells.
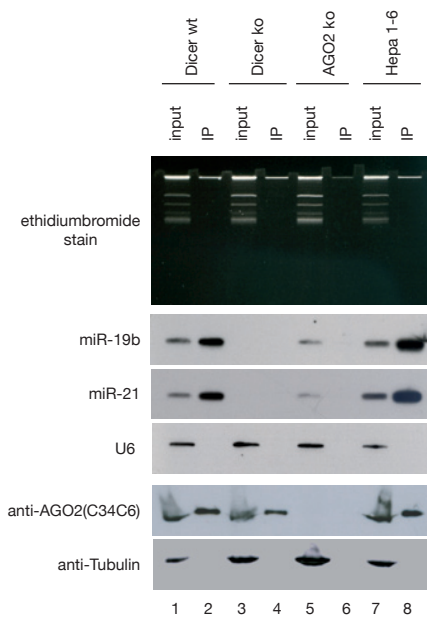
Figure 2.3.4: Coimmunoprecipitation of miRNAs in AGO2-containing RNP complexes isolated with the anti-AGO2(6F4) antibody. RNAs were extracted from whole cell lysate (odd numbered lanes) or AGO2 immunoprecipitations (even numbered lanes) with anti-AGO2(6F4) from Dicer wild type MEFs (Dicer wt, lanes 1-2), Dicer-depleted MEFs (Dicer ko, lanes 3-4), AGO2-depleted MEFs (AGO2 ko, lanes 5-6) or Hepa 1-6 (lanes 7-8). After size separation by denaturing electrophoresis (upper panel) the RNAs were transferred to membrane and probed for miR-19b (2nd panel) and miR-21 (3rd panel). U6 was used as a loading control (4th panel). AGO2 protein abundance in the samples was monitored by Western blotting with anti-AGO2(C34C6) (5th panel). Tubulin was used as loading control for input protein (lower panel).

The amount of AGO2 protein was assessed by Western blotting using anti-AGO2(C34C6). As expected, no AGO2 was detected in lysate and IP from the AGO2-depleted cells. AGO2 was present in the lysates and in the IPs from the other three cell lines. It is noticeable that the AGO2 abundance in the Dicer-depleted MEFs was slightly decreased compared to the level in the wild type cells. Overall, the experiment demonstrated that the anti-AGO2(6F4) antibody specifically coimmunoprecipitatesd AGO2 bound miRNAs.

In mammals, AGO2 is the only AGO protein that has slicer activity and target cleavage is a sign for active and functional RISC. We performed *in vitro* cleavage assays to analyze if the anti-AGO2(6F4) precipitates functional RISC from mouse cell lysates. AGO2-containing protein complexes were immunoprecipitated from wild type Dicer, Dicer-depleted or AGO2-depleted MEFs and from Hepa 1-6 cells (Figure 2.3.5A). The eluates were incubated with a radiolabeled substrate RNA containing the fully complementary target site for the endogenous miRNA 19b (Figure 2.3.5B, left panel). A specific cleavage
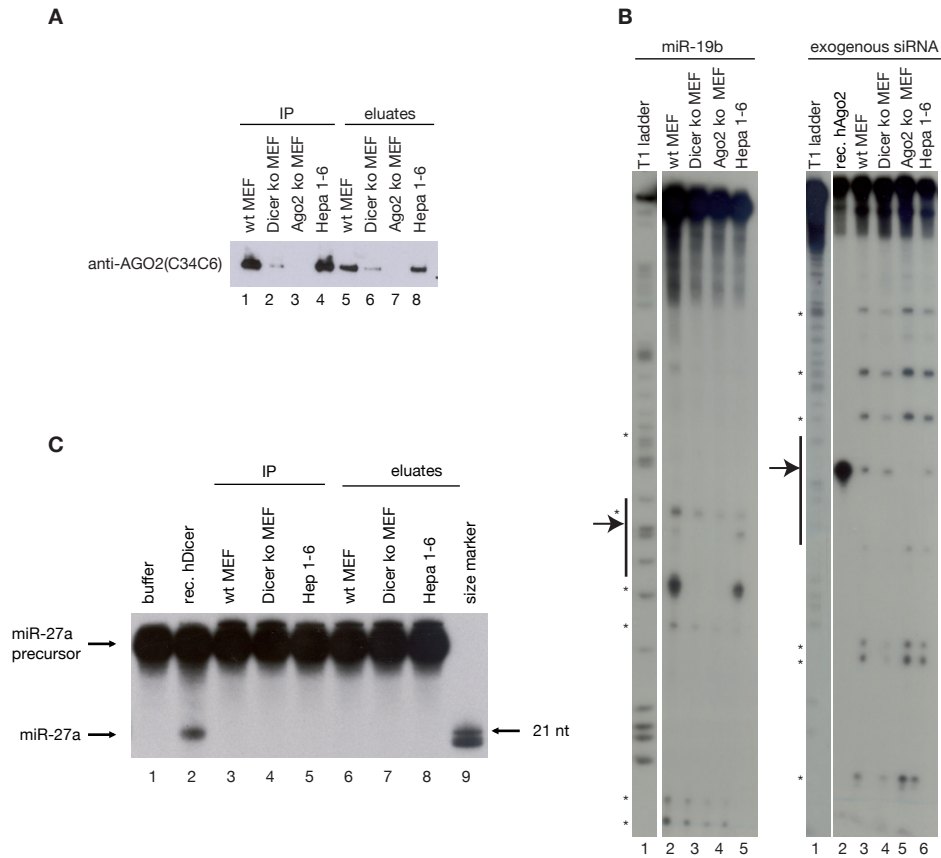
Figure 2.3.5: RISC and Dicer activity of endogenous AGO2-containing RNP complexes. A) Protein complexes were immunoprecipitated from Dicer wild type MEFs (lane 1 and 5), Dicer-depleted MEFs (lanes 2 and 6), AGO2-depleted MEFs (lanes 3 and 7) and Hepa 1-6 (lanes 4 and 8) whole cell lysates with the anti-AGO2(6F4) antibody (lanes 1-4). Bound protein was eluted with competing peptide (lanes 5-8). The presence of AGO2 in the samples was verified by Western blotting with the anti-AGO(C34C6) antibody. B) For RISC activity assays, the eluates were incubated with a ^{32}P cap-labeled substrate RNA containing a target site for the endogenous miRNA-19b (left panel) or were preincubated with an exogenous single stranded siRNA prior to cleavage reaction with a ^{32}P cap-labeled substrate RNA containing a target site for the exogenous siRNA (right panel). Cleavage products were separated by denaturing PAGE and visualized by autoradiography. In the experiment with the exogenous single stranded siRNA, purified recombinant human AGO2 was used as a positive control (lane 2). C) To test for Dicer activitiy, the IPs and eluates were incubated with an internally ^{32}P-labeled miR-27a precursor RNA. Cleavage products were analyzed by denaturing PAGE and autoradiography. ^{32}P-end labeled RNAs with lengths of 16, 18 and 21 nt served as a size standard (lane 9) and recombinant human Dicer protein was used as a positive control (lane 2).

product was observed for the wild type MEFs and the Hepa 1-6. As to be expected, we saw no RISC activity in the Dicer-depleted and the AGO2-depleted MEFs. The RISC activity can be reconstituted *in vitro* in the Dicer-depleted MEFs by loading AGO2 with an exogenous single stranded siRNA (Figure 2.3.5B, right panel). After incubation with the radiolabeled exogenous target RNA, specific degradation products were visible for all samples except the AGO2-depleted MEFs. These results clearly show that the anti-AGO2(6F4) precipitated active endogenous RISC and that the complex was not only cleavage competent but was also able to load single stranded siRNAs into the AGO2 protein.

Earlier studies showed that Dicer associates stably with AGO2 [102, 221]. To test whether Dicer is a component of the endogenous AGO2 complex that is precipitated with the anti-AGO2(6F4), we analyzed Dicer activity in IPs and eluates from different cell lines (Figure 2.3.5A and C). Immunoprecipitates and eluates were incubated with an internally radiolabeled miR-27a precursor. Cleavage products were analyzed by denaturing PAGE and autoradiography (Figure 2.3.5C). Recombinant Dicer was used as a positive control and gave a clear signal for the mature miRNA with the expected size of 21 nt. We observed no Dicer activity in the IPs or the eluates. This result was quite striking because the AGO-Dicer association is a well-studied and established interaction [208, 289, 311]. From the presence of mature miRNAs in whole cell lysates (Figure 2.3.4) we can assume that Dicer is present and active in the input samples. The lack of Dicer activity indicated that Dicer is not stably associated with endogenous AGO2 in the protein complex immunoprecipitated with anti-AGO2(6F4). The absence of Dicer in the immunoprecipitated AGO2 complex was verified by mass spectrometry analysis at a later point in time (see Section 2.4.1).

We aimed to get an overview about the proteins stably associated with AGO2 in our immunoprecipitations. For this purpose, we analyzed the band pattern of bound proteins from stringently washed IPs by SDS-PAGE and silver staining (Figure 2.3.6A). A band with the expected size for AGO2 was clearly visible and we also observe a strong band with a molecular weight of about 120 kDa. Both bands were analyzed by mass spectrometry. The 100 kDa band was identified as AGO2 and contained small contaminations of AGO1 and 3. The 120 kDa band was identified as the coat protein complex II (COPII) component protein SEC24C. The COPII machinery mediates the first step of the exocytic pathway at the endoplasmatic reticulum and SEC24 is an adapter protein involved in cargo recognition and selection. In mammalian cells, SEC24 has four isoforms (SEC24 A-D) [112]. Since components of the miRNA effector complex are enriched on multivesicular bodies in the endocytic pathway [97], we investigated if SEC24C specifically interacts with AGO2 and thereby connects it to the exocytic pathway. Because of the

Figure 2.3.6: Cross reactivity of the anti-AGO2(6F4) antibody with the COPII component SEC24C. A) An anti-AGO2(6F4) IP from N2A whole cell lysate was washed stringently and analyzed by SDS-PAGE and silver staining. Proteins of interest were cut out and identified by mass spectrometry. Antibody chains are indicated by asterisks. B) Protein complexes were isolated from HEK293T cells with either the anti-AGO2(11A9) (lane 1) or a polyclonal antibody against SEC24 (lane 2) and analyzed for the presence of AGO2 (upper panel) and SEC24 (lower panel) by Western blotting.
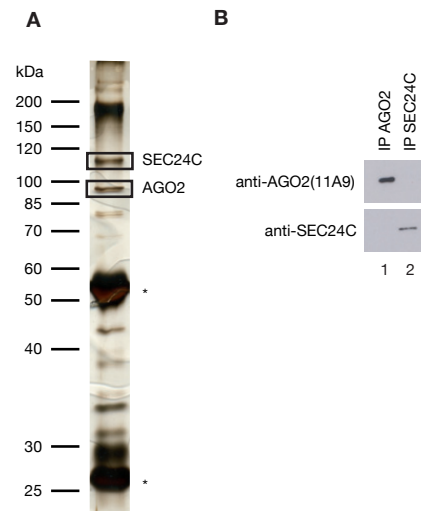
lack of suitable antibodies against mouse SEC24C, the specificity of the interaction was tested in human cells (Figure 2.3.6B). We performed IPs from HEK 293 whole cell lysate with either the anti-human AGO2(11A9) or an antibody specific for SEC24C and tested the precipitates for the presence of the proteins by Western blotting. Both proteins were only present in the IPs with their specific antibody and showed no interaction. Therefore, the presence of SEC24C in the anti-AGO2(6F4) IPs was not a specific protein-protein interaction but was most likely based on a cross reactivity of the antibody.

The cellular localization of proteins is of high interest for functional studies. With an antibody specific against an endogenous protein the problems caused by tagging and overexpressing, for example aggregation, can be avoided. We tested the anti-AGO2(6F4) for its suitability for localization studies in immunofluorescence experiments using confocal microscopy (Figure 2.3.7). N2A cells or AGO2-depleted MEFs were fixed and stained with anti-AGO2(6F4). Since the AGO2-depleted cell line contains no AGO2, we expected no signal in these samples. Instead, we observed a diffuse cytoplasmic staining in both cell lines. In order to rule out that this diffuse staining is background caused by the secondary antibody, we omitted the anti-AGO2(6F4) antibody from the experiment. In this setup, the background staining was clearly reduced. In summary, these results imply that the anti-AGO2(6F4) is not specific for AGO2 but cross-reacted with other proteins in immunofluorescence experiments. The antibody is therefore not suitable for localization studies.
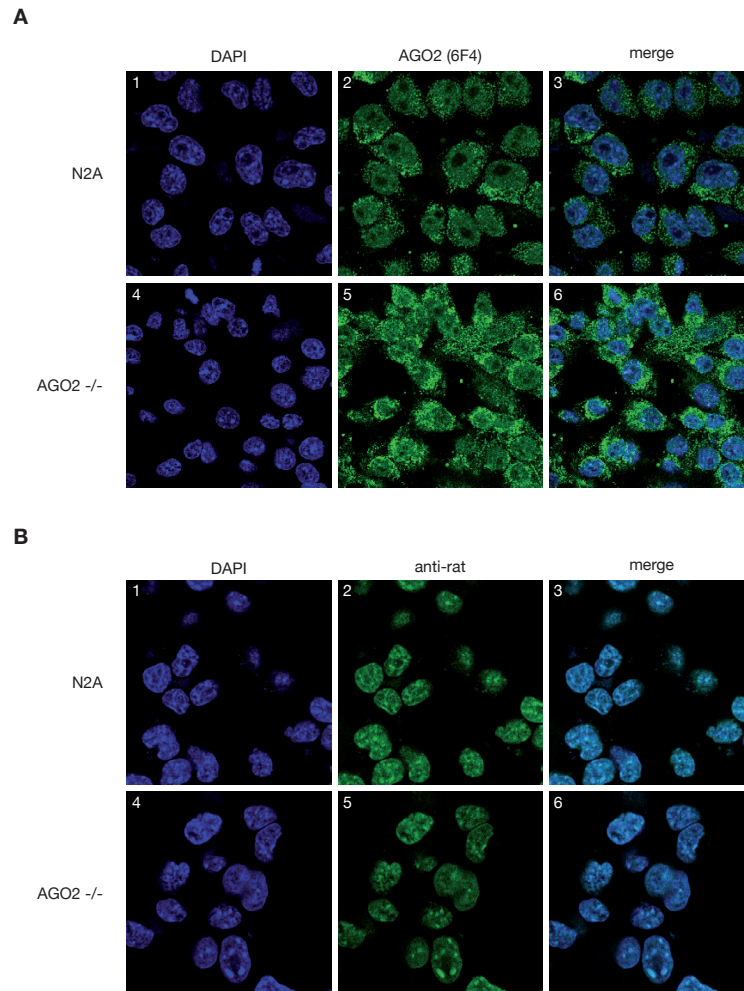
Figure 2.3.7: Immunofluorescence experiments with the anti-AGO2(6F4) antibody.
A) N2A cells (panels 1-3) and AGO2-depleted MEFs (panels 4-6) were fixed and stained with
DAPI (panels 1 and 4) or anti-AGO2(6F4) (panels 2 and 5). Merged images are shown in panels
3 and 6. B) In a control experiment, both cell lines were stained with the secondary antibody
only.

We characterized the monoclonal antibody anti-AGO2(6F4). The antibody specifically
detected mouse AGO2 in Western blot analysis. It immunoprecipitated AGO2 and the
bound protein could be eluted from the antibody with a competing peptide encom-
passing the antibody epitope tag. MiRNAs were coimmunoprecipitated with AGO2
and the immunoprecipitated RISCs show cleavage activity and are able to load single
stranded siRNAs. The antibody is therefore suitable for miRNA profiling and RISC
activity studies. It is an interesting observation that Dicer is not present in the AGO2-

containing complexes bound by the anti-AGO2(6F4) antibody. The antibody showed a weak binding affinity for AGO1 and 3 and strongly cross-reacted with the COPII vesicle component SEC24C. Due to this strong cross reactivity the antibody was not suitable for localization studies by immunofluorescence under the tested conditions.

2.4 Identification of MicroRNA-Dependent AGO2 Interactors from Endogenous Ribonucleoprotein Complexes

2.4.1 A Modified QUICK Approach for the Identification of Specific AGO2 Interactors

Several studies [127, 171, 221] contributed to the present picture of the AGO2 interactome. In these studies, tagged human AGO2 was overexpressed and RNPs were purified via the affinity tag by several purification steps prior to semiquantitative proteomic analysis. The anti-AGO2(6F4) antibody now provides a tool that allowed us to study endogenous AGO2 complexes in mouse by AP-MS. For the high confidence identification of interaction partners of endogenous proteins, quantitative immunoprecipitations can be combined with knockdown in a so called QUICK approach ([296], see page 28). Since we accounted frequent problems with the transfection and knockdown efficiency in the MEF cell line (data not shown), we modified the QUICK approach. Instead of a knockdown of AGO2 by RNAi, we used an AGO2-depleted MEF cell line [55] and applied the method to identify specific interaction partners of endogenous AGO2 as depicted in Figure 2.4.1.

Wild type and AGO2-depleted MEFs were SILAC labeled with light or heavy arginine and lysine. The incorporation rate was above 95% and no arginine to proline conversion was observed (data not shown). AGO2-containing protein complexes were immunoprecipitated with the anti-AGO2(6F4) antibody for each SILAC state separately to prevent heavy to light exchange of specific interaction partners during the purification procedure [231, 342]. After washing, the samples were combined for the elution with a competing peptide. The quality of the immunoprecipitations was analyzed by Western blot as shown for the reverse experiment in Figure 2.4.2A. AGO2 was present in the wild type cell line and enriched in the eluate but it was not detected in the AGO2-depleted cell line. We worked with an excess of lysate and the significant amount of AGO2 remaining in the supernatant after the IP (Figure 2.4.2A, lane 3) indicates that the amount of AGO2 in the sample exceeded the AGO2 binding capacity of the antibody. The eluates
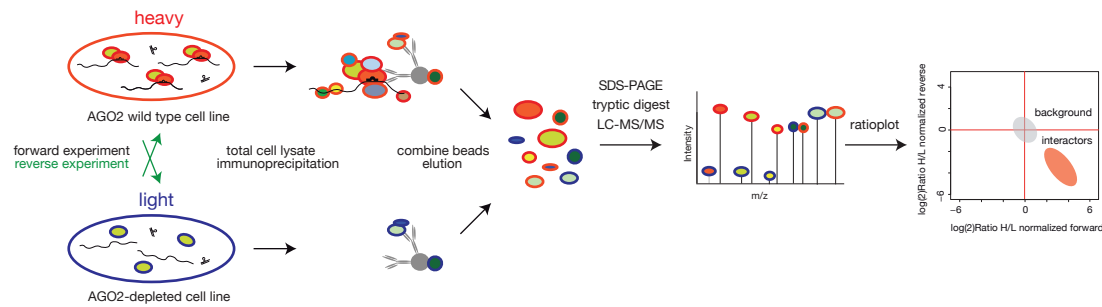
Figure 2.4.1: Experimental setup of a modified QUICK approach to identify specific AGO2 interactors. AGO2-containing complexes were immunoprecipitated from heavy labeled wild type (wt) AGO2 and light labeled AGO2-depleted (ko) MEFs with the anti-AGO2(6F4) antibody. Samples were washed and combined for elution with a competing peptide. Proteins were separated by one-dimensional gel electrophoresis and in-gel digested with trypsin. Peptides were analyzed by LC-MS/MS. For the reverse experiment the SILAC label was swapped between the cell lines. Specific AGO2 interactors are expected to show high H/L ratios in the forward and low ratios in the reverse experiment. Background binders show ratios around one in both experiments. For data visualization the logarithmized, normalized ratios of the forward and reverse experiments are plotted. Background binders are clustered around zero, as highlighted by the grey sphere. Specific interactors can be found in the lower right quadrant as indicated by the red sphere.

were separated by one-dimensional SDS-PAGE, stained with Coomassie (Figure 2.4.2B) and in-gel digested with trypsin. Peptides were analyzed by LC-MS/MS on an LTQ Orbitrap Velos.

We applied several filter criteria to the dataset to ensure a high quality of identification and quantification of the reported proteins. The raw data contained 1385 protein identifications and was reduced to 1279 identified proteins after removing contaminants and reverse identifications. We required two unique peptides and two quantification events per protein for a valid identification. This reduced the number of identified proteins to 500. Figure 2.4.3 shows full scans and fragmentation spectra typical for the bait protein or a background binder. In the full scans, the two SILAC pairs were clearly visible as indicated by the arrows. For the AGO2 peptide (Figure 2.4.3A) the heavy peptide was detected with a higher intensity in the forward experiment and in the reverse experiment the light peptide had a higher intensity. These ratios are characteristic for the bait protein and specific interactors. Background binders show ratios close to one between the SILAC pairs. In Figure 2.4.3B, a peptide from the protein DNAJ is shown. There were no differences in the intensities between the SILAC states and the protein was classified as a background binder.

A

anti-AGO2(C34C6)

1 2 3 4 5

B

kDa

191 —
97 —
64 —
51 —
39 —
28 —
19 —
14 —

Figure 2.4.2: Representative immuno-precipitation of the modified QUICK approach. A) 1,25% input samples (lanes 1 and 2) or supernatant (lanes 3 and 4) from the immunoprecipitations from light labeled wild type (wt, lanes 1 and 3) and heavy labeled AGO2-depleted cells (ko, lanes 2 and 4) and 9% of the eluate (lane 5) were loaded. AGO2 was detected by Western blotting. B) The eluate was separated by SDS-PAGE and stained with Coomassie prior to in-gel digestion.
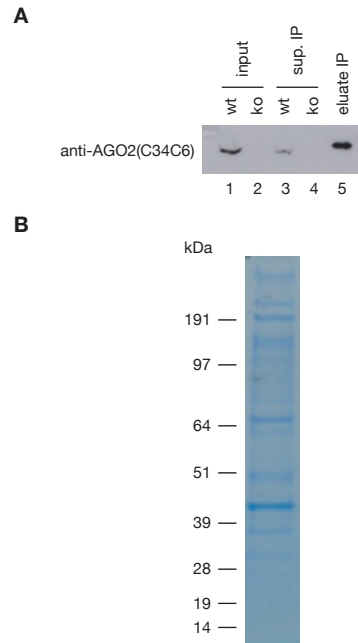
AGO2 was detected with more than 30 unique peptides and more than 100 quantification events both in the forward and the reverse experiment. The sequence coverage was 74%. Ratios of 14.6 and 0.06 in the forward and reverse experiments, respectively, showed that AGO2 is specifically enriched in this experimental setup (Table 2.4.1). As described previously (see Figure 2.3.6), the anti-AGO2 (6F4) strongly cross-reacts with the COPII vesicle component SEC24C. This protein was detected with more than 40 unique peptides, more than 80 counts and a sequence coverage of 56%. It could be clearly identified as a background binder by its ratios of 1.3 in the forward and 0.8 in the reverse experiment (Table 2.4.1). This demonstrated that the modified QUICK approach successfully shifted antibody specific cross reactants into the background.

We visualized the data by ratio plots (Figure 2.4.4). As described in Figure 2.4.1, the background binders are clustered around zero whereas specific interactors can be found in the lower right quadrant. The data set did not display the ratio distribution expected for a typical SILAC data set. Instead, we observed a wide scattering of the background binders and a significant number of contaminants in the lower left quadrant. A high number of proteins were located in the upper left quadrant. These are proteins that were enriched in the IP in the absence of AGO2. This group includes the insulin receptor substrate 1 (IRS1) but mainly comprises proteins involved in cell adhesion such as laminins (LAMB2, LAMA5), glycoproteins (THBS1) and collagens (COL18A1). A set
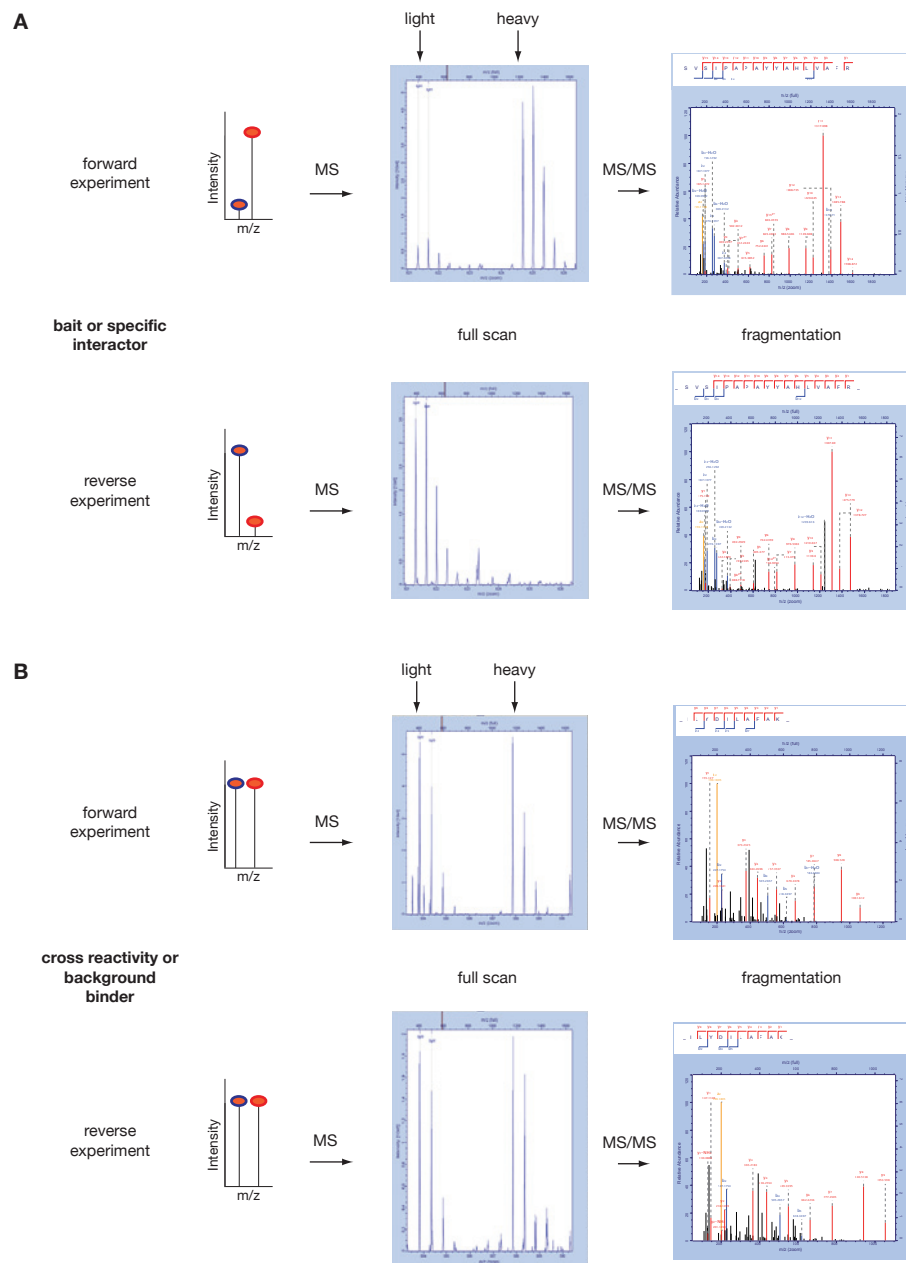
Figure 2.4.3: Full scans and fragmentation spectra for representative peptides. Full scans and fragmentation spectra of a selected peptide are shown for the forward (upper row) and the reverse experiment (lower row) for A) a peptide from the bait protein AGO2 and B) a peptide from the background binder DNAJ.
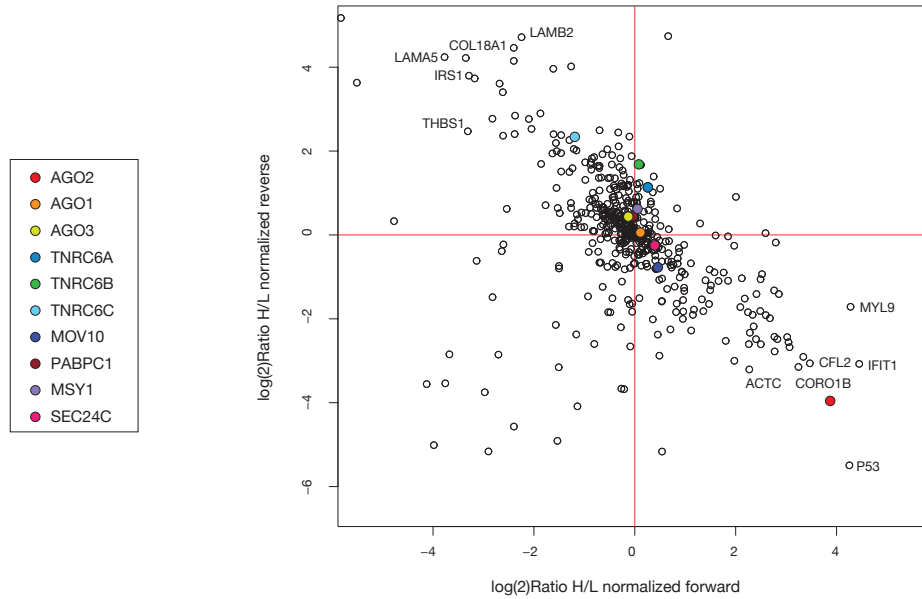
Figure 2.4.4: Modified QUICK approach for the identification of AGO2 interactors.
Logarithmized normalized ratios of forward and reverse experiments are plotted as described in
Figure 2.4.1. Every dot represents an identified and quantified protein. Top outliers are labeled
and a selection of proteins reported to interact with AGO2 are indicated in color.

of proteins, among them AGO2 and the tumor suppressor p53, appeared as clear outliers
and were thereby defined as specific interactors. The top 30 outliers and a selection of
proteins reported to interact with AGO2 as well as the cross reactant SEC24C and
detected AGO proteins are summarized in Table 2.4.1. Dicer and its cofactor TARBP2
were not identified in the dataset. When analyzing the functions of the outliers (see
keywords in Table 2.4.1), the vast majority of these proteins were classified as cytoskeletal
proteins such as myosins (MYH9 and 10, MYO1b, 1c and 6), actin and actin binding
proteins (Cofilin 1 and 2, LIMA1 and Coronin 1B). We highlighted reported AGO2
interacting proteins including TNRC6 A-C, MOV10 and YB1 in the ratio plot and
these proteins were identified as background binders based on their ratios. Among the
background binders we also found the mRNA-binding proteins IGF2BP 1-3, HSP90 and
AGO1 and 3 (Table 2.4.1). It might be possible that the presence of these two AGO
proteins in the IP accounts for the background ratios of some of the reported AGO2
interactors. The majority of the established interactors we selected for analysis associate
with all AGO proteins [171] and therefore it is possible that we detected peptides from
these proteins in association with AGO1, 2 or 3 in our samples. A peptide from a protein
in complex with AGO2 had a high ratio, but since the same peptide from proteins in

Protein Name	Gene Name	Uniprot ID	Keywords	Unique Peptides		Ratio H/L	
				forward	reverse	forward	reverse
Bait							
Protein argonaute-2	Eif2c2	Q8CJG0	RNA-mediated gene silencing	35	31	14,677	0,064
Cross reactivity							
Sec24c protein	Sec24c	Q8R2V9	COPII vesicle coat component	46	41	1,301	0,828
Other AGO proteins							
Protein argonaute-1	Eif2c1	Q8CJG1	RNA-mediated gene silencing transcriptional gene silencing	19	7	1,087	1,046
Protein argonaute-3	Eif2c3	Q8CJF9	RNA-mediated gene silencing	23	16	0,930	1,352
Outliers							
Interferon-induced protein with tetratricopeptide repeats 1	Ifit1	Q64282	unknown function	6	2	21,835	0,119
Myosin regulatory light polypeptide 9	Myl9	Q9CQ19	cytoscleletal protein	4	3	19,376	0,305
Cellular tumor antigen p53	Tp53	P02340	tumor suppressor	2	3	19,086	0,022
Cofilin-2	Cfl2	P45591	actin binding cytoplasmic actin rods	5	10	11,080	0,120
LIM domain and actin-binding protein 1	Lima1	Q9ERG0	actin binding LIM domain	8	7	10,132	0,133
Coronin-1B	Coro1b	Q9WUM3	actin binding interacts with Arp2/3 complex	11	13	9,474	0,113
Cofilin-1	Cfl1	P18760	actin binding cytoplasmic actin rods	6	9	8,378	0,156
Contactin associated protein 1	Cntnap1	O54991	contactin interactor membrane protein	15	10	8,265	0,170
Coronin-1C	Coro1c	Q9WUM4	actin binding	21	29	8,112	0,185
MCG5400	2900073 G15Rik	Q6ZWQ9	unknown function calcium binding	2	2	7,239	0,377
WD repeat-containing protein 1	Wdr1	O88342	actin binding	11	22	7,097	0,179
Myosin-14	Myh14	Q6URW6	myosin	2	4	6,941	0,882
Cysteine and glycine-rich protein 2	Csrp2	P97314	LIM domain protein interacts with ATAC complex (histone acteylation)	3	2	6,832	0,146
Actin-related protein 2/3 complex subunit 4	Arpc4	P59999	actin binding Arp2/3 complex	5	6	6,818	0,186
Twinfilin-1	Twf1	Q91YR1	actin binding	7	7	6,783	0,400
Tropomyosin beta chain	Tpm2	P58774	actin binding	2	3	6,408	0,252
Calmodulin	Calm1	P62204	calcium binding protein stimulates kinases and phosphatases	3	5	6,051	0,266
Myosin-9	Myh9	Q8VDD5	myosin	88	111	6,030	1,029
Myosin-10	Myh10	Q61879	myosin	39	60	5,745	0,523
Ltbp2 protein	Ltbp2	Q0VD84	unknown function calcium binding	3	4	5,656	0,164
Actin-related protein 2	Actr2	P61161	ATP binding Arp2/3 complex (actin polymerization)	5	8	5,626	0,480
Tropomyosin alpha-4 chain	Tpm4	Q6IRU2	actin binding	14	18	5,612	0,284
Myosin-Ic	Myo1c	Q9WTI7	myosin isoform 3 required for transcription initiation	30	37	5,317	0,377
Myosin light chain 1	Myl3	P09542	myosin light chain	2	2	5,292	0,179
Histone H1.0	H1f0	P10922	histone	3	3	5,121	0,221
Filamin-B	Flnb	Q80X90	connects membrane to actin cytoskeleton	88	103	5,045	0,267
Actin-related protein 3	Actr3	Q99JY9	ATP binding Arp2/3 complex	9	12	4,862	0,199
Actin, alpha cardiac muscle 1	Actc1	P68033	actin	9	9	4,822	0,108
Dynactin subunit 4	Dctn4	Q8CBY8	Dynactin	2	7	4,791	0,164
selected reported AGO2 interactors							
Trinucleotide repeat-containing gene 6A protein	Tnrc6a	Q3UHK8	RNA-mediated gene silencing	14	8	1,197	2,193
Trinucleotide repeat-containing gene 6B protein	Tnrc6b	Q8BKI2	RNA mediated gene silencing	62	51	1,058	3,213
Trinucleotide repeat-containing gene 6C protein	Tnrc6c	Q3UHC0	RNA-mediated gene silencing	7	3	0,438	5,058
Polyadenylate-binding protein 1	Pabpc1	P29341	poly(A) tail of mRNA binding	17	12	0,956	1,374
Poly(A) binding protein, cytoplasmic 4	Pabpc4	Q99LF8	RNA binding	16	8	0,559	0,873
Putative helicase MOV-10	Mov10	P23249	RNA-mediated gene silencing	40	29	1,376	0,582
Nuclease-sensitive element-binding protein 1	Ybx1	P62960	transcription pre-mRNA splicing mRNA processing	11	6	1,039	1,539
Insulin-like growth factor 2 mRNA-binding protein 1	Igf2bp1	O88477	mRNA 5'UTR binding	14	3	0,551	2,943
Insulin-like growth factor 2 mRNA-binding protein 2	Igf2bp2	Q5SF07	mRNA translation mRNA 5'UTR binding	15	4	0,536	1,797
Insulin-like growth factor 2 mRNA-binding protein 3	Igf2bp3	Q9CPN8	RNA binding mRNA translation and stabilty	13	4	0,801	1,932
Heat shock protein HSP 90-alpha	Hsp90aa1	P07901	molecular chaperone ATPase activity	18	14	0,347	1,561

Table 2.4.1: List of selected proteins identified in the modified QUICK approach.
A subset of values is listed for the outliers, known cross reactants, AGO family proteins and a selection of proteins reported to interact with AGO2. Keywords describing reported functions were added. The data is visualized in Figure 2.4.4.
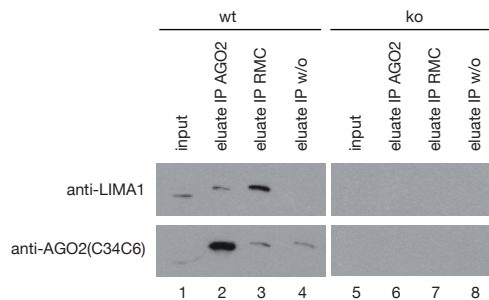
Figure 2.4.5: Comparison of LIMA1 abundance in wild type and AGO2-depleted MEF cell lines by Western blot analysis. Whole cell lysates were prepared from wild type (wt) and AGO2-depleted (ko) MEFs (lanes 1 and 5). AGO2 was immunoprecipitated with the anti-AGO2(6F4) antibody (lanes 2 and 6). As controls the RMC antibody (lanes 3 and 7) and beads without antibody (w/o) was used (lanes 4 and 8). Proteins were detected antibodies against AGO2 (upper panel) or LIMA1 (lower panel).

the AGO1 or 3 complexes was equally present in both SILAC states, the overall ratio computed for the peptide was decreased to a background value and the protein appeared as a background binder. As an alternative, the background binding behavior of the reported interactors might also be caused by non-specific binding to the sepharose that was used as matrix in the IP.

Wide scattering of the data points in ratio plots is an indication for differential background binding caused by significant differences in the whole proteome of the samples used in the experiment. Both of the cell lines we used are mouse embryonic fibroblasts but we observed a strong deviation of the cell shape of the AGO2-depleted cells from other MEF cell lines (data not shown). The shape of the cell is based on the cytoskeleton, so cells with different appearance are likely to differ in the composition of their cytoskeletal proteins. If this applies to this set of cell lines, it could account for the high number of cytoskeletal proteins among the outliers. To test this hypothesis, we analyzed the amount of the actin-binding protein LIMA1, one of the top outliers, in the two cell lines by Western blotting (Figure 2.4.5). The experiment showed that the LIMA1 expression level was higher in the wild type cell line than in the AGO-depleted cells. LIMA1 did not specifically interact with AGO2 but bound non-specifically to the antibody. Due to the different expression levels in the two cell lines it was only enriched on the antibody in the wild type cell line and thus appeared as a false positive AGO2 interactor in the QUICK approach.

We were not able to identify specific AGO2 interactors with the modified QUICK approach despite the fact that cross reactants such as SEC24C were successfully shifted

the to the background. Instead, this experimental setup demonstrated two aspects that we needed to address with further experiments. One aspect was the cross reactivity of the anti-AGO2(6F4) antibody with AGO1 and AGO3. The second aspect was the influence of the whole proteome of the input samples on background binding in the immunoprecipitation.

2.4.2 Comparison of Antibody Performance Between the anti-AGO2(6F4) and the Commercially Available Argonaute2 (C34C6) Antibody

The anti-AGO2(6F4) antibody displayed a strong non-specific association with cytoskeletal proteins in the modified QUICK approach. To test if these reactivities are specific for the anti-AGO2(6F4) antibody, we compared it to the commercially available monoclonal Argonaute 2 (C34C6) antibody (anti-AGO2(C34C6)).

We immunoprecipitated AGO2-containing complexes from heavy labeled wild type MEFs and light labeled AGO2-depleted MEFs with the anti-AGO2(C34C6). After the washing steps the beads were combined and bound protein was non-specifically eluted from the beads by the addition of denaturing sample buffer. Samples were processed further as described before (Figure 2.4.1). The quality of the IP was checked in a Western blot and Coomassie stain (Figure 2.4.6). As for the IPs with the anti-AGO2(6F4) (Figure 2.4.2A) we worked with an excess of input sample and the amount of AGO2 in the sample surpasses the binding capacity of the anti-AGO2(C34C6) antibody as seen by the high amount of AGO2 still present in the supernatant after the IP (Figure 2.4.6A). The saturation of the binding capacity ensures that the amount of AGO2 bound is comparable in all samples and allows for a reliable quantification independently of the AGO2 concentration in the input samples. The protein profile in the Coomassie stain (Figure 2.4.6B) showed no significant differences to the anti-AGO2(6F4) IP (Figure 2.4.2B) except for stronger antibody chain bands caused by the unspecific elution with sample buffer. A possibility to reduce the amount of antibody chains in unspecific elutions is covalent coupling of the antibody. Direct coupling of the anti-AGO2(C34C6) resulted in a loss of antibody binding activity (data not shown). Therefore, the method could not be applied for the anti-AGO2(C34C6) antibody.

For data analysis the raw data from the forward experiment from the modified QUICK approach was defined as forward experiment and the data from the IP with the anti-AGO2(C34C6) antibody was defined as the reverse experiment. With the combination of the two experiments into one dataset, we directly compare the ratios for the identified proteins between the two experiments instead of identifying outliers. After processing, we filtered the dataset as described (Section 2.4.1) and obtained 446 identified

Figure 2.4.6: Immunoprecipitation of AGO2 complexes with the anti-AGO2(C34C6) antibody. A) 1,28% of input samples (lanes 1 and 2) or supernatants of the immunoprecipitations (lanes 3 and 4) from heavy labeled wild type (lanes 1 and 3) and light labeled AGO2-depleted cells (lanes 2 and 4) and 2% of the eluate (lane 5) were loaded and probed with an antibody against AGO2. Lane 6 shows a longer exposure of the eluate. B) The eluate was separated by SDS-PAGE and stained with Coomassie.
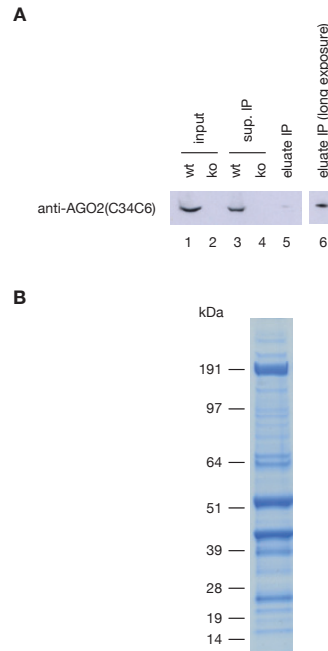
proteins. Selected values for proteins of interest are summarized in Table 2.4.2. The anti-AGO2(6F4) precipitated more AGO2 then the anti-AGO2(C34C6), as can be seen by the higher numbers of unique peptides and quantification events for AGO2. The ratios in the anti-AGO2(C34C6) experiment are lower for all identified proteins, which we attributed to a lower incorporation rate for the cells used in this experiment. The comparison of the values for the AGO proteins 1 and 3 and a selection of reported AGO2 interactors including the TNRC6 and IGF2BP protein families showed no significant differences between the two antibodies in respect to unique peptides or quantification events. We observed differences in the ratios for some proteins, especially for the AGO1 and 3 and the TNRC6 proteins, but all proteins clearly did not appear as specific interactors in both experiments. Dicer and its interaction partners were not detected in any of the experiments. SEC24C, the protein identified as a specific cross reactor for the anti-AGO2(6F4) antibody, was also identified in the IP with the commercial antibody, yet in a significantly lower amount. In both IPs, SEC24C was identified as a background binder. Overall, both antibodies showed very similar binding profiles in respect to reported AGO2 interactors, cross reactivity with other AGO proteins and known background binders. When comparing the proteins with the highest ratios, we also saw a big overlap between the two experiments. In both cases the majority of these proteins are cytoskeletal proteins (Table 2.4.2). Therefore, the high amount of cytoskeletal prote-

Protein Names	Gene Name	Uniprot ID	Keywords	Unique Peptides		Ratio H/L		Ratio H/L Count	
				anti-AGO2 (6F4)	anti-AGO2 (C34C6)	anti-AGO2 (6F4)	anti-AGO2 (C34C6)	anti-AGO2 (6F4)	anti-AGO2 (C34C6)
Bait									
Protein argonaute-2	Eif2c2	Q8CJG0	RNA-mediated gene silencing	36	26	14,497	9,156	154	69
Other AGO proteins									
Protein argonaute-1	Eif2c1	Q8CJG1	RNA-mediated gene silencing transcriptional gene silencing	18	18	1,085	0,363	40	37
Protein argonaute-3	Eif2c3	Q8CJF9	RNA-mediated gene silencing	22	17	0,904	0,396	31	30
Comparison of selected reported AGO2 interaction partners									
Trinucleotide repeat-containing gene 6A protein	Tnrc6a	Q3UHK8	RNA-mediated gene silencing	14	16	1,506	0,024	18	20
Trinucleotide repeat-containing gene 6B protein	Tnrc6b	Q8BKI2	RNA-mediated gene silencing	62	56	0,841	0,226	139	118
Trinucleotide repeat-containing gene 6C protein	Tnrc6c	Q3UHC0	RNA-mediated gene silencing	7	16	0,600	0,048	7	22
Polyadenylate-binding protein 1	Pabpc1	P29341	poly(A) tail of mRNA binding	18	18	0,946	0,898	110	74
Poly(A) binding protein, cytoplasmic 4	Pabpc4	Q99LF8	RNA binding	15	12	0,560	0,512	30	20
Putative helicase MOV-10	Mov10	P23249	RNA-mediated gene silencing	36	33	1,367	1,321	43	37
Nuclease-sensitive element-binding protein 1	Ybx1	P62960	transcription pre-mRNA splicing mRNA processing	11	7	1,067	1,023	50	17
Insulin-like growth factor 2 mRNA-binding protein 1	Igf2bp1	O88477	mRNA 5'UTR binding	14	16	0,561	0,630	25	19
Insulin-like growth factor 2 mRNA-binding protein 2	Igf2bp2	Q5SF07	mRNA translation mRNA 5'UTR binding	15	12	0,523	0,547	24	15
Insulin-like growth factor 2 mRNA-binding protein 3	Igf2bp3	Q9CPN8	RNA binding mRNA translation and stabilty	15	13	0,784	0,788	22	17
Heat shock protein 84b	Hsp90ab1	Q71LX8	molecular chaperone ATPase activity	2	2	0,480	0,953	66	33
Heat shock protein HSP 90-alpha	Hsp90aa1	P07901	molecular chaperone ATPase activity	19	16	0,347	0,592	24	19
Comparison of selected contaminants									
Sec24c protein	Sec24c	Q8R2V9	COPII vesicle coat component	45	19	1,276	1,172	83	20
Caseinolytic peptidase B protein homolog	Clpb	Q60649	ATPase secretion/protein trafficking	2	25	84,784	1,879	3	41
Myosin regulatory light polypeptide 9	Myl9	Q9CQ19	myosin cytoscleletal protein	3	5	25,503	44,205	4	5
Interferon-induced protein with tetratricopeptide repeats 1	Ifit1	Q64282	unknown function	6	3	23,415	7,451	5	2
Cellular tumor antigen p53	Tp53	P02340	tumor suppressor	3	6	18,519	12,297	4	4
Cofilin-2	Cfl2	P45591	actin binding cytoplasmic actin rods	5	5	10,977	20,324	7	5
Coronin-1B	Coro1b	Q9WUM3	actin bindin interacts with Arp2/3 complex	11	7	9,731	25,584	13	12
Coronin-1C	Coro1c	Q9WUM4	actin binding	21	19	8,833	8,882	29	32
Tropomyosin beta chain	Tpm2	P58774	actin binding	2	3	8,284	6,064	9	15
WD repeat-containing protein 1	Wdr1	O88342	actin binding	11	21	7,409	22,330	13	24
MCG5400	2900073 G15Rik	Q6ZWQ9	unknown function calcium binding	2	4	7,139	14,765	22	87

Table 2.4.2: List of proteins of interest identified in the anti-AGO2(6F4) and anti-AGO2(C34C6) immunoprecipitations. Selected values are summarized for the identified AGO proteins, reported AGO2 interactors and a set of contaminants and known cross reactants. Keywords describing reported functions were added.

ins in the IPs was not based on the specific binding characteristic of the anti-AGO2(6F4) antibody. Instead, it supported our previous observation that this background binding of cytoskeletal proteins is a general problem caused by the significant differences of the whole proteome between the two cell lines used in this experimental setup.

## 2.4.3 Identification of Specific AGO2 Interacting Proteins from Hepa 1-6 Cells

In the QUICK approach, the same antibody was used for IPs from different cell lines which led to the strong differences in background binding (see Section 2.4.1). Further experiments revealed that this binding behavior is not specific for the anti-AGO2(6F4) antibody (see Section 2.4.2). In order to address the influence of the whole proteome of

the input samples on the quality of the IP, we now went back to the classical approach of using a control antibody to define background binding. This allowed the use of the same cell line as input sample and should prevent the identification of proteome-based false positives.

Hepa 1-6 cells were SILAC labeled and protein complexes were immunoprecipitated with the anti-AGO2(6F4) or a control antibody from the different SILAC states separately. As control antibody we used the anti-RmC(16D2), an antibody directed against mouse complement C4 protein. Samples were combined at the elution step and further processed for MS analysis as described previously. The quality of the IPs was assessed by Western blot analysis and Coomassie stain of the eluates (Figure 2.4.7).

Figure 2.4.7: Immunoprecipitations with the anti-AGO2(6F4) or the anti-RMC antibody from Hepa 1-6 cells. A) 1.2% of heavy (lane 1) or light labeled (lane 2) input samples and supernatants from IPs for the forward (lanes 3 and 4) or the reverse (lanes 6 and 7) experiments were loaded. 24% of the eluates from the forward and reverse experiment were loaded in lanes 5 and 8, respectively. B) The eluate from the forward experiment was separated by SDS-PAGE and stained with Coomassie.
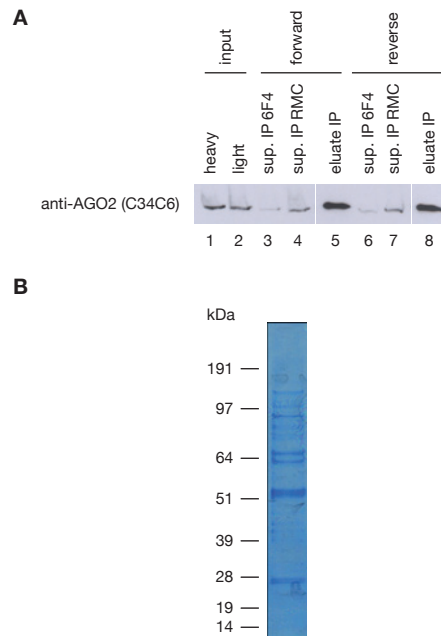
Equal amounts of heavy or light labeled whole cell lysate were used for all IPs. The amount of AGO2 remaining in the supernatant is unchanged in the control IPs with the anti-RmC(16D2), suggesting that there is no unspecific AGO2 precipitation. As with the anti-AGO2(6F4) IPs from MEF cells, AGO2 is strongly detected in the eluates. First differences to the previous experiments became apparent in the Coomassie stain of the eluate (Figure 2.4.7B). The band pattern of the proteins showed clear differences to the band pattern in IPs from MEF cell lines (Figure 2.4.2B). The high molecular weight bands above 191 kDa are either missing or very weak. Between the 97 and 64 kDa marker the proteins bands are clearer and a distinct band appears at approximately 90 kDa.
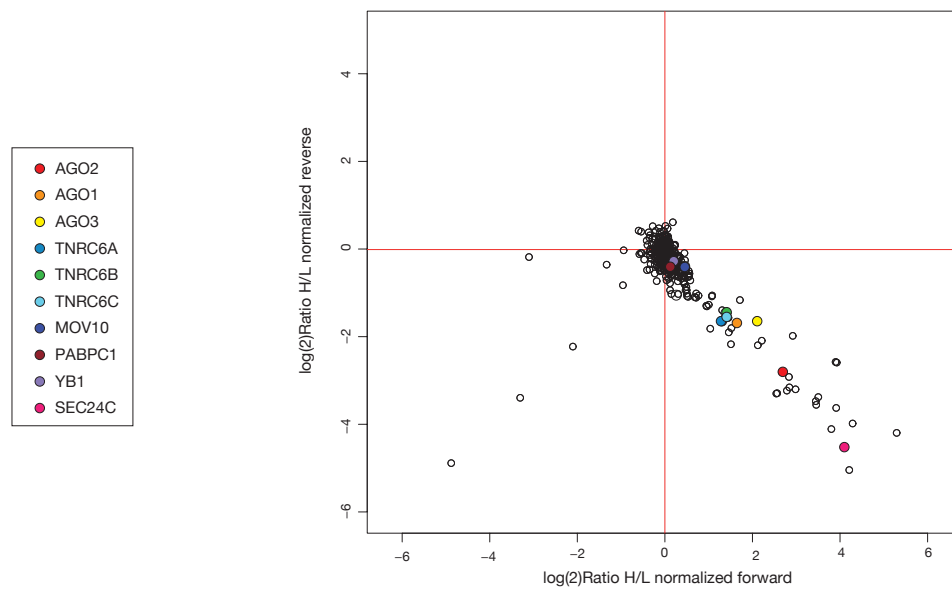
Figure 2.4.8: Immunoprecipitation of endogenous AGO2-containing RNP complexes from Hepa 1-6 cells. Logarithmized, normalized ratios from the forward and reverse experiments are plotted against each other. Every dot represents an identified and quantified protein. Specific interactors appear in the lower right quadrant whereas background binder cluster around zero. Selected proteins are indicated in colors.

In the LC-MS/MS analysis, 643 proteins were identified and 348 identifications passed our filter criteria. AGO2 was identified with more than 40 unique peptides per experiment and a high sequence coverage of 78% (Table 2.4.3). The ratios of 6.38 and 0.14 in forward and reverse experiments were relatively low but still defined AGO2 as a clear outlier. The cross reacting protein SEC24C was identified with more than 30 unique peptides and was clearly defined as an outlier by the ratios of 17.09 and 0.04. No Dicer petides were detected in the experiments. The data was visualized in a ratio plot (Figure 2.4.8). As for the modified QUICK approach, background binders cluster around zero and outliers appear in the lower right quadrant.

The dataset showed a distribution typical for a high quality SILAC dataset. There was almost no scattering and background binders were tightly clustered at the crossing of the zero base lines of the forward and reverse experiments. In the lower left quadrant only very few contaminants were visible. A set of proteins appeared as outliers in the lower right quadrant and could be clearly distinguished from the background cloud. From the ratio plot, we could conclude that the wide scattering of data points and the high amount of outliers in the previous experiments was indeed caused by using cell lines showing dif-

Protein Names	Gene Names	Uniprot ID	Keywords	Unique Peptides		Ratio H/L	
				forward	reverse	forward	reverse
Bait							
Protein argonaute-2	Eif2c2	Q8CJG0	RNA-mediated gene silencing	40	45	6,383	0,144
Outliers							
Programmed cell death 6 interacting protein	Pdcd6ip	Q9WU78	multivesicular body protein	40	46	39,247	0,055
Insulin receptor substrate 1	Irs1	P35569	insulin receptor signaling pathway	43	47	19,529	0,064
Protein FAM110A	Fam110a	Q8R184	cytoskeleton spindel pole organizer	5	5	18,503	0,031
Sec24c protein	Sec24c	Q8R2V9	COPII vesicle coat component	34	41	17,090	0,044
Peptidyl-prolyl cis-trans isomerase FKBP5	Fkbp5	Q64378	heteromeric cytoplasmic complex with Hsp90 and Hsp70	8	7	15,199	0,167
Ras GTPase-activating protein 2	Rasa2	P58069	membrane, Ras c-AMP pathway	22	23	15,047	0,082
Contactin associated protein 1	Cntnap1	O54991	membrane protein	18	20	14,905	0,169
Protein transport protein Sec23A	Sec23a	Q01405	COPII vesicle coat component	24	27	13,940	0,058
Syntenin-1	Sdcbp	O08992	membrane protein	8	6	11,337	0,097
Protein transport protein Sec23B	Sec23b	Q9D662	COPII vesicle coat component	31	32	10,988	0,086
Glutamine and serine rich 1	Qser1	A2BIE1	unknown function	14	14	10,895	0,091
Latent-transforming growth factor beta-binding protein 3	Ltbp3	Q61810	TGF beta1 signalling pathway	3	6	7,903	0,110
Ubiquitin carboxyl-terminal hydrolase 19	Usp19	Q3UJD6	deubiquitination	7	12	7,563	0,255
Phosphate carrier protein, mitochondrial	Slc25a3	Q8VEM8	phosphate group transport cytosol-mitrochondrial matrix	10	10	7,174	0,113
Heat shock protein HSP 90-alpha	Hsp90aa1	P07901	molecular chaperone ATPase activity	11	14	7,126	0,133
Heat shock protein 84b	Hsp90ab1	Q71LX8	molecular chaperone, ATPase activity	2	2	6,898	0,107
Ubiquitin-associated protein 2	Ubap2	Q91VX2	unknown function	7	8	5,912	0,103
SUN domain containing protein1	Sun1	Q9D666	nucleoskeleton/cytoskeleton	6	4	5,841	0,103
Heterogeneous nuclear ribonucleoprotein H1	Hnrnph1	O35737	pre mRNA alternative splicing RNA binding	10	11	4,639	0,236
Heterogeneous nuclear ribonucleoprotein H2	Hnrnph2	P70333	hnRNP complex RNA binding	8	8	4,350	0,220
Protein argonaute-3	Eif2c3	Q8CJF9	RNA-mediated gene silencing	5	5	4,274	0,325
Annexin A2	Anxa2	P07356	calcium binding sectreted	3	3	3,279	0,450
Protein argonaute-1	Eif2c1	Q8CJG1	RNA-mediated gene silencing transcriptional gene silencing	11	15	3,123	0,313
Ythdc1 protein	Ythdc1	Q8R5E6	unknown function	9	8	2,867	0,289
Ubiquitin-40S ribosomal protein S27a	Rps27a	P62983	cleaved into Ubiquitin and 40S ribosomal protein27a, modification translation	5	4	2,848	0,223
Sarcoplasmic/endoplasmic reticulum calcium ATPase 2	Atp2a2	O55143	ATP-dependent Ca2+ transport cytosol-sarcoplasmatic reticulum	2	2	2,750	0,270
Myoferlin	Myof	Q69ZN7	Calcium binding transmembrane protein	5	8	2,736	0,340
Trinucleotide repeat-containing gene 6C protein	Tnrc6c	Q3UHC0	RNA-mediated gene silencing	9	9	2,644	0,339
Trinucleotide repeat-containing gene 6B protein	Tnrc6b	Q8BKI2	RNA-mediated gene silencing	23	25	2,630	0,366
14-3-3 protein epsilon	Ywhae	P62259	Signaling recognizes phosphoserine and phosphothreonines	6	7	2,476	0,384
Trinucleotide repeat-containing gene 6A protein	Tnrc6a	Q3UHK8	RNA-mediated gene silencing	13	15	2,471	0,322
Selected reported AGO2 interactors							
Fragile X mental retardation syndrome-related protein 1	Fxr1	Q61584	RNA binding	15	13	1,945	0,407
Fragile X mental retardation protein 1 homolog	Fmr1	P35922	RNA binding RNA transport translation	11	10	1,927	0,411
Polyadenylate-binding protein 1	Pabpc1	P29341	poly(A) tail of mRNA binding	20	21	1,140	0,769
Poly(A) binding protein, cytoplasmic 4	Pabpc4	Q99LF8	RNA binding	19	19	1,230	0,760
Putative helicase MOV-10	Mov10	P23249	RNA-mediated gene silencing	42	40	1,352	0,766
Nuclease-sensitive element-binding protein 1	Ybx1	P62960	transcription pre-mRNA splicing mRNA processing	9	8	1,148	0,776
Insulin-like growth factor 2 mRNA-binding protein 1	Igf2bp1	O88477	mRNA 5'UTR binding	14	13	1,109	0,839
Insulin-like growth factor 2 mRNA-binding protein 2	Igf2bp2	Q5SF07	mRNA translation mRNA 5'UTR binding	14	14	1,113	0,808
Insulin-like growth factor 2 mRNA-binding protein 3	Igf2bp3	Q9CPN8	RNA binding mRNA translation and stabilty	17	19	1,301	0,762
Regulator of nonsense transcripts 1	Upf1	Q9EPU0	nonsense mediated mRNA decay	47	48	1,452	0,648

Table 2.4.3: List of selected values for proteins of interest identified in AGO2-containing RNP complexes from Hepa 1-6 cells. A subset of values is given for the top 40 outliers and reported AGO2 interactors. Keywords describing protein functions are added.

ferences in their proteome as input samples and that this problem can be circumvented by working with samples from identical or at least very similar cell lines.

The antibody specific cross reactant SEC24C and other vesicle components such as PDCD6IP and SEC23A and B are the top outliers together with membrane proteins such as RASA2, CNTNAP1 and SDCBP. The TNRC6 proteins and AGO1 and 3 also appear as clear outliers (Figure 2.4.8). In combination with the background ratios in the QUICK approach (see Section 2.4.1), the high ratios for AGO1 and 3 clearly identify the latter two proteins as cross reactants of the anti-AGO2(6F4) antibody. HSP90, FXR1 and FMR are proteins that have been reported to interact with AGO2 [144, 255] and these proteins were identified as specifically interacting proteins in this dataset. Another set of reported interactors including MOV10, YB1, PABPC1, the IGF2BP proteins 1-3 and UPF1 appeared as background binders (Table 2.4.3). An association with AGO1 and 3 cannot explain this binding behavior because, unlike in the QUICK approach, AGO1 and 3 were detected with high ratios in this experimental setup. Therefore, the background binding of these established AGO2 interactors was not caused by binding to other AGO proteins as previously suggested (see Section 2.4.1) but is more probably based on non-specific interactions with the control antibody or the sepharose matrix. To investigate this possibility, we analyzed the binding behavior of YB1 and UPF1 by Western blot analysis (Figure 2.4.9). Proteins were immunoprecipitated from whole cell lysate of MEF cells with either the anti-AGO2(6F4) or the anti-RmC(16D2) antibody and the IPs were tested for the presence of AGO2, YB1 and UPF1. AGO2 was present only in the IP with the anti-AGO2(6F4) antibody but YB1 and UPF were present in the control IP with the anti-RmC(16D2) antibody as well. Therefore the background binding behavior of YB1 and UPF1 was based on non-specific binding to the control antibody or the sepharose matrix.
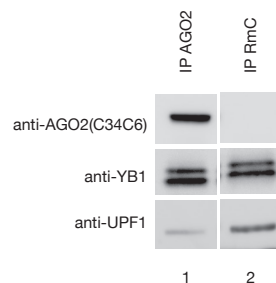

Figure 2.4.9: Cross reactivity of the anti-RMC(16D2) antibody with the reported AGO2 interacting proteins YB1 and UPF1. Protein complexes were immunoprecipitated from wild type MEFs with the anti-AGO2(6F4) (lane 1) or the anti-RMC(16D2) antibody (lane 2). Eluates were analyzed for the presence of AGO2 (upper panel), YB1 (middle panel) and UPF1 (lower panel) by Western blotting.

Taken together, our results on the analysis of endogenous AGO2 complexes (see Sections 2.4.1, 2.4.2 and 2.4.3) it becomes apparent that our current experimental approach does not allow a confident identification of the endogenous AGO2 complex components. Further changes to the experimental setup might enable us to reduce the non-specific binding of reported AGO2 interactors to the control antibody or the sepharose matrix and to diminish the influence of the whole proteome on the binding profile. But since the cross reactivity of the anti-AGO2(6F4) antibody with other AGO proteins is a problem that cannot be solved without significant time and effort, the project was discontinued.

2.4.4 Characterization of the MicroRNA Dependency of AGO2-Specific Interactors

Quantitative proteomics cannot only be used for the identification of specific interaction partners but can be applied to monitor stimulus-specific changes of complex composition. As described previously, several proteins specifically interacting with AGO2 also bind non-specifically to the affinity matrix and thereby appear as background binders (see Sections 2.4.1 and 2.4.3). In addition, the cross reactivity of the anti-AGO2(6F4) antibody with AGO1 and 3 renders it impossible to define the composition of the basal AGO2 protein complex since proteins associating with all three AGO proteins can not be distinguished from those only interacting with AGO2 in the MS analysis. Nevertheless,
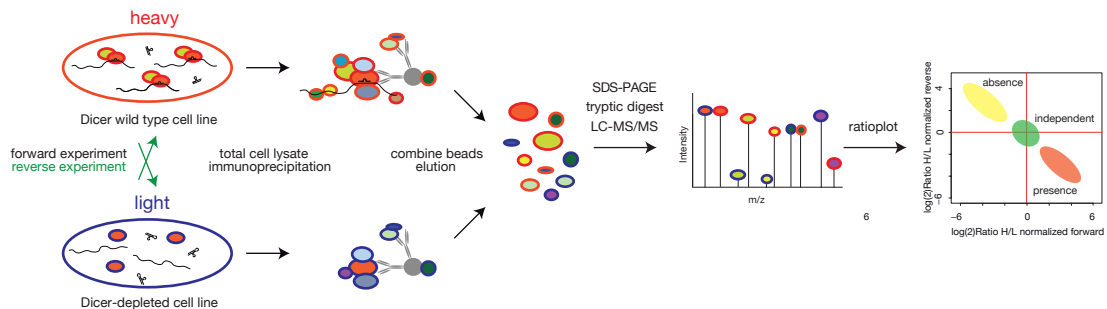
Figure 2.4.10: Experimental setup for the identification of the miRNA-dependency of AGO2 interactions. AGO2-containing complexes were immunoprecipitated from SILAC labeled Dicer wild type and Dicer-depleted MEFs with the anti-AGO2(6F4) antibody. Samples were combined at the elution step and analyzed by MS. Proteins interacting with AGO2 in the presence of Dicer and miRNAs are expected to show high ratios in the forward and are located in the lower right quadrant (red area) in a ratio plot. Background binders and Dicer and miRNA-independent interactors show ratios around one in both experiments and cluster around zero (green area). Proteins with low forward and high reverse ratios bind to AGO2 preferentially in the absence of Dicer and miRNAs and appear in the upper left quadrant (yellow area).

we should theoretically be able to monitor changes of specific AGO interactors in similar cell lines under different cellular conditions. Performing immunoprecipitations with the anti-AGO2(6F4) in Dicer wild type and Dicer-depleted MEFs provides a system that enabled us to study the influence of the presence or absence of Dicer and miRNAs on the protein composition of endogenous AGO2-containing RNPs.

We carried out AGO2 IPs with the anti-AGO2(6F4) from SILAC-labeled Dicer wild type and Dicer-depleted cells as depicted in Figure 2.4.10. The quality of the IPs was checked by Western blotting and Coomassie staining of the eluates (Figure 2.4.11). As the cellular concentration of AGO2 is decreased in the Dicer-depleted cells, we worked with an excess of input sample to reach full saturation of the antibody binding capacity and to facilitate quantitative analysis between the samples. The eluates (Figure 2.4.11B) showed the typical protein band pattern previously observed for MEFs (see Figure 2.4.2) and were further processed for MS analysis as described earlier (Section 2.4.1).
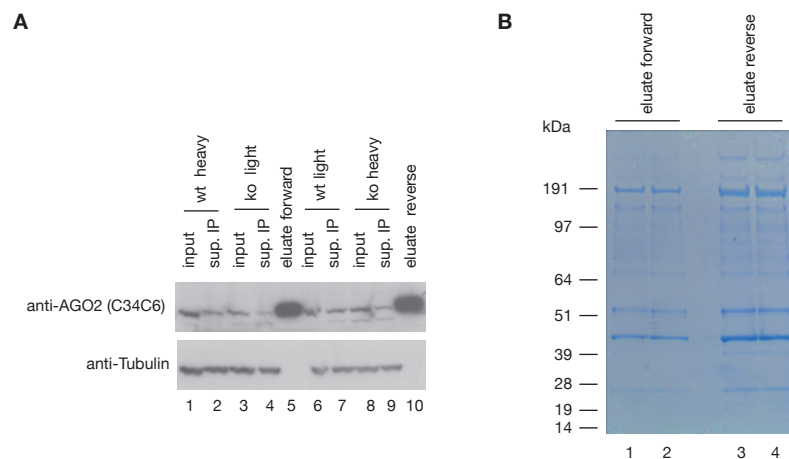
Figure 2.4.11: Immunoprecipitations for the identification of miRNA-dependent AGO2 interaction partners. A) 0,6% input samples (lanes 1, 3, 6 and 8), supernatants after IPs (sub. IP, lanes 2, 4, 7 and 9) and 10% eluates (lanes 5 and 10) for forward (lanes 1-5) and reverse (lanes 6-10) experiments were probed for AGO2 (upper panel) and tubulin as loading control (lower panel) by Western blot. B) Eluates from the forward (lanes 1-2) and the reverse (lanes 3-4) experiments were separated by one dimensional PAGE and stained with Coomassie.

With only 374 identified proteins after filtering, this was the smallest dataset we obtained so far. This can be partly attributed to the fact that the data was measured on a LTQ Orbitrap, a mass spectrometer which is less sensitive than the LTQ Orbitrap Velos, which was used for the previous measurements. In this experimental setup AGO2 was
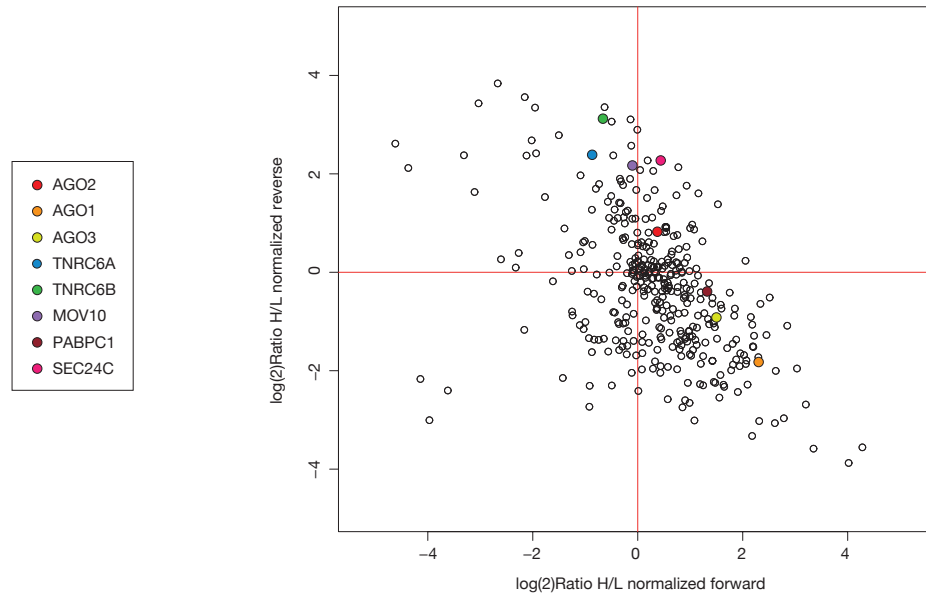
Figure 2.4.12: Identification of miRNA-dependent interactors in endogenous AGO2-containing RNPs. Logarithmized normalized ratios from forward and reverse experiments are plotted. Every dot represents an identified and quantified protein. A selection of proteins of interest are indicated in color.

precipitated in both IPs and this was reflected by the high sequence coverage of 82% and around 50 unique peptides per experiment. Dicer was not detected (Table 2.4.4).

We visualized the data in a ratio plot (Figure 2.4.12) and observed a very wide scattering of the data points. There was no clearly defined background cloud and it was therefore not possible to define a cut off for the numerous outliers. We observed a mixture of cytoskeletal, membrane and mitochondrial proteins as outliers in the forward experiment (Table 2.4.4). Among the background binders we found AGO1 and 3, PABPC, IGF2BP1 and SEC24C. In the reverse experiment, the reported AGO2 interactors HSP90, MOV10, TNRC6A and B as well as IGF2BP3 were identified as outliers. We also saw mRNA binding proteins (DHX9 and HNRNPD), the two SEC proteins 16A and 23 and several membrane proteins in this group. The identification of reported AGO2 interacting and mRNA binding proteins among the outliers was promising, but the quality of the data, as indicated by the low number of identified proteins, was too poor to draw reliable conclusions. Apparently the loss of Dicer and miRNAs changed the whole proteome significantly and led to the wide scattering of the data points that prevented a separation of outliers from the background cloud. This was a problem inherent to the experimental setup and can not be overcome by measuring on an instrument with higher sensitivity.

Protein Names	Gene Names	Uniprot ID	Keywords	Unique Peptides		Ratio H/L	
				forward	reverse	forward	reverse
Bait							
Protein argonaute-2	Eif2c2	Q8CJG0	RNA-mediated gene silencing	50	51	1,296	1,769
Cross reactivity							
Sec24c protein	Sec24c	Q8R2V9	COPII vesicle coat component	49	48	1,139	4,835
Top 20 outliers Dicer wild type							
Ltbp2 protein	Ltbp2	Q0VD84	unknown function calcium binding	2	3	19,421	0,085
Caldesmon 1	Cald1	Q8VCQ8	unknown function actin binding	11	21	16,194	0,068
Phostensin	2310014 H01Rik	Q8BQ30	targets phosphatase 1 to F-actin	2	6	10,197	0,083
Procollagen-lysine,2-oxoglutarate 5-dioxygenase 2	Plod2	Q9R0B9	collagen modification	2	5	9,211	0,155
Filamin-B	Flnb	Q80X90	connects cell membrane to actin	60	91	8,184	0,258
Cytoskeletal protein	Utrn	O08614	actin binding	7	37	7,206	0,471
Serine hydroxymethyltransferase	Shmt2	Q3TFD0	carbon metabolism	4	4	6,890	0,128
Galectin-1	Lgals1	P16045	beta-galactoside binding secreted	2	6	6,181	0,250
Cytospin-A	Cytsa	Q2KN98	cytokinesis spindle organization	30	49	6,119	0,120
Latent-transforming growth factor beta-binding protein 3	Ltbp3	Q61810-1	TGF signalling, secreted	34	31	5,711	0,701
Transforming growth factor beta-3	Tgfb3	P17125	cell differentiation secreted	4	4	5,470	0,413
Regulator of nonsense transcripts 1	Upf1	Q9EPU0	nonsense mediated mRNA decay	36	36	5,053	0,640
Ankycorbin	Rai14	Q9EP71	cytoskeletal protein	14	25	4,978	0,123
Calreticulin	Calr	P14211	calcium binding ER Trim21 interactor	4	4	4,921	0,303
Nidogen-1	Nid1	P10493	extracellular matrix lamin associated	3	2	4,645	0,409
Phenylalanine--tRNA ligase alpha chain	Farsa	Q8C0C7	Aminoacyl-tRNA synthetase	13	10	4,602	0,349
ADP/ATP translocase 2	Slc25a5	P51881	ADP/ATP translocase mitochondrial	6	7	4,570	0,352
ADP/ATP translocase 1	Slc25a4	P48962	ADP/ATP translocase mitochondrial	8	8	4,535	0,478
Glypican-4	Gpc4	P51655	cell surface proteglycan	5	6	4,530	0,100
Peptidyl-prolyl cis-trans isomerase A	Ppia	P17742	protein folding	2	4	4,450	0,533
Top 20 outliers Dicer depleted							
Peptidyl-prolyl cis-trans isomerase FKBP5	Fkbp5	Q64378	heteromultimeric cytoplasmic complex with HSP90 and HSP70	22	22	0,157	14,289
Heat shock protein HSP 90-alpha	Hsp90aa1	P07901	molecular chaperone ATPase activity	19	21	0,225	11,782
Low-density lipoprotein receptor-related protein 2	Lrp2	A2ARV4	high density lipoprotein endocytosis	4	5	0,122	10,806
Neurobeachin	Nbea	Q9EPN1	anchors protein kinase A to membrane	71	67	0,646	10,233
Prostaglandin E synthase 3	Ptges3	Q9R0Q7	molecular chaperone	3	5	0,258	10,179
Trinucleotide repeat-containing gene 6B protein	Tnrc6b	Q8BKI2	RNA-mediated gene silencing	57	49	0,631	8,698
Heterogeneous nuclear ribonucleoprotein D0	Hnrnpd	Q60668	3'UTR ARE binding	4	4	0,910	8,604
EMILIN-1	Emilin1	Q99K41	cell adhesion, secreted	6	4	0,708	8,353
Sec16a protein	Sec16a	Q8K000	unknown function human protein defines ER exit sites and ER-Golgi trafficking	11	9	0,993	7,453
Heat shock protein 84b	Hsp90ab1	Q71LX8	molecular chaperone ATPase activity	2	2	0,352	6,891
Laminin subunit alpha-5	Lama5	Q61001	cell adhesion, secreted	5	3	0,246	6,416
Histone H3	H3	P68433 P84228 P84244	chromatin	4	4	0,041	6,126
Heterogeneous nuclear ribonucleoprotein A/B	Hnrnpab	Q99020	transcriptional repressor	6	7	0,918	5,948
E3 ubiquitin-protein ligase TRIM21	Trim21	Q62191	ubiquitin ligase	2	2	0,261	5,338
Trinucleotide repeat-containing gene 6A protein	Tnrc6a	Q3UHK8	RNA-mediated gene silencing	11	10	0,547	5,241
Histone H4	H4	P62806	chromatin	6	6	0,101	5,199
Protein transport protein Sec23B	Sec23b	Q9D662	COPII vesicle coat component	33	36	0,724	5,186
Insulin-like growth factor 2 mRNA-binding protein 1	Igf2bp1	O88477	mRNA 5'UTR binding	4	4	0,230	5,174
Putative helicase MOV-10	Mov10	P23249	RNA-mediated gene silencing	28	24	0,929	4,501
ATP-dependent RNA helicase A	Dhx9	O70133	CRD-mediated complex transcriptional activator	32	35	1,709	4,392
Other AGO proteins							
Protein argonaute-1	Eif2c1	Q8CJG1	RNA-mediated gene silencing transcriptional gene silencing	12	10	4,936	0,283
Protein argonaute-3	Eif2c3	Q8CJF9	RNA-mediated gene silencing	6	6	2,827	0,529
selected reported AGO2 interactors in background							
Insulin-like growth factor 2 mRNA-binding protein 3	Igf2bp3	Q9CPN8	RNA binding mRNA translation and stabilty	4	4	0,546	2,414
Polyadenylate-binding protein 1	Pabpc1	P29341	poly(A) tail of mRNA binding	7	7	2,501	0,762
Poly(A) binding protein, cytoplasmic 4	Pabpc4	Q99LF8	RNA binding	6	5	2,681	0,697

Table 2.4.4: List of proteins identified in the AGO2 IPs for the identification of miRNA-dependent interactors from endogenous AGO2-containing RNPs. Selected values are given for the top 20 outliers, a set of reported AGO2 interactors, identified AGO proteins and the cross reactant SEC24C. Keywords describing protein functions are added.

2.5 Identification of AGO2 Interactors from Tagged Protein Complexes and Characterization of the RNA Dependency of the Interactions

2.5.1 Establishment of Stable FLAG-HA-tagged AGO2 Expressing MEF Cell Lines

Our approaches to identify AGO2 specific interaction partners from endogenous protein complexes revealed the influence of the whole cell proteome on background binding as one of the major factor preventing a high confidence analysis of AGO2 protein complexes. A second factor is the cross reactivity of the endogenous antibodies with other proteins of the AGO family. One solution to address the latter aspect is to work in a tag-based system. The combination of a FLAG- and HA-tag (F/H-tag) is an established system for the purification and analysis of AGO-containing ribonucleoprotein complexes [127, 171, 221, 349].

We established a set of Dicer wild type or Dicer-depleted mouse embryonic fibroblasts that stably overexpress AGO2 with a FLAG/HA-tag at the N-terminus by using retroviral transfection (Figure 2.5.1). Two sets of constructs were used. One contained the F/H-AGO2 and IRES-GFP as a transfection marker and the other, the control construct, contained only IRES-GFP. The cells were tested for the stability of the Dicer depletion during culturing (Figure 2.5.1A). The expression level of F/H-AGO2 was higher in the Dicer wild type cells than in the Dicer-depleted cells and thereby follows the same trend as the endogenous AGO2 protein levels (Figure 2.5.1B, middle panel). Tagged protein could be immunoprecipitated with the FLAG-antibody and AGO2 could be eluted by incubation with FLAG-peptide (Figure 2.5.1C). The GFP expressing cell lines served as negative controls for all experiments (Figure 2.5.1A-C). The amount of miRNAs was not affected by the expression of F/H-AGO2 in the Dicer wild type cells (Figure 2.5.1D) and an enrichment of miRNAs in the FLAG-IP is only observed for the F/H-AGO2 expressing Dicer wild type cells. Mature miRNAs were not detected in the Dicer-depleted MEFs (Figure 2.5.1D). Some small RNA species are independent of Dicer processing, for example miR-451 [40, 45]. Although miR-451 is not detectable in the MEFs (Anne Dueck, personal communication) it can not be excluded that other Dicer-independent small RNAs species are present in the Dicer-depleted cell lines.

This set of cell lines now enabled us to identify AGO2 interaction partners and to study the Dicer and miRNA requirement of the interactions. By using the FLAG-tag for purification, we avoided the problem of cross reactivity with other AGO proteins. Since the F/H-AGO2 expressing cell lines differ from their respective GFP expressing con-

trol cell lines only in respect to the AGO2 overexpression, the differences in the whole cell proteome between the cell lines should be only minor and the problems caused by differently expressed background binders should be significantly reduced.
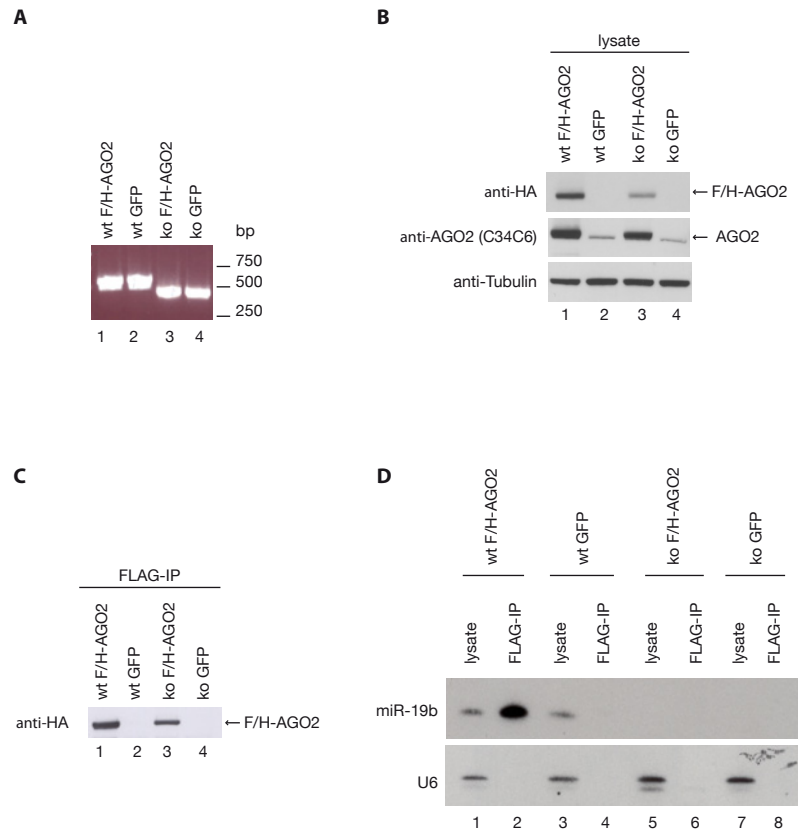

Figure 2.5.1: Characterization of the FLAG/HA-tagged AGO2 expressing MEF cell lines. Wild type (wt) and Dicer-depleted (ko) MEF cells were transduced with retrovirus carrying FLAG/HA-tagged AGO2 (F/H-AGO2) and GFP or GFP (GFP) alone. A) Cultured MEFs were genotyped to verify Dicer depletion. Genomic DNA was isolated from cells three weeks after transduction and amplified by PCR with primers flanking the deleted region in the Dicer gene. PCR products were visualized by ethidiumbromide stain after size separation in an agarose gel. B) The expression of F/H-AGO2 was analyzed by Western blot. 30 µg total cell lysates were probed with anti-HA or anti-AGO2 antibody for detection of F/H-AGO2 (upper panel) or endogenous AGO2 (middle panel). Tubulin was used as a loading control (lower panel). C) F/H-AGO2 was immunoprecipitated from total lysate with anti-FLAG agarose beads and analyzed by Western blot with an anti-HA-antibody. D) RNAs were isolated from lysate or immunoprecipitated F/H-AGO2-containing RNP complexes and probed for miR-19b (upper panel). The membrane was stripped and reprobed for U6 to control equal loading of input RNA (lower panel).

2.5.2 Characterization of the Protein Composition of AGO2-Containing Ribonucleoprotein Complexes and Analysis of the miRNA Dependency of the Interactions

In a first set of experiments, we aimed to define the protein composition of the AGO2 complex. By comparing FLAG-based purifications from the F/H-AGO2 expressing cell line against the corresponding control cell line, we were able to identify specific interactors with high confidence and to define the protein composition of basal AGO2-containing RNPs (Figure 2.5.2A). Protein complexes were immunoprecipitated with the FLAG-antibody from total lysates from SILAC labeled F/H-AGO2 expressing Dicer wild type MEFs (wt F/H-AGO2) and the control MEF cell line transduced with empty virus (wt GFP). Samples were combined at the elution step and analyzed by LC-MS/MS on an LTQ Orbitrap. The experiment was also carried out with the Dicer-depleted (ko F/H-AGO2 and ko GFP) cell lines. In the next step, we performed experiments designed to analyze the Dicer and miRNA dependency of the AGO2 interactions. For this purpose, AGO-containing RNPs from the F/H-AGO2 expressing Dicer wild type and the Dicer-depleted cells were directly compared against each other analogous to the approach carried out for the endogenous protein complexes (Figure 2.5.2B). In contrast to the endogenous approach (see Section 2.4.4), we were looking at a complex with a known protein composition as our first set of experiments (Figure 2.5.2A) predefined the composition of the basal AGO2-containing RNP complex. Thus, the proteins which interact independently of Dicer and miRNAs and therefore show no significant ratios could be tracked among the background binders.

We identified between 1050 and 1350 proteins per experiment. Between 47 and 60% passed the filter criteria of at least two unique peptides and two quantification events per protein. We obtained datasets containing 758, 617 and 641 proteins for the wt F/H-AGO2 versus wt GFP, ko F/H-AGO2 versus ko GFP and the wt F/H-AGO2 versus ko F/H-AGO2 experiments, respectively. AGO2 was identified with more than 37 unique peptides and sequence coverages over 72% in all measurements. Dicer was detected with at least 25 unique peptides and 22% sequence coverage in the wt F/H-AGO2 versus wt GFP and the wt F/H-AGO2 versus ko F/H-AGO2 data, indicating that Dicer stably associates with overexpressed F/H-AGO2. We visualized the data by ratio plots (Figure 2.5.3) and cluster analysis (Figure 2.5.4). For the cluster analysis, the logarithmized normalized ratios of proteins identified as specific AGO2 interactors were hierarchically clustered and the result was displayed as a heat map.
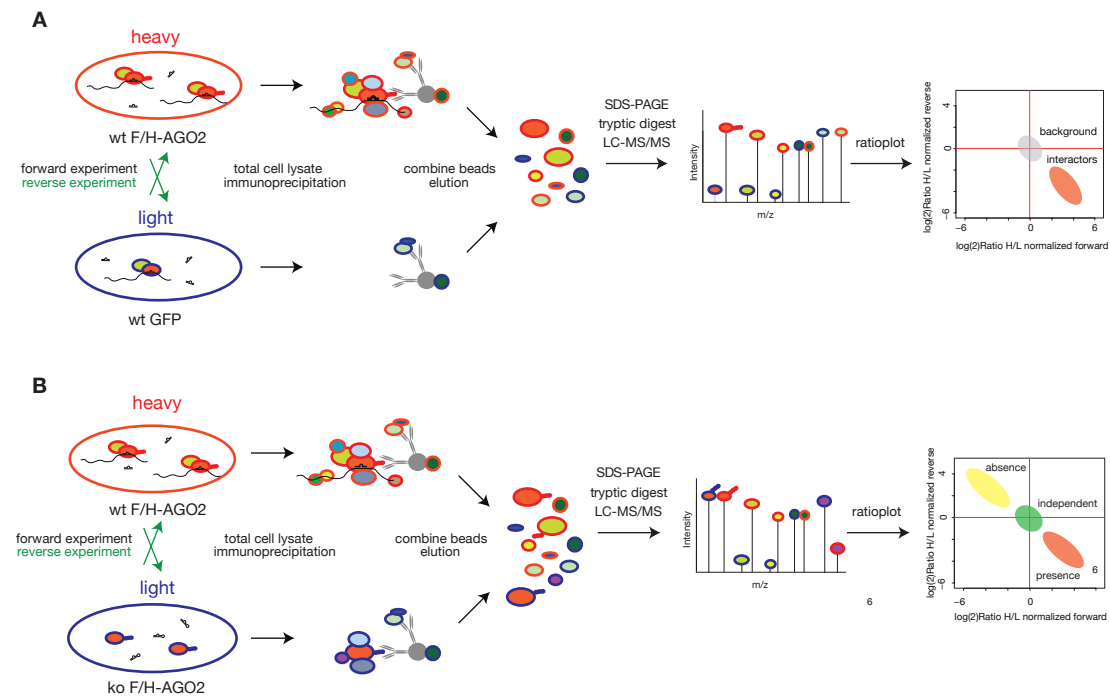
Figure 2.5.2: Experimental setup for the identification of specific AGO2 interactors and analysis of the miRNA requirement of the interaction. A) FLAG-antibody was used for immunoprecipitations of protein complexes from total cell lysates from heavy SILAC labeled F/H-AGO2 expressing Dicer wild type MEFs (wt F/H-AGO2) and a light labeled control MEF cell line transduced with GFP only (wt GFP). Immunoprecipitations were carried out for each SILAC state separately and the beads were combined for elution with 3x FLAG-peptide. Eluates were separated by SDS-PAGE, digested with trypsin and analyzed by LC-MS/MS. For the reverse experiment the SILAC label was swapped between the cell lines. The experiments were also carried out using the F/H-AGO2 expressing Dicer-depleted MEFs (ko F/H-AGO2) and its corresponding control cell line (ko GFP). In the ratio plot, background binders are clustered around zero, as highlighted by the grey area. Specific interactors can be found in the lower right quadrant as indicated by the red area. B) AGO2-containing RNP complexes were immunoprecipitated with the FLAG-antibody from heavy labeled F/H-AGO2 expressing Dicer wild type MEFs and light labeled F/H-AGO2 expressing Dicer-depleted MEFs separately. For the elution with 3xFLAG peptides, the samples were combined and eluates were further processed as described in A. The reverse experiment with swapped labels was also carried out. In a ratio plot, interactions that are independent of the presence or absence of miRNAs and Dicer cluster around zero together with background binders (green sphere). Proteins interacting preferentially in the presence of miRNAs and Dicer appear in the lower right quadrant (red sphere) and proteins preferentially interacting with AGO2 in the absence of miRNAs and Dicer are located in the upper left quadrant (yellow sphere).

More than 90% of the identified proteins could directly be classified as background binders based on their SILAC ratios around 1, among them the methylosome components PRMT5, MEP50 and pICLn. 53 proteins appeared as outliers and were thereby
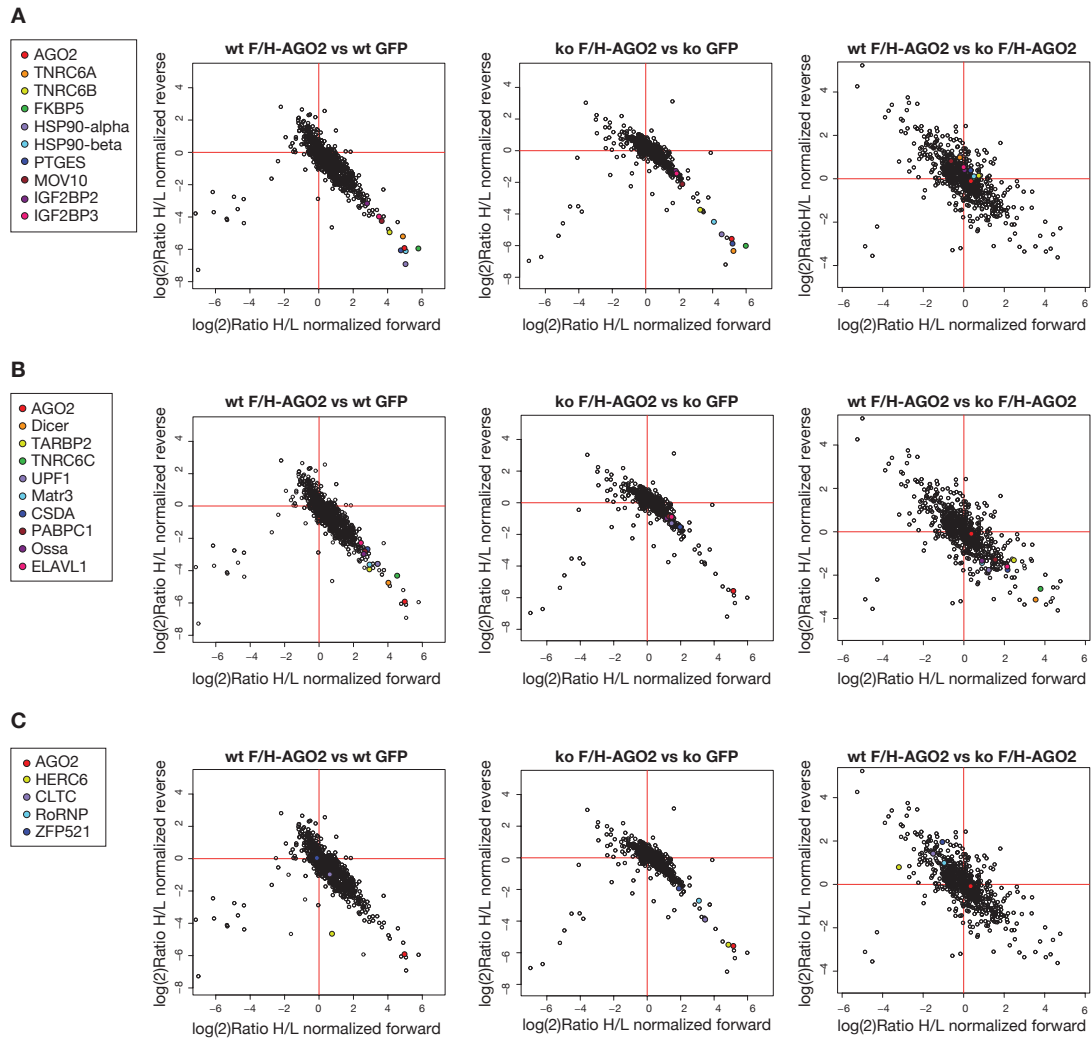
Figure 2.5.3: Identification of AGO2-associated proteins and the miRNA-requirement of the interaction. Logarithmized normalized ratios of forward and reverse experiments for F/H-AGO2 immunoprecipitations from Dicer wild type (wt), Dicer-depleted (ko) and Dicer wild type versus Dicer-depleted MEFs are plotted as described in Figure 2.5.2. Selected proteins binding to AGO2 A) independently of Dicer and miRNAs B) preferentially in the presence of Dicer and miRNAs and C) preferentially in the absence of Dicer and miRNAs are indicated in color.

suggested to be specific interactors (Tables 2.5.1, 2.5.2 and 2.5.3). Among the specific interactors more than 85% are RNA binding proteins or are involved in mRNA processing or degradation, translation or RNA-mediated gene silencing.

We compared our data set to two semiquantitative proteomic data sets for human F/H-AGO2-containing RNP complexes published by Höck and colleagues [127] and by
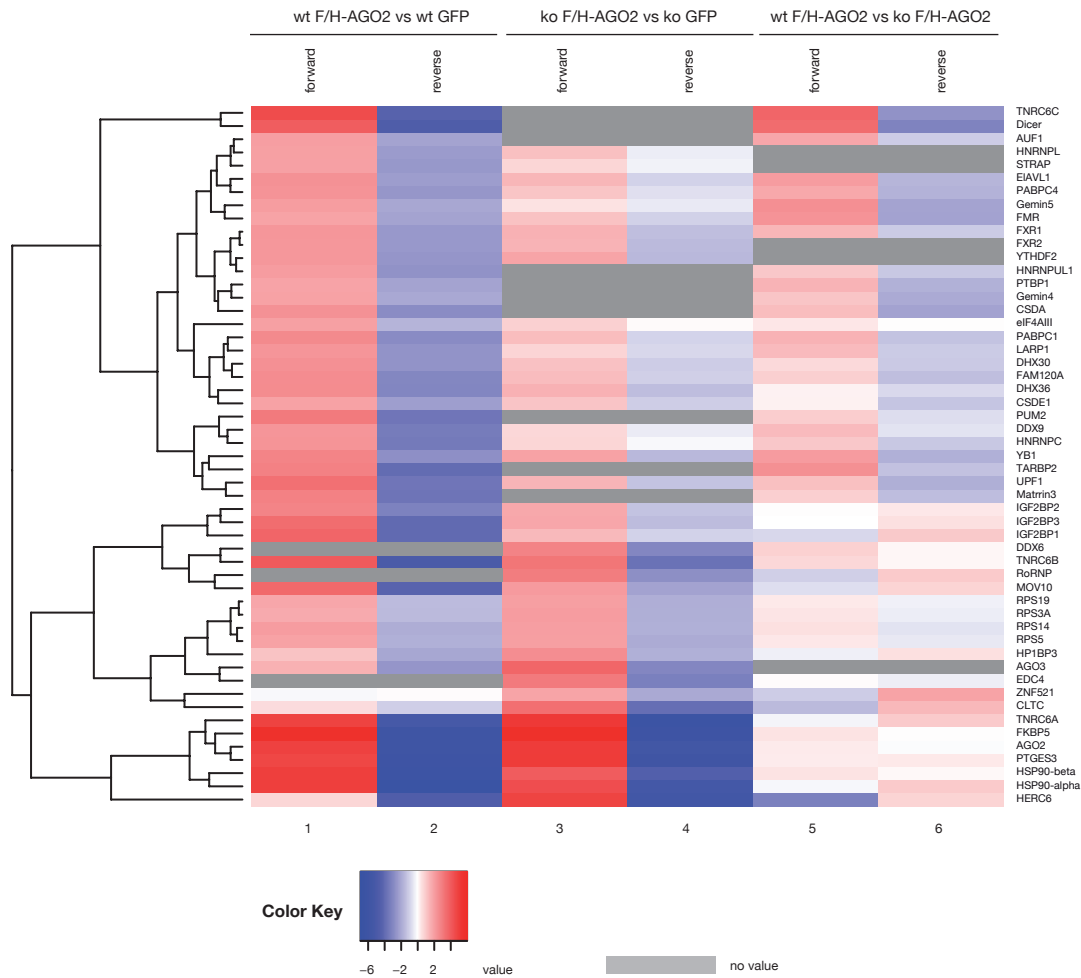
Figure 2.5.4: Hierachical clustering of AGO2-associated proteins and the miRNA requirement of the interaction. Logarithmized normalized ratios of proteins identified as AGO2 interactors either in the presence or absence of Dicer and miRNAs were used for clustering. Proteins included in the cluster analysis were required to have ratios above the cut off manually deduced from ratio distributions for each individual dataset and had to be identified in at least four out of the six measurements. Grey squares indicate that the protein was not quantified in an experiment whereas colors represent the values for the ratios. Red indicates values above, blue below and white around zero. The forward and reverse ratios for an outlier are characterized by a red-blue pair in columns one and two or three and four. Dicer- or miRNA-independent binders show ratios close to zero in the comparative experiment (column 5 and 6). Dicer- or miRNA-dependent interactors show a red-blue pair in these columns, whereas proteins binding preferentially in the absence of Dicer or miRNAs show a blue-red pair.
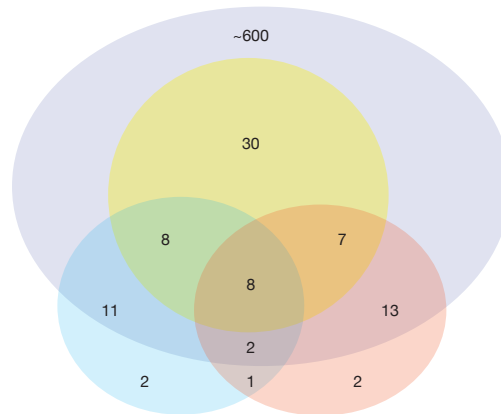
Figure 2.5.5: Comparison between the SILAC data for mouse and semiquantitative datasets for human F/H-AGO2-containing RNP complexes. The complete data set (purple) or outliers (yellow) of the SILAC data for mouse F/H-AGO2-containing RNP complexes were compared to data published by Höck and colleagues (red) [127] and by Landthaler and colleagues (blue) [171] for human F/H-AGO2-containing RNP complexes.

Landthaler *et al.* [171] (Figure 2.5.5). The datasets for human F/H-AGO2 contained around 30 proteins each and showed an overlap of 33%. When comparing the homologues murine proteins identified in at least two out of three of our SILAC datasets with both data sets for the human F/H-AGO2 complexes, we saw that our data covered 90% of the reported interactors from the human datasets. 42% of the proteins reported as AGO2 interactors in human were identified as outliers and therefore as specific interactors in the SILAC data for mouse AGO2 complexes as well. The other 48% of the interactors reported by Höck and Landthaler were classified as background binders in our SILAC approach. Among the outliers identified in our SILAC data, 28% have not been described as specific interactors of AGO2 so far.

We grouped the specific interactors according to the miRNA and Dicer dependency of their binding behavior. Among the proteins binding to AGO2 independently of the presence or absence of Dicer and thus mature miRNAs (Figure 2.5.3A, Table 2.5.1), we identified the heat shock proteins HSP90-alpha and HSP90-beta and their cochaperones FKBP5 and PTGES. HSP90 is involved in loading small RNAs into RISC in mammals and plants [134, 138, 148] and it regulates AGO2 localization [255]. The cochaperones FKBP5 and PTGES have not been described in AGO2 complexes before. Another protein showing miRNA-independent binding behavior is the putative helicase MOV 10 whose *Drosophila* homologue Armitage is involved in RISC formation [318]. Other proteins in this group are the mRNA binding proteins IGF2BP 1-3, PUM2, HN-

				wt F/H-AGO2 vs. wt GFP		ko F/H-AGO2 vs. wt GFP		wt F/H-AGO2 vs. ko F/H-AGO2	
Protein Name	**Gene Name**	**Uniprot ID**	**Keywords**	**Ratio H/L forward**	**Ratio H/L reverse**	**Ratio H/L forward**	**Ratio H/L reverse**	**Ratio H/L forward**	**Ratio H/L reverse**
Bait									
Protein argonaute-2	Eif2c2	Q8CJG0	RNA-mediated gene silencing	31,401	0,017	35,089	0,021	1,288	0,952
Proteins binding independently of the presence or absence of miRNAs and Dicer									
Peptidyl-prolyl cis-trans isomerase FKBP5	Fkbp5	Q64378	heteromultimeric cytoplasmic complex with HSP90 and HSP70	55,043	0,016	63,056	0,016	1,377	1,017
Heat shock protein HSP 90-alpha	Hsp90aa1	P07901	molecular chaperone ATPase activity	33,307	0,008	22,783	0,026	0,903	2,010
Heat shock protein 84b	Hsp90ab1	Q71LX8	molecular chaperone ATPase activity	33,102	0,015	16,950	0,044	1,401	1,066
Trinucleotide repeat-containing gene 6A protein	Tnrc6a	Q3UHK8	RNA mediated gene silencing	29,605	0,027	37,910	0,012	0,878	1,995
Prostaglandin E synthase 3	Ptges3	Q9R0Q7	molecular chaperone	27,236	0,015	36,365	0,017	1,270	1,301
Trinucleotide repeat-containing gene 6B protein	Tnrc6b	Q8BKI2	RNA-mediated gene silencing	17,280	0,032	9,537	0,075	1,665	1,106
Insulin-like growth factor 2 mRNA-binding protein 1	Igf2bp1	O88477	RNA binding mRNA translation and stabilty	13,611	0,064	2,622	0,537	0,571	2,068
Putative helicase MOV-10	Mov10	P23249	RNA-mediated gene silencing	12,604	0,053	4,575	0,229	0,645	1,757
Insulin-like growth factor 2 mRNA-binding protein 3	Igf2bp3	Q9CPN8	RNA binding mRNA translation and stabilty	11,289	0,064	3,601	0,372	1,002	1,452
Enhancer of mRNA-decapping protein 4	Edc4	QQ3UJB9	mRNA decapping	no value	no value	8,772	0,108	1,043	0,785
Probable ATP-dependent RNA helicase DDX6	Ddx6	P54823	mRNA degradation mRNA decapping	no value	no value	7,152	0,129	1,803	1,118
Pumilio homolog 2	Pum2	Q80U58	mRNA translation and stabilty mRNA 3'UTR binding	8,727	0,084	no value	no value	1,910	0,635
Insulin-like growth factor 2 mRNA-binding protein 2	Igf2bp2	Q5SF07	mRNA translation mRNA 5'UTR binding	6,983	0,112	3,477	0,406	1,023	1,330
Probable ATP-dependent RNA helicase DHX36	Dhx36	Q8VHK9	mRNA degradation mRNA deadenylation	6,003	0,125	2,961	0,379	1,165	0,585
Putative ATP-dependent RNA helicase DHX30	Dhx30	Q99PU8	RNA binding ATP dependent helicase	5,459	0,166	2,308	0,483	1,623	0,454
YTH domain family 2	Ythdf2	Q8K325	unknown function	4,820	0,175	3,732	0,350	no value	no value
40S ribosomal protein S14	Rps14	P62264	ribosomal protein	4,387	0,280	4,217	0,298	1,435	0,685
Heterogeneous nuclear ribonucleoprotein L	Hnrnpl	Q8R081	pre-mRNA binding	4,080	0,198	2,338	0,780	no value	no value
Eukaryotic initiation factor 4A-III	Eif4a3	Q91VC3	ATP dependent RNA helicase exon junction complex	4,077	0,319	1,841	1,053	1,350	1,025
Serine-threonine kinase receptor-associated protein	Strap	Q9Z1Z2	SMN complex	3,996	0,187	1,702	0,836	no value	no value
Cold shock domain-containing protein E1	Csde1	Q91W50	RNA binding	3,965	0,208	2,190	0,493	1,179	0,423
40S ribosomal protein S5	Rps5	P97461	ribosomal protein	3,951	0,299	4,169	0,273	1,337	0,740
40S ribosomal protein S19	Rps19	Q9CZX8	ribosomal protein	3,558	0,369	4,152	0,287	1,305	0,827
40S ribosomal protein S3a	Rps3a	P97351	ribosomal protein	3,337	0,362	4,435	0,294	1,370	0,776
Heterochromatin protein 1-binding protein 3	Hp1bp3	Q3TEA8	unknown function	2,229	0,248	5,788	0,297	0,815	1,439

Table 2.5.1: Specific interactors associating with AGO2 independently of the presence or absence of Dicer and miRNAs. Selected values are summarized for proteins identified to interact with AGO independently of the presence or absence of Dicer and miRNAs. Keywords describing reported functions were added.

RNPL, DHX30, several ribosomal proteins (RPS 19, 14, 5 and 3a) and the ARE binding protein DHX36/RHAU. We also found proteins involved in mRNA decay such as the decapping complex proteins EDC4 and DDX6/RCK. The AGO2-associated proteins TNRC6A and TNRC6B also showed a Dicer- and miRNA-independent binding behavior. We characterized several of the newly identified interactors as miRNA-independent interactors by their ratios, among them the uncharacterized protein YTHDFH2 and the heterochromatin binding protein HB1BP3. EIF4A3 also belongs to this group. This ATP-dependent RNA helicase is part of the Exon Junction Complex [38] that is required for the degradation of aberrant mRNAs through UPF1-mediated NMD [92, 93]. The two novel AGO2 interacting proteins STRAP/UNRIP [104] and CSDE1/UNR interact with poly-A binding proteins and are involved in translational repression in *Drosophila* [60, 61].

In Figure 2.5.3B and Table 2.5.2, we highlight proteins that bound to AGO2 preferen-

| Protein Name	Gene Name	Uniprot ID	Keywords	wt F/H-AGO2 vs. wt GFP		ko F/H-AGO2 vs. wt GFP		wt F/H-AGO2 vs. ko F/H-AGO2	
				Ratio H/L forward	Ratio H/L reverse	Ratio H/L forward	Ratio H/L reverse	Ratio H/L forward	Ratio H/L reverse
Bait									
Protein argonaute-2	Eif2c2	Q8CJG0	RNA-mediated gene silencing	31,401	0,017	35,089	0,021	1,288	0,952
Proteins preferentially binding in the presence of miRNAs and Dicer									
Trinucleotide repeat-containing gene 6C protein	Tnrc6c	Q3UHC0	RNA-mediated gene silencing	23,986	0,050	no value	no value	13,655	0,161
Endoribonuclease Dicer	Dicer	Q8R418	RNA-mediated gene silencing	16,371	0,037	no value	no value	11,599	0,115
Regulator of nonsense transcripts 1	Upf1	Q9EPU0	nonsense mediated mRNA decay	10,406	0,085	2,786	0,411	2,350	0,294
Matrin-3	Matr3	Q8K310	RNA binding nuclear matrix	7,601	0,081	no value	no value	1,867	0,378
RISC-loading complex subunit TARBP2	Tarbp2	P97473	RNA-mediated gene silencing	7,550	0,066	no value	no value	5,522	0,403
Nuclease-sensitive element-binding protein 1	Ybx1	P62960	transcription pre-mRNA splicing mRNA processing	7,006	0,158	3,917	0,348	4,475	0,300
Polyadenylate-binding protein 1	Pabpc1	P29341	poly(A) tail of mRNA binding	6,248	0,142	2,471	0,549	2,908	0,408
Constitutive coactivator of PPAR-gamma-like protein 1	FAM120A	Q6A0A9	RNA binding oxidative stress	6,071	0,129	2,512	0,516	1,861	0,385
ELAV-like protein 1	Elavl1	P70372	AU-rich element binding	5,352	0,204	2,716	0,530	4,400	0,325
Cold shock domain-containing protein A	Csda	Q9JKB3	mRNA binding translational repression transcription	5,349	0,144	no value	no value	2,444	0,229
Poly(A) binding protein, cytoplasmic 4	Pabpc4	Q99LF8	RNA binding	5,161	0,178	2,166	0,651	3,487	0,311
Heterogeneous nuclear ribonucleoproteins C1/C2	Hnrnpc	Q9Z204	pre-mRNA binding mRNA binding	5,136	0,093	1,691	0,919	2,079	0,446
ATP-dependent RNA helicase A	Dhx9	O70133	transcription RNA binding helicase	4,962	0,099	1,676	0,764	2,539	0,685
La-related protein 1	Larp1	Q6ZQ58	RNA binding	4,932	0,169	1,718	0,581	2,564	0,464
Fragile X mental retardation syndrome-related protein 1	Fxr1	Q61584	RNA binding	4,897	0,191	2,945	0,386	2,713	0,469
Fragile X mental retardation syndrome-related protein 2	Fxr2	Q9WVR4	RNA binding	4,806	0,190	2,855	0,360	no value	no value
Heterogeneous nuclear ribonucleoprotein U-like protein 1	Hnrnpul1	Q8VDM6	transcription mRNA processing and transport	4,388	0,161	no value	no value	2,087	0,438
Gem-associated protein 5	Gemin5	Q8BX17	RNA binding SMN complex	4,279	0,251	1,407	0,744	5,662	0,232
Heterogeneous nuclear ribonucleoprotein D	Hnrnpd	Q60668	3'UTR ARE binding	4,199	0,235	no value	no value	3,539	0,489
Gem (Nuclear organelle) associated protein 4	Gemin4	Q8K1K1	RNA binding SMN complex	3,916	0,257	no value	no value	2,172	0,267
Fragile X mental retardation protein 1 homolog	Fmr1	P35922	RNA binding RNA transport translation	3,849	0,232	2,270	0,527	5,165	0,231
Polypyrimidine tract binding protein 1	Ptbp1	P17225	pre-mRNA splicing	3,812	0,236	no value	no value	2,834	0,306

Table 2.5.2: Specific interactors preferentially associating with AGO2 in the absence of Dicer and miRNAs. Selected values are summarized for proteins identified as specific AGO2 interactors and keywords describing reported functions were added.

tially in the presence of Dicer and miRNAs. As expected, we found Dicer and its cofactor TARBP2 [43, 114] in this group, but we did not identify the reported Dicer cofactor PACT [167, 178] in any of the datasets. In contrast to the binding behavior of its paralogs TNRC6A and B, the interaction between TNRC6C and AGO2 seemed to be Dicer- and miRNA- dependent. The RNA helicase A/DHX9 has been implicated in siRNA loading [278] and is the only protein involved in RISC assembly that showed miRNA or Dicer dependency. A number of RNA binding proteins including YB1, Gemin 4 and 5, HNRNPC and HNRNPUL were found in this group along with the ARE binding proteins HNRNPD/AUF1 and ELAVL1/HuR, the cytoplasmic poly-A binding proteins 1 and 4, the mitochondrial protein Matrin3 as well as UPF1. The latter is involved in nonsense mediated mRNA decay and has been reported to function in the miRNA pathway [143]. The fragile X mental retardation protein and its paralog FXR2 have been reported to associate with AGO [37, 136] and Dicer activity [144] and the paralog FXR1 is involved in miRNA-regulated upregulation of translation [331, 332]. We also identified these

Protein Name	Gene Name	Uniprot ID	Keywords	wt F/H-AGO2 vs. wt GFP		ko F/H-AGO2 vs. wt GFP		wt F/H-AGO2 vs. ko F/H-AGO2	
				Ratio H/L forward	Ratio H/L reverse	Ratio H/L forward	Ratio H/L reverse	Ratio H/L forward	Ratio H/L reverse
Bait									
Protein argonaute-2	Eif2c2	Q8CJG0	RNA-mediated gene silencing	31,401	0,017	35,089	0,021	1,288	0,952
Proteins preferentially binding in the absence of miRNAs and Dicer									
Putative uncharacterized protein	Herc6	Q3UEA7	E3 ubiquitin-protein ligase ISGylation	1,690	0,040	28,888	0,022	0,109	1,732
Protein argonaute-3	Eif2c3	Q8CJF9	RNA-mediated gene silencing	2,976	0,176	13,360	0,129	no value	no value
Clathrin heavy chain 1	Cltc	Q68FD5	vesicel coating	1,537	0,507	10,934	0,068	0,360	2,680
60 kDa SS-A/Ro ribonucleoprotein	RoRNP	O08848	RNA binding protein	no value	no value	8,421	0,153	0,512	1,990
Zinc finger protein 521	Znf521	Q6KAS7	transcription factor	0,923	1,034	3,739	0,261	0,484	3,891

Table 2.5.3: Specific interactors preferentially associating with AGO2 in the presence of Dicer and miRNAs. Selected values are summarized for proteins identified as specific AGO2 interactors. Keywords describing reported functions were added.

proteins as Dicer- and miRNA-dependent AGO2 interactors. Among the newly identified AGO2 interacting proteins, we observed a preference for binding in the presence of miRNAs for the PABPC1-binding protein LARP1 [34], the mRNA binding protein FAM120A/Ossa, the YB1-associating protein PTBP1 [46] and for CSDA, a protein that shares cellular functions with YB1 [201].

The third group contains proteins that preferentially interacted with AGO2 in the absence of Dicer or miRNAs (Figure 2.5.3C, Table 2.5.3) and which are hereby described for the first time. In this group we found the RNA binding protein RoRNP [21], the zinc finger protein ZNF521 [28] and the vesicle coat protein Clathrin (CLTC). It was very interesting to see that AGO3 showed an increased association with AGO2 in the absence of Dicer and miRNAs. We also identified HERC6, a HECT-type E3 protein ligase that mediates conjugation of ISG15 to target proteins in human [351] in this group.

2.5.3 AGO2 Associates with Large RNAs Independently of the Presence or Absence of Dicer and Mature miRNAs

Our data revealed a high number of RNA binding proteins in complex with AGO2. The RNA binding proteins PUM2, IGF2BP1-3 and TNRC6A-C have been studied in respect to their bound mRNAs [115] recently and the role of the TNRC6 proteins in miRNA-dependent gene silencing is well established [324]. An analysis of PUM2-RNA target sites showed that these are enriched around predicted miRNA binding sites, which suggests a link between PUM2 and the miRNA pathway [91]. To our surprise, we noticed that these and other RNA binding proteins show a miRNA-independent binding behavior. If these proteins associate with AGO2 in an RNA-dependent manner as it has been reported for IGF2BP1 and 3 [127], this strongly suggests that AGO2 associates with large RNAs in
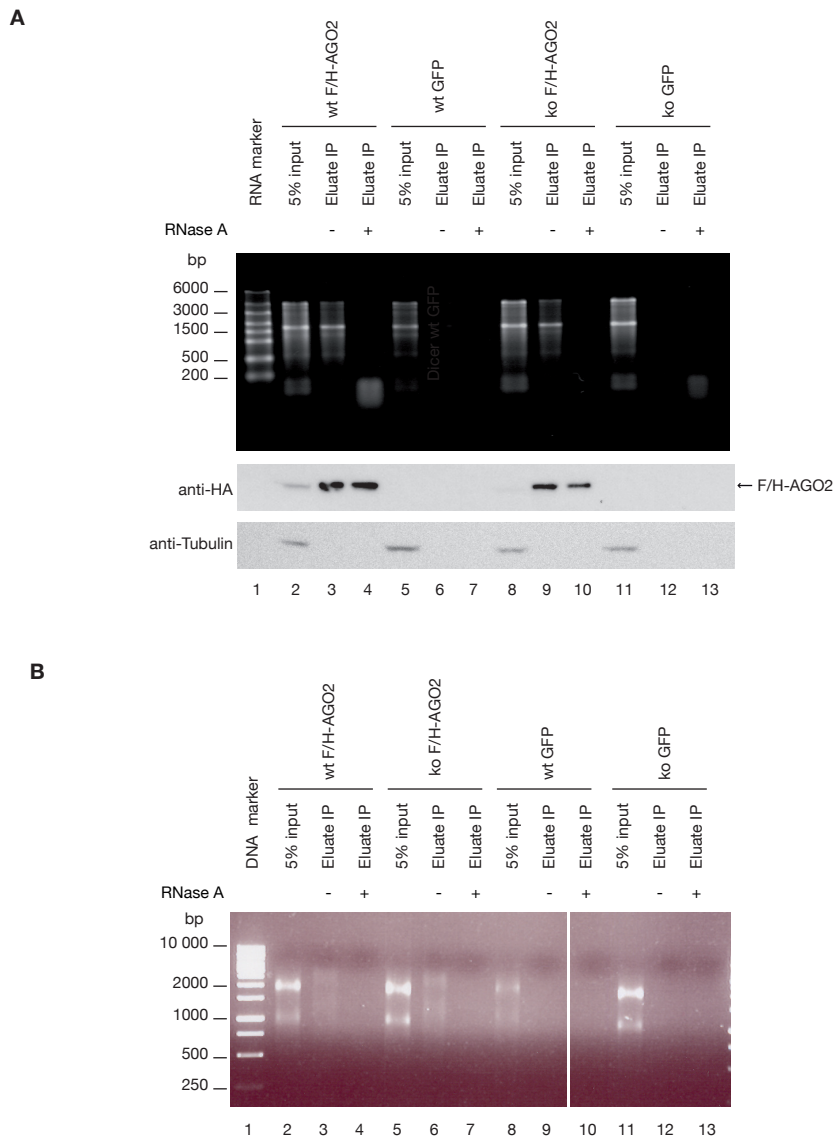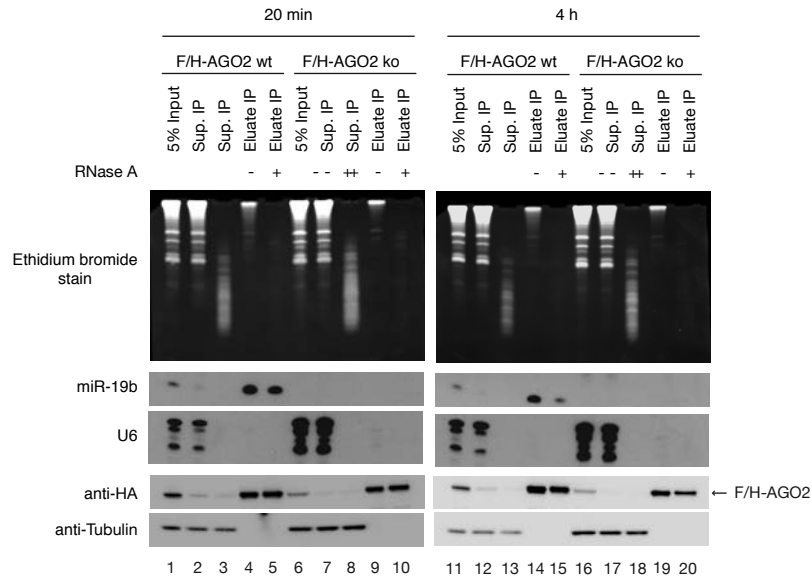
Figure 2.5.6: RNA-binding behavior of AGO2 in Dicer wild type and Dicer-depleted MEFs. A) AGO2-containing RNP complexes were precipitated from equal amounts of whole cell lysate from Dicer wild type (lanes 2-4) and Dicer-depleted (lanes 8-10) F/H-AGO2 expressing MEFs or from the corresponding GFP-expressing control cell lines (lanes 5-7 and 11-13) with (lanes 4, 7, 10 and 13) or without (lanes 3, 6, 9 and 12) RNase A treatment. RNA was isolated from immunoprecipitates and lysates and visualized by ethidiumbromide staining after size separation in an agarose gel (upper panel). The presence of AGO2 in the samples was analyzed by Western blot (middle panel). Tubulin was used as a loading control in the Western blot analysis (lower panel). B) A fraction of the extracted RNA samples were reverse transcribed into DNA using an oligo-(dT) primer. The first strand cDNA was separated according to size in an agarose gel and visualized by staining with ethidiumbromide.

the absence of Dicer and mature miRNAs. To test this hypothesis, we immunoprecipi-
tated F/H-AGO2-containing RNP complexes from the F/H-AGO2 expressing Dicer wild
type and Dicer-depleted MEF cell lines and extracted the bound RNAs (Figure 2.5.6A).
To be able to distinguish specifically bound RNAs from background, we used two dif-
ferent controls. First, we used the GFP expressing control cell lines and second, IPs
were treated with RNase A to completely degrade all contained RNAs. The RNAs were
analyzed in an agarose gel stained with ethidiumbromide (upper panel) and the AGO2
amount was assesed by Western blot analysis (middle panel). It is clearly visible that a
significant amount of large RNAs is bound to AGO2 in the Dicer depleted cells (lane 9),
suggesting that AGO2 may stably associate with large RNAs in the absence of miRNAs.
To analyze whether the large RNAs coprecipitating with AGO2 are polyadenylated, the
extracted RNAs were reverse transcribed into cDNA with oligo-d(T) primers and ana-
lyzed in an agarose gel stained with ethidiumbromide (Figure 2.5.6B). The detection of
oligo-d(T) primed cDNAs in the untreated IPs from the Dicer-wild type as well as the
Dicer-depleted cells suggests that the large RNAs associated with AGO2 in the absence
of Dicer and miRNAs contain polyadenylated RNAs.

2.5.4 The large RNA and MicroRNA Dependency of AGO2 Interactions Is Not Coupled

The observation that RNA binding proteins might associate with AGO2 through larger
RNAs bound independently of miRNAs sheds a new light on the role of large RNAs on the
protein composition of AGO2-containing RNPs. To be able to analyze the dependency
of the specific AGO2 interactors on the presence of large RNAs without disturbing the
influence of miRNAs on the binding behavior, it was necessary to establish conditions
under which large RNAs are completely degraded and miRNAs are still intact.
F/H-AGO2-containing RNPs were isolated from Dicer wild type or Dicer-depleted MEFs
and treated with RNAse A for either 20 min or 4 h at 4°C prior to the washing steps.
RNAs were isolated and analyzed by Northern Blotting (Figure 2.5.7). After RNAse A
treatments, no miRNAs were detected in the supernatants of the IPs. For the RNAse A
treated IPs, we saw a strong influence of the duration of the treatment on miRNA
stability. After a short treatment, the amount of miRNAs was only slightly reduced
compared to the untreated sample whereas a long treatment led to a strong reduction
of miRNAs. However, longer RNA species were effectively degraded with both the long
and the short RNAse A treatment. This experiment established a 20 min long treatment
with 100 µg/ml RNase A at 4°C as suitable conditions for the analysis of the large RNA
requirement without interfering with miRNA binding and stability.

Figure 2.5.7: Analysis of large RNA and miRNA degradation by RNase A treatment. AGO2-containing RNP complexes were precipitated from whole cell lysate from Dicer wild type (lanes 1-5 and 11-15) or Dicer-depleted (lanes 6-10 and 16-20) F/H-AGO2 expressing MEFs with (lanes 3, 5, 8, 10 and 13, 15, 18 and 19) or without (lanes 2, 4, 7, 9 and 12, 14, 17 and 20) treatment with 100 μg/ml RNase A for 20 min (left panel) or 4 h (right panel) at 4° C. RNA was isolated from lysate or immunoprecipitated F/H-AGO2, separated by 12% denaturing PAGE and visualized by ethidiumbromide staining (upper panel). The RNA was then blotted and probed for miR-19b (second panel). The membrane was stripped and reprobed with U6 to control equal loading of input RNA (third panel). The presence of AGO2 in the samples was analyzed by Western blot (fourth panel). Tubulin was used as a loading control in the Western blot analysis (lowest panel).

As observed previously (Figure 2.5.1B), the expression level of F/H-AGO2 was lower in the Dicer-depleted cells, which was compensated by increasing the amount of input sample to achieve full saturation of the binding capacity of the antibody for all experiments. The short RNase A treatment did not influence the amount of AGO2 protein in the IP but after the long treatment less AGO2 was present in the eluates. This observation is another indication for the importance of miRNA abundance on AGO2 stability.

We modified our SILAC based experimental set up for the analysis of the large RNA dependency of the interactions as shown in Figure 2.5.8. Immunoprecipitations for the isolation of AGO2-containing mRNPs were carried out from SILAC labeled F/H-AGO2 expressing Dicer wild type MEFs for each SILAC label separately as described before. To be able to see a large RNA dependency of the interaction, we degraded the RNA in the IP from the light labeled cells by treatment with RNase A for 20 min at 4° C directly
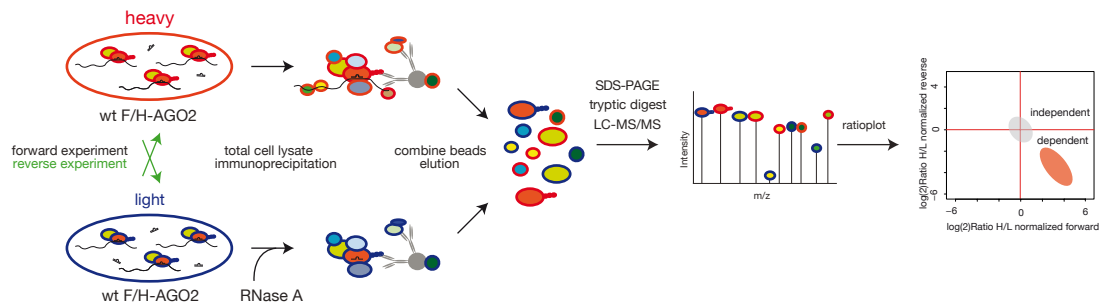
Figure 2.5.8: Experimental setup for the analysis of large RNA-dependent binding behavior of AGO2 interactors. The experimental setup shown in Figure 2.5.2 was adapted to analyze the large RNA dependency of the AGO2 interaction. F/H-AGO2-containing RNP complexes were immunoprecipitated from total cell lysates from SILAC labeled, F/H-AGO2-expressing Dicer wild type (wt F/H-AGO2) MEFs. One sample was treated with RNase A and beads were combined for elution after washing. For the reverse experiment, the label of the RNAse A treated sample was swapped. The large RNA-dependent AGO2 interactors are expected to show high H/L ratios in the forward and low ratios in the reverse experiment. Background binders show ratios around one in both experiments. The experiments were also carried out using the F/H-AGO2 expressing Dicer-depleted MEFs.

before the washing steps. The heavy labeled sample was not treated with RNase A and contained intact large RNAs. For the reverse experiments the heavy labeled sample was treated with RNAse A. The experiment was also carried out with the F/H-AGO2 expressing Dicer-depleted MEF cell line.

With 985 identifications the number of identified proteins in the Dicer-depleted cell line (ko F/H-AGO2, 20 min RNAse A treated) was lower then in the Dicer wild type cell lines (wt F/H-AGO2, 20 min RNAse A treated, 1074 identified proteins) as it was also the case for the previous experiments. We obtained 681 identifications in the Dicer wild type and 520 in the Dicer-depleted cell lines after filtering. We focused the analysis on those proteins already identified as potential interactors in previous experiments (see Section 2.5.2). The identification and quantification for the interactors was better in the data from the Dicer wild type cells than in the data set from the Dicer-depleted and reflects the higher number of identifications (Table 2.5.4). Seven interactors (EDC4, DDX6, FXR2, TARBP2, RoRNP, HERC6 and PUM2) either did not pass the filter criteria or were not identified at all in the datasets. All of these proteins had either low peptide numbers or were not identified in all of the measurements for the miRNA dependency experiment.

For the identified specific interactors, the data was visualized in ratio plots (Figure 2.5.9) and a heat map (Figure 2.5.10). In the heat map no cut off was set but only interactors

Protein Name	Gene Name	Uniprot ID	wt F/H-AGO2 20 min RNAse A treated		ko F/H-AGO2 20 min RNAse A treated	
			Ratio H/L forward	Ratio H/L reverse	Ratio H/L forward	Ratio H/L reverse
Bait						
Protein argonaute-2	Eif2c2	Q8CJG0	0,964	1,077	0,988	1,030
large RNA dependent interactors						
ELAV-like protein 1	Elavl1	P70372	23,522	0,075	no value	0,047
Heterogeneous nuclear ribonucleoprotein L	Hnrnpl	Q8R081	18,787	0,039	11,405	0,040
Putative helicase MOV-10	Mov10	P23249	17,880	0,026	15,032	0,084
Nuclease-sensitive element-binding protein 1	Ybx1	P62960	16,441	0,042	8,083	0,115
Insulin-like growth factor 2 mRNA-binding protein 1	Igf2bp1	O88477	16,224	0,028	13,345	0,043
Heterochromatin protein 1-binding protein 3	Hp1bp3	Q3TEA8	15,491	0,091	8,570	0,114
Insulin-like growth factor 2 mRNA-binding protein 3	Igf2bp3	Q9CPN8	15,403	0,040	10,633	0,058
Cold shock domain-containing protein A	Csda	Q9JKB3	14,131	0,035	no value	no value
Insulin-like growth factor 2 mRNA-binding protein 2	Igf2bp2	Q5SF07	13,066	0,046	10,980	0,064
Probable ATP-dependent RNA helicase DHX36	Dhx36	Q8VHK9	12,600	0,042	6,981	0,117
Poly(A) binding protein, cytoplasmic 4	Pabpc4	Q99LF8	11,727	0,071	6,775	0,117
Polyadenylate-binding protein 1	Pabpc1	P29341	10,879	0,071	5,477	0,118
Regulator of nonsense transcripts 1	Upf1	Q9EPU0	9,236	0,081	6,314	0,133
Heterogeneous nuclear ribonucleoprotein U-like protein 1	Hnrnpul1	Q8VDM6	9,222	0,088	no value	no value
Heterogeneous nuclear ribonucleoproteins C1/C2	Hnrnpc	Q9Z204	7,047	0,112	no value	no value
La-related protein 1	Larp1	Q6ZQ58	6,910	0,107	4,889	0,189
40S ribosomal protein S14	Rps14	P62264	6,142	0,161	5,439	0,170
Polypyrimidine tract binding protein 1	Ptbp1	P17225	4,806	0,224	no value	no value
Constitutive coactivator of PPAR-gamma-like protein 1	FAM120A	Q6A0A9	4,762	0,186	2,808	0,299
ATP-dependent RNA helicase A	Dhx9	O70133	4,561	0,233	1,856	0,498
Eukaryotic initiation factor 4A-III	Eif4a3	Q91VC3	4,505	0,202	1,350	0,583
Putative ATP-dependent RNA helicase DHX30	Dhx30	Q99PU8	4,105	0,219	no value	no value
Fragile X mental retardation protein 1 homolog	Fmr1	P35922	3,847	0,245	no value	0,430
Matrin-3	Matr3	Q8K310	3,789	0,201	2,140	0,331
Proteins binding preferntially in the presence of large RNAs						
40S ribosomal protein S19	Rps19	Q9CZX8	3,604	0,319	3,291	0,332
Fragile X mental retardation syndrome-related protein 1	Fxr1	Q61584	3,208	0,276	1,885	0,601
40S ribosomal protein S5	Rps5	P97461	3,115	0,356	2,764	0,374
Gem-associated protein 5	Gemin5	Q8BX17	2,181	0,383	0,792	1,100
Heterogeneous nuclear ribonucleoprotein D	Hnrnpd	Q60668	2,139	0,397	no value	no value
Gem (Nuclear organelle) associated protein 4	Gemin4	Q8K1K1	1,918	0,462	0,756	1,205
YTH domain family 2	Ythdf2	Q8K325	1,915	0,329	no value	0,326
Serine-threonine kinase receptor-associated protein	Strap	Q9Z1Z2	1,591	0,458	no value	no value
Cold shock domain-containing protein E1	Csde1	Q91W50	1,569	0,437	1,512	0,648
direct interactors						
Clathrin heavy chain 1	Cltc	Q68FD5	1,152	0,991	0,911	1,024
Zinc finger protein 521	Znf521	Q6KAS7	1,027	0,864	0,810	0,785
Heat shock protein HSP 90-alpha	Hsp90aa1	P07901	1,005	1,096	1,007	1,055
Heat shock protein 84b	Hsp90ab1	Q71LX8	1,003	1,118	1,018	1,084
Endoribonuclease Dicer	Dicer	Q8R418	0,992	0,843	no value	no value
Protein argonaute-3	Eif2c3	Q8CJF9	0,990	1,059	no value	no value
Peptidyl-prolyl cis-trans isomerase FKBP5	Fkbp5	Q64378	0,973	1,147	0,980	0,968
Prostaglandin E synthase 3	Ptges3	Q9R0Q7	0,960	1,345	0,861	1,242
Trinucleotide repeat-containing gene 6C protein	Tnrc6c	Q3UHC0	0,916	1,101	no value	no value
Trinucleotide repeat-containing gene 6B protein	Tnrc6b	Q8BKI2	0,894	1,080	0,784	1,073
Trinucleotide repeat-containing gene 6A protein	Tnrc6a	Q3UHK8	0,865	0,975	0,836	0,896

Table 2.5.4: Large RNA dependency of specific AGO2 interaction partners. Selected values are listed for proteins previously identified as specific AGO2 interactors. The data was visualized by ratio plots (Figure 2.5.9) and a heat map (Figure 2.5.10).

identified in at least two out of the four measurements were included. Proteins were not clustered but displayed in the heat map according to the ratios of the forward experiment ratios in the Dicer wild type cells. Interactors associating with AGO2 in a large RNA-dependent way appeared as outliers in the lower right quadrant in ratio plots and showed intensively colored red-blue ratio pairs in the heat map. The binding of the interactors that bind to AGO2 via protein-protein interactions was not affected by the RNase A treatment and therefore these proteins appeared together with the background binders in the ratio plots and showed white or weak coloring in the heat map.
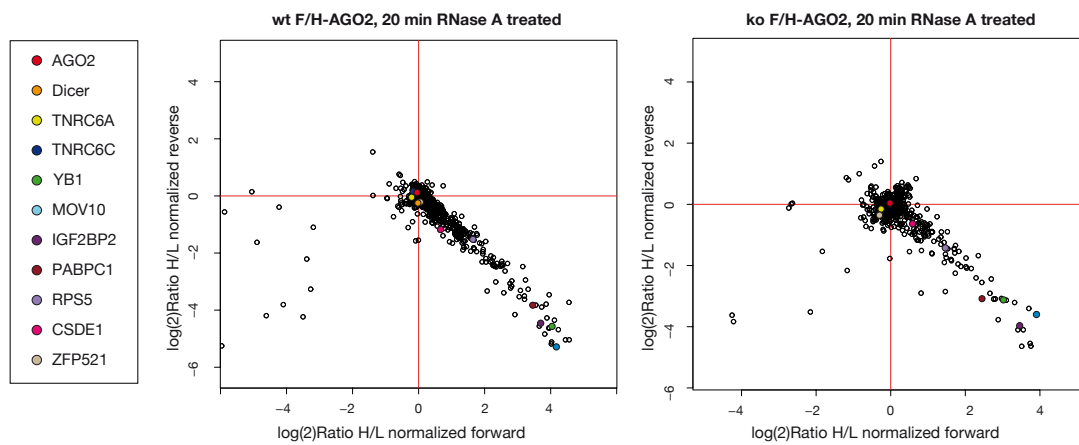
Figure 2.5.9: Ratio plots for the large RNA requirement of AGO2 interacting proteins. Normalized H/L ratios were plotted as described in Figure 2.5.8. Every dot represents an identified and quantified protein. Selected proteins are indicated in color.

We saw a high number of proteins that associate with AGO2 in a strongly large RNA-dependent manner. In this group we found many RNA binding proteins including IGF2BP1-3, RHAU/DHX36, PUM2, DHX30, HNRNPL, HNRNPUL and the ribosomal proteins RPS14 and RPS3a. Other large RNA-dependent binders were MOV10 and HP1BP3. All these proteins showed a miRNA-independent binding behavior and therefore associated with AGO2 via large RNAs bound to AGO2 independently of the presence or absence of miRNAs.

Among the Dicer- and miRNA-dependent interactors, UPF1, FAM120A, PTBP1, YB1, CSDA, FMR, HNRNPD/AUF1, ELAVL1/HuR, Matrin3, HNRNPC and LARP1 exhibited a strong large RNA requirement for their association with AGO2. PABPC1 and 4 also associated with AGO2 in a large RNA-dependent way. This binding behavior indicates that they associated with AGO2 via large RNAs bound to AGO2 only in the presence of miRNAs and Dicer.

A group of proteins showed a preference for binding to AGO2 when large RNAs were present. Here, we saw members of the group of miRNA-independent binders (RPS19 and 5, YTHDF2, STRAP and CSDE1) and the miRNA-dependent interactors FXR1, HNRNPD/AUF1 as well as Gemin 4 and 5. This subgroup appeared to be enriched on large RNAs specifically bound by AGO2 in the presence of miRNAs and Dicer but could also be found on large RNAs associated with AGO2 in the absence of miRNAs and Dicer.

A set of proteins associated with AGO2 in a large RNA-independent manner. This
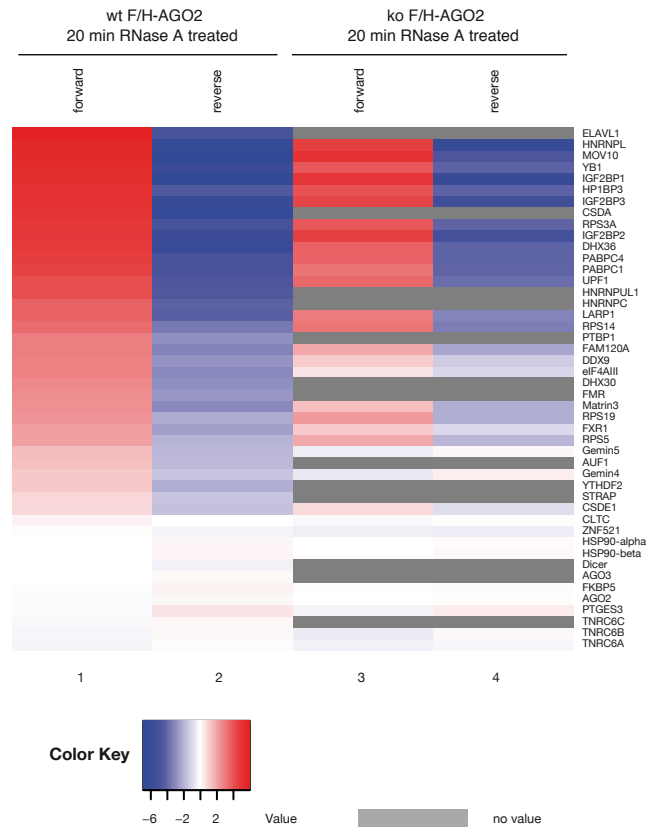
Figure 2.5.10: Heat map analysis of the large RNA requirement of AGO2 interactions. The normalized H/L ratios are displayed in form of a heat map. Red indicates values above, blue below and white around zero. Grey squares indicate that the protein was not quantified in the experiment. The color intensity indicates the strength of the large RNA dependency. Proteins were not clustered but sorted according to the ratio in the forward experiment for the Dicer-wild type sample.

includes the TNRC6 proteins that directly interact with AGO2 via their N-terminal GW-repeat containing region [324]. This direct interaction did not require Dicer and miRNAs for TNRC6A and B. TNRC6C on the other hand showed a strong dependency on Dicer and miRNAs. Dicer and AGO2 interact directly via the AGO PIWI-box and the RNase III domain of Dicer [311], so this interaction is also clearly RNA-independent. Other Dicer- and miRNA-independent interactors directly associating with AGO2 in an RNA independent manner were the HSP90 alpha and beta proteins with their cochaperones PTGES and FKBP5. Among the interactors preferentially binding to AGO2 in the absence of Dicer and miRNAs, only AGO3, CLTC and ZNF521 were identified in the datasets and they all showed a direct protein-protein binding behavior.
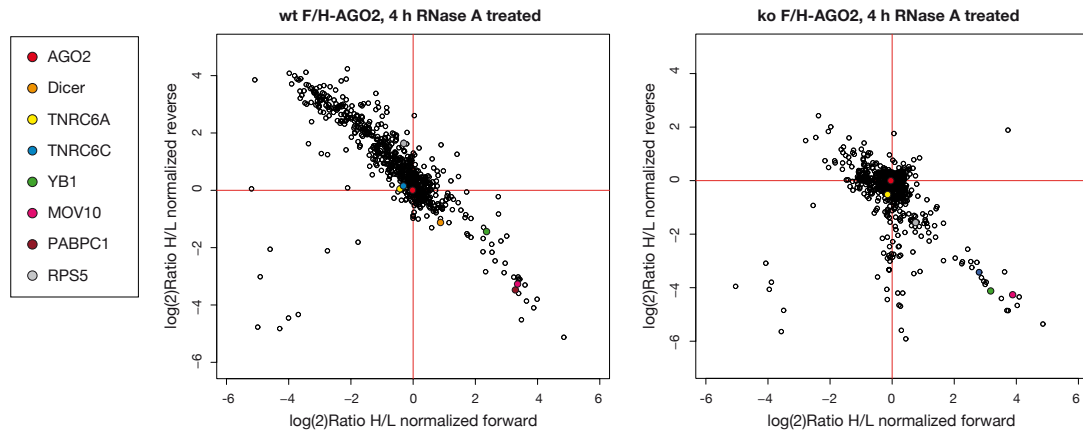
Figure 2.5.11: Ratio plots for the large RNA requirement of AGO2 interacting proteins after long RNase A treatment. H/L ratios were plotted as described in Figure 2.5.8. Selected proteins are indicated in color.

For the two proteins DHX9 and eIF4AIII the ratios between the data sets from wild type and Dicer-depleted cells showed an inconsistency, making it impossible to clearly define their binding behavior. According to the ratios they are strongly RNA-dependent binders in the wild type cells but in the Dicer-depleted cells they showed only weak large RNA dependency (Table 2.5.4 and Figure 2.5.10). This could be attributed to the quality differences of the data sets or it might indicate that the two proteins have different functions in the presence and absence of mature miRNAs and Dicer.

To be able to compare the influence of the duration of the RNase A treatment on the stability of the AGO2-containing RNPs, we measured samples treated with RNase A for 4 h in the same setup as for the samples treated for 20 min only. The datasets were of comparable size (1169 and 1202 identifications for the Dicer wild type (F/H-AGO2 wt, 4 h RNAse A treated) and Dicer-depleted (F/H-AGO2 ko, 4 h RNAse A treated) cell lines, respectively) and over 50% of identified proteins passed the filter criteria. Final datasets contained 679 proteins in the Dicer wild type and 647 proteins in the Dicer-depleted experiments. In the visualization of the data as ratio plots (Figure 2.5.11), we observed scattering of the datapoints and tailing into the upper left quadrant. This tailing is very strong for the experiment in the Dicer wild type cells and is an indication for significant changes in protein composition in the sample upon degradation of miRNAs and large RNAs.

Despite comparable or even higher numbers of proteins in the datasets, the number of previously identified AGO2 interactors was lower than in the samples treated with

Protein Name	Gene Name	Uniprot ID	wt F/H-AGO2 4 h RNAse A treated		ko F/H-AGO2 4 h RNAse A treated	
			Ratio H/L forward	Ratio H/L reverse	Ratio H/L forward	Ratio H/L reverse
Bait						
Protein argonaute-2	Eif2c2	Q8CJG0	0,980	1,011	0,964	0,999
large RNA dependent interactors						
ELAV-like protein 1	Elavl1	P70372	28,757	0,029	17,041	0,049
Heterogeneous nuclear ribonucleoprotein L	Hnrnpl	Q8R081	10,390	0,117	11,460	0,047
Putative helicase MOV-10	Mov10	P23249	10,340	0,104	14,660	0,051
Nuclease-sensitive element-binding protein 1	Ybx1	P62960	5,079	0,375	9,116	0,057
Insulin-like growth factor 2 mRNA-binding protein 1	Igf2bp1	O88477	14,699	0,058	13,349	0,035
Heterochromatin protein 1-binding protein 3	Hp1bp3	Q3TEA8	2,749	1,396	6,877	0,092
Insulin-like growth factor 2 mRNA-binding protein 3	Igf2bp3	Q9CPN8	10,409	0,104	8,999	0,058
Cold shock domain-containing protein A	Csda	Q9JKB3	no value	no value	no value	no value
Insulin-like growth factor 2 mRNA-binding protein 2	Igf2bp2	Q5SF07	10,365	0,123	7,982	0,068
Probable ATP-dependent RNA helicase DHX36	Dhx36	Q8VHK9	4,757	0,312	4,804	0,122
Poly(A) binding protein, cytoplasmic 4	Pabpc4	Q99LF8	10,490	0,083	7,738	0,074
Polyadenylate-binding protein 1	Pabpc1	P29341	9,887	0,089	6,968	0,093
Regulator of nonsense transcripts 1	Upf1	Q9EPU0	12,494	0,069	7,344	0,081
Heterogeneous nuclear ribonucleoprotein U-like protein 1	Hnrnpul1	Q8VDM6	3,317	0,350	no value	no value
Heterogeneous nuclear ribonucleoproteins C1/C2	Hnrnpc	Q9Z204	1,542	1,226	no value	no value
La-related protein 1	Larp1	Q6ZQ58	6,205	0,182	5,786	0,123
40S ribosomal protein S14	Rps14	P62264	0,512	2,412	1,451	0,423
Polypyrimidine tract binding protein 1	Ptbp1	P17225	3,630	0,321	no value	no value
Constitutive coactivator of PPAR-gamma-like protein 1	FAM120A	Q6A0A9	2,223	0,458	no value	no value
ATP-dependent RNA helicase A	Dhx9	O70133	0,376	4,483	1,066	0,729
Eukaryotic initiation factor 4A-III	Eif4a3	Q91VC0	1,471	1,181	0,860	0,833
Putative ATP-dependent RNA helicase DHX30	Dhx30	Q99PU8	0,277	5,592	0,535	0,713
Fragile X mental retardation protein 1 homolog	Fmr1	P35922	no value	no value	no value	no value
Matrin-3	Matr3	Q8K310	4,743	0,226	2,637	0,231
Proteins binding preferntially in the presence of large RNAs						
40S ribosomal protein S19	Rps19	Q9CZX8	0,866	3,072	1,744	0,343
Fragile X mental retardation syndrome-related protein 1	Fxr1	Q61584	0,139	9,027	0,277	1,670
40S ribosomal protein S5	Rps5	P97461	0,812	3,183	1,685	0,339
Gem-associated protein 5	Gemin5	Q8BX17	1,132	0,822	0,685	1,100
Heterogeneous nuclear ribonucleoprotein D	Hnrnpd	Q60668	1,627	0,685	no value	no value
Gem (Nuclear organelle) associated protein 4	Gemin4	Q8K1K1	no value	no value	0,551	1,320
YTH domain family 2	Ythdf2	Q8K325	1,668	0,581	no value	no value
Serine-threonine kinase receptor-associated protein	Strap	Q9Z1Z2	no value	no value	no value	no value
Cold shock domain-containing protein E1	Csde1	Q91W50	0,463	3,007	no value	no value
direct interactors						
Clathrin heavy chain 1	Cltc	Q68FD5	0,569	2,627	0,693	1,192
Zinc finger protein 521	Znf521	Q6KAS7	no value	no value	0,753	0,882
Heat shock protein HSP 90-alpha	Hsp90aa1	P07901	1,051	0,968	0,936	0,990
Heat shock protein 84b	Hsp90ab1	Q71LX8	1,020	0,978	0,966	1,030
Endoribonuclease Dicer	Dicer	Q8R418	1,836	0,470	no value	no value
Protein argonaute-3	Eif2c3	Q8CJF9	no value	no value	no value	no value
Peptidyl-prolyl cis-trans isomerase FKBP5	Fkbp5	Q64378	1,021	0,927	0,965	1,157
Prostaglandin E synthase 3	Ptges3	Q9R0Q7	1,839	0,505	0,974	1,097
Trinucleotide repeat-containing gene 6C protein	Tnrc6c	Q3UHC0	0,812	1,095	no value	no value
Trinucleotide repeat-containing gene 6B protein	Tnrc6b	Q8BKI2	0,875	1,050	0,779	1,062
Trinucleotide repeat-containing gene 6A protein	Tnrc6a	Q3UHK8	0,905	0,704	0,905	0,704

Table 2.5.5: Large RNA requirement of specific AGO2 interaction partners after long RNase A treatment. Selected values are listed for proteins previously analyzed in Table 2.5.4. The data was visualized in the ratio plots in Figure 2.5.11.

RNAse A for only 20 min (Table 2.5.5). The majority of the identified specific AGO2 interactors showed the same large RNA dependency as in the samples with the short RNase treatment, for example PABPC1, MOV10 and YB1 (strong large RNA dependency) and TNRC6A (direct protein-protein interaction). However, in the group of proteins classified to bind preferentially in the presence of large RNAs, the deviation of the binding behavior between the short and the long RNAse A treatment is quite strong. One example is the protein FXR1, which was shown to bind to AGO2 preferentially in the presence of Dicer and miRNAs in our previous experiments. FXR1 was shifted into the upper left quadrant in the long RNase A treated samples, which is an indication for an

increased binding to AGO2 in the absence of large RNAs and the decreased abundance of miRNAs. In the short RNase A treated samples, FXR1 appeared in the lower right quadrant and was classified to bind preferentially in the presence of large RNAs (see Figure 2.5.9 and Table 2.5.4). RPS5, a protein associating with AGO2 independently of the presence of absence of miRNAs and Dicer, showed a weak large RNA-dependent binding behavior in the short RNase A treated samples as well as in the long RNAse A treated samples from the Dicer-depleted cells. Contrary to the similar behavior in those three samples, RPS5 was shifted into the upper left quadrant in the long RNAse A treated Dicer wild type sample. Taken together, these observations suggested that the long treatment with RNase A leading to the degradation of miRNAs within the AGO2 protein did not only lead to the destabilization of Dicer- and miRNA-dependent interactions and a reduced stability of AGO2 itself (see Figure 2.5.7) but might also destabilize miRNA-independent interactions. It is possible that, as indicated by the low number of reported interactors identified in this experiment, the AGO2-containing RNPs dissociated upon the degradation of large RNAs and AGO2-bound miRNAs. As a consequence of the reduced size of the specifically bound AGO2-containing RNP complexes, more surface of the agarose matrix becomes available for non-specific binding and the amount of background binders increases, as indicated by the strong tailing observed in the ratio plots (Figure 2.5.11).

2.5.5 Verification of Interactions and Their RNA Dependency by Western Blot Analysis

In general, the identification of proteins by mass spectrometry is very reliable when stringent filter criteria are applied. The great progress in the field of quantitative proteomics now even allows a reliable quantitation of proteins by mass spectrometry and facilitates the confidential identification of interaction partners by AP-MS. Nevertheless, for our data a false discovery rate of 1% remains and it is necessary to verify the data using a second, independent method. Therefore, we performed Western Blot analysis of a subset of identified AGO2 interactors (Figure 2.5.12). F/H-AGO2-containing RNP complexes were immunoprecipitated from the F/H-AGO2-expressing cell lines. To test the RNA dependency of the interactors, a set of samples was treated with RNase A for 4 h. IPs from the GFP expressing control cell lines served as background control. Equal amounts of AGO2 were loaded for the analysis to allow for a direct comparison of protein amounts. We selected twelve antibodies specific against various of the interactors and tested the F/H-AGO2 immunoprecipitation for the presence of these proteins by Western blotting. Of the twelve antibodies, only four showed no or only low background signals

Figure 2.5.12: Western Blot analysis of identified AGO2 interactors. F/H-AGO2-containing RNP complexes were immunoprecipitated from the MEF cell lines as described before (lanes 1, 2, 5 and 6). To analyze the large RNA dependency of the interaction, the samples were treated with RNase A for 4h at 4°C (lanes 3 and 4). IPs from the GFP-expressing cell lines were used as controls for background binding (lanes 5 and 6). Proteins were separated by SDS-PAGE, transferred to membrane and probed with antibodies against the endogenous proteins or the HA-tag. Arrows indicate signals specific for the target protein, asterisks indicate background signals.
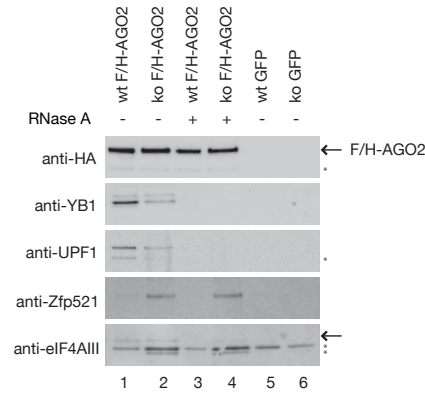
and detectable signals at the expected size. The others either showed no signals at all, no signal at the size expected for their target protein or a vast number of additional, strong and non-specific bands that greatly reduced our confidence in the specificity of the antibody.

YB1 and UPF1 were both found to be miRNA- and large RNA-dependent interactors in our mass spectrometry approach. In the Western blot analysis, we saw a strong signal in the Dicer wild type sample and a reduced signal in the Dicer-depleted cells for these two proteins. This validated the miRNA dependency of the interaction. The large RNA requirement of the interaction was confirmed by the disappearance of the signal after RNAse A treatment. The Western blot signals were specific as can be seen by the absence of signals in the control samples. ZNF521 is a protein that directly interacts with AGO2 in the absence of miRNAs and Dicer. As predicted based on the mass spectrometry data, we saw signals in the samples from the Dicer-depleted cells only and the signal intensity was not affected by the RNAse treatment. The lowest panel shows the Western blot analysis of eIF4AIII. This protein is a Dicer- and miRNA-independent interactor and bound equally in the Dicer wild type and Dicer-depleted cells according to our mass spectrometry data. The ratios for the large RNA dependency differed between the two cell lines. In the Dicer wild type cell lines, the interaction showed a strong large RNA dependency and we also observed that there was no signal in the western blot for the RNase A treated Dicer wild type sample. In the Dicer-depleted cells, the large RNA requirement seemed to be reduced and in accordance with the mass spectrometry data, we still observed a very weak signal in the RNAse A treated sample.

In summary, the results of the Western blot analysis were in good agreement with the mass spectrometry data and supported our results.

3 Discussion

3.1 Single-Particle Electron Microscopy Analysis of the AGO2 Complex I and Methylosome Components

Our current knowledge of the architecture of AGO and Dicer derives from crystallization studies of full length homologous proteins from archaea or unicellular eukaryotes [207, 258, 344, 345]. For eukaryotic AGO and Dicer, structural insights are only available for individual domains or truncated proteins [26, 27, 59, 85, 206, 305, 312]. These crystal structures reveal detailed information about the individual proteins and their catalytic functions, but they do not give insights into the structural details underlying the interaction between the RISC components. Therefore, we aimed to analyze the structure of the human RISC loading complex by electron microscopy to gain insights into RISC architecture and the mechanism of RISC loading.

The human RISC loading complex consists of AGO2, Dicer and TRBP [102, 208, 212]. We assumed that the AGO2 complex I described by Höck *et al.* [127] corresponds to the RISC loading complex and we refined the purification strategy to isolate this complex from HEK cells. In the last purification step, a GraFix gradient designed to gradually cross-link protein complexes while simultaneously separating them according to their size, the AGO2 complex I subdivided into free AGO2 and a heterodimeric complex consisting of AGO2 and Dicer. TRBP was not copurified with the AGO2-Dicer complex in this experimental set up. RISC assembly in *Drosophila* involves two intermediate complexes [318] and it is possible that the free AGO2 and the AGO2-Dicer heterodimer represent similar intermediate complexes in human. Micrographs of negatively stained GraFix fractions containing the AGO2-Dicer complex revealed a low number of particles with a strong heterogeneity that were not suitable for 3D reconstruction. This heterogeneity is very likely caused by dissociation of the complex during sample preparation. In 2009, Wang *et al.* [342] presented a low resolution structure of a reconstituted human RISC loading complex reconstructed by single particle EM analysis. They reported similar problems with complex stability at the dilute conditions applied during sample preparation for the negative stain EM analysis. In their hands, the AGO2-Dicer complex dissociated completely during grid preparation. This instability of the complex reflects

a very low affinity among the RLC components. The complex is stabilized by the addition of TRBP, probably by enhancing the affinity of Dicer for AGO2 [43]. However, we did see a rather stable AGO2-Dicer complex without TRBP until the grid preparation. In the hands of Wang *et al.*, GraFix stabilized ternary RLC particles appeared mono-dispersed in EM and facilitated the reconstruction of the RLC structure with a resolution of 33 Å [342]. Dicer has a distinct L-shape in which the base branch is constituted by the DEXH/D domain. AGO2 binds in a way that it connects with the top and the base branch of Dicer, giving the complex an overall triangular structure. TRBP binds to the Dicer DEXH/D domain [114, 167] and additional densities observed at the base branch of Dicer might correspond to TRBP in this study [342]. A simultaneously published study presented the EM structure of the Dicer-TRBP complex with the moderate resolution of 18 Å [173]. In this study Dicer likewise has an L-shape structure and the higher resolution reveals a surface trench for dsRNA binding. The dimeric TRBP-Dicer complex is very stable and sample preparation for EM analysis did not require cross-linking. This is a clear indication that the affinity of Dicer to its cofactor TRBP is significantly higher than its affinity for AGO2 and is in support of the theory that TRBP enhances the affinity between AGO2 and Dicer. For further insights into the RLC structure, for example the identification of individual proteins and domains, it is necessary to improve quality and resolution of the structure. One approach is to use cryo-EM since it is possible that the RLC is more stable during vitrification than during grid preparation for negative stain. This approach requires highly concentrated, pure RLC and an input sample with this quality is more likely to be provided by an *in vitro* reconstitution approach than by the purification of the complex from human cells.

During our efforts to establish a purification strategy for the AGO2 complex I, we frequently copurified the methylosome core components PRMT5 and MEP50. PRMT5 symmetrically dimethylates the PIWI proteins in mouse, fly and *X. laevi* and these posttranslational modifications are required for the interaction of PIWI proteins with TDRD proteins [304]. The methylosome stably associates with murine and fly PIWI proteins and has been observed in FLAG-based purification procedures for AGO2 [221]. We showed that the copurification of this protein complex is not based on a specific interaction between the methylosome and AGO2. It has been previously observed that the methylosome components are contained in FLAG immunoprecipitations [23]. We now established it as a cross-reactivity of the FLAG agarose matrix used for the immunoprecipitation. We utilized this unspecific affinity to isolate endogenous PRMT5-MEP50 complex from HEK cells. With this highly pure sample of the PRMT5-MEP50 complex at hand, we aimed to reconstruct the methylosome core structure by single particle EM

analysis. Electron micrographs of the GraFix cross linked, negatively stained complex showed that the sample contains particles with varying sizes and structural features. We tried to reconstruct the structure but the refinement of an initial model failed despite our efforts to reduce sample heterogeneity by sub-classifying the particles according to their size. Endogenous PRMT5 forms homo-oligomeric complexes and is mostly present as tetramers [275]. Our purified endogenous PRMT5-MEP50 complex had an approximate size of 300 kDa, which corresponds to the size of a PRMT5 tetramer in association with one MEP50 protein. It is suggested that large endogenous PRMT5 homo-oligomeric complexes are very unstable and dissociate into smaller, more stable complexes during the purification procedure [275]. Therefore, it is possible that our sample contained oligomeric complexes that dissociated into smaller complexes during grid preparation. This theory is supported by the fact that non-cross-linked PRMT5-MEP50 particles showed an even stronger heterogeneity after negative staining. PRMT5 has an indiscriminate activity towards a variety of substrates and depends on the association with adapter proteins for substrate specificity [108, 261]. The best characterized of these adapter proteins is pICln, a methylosome component that stimulates the methylation of Sm proteins through PRMT5 [87, 218]. It enhances the solubility and activity of recombinant PRMT5 [261], an observation which indicates that the adapter proteins might be important for methylosome stability. We do not detect adapter proteins or substrates in our sample preparations and it might be possible that the absence of these proteins further contributes to the instability of the methylosome core complex.

So far the molecular mechanism underlying the association of PRMT5 to the PIWI proteins remains unknown. Future projects such as the recently initiated reconstruction of an *in vitro* reconstituted methylosome in combination with a PIWI protein as substrate will give insights into methylosome architecture and substrate binding and will provide a better understanding of PRMT5 function.

3.2 The Mouse AGO2 Specific Rat Monoclonal anti-AGO2(6F4) Antibody

AGO-containing RNPs have been purified using different biochemical approaches ranging from the reconstruction of RISC on tagged RNAs and density centrifugation to affinity chromatography of tagged AGO proteins [127, 171, 214, 221]. Aside from giving insights into the proteomic composition of AGO-containing RNPs, these approaches also facilitated the cloning and deep sequencing of small RNAs associated with AGO proteins and greatly advanced the knowledge of small RNA profiles and enabled miRNA target iden-

tification [20, 63, 115]. The majority of these studies employed overexpressed, tagged
AGO proteins because of the lack of suitable antibodies against the endogenous proteins.
Overexpression of proteins can cause artificial protein-protein interactions and the added
affinity tag can interfere with protein function. In addition, these approaches can only be
implemented in transfectable cell lines and thereby exclude tissues samples and primary
cells. Although an N-terminal FLAG/HA-tag does not interfere with the activity of
AGO2, the impact of AGO2 overexpression on protein interactions remains elusive. The
establishment of highly specific monoclonal antibodies against the human AGO proteins
[20, 282, 349] greatly advanced the analysis of endogenous AGO complexes in the hu-
man system. We have generated a monoclonal antibody specific for mouse AGO2. The
anti-AGO2(6F4) detected and immunoprecipitated catalytically active AGO2 with its
associated small RNAs from various murine cell lines. Bound proteins could be eluted
from the antibody matrix with a competing peptide, a property especially useful for
interaction studies since it allows to circumvent denaturing elution conditions that often
result in the elution of contaminating proteins. The anti-AGO2(6F4) had weak affinities
for AGO1 and 3 and a strong cross-reactivity for the COP II vesicle component SEC24C.
These additional affinities complicate the utilization of the antibody for proteomic stud-
ies (see Section 2.4), localization studies and the profiling of AGO2 associated RNAs.
Despite the cross-reactivities, the affinity of the antibody for AGO2 is very high and
bound miRNAs were coimmunoprecipitated with high reliability. Therefore, the anti-
body is well suited for the verification of novel miRNAs as recently demonstrated by
Zhu *et al.* [365].

3.3 Quantitative Proteomic Analysis of Endogenous AGO2-containing Ribonucleoprotein Complexes

MiRNA-guided gene silencing is important for almost all cellular processes and miRNA
function is therefore heavily regulated at many different steps. AGO proteins are em-
bedded into large protein-RNA structures containing si- and miRNAs as well as trans-
lationally repressed mRNAs [127, 171, 349]. It is becoming more and more apparent
that the proteins associating with AGO in the RNPs have a strong regulatory effect
on AGO activity and function. Several large scale semiquantitative proteomic studies
of tagged AGO protein complexes contributed to our current knowledge of the protein
composition of AGO-containing RNPs [95, 127, 171, 221, 349]. However, many of the
interactions have not been further classified or validated and little is known about how

well these observations apply to the endogenous complexes. In order to investigate the protein composition of endogenous murine AGO2-containing RNPs, we used a SILAC-based quantitative proteomic approach to identify specific AGO2 interactors and aimed to characterize the miRNA-dependency of the associations. In a modified QUICK approach, we used the anti-AGO2(6F4) antibody to isolate AGO2-containing RNPs from SILAC-labeled AGO2 wild type and AGO2-depleted MEFs. Although AGO2 was identified with a high sequence coverage and clear ratios, and known cross reactants were identified as background binders, this approach did not allow us to define AGO2 interacting proteins with high confidence. The group of outliers contained predominantly highly abundant cytoskeletal proteins. Actins and Myosins, amongst others, often bind non-specifically to sepharose and are frequently found in immunoprecipitations carried out with sepharose as an affinity matrix [323]. In quantitative AP-MS approaches, such contaminants usually appear as background binders and are only occasionally identified as outliers due to variabilities inherent to sample handling and quantification. Subsequent analysis showed that the cytoskeletal proteins were differently expressed in the two cell lines used in our modified QUICK approach. Consequently, non-specific binding of these proteins was stronger in one of the samples and generated high ratios for these proteins. Similar differential background binding also prevented the analysis of the miRNA dependency of AGO2 interactions. This observation highlighted the influence of the whole proteome on interaction proteomics. Upon cellular stimuli, not only the composition of individual protein complexes might be altered but the whole cell proteome can undergo significant changes that might have severe effects on the composition of the non-specific background binders associated with the affinity matrix and lead to the identification of false positive interactors.

Many previously reported AGO2 interacting proteins, in part with established functions in miRNA-mediated gene silencing, were identified as background binders in the modified QUICK approach. It is not likely that anti-AGO2(6F4) binding interferes with complex formation or that the antibody recognizes a sub-complex lacking these interactors because a commercially available antibody with a different epitope produced a very similar protein profile. Both antibodies precipitated AGO1 and AGO3 in significant amounts. This could reflect a specific interaction between the different AGO proteins. AGO1 and 2 interact with each other *in vivo* [298, 359]. Different AGO proteins were identified in the same complex in AGO 1-4 immunoprecipitations [171] but the non-bait AGO proteins were identified with low sequence coverages and only one unique peptide each, thus the identification is not very reliable. In addition, the murine AGO proteins share a high sequence homology, so it is probable that the presence of AGO1 and 3 in the

immunoprecipitations were based on a cross-reactivity of the antibodies. This theory is supported by the observation that AGO1 and 3 showed background ratios in the QUICK approach but appear as specific interactors in an approach with a control antibody. All four human AGO proteins associate with highly similar sets of proteins and the majority of the analyzed reported AGO2 interactors in our data set interact with all four AGO proteins. This interaction with cross reacting AGO proteins could cause a shift of the ratios below the threshold for specific interactors. But since AGO 1, 2 and 3 all show high ratios in the approach with a control antibody and the reported interactors retain their background ratios, it is necessary to consider non-specific associations with the affinity matrix for this set of proteins. As described by Trinkle-Mulcahy *et al.*, for some cases, especially for low abundance proteins, the SILAC ratios alone are not sufficient to define specificity and it is necessary to apply special filters for the identification of such interactors [323].

Dicer and its cofactors TRBP/TARBP2 and PACT/PRKRA were not identified in any of the immunoprecipitations of endogenous AGO2-containing RNPs. As our experiments showed, the lack of Dicer and TRBP in these complexes was not cell line or antibody specific. The absence of Dicer in endogenous AGO2-containing RNPs is an interesting observation since the association between Dicer and AGO is well studied at the molecular level [208, 311]. RISCs undergo several intermediates during their formation and protein composition is likely to vary considerably depending on the current function of an individual RISC. A Dicer-free AGO2 complex was identified in human cells after fractionation of tagged-AGO2 complexes [127] but we did not apply comparable fractionation to our samples. As discussed above (see Section 3.1) the AGO2-Dicer complex appears to be rather unstable, which reflects a low affinity between the two proteins. *In vitro* reconstitution of the human RLC complex indicates that AGO2 dissociates from the RLC after miRNA loading [208]. Once loaded with a small RNA, AGO2 does not necessarily have to be associated with Dicer for its function in target RNA degradation and translational repression. Thus, Dicer is possibly not a part of active RISCs. This hypothesis is strengthened by two observations. First, although Dicer coimmunoprecipitates with AGO, immunoprecipitations of Dicer do not contain the majority of AGO interactors and second, Dicer-associated mRNAs share no sequence similarity with AGO-associated miRNA targeted mRNAs [171]. However, Dicer is frequently observed in immunoprecipitations of overexpressed, tagged AGO proteins. Is the association between AGO and Dicer concentration dependent? Does a higher abundance of AGO trigger a more stable association? If yes, how does this influence the association with other protein components and AGO function? These and other questions concerning the

presence and function of Dicer in RISCs need to be carefully addressed in future studies on endogenous AGO2-containing RNP complexes.

3.4 Identification of Differential AGO2 Interactions by SILAC-based Quantitative Proteomics

Several semiquantitative proteomic studies and various genetic or RNAi-based screens have been performed in plants and animals leading to the identification of proteins that are involved in the different aspects of small RNA-guided gene silencing. However, none of these studies were aimed at the discrimination of protein-protein or protein-RNA interactions within AGO-containing RNPs but mostly focused on the identification of AGO interaction partners. We used affinity purification of FLAG/HA-tagged AGO2-containing RNPs in combination with SILAC-based quantitative proteomics to provide a comprehensive list of proteins associating with AGO2 either through protein-protein interactions or by indirect binding via RNAs. We identified 94% of the AGO2 interaction partners previously identified by proteomic studies [127, 171] and the high sensitivity of our measurements facilitated the identification of additional, so far unreported potential AGO2 interaction partners. The quantitative aspect of our analysis allowed us to discriminate between background binders and specific interactions and several previously reported interaction partners, for example the methylosome components [221], were classified as non-specific binders.

In order to analyze the miRNA dependency of AGO2 interactions, we used MEF cell lines in which Dicer has been genetically inactivated [101]. As a consequence, miRNA precursors are not processed into mature miRNAs in these cells. AGO2 complexes in these MEFs are most likely free of miRNAs as miR-451, the only known miRNA processed by AGO2 independently of Dicer [40, 45], is not expressed in these cells.

We hypothesized that unloaded, miRNA-free AGO2 associates with different proteins than miRNA-loaded AGO2. To test this hypothesis, we compared AGO2-containing RNPs from Dicer wild type and Dicer-deficient MEFs. Indeed, we found a number of proteins that interacted with AGO2 specifically in the presence or absence of Dicer and miRNAs, while other proteins associated with AGO2 under both conditions (Figure 3.4.1). Among the specific interactions not affected by the miRNA loading status of the AGO2 protein, we identified a high number of RBPs reported to associate with mRNAs. MiRNAs are generally regarded as sequence-specific guides that target AGO

protein complexes to distinct sites on mRNAs with partial sequence complementary to the miRNA [82]. Following this assumption, we presumed that AGO proteins would not interact with mRNAs in the absence of Dicer and mature miRNAs. The miRNA-independent binding behavior of the RBPs with AGO2 now lead us to hypothesize that AGO2 binds large RNAs with its associated RBPs irrespective of miRNAs. We showed that AGO2 stably associates with large RNAs in the absence of miRNAs and that large RNA binding strongly influences the protein composition of AGO2 containing RNPs (Figure 3.4.1). Our proteomic based observation of miRNA-independent large RNA binding is confirmed by deep-sequencing studies. Chi and colleagues [44] described so called "orphan cluster" mRNAs that have no predicted seed matches with known miR-NAs but nevertheless associate with AGO2. Leung *et al.* observed that a G-rich motif containing mRNAs associate with AGO2 in an miRNA independent manner. They speculate that the presence of a G-rich motif in the close proximity of a miRNA binding site strengthens the affinity of the AGO-miRNA complex for the binding site and increases the probability for miRNA-mediated repression [183]. It might also be possible that miRNA-independent mRNA binding is the basis for a so far unknown regulatory mechanism in which mRNA target recognition and binding is mediated by RBPs and AGO2 only serves as a scaffold protein for the recruitment of factors involved in translational repression and mRNA degradation. With our current knowledge, the exact mechanism and function of non-miRNA-guided mRNA binding remains elusive and needs to be investigated in future studies.

A current model of the mechanism of miRNA-guided gene silencing is that AGO proteins interact with a member of the GW128 protein family, which in turn interacts with the PABP bound to the poly(A)-tail of the mRNA. This interaction interferes with PABP function and inhibits translation or induces deadenylation. *Drosophila* GW182 predominantly binds to the RRMs of PABP through its N- and C-terminal domains, whereas human TNRC6C and PABP interact via binding between the PAM2 motif and the Mlle domain. It is hypothesized that the different modes of interaction cause fundamental differences in the silencing mechanism [324]. Our finding that TNRC6C binds to AGO2 only in the presence of miRNAs and Dicer, while TNRC6A and B show a Dicer and miRNA-independent binding behavior, supports this theory of differential silencing mechanisms of the TNRC6 proteins.

Messenger RNA destabilization has emerged as a widespread effect of miRNA mediated regulation. The interactions of miRNPs with the deadenlyase complex has been characterized in molecular detail [79, 363], yet not much is known about functional interactions
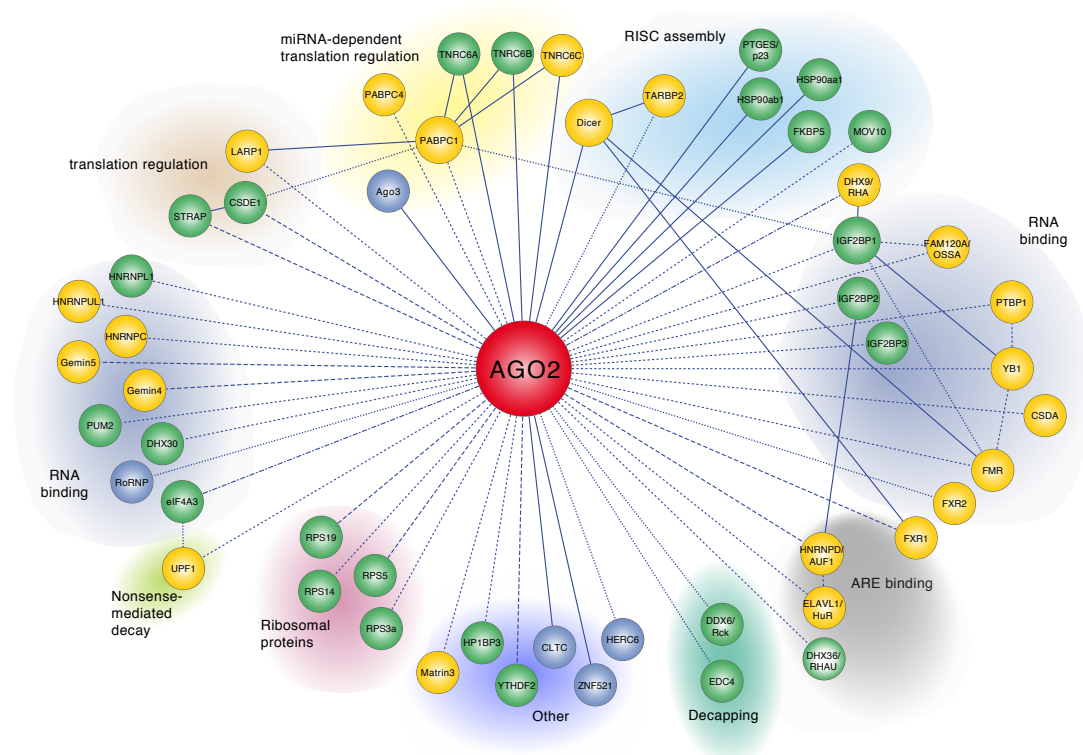
Figure 3.4.1: AGO2 Interaction Network. The proteomic data was combined into an interaction network. Proteins were grouped according to their biological functions and reported interactions between the AGO2-associated proteins were added. AGO2 is depicted in red. Proteins interacting with AGO2 independently of Dicer and the miRNA loading status of AGO2 are shown in green. Interactors binding to AGO2 only in the presence or absence of miRNAs and Dicer are indicated in yellow and blue, respectively. The style of the connecting lines represents the large RNA dependency. Solid lines indicate protein-protein interactions. Short dashed lines represent a strong large RNA dependency of the interactions. A weak influence of large RNA presence on the binding behavior is depicted by long dashed lines. Broken dashed lines indicate differential large RNA dependencies in the presence of absence of miRNAs and Dicer. Proteins not identified in the large RNA dependency screen are connected to AGO2 by dotted lines.

with the decapping machinery. DDX6, a DEAD box helicase more widely referred to as RCK, is involved in translational regulation and associates with AGO1 and 2 in human cells [359]. RCK and the decapping enhancer Ge-1 are required for miRNA-guided gene silencing in flies [75]. Based on our observation that AGO2 interacts with DDX6/RCK and the Ge-1 homologue EDC4, it is tempting to suggest a model in which AGO2 does not only stimulate deadenylation via the GW182 proteins but also triggers subsequent decapping and efficient mRNA decay by recruiting the decapping factors RCK and EDC4. Other proteins identified as interactors in our proteomic screen might also

connect AGO2 and the miRNA machinery to mRNA decay. The RNA helicase UPF1 is a miRNA- and large RNA-dependent AGO2 interactor and is known to interact with decapping, deadenylation and exosome components. RISC bound mRNAs accumulate due to inefficient degradation in the absence of UPF1, so one might speculate that UPF mediates the interaction between RISC and mRNA decay factors [143]. In addition, UPF1 and the exon junction complex component eIF4A3 are involved in NMD and represent a possible connection between this degradation process and miRNA-mediated repression [92, 93]. Another helicase, DHX36/RHAU, is involved in deadenylation of AU-rich mRNAs and might link AGO2 to ARE-mediated messenger RNA decay. A connection between miRNA-mediated repression and ARE-mediated translation regulation is suggested by our data by the miRNA- and large RNA-dependent AGO2 interactor HuR and its cofactor AUF1 [39].

Aside from various RBPs and mRNA decay factors, we identified components involved in RISC assembly and maturation. Dicer and AGO interact through their RNase III and PIWI domains [311]. This direct protein-protein interaction is reflected by an RNA-independent binding behavior in our data. TRBP seems to have no affinity for AGO in the absence of miRNAs and Dicer, and its presence in the RNP complex appears to be coupled to its association with Dicer. HSP90 regulates AGO localization and its ATPase activity is required for the conformational changes of the AGO protein during the process of small RNA loading [134, 138, 255]. Together with its cochaperones, HSP90 associated with AGO2 in an RNA-independent manner, suggesting a stable protein-protein interaction that could have additional functions besides small RNA loading. The only RISC loading factor binding in a miRNA-dependent manner is the RNA helicase A (RHA/DHX9). This is in good agreement with its proposed function of promoting the interaction between Dicer products and AGO [278]. It is puzzling that RHA binding to AGO2 displayed differently strong large RNA dependencies in the presence and absence of Dicer and miRNAs and it could be worthwhile to elucidate the function underlying this binding behavior. Another protein involved in RISC maturation is the putative helicase MOV10 [221, 318]. Among the identified RISC assembly components, MOV10 is the only factor showing a large RNA-dependent association with AGO. This binding behavior suggests a function downstream of RISC loading, possibly at the step of large RNA binding by the RISC.

We identified a number of proteins that specifically associated with AGO2 preferentially in the absence of miRNAs. These proteins bind to AGO2 through protein-protein interactions. It is interesting that one of these proteins is AGO3. AGO1 and 2 are known

to interact with each other [298, 359], but why and with which functional consequences AGO3 associates specifically with unloaded AGO2 can only be speculated. ZNF521 is a nuclear factor suggested to be involved in transcription regulation [28] and its discovery in RNA-free AGO2 complexes points towards a possible miRNA-independent nuclear function for AGO2. We observed that AGO2 abundance is significantly lower in the Dicer-deficient cells compared to the wild type cells, not only at endogenous levels but also when AGO2 was overexpressed. This lower abundance seems to be caused by an instability of AGO2 in the absence of miRNAs. In addition, large RNA binding also seemed to have a stabilizing effect on AGO2 since AGO2 stability decreased upon long RNase treatment (Figure 2.5.7). Is AGO2 targeted for degradation when it can not execute its function in the absence of miRNAs? Murine AGO2 turnover is regulated by ubiquitinylation [283] and we identified the HECT-type E3 ligase HERC6 in association with RNA-free AGO2. HERC6 mediates the conjugation of ISG15 to target proteins in human [351]. ISG15 functions as a ubiquitin homolog and it is therefore tempting to speculate that RNA-free AGO2 might be subjected to this specific form of post translational modification in the absence of mature miRNAs.

We combined our proteomic data into an interaction network that presents an overview of the protein components of AGO2-containing RNPs and displays the miRNA and Dicer as well as the large RNA requirements of the interactions (Figure 3.4.1). Reported interactions between the AGO2-associated proteins were included into the network to point out possible regulatory pathways and AGO2-independent interactions between the RNP components. Our experimental set up does not discriminate between proteins present in the RNPs with a clear AGO2-related function and RBPs without related functions that "hitchhike" to the RNPs on the associated large RNAs. One transcript is bound and regulated by multiple RBPs and a single RBP can bind to up to 30% of the RNA transcripts in human cells [115]. In the end it is the combination of the associated factors that determines the regulatory outcome. It is suggested that RBPs and miRNAs mediate each others activities by competition or complementation for target RNA binding. Indeed, there seems to be a strong interplay between RBPs and miRNAs, which is represented by several proteins in our data set. One example is FMR, a protein that facilitates the assembly of miRNAs on specific targets [266]. Another example is the ARE-binding protein HuR. Its binding sites are found in close proximity to miRNA binding sites [175] and HuR mediates translation either by acting cooperatively with miRNAs in RISC recruitment or by relieving miRNA-mediated repression [23, 39, 159]. Target sites for the mRNA binding protein PUM2 are also enriched around predicted miRNA binding sites and it is suggested that PUM proteins recruit the miRNA machinery to regulate

their targets [91]. RBP-mediated regulation of miRNA activity is also dependent on cellular conditions, as seen for FXR1 that relieves miRNA-mediated repression during cell cycle arrest [331, 332]. Our proteomic data does not reveal the composition of such highly individual RNPs but gives an average of protein complexes and binding partners associated with AGO2. It would therefore be interesting to refine our present interaction network by further separating the different RNPs to allow for a more detailed analysis of the proteomic composition of the individual RNPs with a special focus on how the associated proteins influence AGO2 function under varying cellular conditions.

4 Material and Methods

4.1 Material

4.1.1 Chemicals, Enzymes, Peptides and Oligonucleotides

All chemicals were, unless stated otherwise, purchased from one of the following companys: Amersham Bioscience (Buckinghamshire, UK), Biorad (Hercules, USA), Merck (Darmstadt, Germany), Qiagen (Hilden, Germany), Roche (Basel, Switzerland), Roth (Karlsruhe, Germany) and Sigma-Aldrich (Munich, Germany). Radiochemicals were provided by Perkin Elmer (Waltham, USA). Enzymes were purchased from New England Biolabs (Ipswich, USA) or Fermentas (Burlington, Canada). Unless specified otherwise, peptides were synthesized by the Peptide Service of the Core Facility at the Max Planck Institute of Biochemistry (Martinsried, Germany). DNA oligonucleotides were synthesized by Metabion (Martinsried, Germany).

4.1.2 Plasmids

pVP5: This mammalian expression vector has been kindly provided by the Bob Roeder laboratory. It is based on the pIRES1neo expression vector (Clontech, Mountain View, USA) but contains a Kozak Sequence followed by a FLAG- and an HA-tag, which has been inserted between the *Eco*RV and *Nhe*I restriction site in the multiple cloning site. The pVP5 is used in this work for the overexpression of FLAG/HA-tagged (F/H-tagged) proteins in mammalian cells.

pDest26cMyc: This mammalian expression vector is based on the pDest26 vector (Invitrogen, Carlsbad, USA) and has been engineered to contain an N-terminal cMyc-tag instead of a 6xHis-tag. In this work the vector is used for the overexpression of cMyc-tagged Dicer in HEK293T cells.

4.1.3 Antibodies

- anti-AGO1(4B8): rat monoclonal, hybridoma supernatant [20]
- anti-human AGO2(11A9): rat monoclonal, hybridoma supernatant [282]

- anti-human AGO3(5A3): rat monoclonal, hybridoma supernatant [349]
- anti-AGO4(6C10): rat monoclonal, hybridoma supernatant [349]
- anti-RmC(16D2): rat monoclonal, hybridoma supernatant
- anti-mouse AGO2(6F4): rat monoclonal, hybridoma supernatant
- anti-human SEC24C: rabbit polyclonal [248]
- anti-HA: mouse monoclonal 16B12 (Covance, Berkely, USA)
- anti-β-tubulin: mouse monoclonal DM1A (Sigma, St. Louis, USA)
- anti-β-actin: mouse monoclonal AC15 (Abcam, Cambridge, UK)
- anti-AGO2(C34C6): rabbit monoclonal C34C6 (Cell Signaling, Danvers, USA)
- anti-mouse IgG: rabbit, peroxidase conjugated (Sigma, St. Louis, USA)
- anti-rat IgG: goat, peroxidase conjugated (Jackson Laboratory, West Grove, USA)
- anti-rabbit IgG: goat, peroxidase conjugated (Jackson Laboratory, West Grove, USA)
- fuorescein anti-rat IgG: rabbit, fluorescein conjugated (Vector Laboratories, Burlingame, USA)

4.1.4 Bacterial Strains and Cell Lines

Bacterial strains

- *E. coli* XL1 blue

Mammalian cell lines

- human embryonic kidney 293 T cells (HEK293T)
- AGO2 (-/-) mouse embryonic fibroblasts [55]
- Dicer (+/+) mouse embryonic fibroblasts (1C1) [101]
- Dicer (-/-) mouse embryonic fibroblasts (2G4) [101]
- Dicer (+/+) FLAG/HA expressing AGO2 embryonic fibroblasts (1C1)
- Dicer (-/-) FLAG/HA AGO2 expressing embryonic fibroblasts (2G4)
- mouse hepatoma cells (Hepa 1-6)
- mouse neuroblastoma cells (N2A)
- mouse fibroblast cells (NIH 3T3)

4.1.5 Media

Bacteria media

Lysogeny broth media (LB)	1% (w/v)	Trypton
	1% (w/v)	NaCl
	0.5% (w/v)	Yeast extract

Cell culture media

Normal DMEM: DMEM with high glucose (PAA, Pasching, Austria) with 10% fetal bovine serum (Biochrom, Berlin, Germany) and 10% Penicillin/Streptomycin (PAA, Pasching, Austria.)

SILAC media: DMEM with high glucose devoid of arginine and lysine (PAA, Pasching, Austria) supplemented with 10% dialyzed FBS (Invitrogen, Carlsbad USA), 10% Penicillin/Streptomycin (PAA, Pasching, Austria), 2 nM stable glutamine (PAA, Pasching, Austria) and either with normal lysine and arginine or the heavy counterparts ($^{13}C_6{}^{15}N_4$-L-arginine, $^{13}C_6{}^{15}N_2$-lysine, Sigma-Aldrich, Munich, Germany) at a concentration of 42 mg/l and 72 mg/l, respectively.

4.1.6 Buffers and Solutions

General Buffers

Phosphate buffered saline (PBS)	135 mM	NaCl
	1.3 mM	KCl
	3.2 mM	Na_2HPO_4
	0.5 mM	NaH_2PO_4, pH 7.4

TBE buffer	89 mM	Tris-HCl, pH 8.3
	89 mM	boric acid
	2.5 mM	EDTA

HEPES (2x)	274 mM	NaCl
	54.6 mM	HEPES
	1.5 mM	Na_2HPO_4

MOPS buffer (50x)	1 M	MOPS, pH 7.0

SDS-PAGE

Protein sample buffer (5x)	400 mM	Tris-HCl, pH 6.8
	5 mM	EDTA
	0.01% (w/v)	bromphenol blue
	50% (w/v)	glycerol
	1% (w/v)	SDS
5% stacking gel	5% (v/v)	acrylamide (37%, 5:1)
	75 mM	Tris-HCl, pH 6.8
	0.1% (w/v)	SDS
	0.1 % (w/v)	APS
	4 µM	TEMED
10% separation gel	10% (v/v)	acrylamide (37%, 5:1
	400 mM	Tris HCl, pH 8.0
	0.1% (w/v)	SDS
	0.1% (w/v)	APS
	4 µM	TEMED
SDS running buffer	200 mM	glycerol
	25 mM	Tris-HCl, pH 7.5
	25 mM	SDS

Coomassie Staining

Coomassie solution	0.25% (w/v)	Coomassie R250
	50% (v/v)	methanol
	10 % (v/v)	acetic acid
Destaining solution	30% (v/v)	methanol
	10% (v/v)	acetic acid

Colloidal Coomassie staining	0.08% (w/v)	Coomassie G250
solution	1.6% (v/v)	H_3HPO_4
	8.0% (w/v)	$(NH_4)_2SO_4$
	20% (v/v)	methanol

Silver Staining Solutions

Fixing solution	50% (v/v)	methanol
	12% (v/v)	acetic acid
	0.5 ml/l	37% formaldehyde

Washing solution	30% (v/v)	ethanol

Sodium thiosulfate solution	0.2 g/l	NaS_2O_3 x 5 H_2O

Silver nitrate solution	2 g/l	$AgNO_3$
	0.75 ml/l	37% formaldehyde

Developer	60 g/l	$NaCO_3$
	0.5 ml/l	37% formaldehyde

Stopping solution	50% (v/v)	methanol
	12 % (v/v)	acetic acid

Buffers for Western Blotting

TBS-T	137 mM	NaCl
	20 mM	Tris-HCl, pH 7.6
	0.1% (v/v)	Tween-20

Towbin buffer	192 mM	glycin
	25 mM	Tris-HCl, pH 8.3
	20% (v/v)	methanol
	0,037% (w/v)	SDS

Transfer buffer	25 mM	Tris HCl
	192 mM	glycine
	20% (v/v)	methanol

Western blot wash buffer	300 mM	Tris-HCl, pH 7.5
	150 mM	NaCl
	0.25% (v/v)	Tween-20

Chemiluminescence detection	100 mM	Tris-HCl, pH 8.5
	1.2 mM	Luminol
	0.68%	p-coumaric acid
	0.02%	H_2O_2

Buffers for Immunofluorescence

Fixing Solution	130 mM	NaCl
	774 mM	Na_2HPO_4, pH 7.4
	226 mM	NaH_2PO_4
	3.7% (w/v)	formaldehyde

Stopping solution	130 mM	NaCl
	774 mM	Na_2HPO_4, pH 7.4
	226 mM	NaH_2PO_4
	0.2% (w/v)	Triton 100
	3% (w/v)	Albumin fraction V

Wash buffer	130 mM	NaCl
	774 mM	Na_2HPO_4, pH 7.4
	226 mM	NaH_2PO_4
	0.1% (w/v)	Tween 20
	0.2% (w/v)	Albumin fraction V

Buffers for RNA Isolation and Northern Blotting

Protease K buffer (2x)	300 mM	NaCl
	200 mM	Tris-HCl, pH 7.5
	25 mM	EDTA
	2% (w/v)	SDS

RNA loading dye (1x)	89 mM	Tris-HCl, pH 8.3
	89 mM	boric acid
	2.5 mM	EDTA
	90% (v/v)	formamide
	0.025% (w/v)	xylene cyanol
	0.025% (w/v)	bromophenol blue

Denaturing polyacrylamide gels	25.2 g	urea
for RNA	18 ml	acrylamide (40%; 19:1)
	1.2 ml	1 M MOPS-NaOH, pH 7.0
	360 µl	APS
	21 µl	TEMED

Cross-link solution	0.13 M	1-methylimidazole, pH 8.0
	0.16 M	1-ethyl-3-(3-dimethylaminopropyl) carbodiimide

SSC (20x)	3 M	NaCl
	0.3 M	sodium citrate, pH 7.1

Denhardt's solution (50x)		
	1% (w/v)	Albumin fraction V
	1% (v/v)	Polyvinylpyrrolidon K30
	1% v(v/v)	Ficoll 400

Hybridization solution	5x	SSC
	7% (w/v)	SDS
	20 mM	Na_2HPO_4, pH 7.2
	1x	Denhardt's solution

| Wash buffer I | 5x | SSC |
| | 1% (w/v) | SDS |

| Wash buffer II | 1x | SSC |
| | 1% (w/v) | SDS |

Buffers for *In Vitro* RISC Activity Assays

in vitro transcription buffer	1x	T7 RNA polymerase buffer
	1 mM	ATP
	1 mM	CTP
	1.6 mM	GTP
	0.4 mM	UTP
	5 mM	DTT

| RNA elution buffer | 300 mM | NaCl |
| | 2 mM | EDTA, pH. 8.0 |

GT buffer	40 mM	Tris-HCl, pH 8.0
	60 mM	$MgCl_2$
	10 mM	DTT
	2 mM	spermidine

Reaction buffer	1 mM	ATP
	0.2 mM	GTP
	10 U/ml	RNasin (Promega, Madison, USA)
	100 mM	KCl
	1.5 mM	$MgCl_2$
	0.5 mM	DTT

T1 digestion buffer	1 mM	ATP
	10 mM	urea
	1.5 mM	EDTA
	0.05% (w/v)	bromphenol blue
	0.05% (w/v)	xylene cyanol

Buffers for *In Vitro* Dicer Activity Assays

in vitro transcription buffer	1x	T7 RNA polymerase buffer
	1 mM	ATP
	1 mM	CTP
	1.6 mM	GTP
	20 µM	UTP
	5 mM	DTT
Reaction buffer	135 mM	NaCl
	1.3 mM	KCl
	3.2 mM	Na_2HPO_4, pH 7.4
	0.5 mM	NaH_2PO_4
	5 mM	ATP
	7.5 mM	$MgCl_2$

Buffers for AGO2 Complex I Purification from HEK293T Cells

Cell lysis buffer	150 mM	KCl
	25 mM	HEPES-KOH, pH 7.4
	2 mM	EDTA
	1 mM	NaF
	0.5% (v/v)	NP-40
	5% (v/v)	glycerol
	5 mM	DTT
	1 mM	AEBSF
Sucrose gradient buffer	150 mM	KCl
	25 mM	HEPES-KOH, pH 7.4
	15 or 55% (w/v)	sucrose
IP wash buffer	150 mM	KCl
	50 mM	HEPES-KOH, pH 7.4
	5 mM	$MgCl_2$
	0.01% (v/v)	NP-40
	5% (v/v)	glycerol

Elution buffer	150 mM	KCl
	25 mM	HEPES-KOH, pH 7.4
	5 mM	$MgCl_2$
	5% (v/v)	glycerol

Buffers for PRMT5-MEP50 Complex Purification from HEK293T Cells

Cell lysis buffer	150 mM	KCl
	25 mM	Tris-HCl, pH 7.4
	2 mM	EDTA
	1 mM	NaF
	0.5% (v/v)	NP-40
	5% (v/v)	glycerol
	5 mM	DTT
	1 mM	AEBSF

Sucrose gradient buffer	150 mM	KCl
	25 mM	Tris-HCl, pH 7.5, pH 7.4
	15 or 55% (w/v)	sucrose

IP wash buffer	150 mM	KCl
	50 mM	Tris-HCl, pH 7.5, pH 7.4
	5 mM	$MgCl_2$
	0.01% (v/v)	NP-40
	5% (v/v)	glycerol

Elution buffer	150 mM	KCl
	25 mM	Tris-HCl, pH 7.5, pH 7.4
	5 mM	$MgCl_2$
	5% (v/v)	glycerol

Buffers for Glycerol Gradients

Glycerol gradient buffer	150 mM	KCl
	25 mM	HEPES-KOH, pH 7.4
	10 or 30% (v/v)	glycerol

Buffers for Immunoprecipitation of AGO2-Containing RNP Complexes for Mass Spectrometry Analysis

Cell lysis buffer	150 mM	KCl
	25 mM	Tris-HCl, pH 7.5
	2 mM	EDTA
	1 mM	NaF
	0.5% (v/v)	NP-40
	5 mM	DTT
	5% (v/v)	glycerol
	1x	complete protease inhibitor cocktail (Roche, Basel, Switzerland)

IP wash buffer (for FLAG-IPs)	300 mM	NaCl
	50 mM	Tris-HCl, pH 7.5
	5 mM	MgCl$_2$
	0.01% (v/v)	NP-40
	5% (v/v)	glycerol

IP wash buffer (for anti-AGO2(6F4) and anti-AGO2(C34C6) IPs)	150 mM	NaCl
	50 mM	Tris-HCl, pH 7.5
	5 mM	MgCl$_2$
	0.01% (v/v)	NP-40
	5% (v/v)	glycerol

Elution buffer	150 mM	NaCl
	25 mM	Tris-HCl, pH 7.4
	5 mM	MgCl$_2$
	5% (v/v)	glycerol

Buffers Peptide Extraction, Stage Tipping and Mass Spectrometry Analysis

| Buffer A* | 2% (v/v) acetonitrile |
| | 0.1% (v/v) trifluoroacetic acid |

| Buffer A | 0.5% (v/v) acetic acid |

| Buffer B | 0.5% (v/v) acetic acid |
| | 80% (v/v) acetonitrile |

4.2 Methods

4.2.1 General Methods

General Molecular Biological Methods

Standard molecular biology methods, for example DNA gelelectrophoresis, extraction and precipitation of nucleic acids and transformation of *E.coli* with plasmid DNA were performed as described by Sambrook *et al.* [288].

Cloning of Murine Argonaute Genes

The murine Argonaute genes 1-4 (AGO1-4) were cloned into pVP5 using the templates, primers and restriction sites indicated in Table 4.2.1. Genes were amplified from template DNA with Phusion^{TM} DNA Polymerase (Finnzymes, Espoo, Finnland) and PCR Products were isolated from agarose gels with the NucleoSpin-Kit (Macherey Nagel, Düren, Germany). Vector DNA and PCR products were digested with the respective restriction enzymes, ligated using T4 DNA Ligase (Fermentas, Burlington, Canada) and transformed into *E. coli* XL1 blue. Isolation of plasmid DNA from *E. coli* was carried out using the NucleoBond® XtraMini or the NucleoBond® XtraMidi Kit (Macherey Nagel, Düren, Germany). All kits and enzymes were used according to the manufacturers instructions.

Whole Cell Lysate Preparation

Cells were cultured to 80-90% density, washed three times with PBS, scraped off and pelleted at 200 g for 10 min at RT. The cell pellets were flash frozen in liquid nitrogen and stored at -80°C. For lysate preparation, the cells were thawed on ice, suspended in lysis buffer freshly supplemented with DTT and protease inhibitor by pipetting up and

AGO1	
template	IMAGE clone 40111808 (RZPD, Berlin, Germany)
forward primer	5'-CGCTGCGGCCGCATGGAAGCGGGACCCTCGGG-3'
reverse primer	5'-CGCTGAATTCTCAAGCGAAGTACATGGTGCGT-3'
restriction sites	*Not*I/*Eco*RI

AGO2	
template	IMAGE clone 40111875 (Geneservice, Cambridge, UK)
forward primer	5'-CGCTGCGGCCGCATGGACTCGGGAGCCGGCCC-3'
reverse primer	5'-CGCTGAATTCTCAAGCAAAGTACATGGTGCGC-3'
restriction sites	*Not*I/*Eco*RI

AGO3	
template	cDNA clone (Alexa Dittmer, Research Group Klaus Förstemann)
forward primer	5'-CGCTGCGGCCGCATGGAAATCGGCTCCGCAGG-3'
reverse primer	5'-CGCTCAATTGTTAAGCGAAGTACATTGTGCGT-3'
restriction sites	*Not*I/*Mfe*I

AGO4	
template	IMAGE clone 30607807 (RZPD, Berlin, Germany)
forward primer	5'-CGCTGCGGCCGCATGGAGGCGGTGGGACCCGG-3'
reverse primer	5'-CGCTCAATTGTCAGGCAAAATACATAGTGTGC-3'
restriction sites	*Not*I/*Mfe*I

Table 4.2.1: Templates, primers and restriction sites used for cloning of murine Argonaute genes into the vector pVP5.

down and incubated on ice for 20 min. The cell debris was pelleted by centrifugation ($17\,000\,g$, $10\,min$, $4°C$) and the supernatant transferred to a fresh reaction tube. The total protein concentration was either determined by measurement of the A_{280} or by Bradford Protein Assay (Biorad, Hercules, USA).

Antibody Matrix Preparation

Protein G Sepharose beads (GE Healthcare, Fairfield, USA) were washed twice with PBS. Hybridoma supernatant was cleared of precipitated protein by centrifugation ($5\,min$, $17\,000\,g$, $4°C$) and 20 fold the volume of beads was added to the prepared beads. For purified antibodies, $1\,µg$ of antibody was used per µl of beads. PBS buffer was added until the desired volume and the mixture was incubated over night at $4°C$ with slow

rotation. The beads were then washed twice with PBS and resuspended in a small volume of buffer.

SDS-PAGE, Coomassie Staining and Silver Staining

Proteins from lysates or IPs were separated on polyacrylamide gels with 5% and 10% acrylamide in stacking and separation gel, respectively, or NuPAGE 4-12 % Bis-Tris Gels (Invitrogen, Carlsbad, USA). For Coomassie staining and destaining of separated proteins either Coomassie R-250 and destaining solution or Coomassie G-250 and water were used. NuPAGE gels were stained using the Novex Colloidal Blue Stain Kit (Invitrogen, Carlsbad, USA). For silver staining of separated proteins, gels were fixed in fixing solution for 1 h and washed with washing solution 3x for 20 min. Sodium thiosulfate solution was applied for 1 min followed by rinsing with water for 3x 20 sec. The gel was then soaked with silver nitrate for 20 min and rinsed with water for 2x 20 sec. Developer was applied until the desired stain intensity was reached and the reaction was stopped by discarding the developer followed by rinsing with water. The gel was then incubated in stopping solution for 10 min and transferred into water.

Western Blotting

Proteins were separated by SDS-PAGE and transferred to Amersham Hybond ECL membrane (GE Healthcare, Fairfield, USA) by semi dry electroblotting in Towbin buffer. Proteins run in NuPAGE gels were transferred to nitrocellulose membrane (Whatmann, Maidstone, UK) by wet blotting in transfer buffer. The membranes were blocked in Western blot wash buffer or TBS-T with 10% (w/v) dry milk. Rat hybridoma supernatants or purified monoclonal primary antibodies were diluted with Western blot wash buffer. Commercially available primary antibodies were used according to the manufacturer's instruction. Secondary antibodies were used in the same buffer as the corresponding primary antibody with the addition of 5% (w/v) dry milk. Dilution factors for secondary antibodies were as indicated by the manufacturer.

Immunofluorescence

Cells were grown on cover slips to 50% confluency, the medium was aspirated and the cells were fixed in fixing buffer at 4°C for 15 min. The reaction was stopped by incubation of the cells in stopping buffer for 5 min at 4°C. After incubation in blocking buffer for 10 min at 4°C the cells were washed three times with wash buffer. The primary antibody anti-AGO2(6F4) was diluted 1:50 in wash buffer and incubated with the cells for 1 h at RT followed by five washing steps with wash buffer. The fluorescein coupled anti-rat

secondary antibody was diluted 1:100 with wash buffer. After incubation for 1 h at RT in the dark, the antibody solution was aspirated. The cells were incubated in wash buffer containing 0.1 mg/ml DAPI for 5 min at RT and washed five times with wash buffer. The cover slips were then mounted on object holders with Hard Set Mounting Medium (Vector Laboratories, Burlingame, USA). Confocal images were recorded on a TCS SP2 confocal laser microscope (Leica Microsystems, Wetzlar, Germany).

RNA Isolation

Total RNA was extracted from cultured cells using the PrepEase^{TM} RNA Spin Kit (USB, Cleaveland, USA) according to the manufacturer's instructions. For the isolation of RNA from IPs and input samples, the beads or lysates were mixed with Protease K buffer containing 40 µg/ml Proteinase K and incubated for 15 min at 65°C. RNA was extracted with phenol/chlorophorm/isoamylalkohol (25:24:1) and precipitated in ethanol at -20°C over night. After pelleting by centrifugation (30 min, 17 000 g, 4°C) the isolated RNA was dried at room temperature and dissolved in an appropriate volume of water.

Northern Blotting

Isolated RNAs were separated on denaturing 12% polyacrylamide gels by electrophoresis and the gels were stained with ethidium bromide to control RNA quality. RNAs were transferred to Hybond-N membrane (Amersham Biosciences, Buckinghamshire, UK) by semidry electroblotting in water at 20 V for 30 min and crosslinked to the membrane with 1-Ethyl-3-[3-dimethylaminopropyl]carbodiimide hydrochloride [252] at 50°C for 1 h. After crosslinking the membrane was rinsed with water, dried and incubated in hybridization solution at 50°C for 1h. Northern blot probes were prepared by radiolabeling 10 pmol of DNA oligonucleotides with T4 polynucleotide kinase (Fermentas, Burlington, Canada) in the presence of ^{32}P-ATP according to the manufactures' instruction. The labeled probe was purified using MicroSpin G-25 columns (GE Healthcare, Fairfield, USA) as described by the manufacturer and the purified probe was added into the hybridization solution and incubated with the membrane over night at 50°C. The membrane was then washed twice with Northern blot wash buffer I for 10 min at 50°C and once with Northern blot wash buffer II for 10 min at 50°C. Signals were detected by audioradiography with MS film and an intensifying screen (Kodak, Stuttgart, Germany) at -80°C. The probes used in this work are summarized in Table 4.2.2.

mmu-miR-19b	5'-TCAGTTTTGCATGGATTTGCACA-3'
mmu-miR-21	5'-TCAACATCAGTCTGATAAGCTA-3'
lysin-tRNA	5'-CTGATGCTCTACCGACTGAGCTATCCGGGC-3'
U6-snRNA	5'-CTGATGCTCTACCGACTGAGCTATCCGGGC-3'

Table 4.2.2: Sequences of DNA oligos used as Northern blot probes.

cDNA Synthesis

Total RNA was isolated as described previously (see Section "RNA Isolation" on page 115) and cDNA was synthesized with oligo-d(T) primers using the First Strand cDNA Synthesis Kit (Fermentas, Burlington, Canada) as instructed by the manufacturer.

Genotyping

Mouse embryonic fibroblast were genotyped approximately every 10 passages when in culture. DNA was isolated using a QIAamp DNA Mini Kit (Qiagen, Hilden, Germany) according to the manufacturer's instructions for isolation of genomic DNA from cultured cells. A touch down PCR was performed with the primers 23F (5'-ATTGTTACCAGCG CTTAGAATTCC-3'), 458F (5'-TCGGAATAGGAACTTCGTTTAAAC-3') and 460R (5'-GTACGTCTACAATTGTCTATG-3') as described elsewhere [4]. PCR products were analyzed on a 1% agarose gel stained with ethidiumbromide.

In Vitro RISC Activity Assay

Two different RNAs were used as *in vitro* cleavage substrates in this study. The RNA targeted by the exogenous siRNA 5'-UCGAAGUAUUCCGCGUACGUdT-3' has been described by Martinez et al. in 2002 [214] and contains the target site flanked by sequences of firefly luciferase. For cleavage directed by the endogenous miR-19b an RNA described by Meister et al. in 2004 [220] was used. RNA was *in vitro* transcribed from PCR transcripts with T7 RNA polymerase (Fermentas, Burlington, Canada) in *in vitro* transcription buffer at 37°C for 3 h. The RNA was purified on an 8% denaturing polyacrylamide gel (SequaGel®-Kit, National Diagnostics, Atlanta, USA), detected by UV shadowing and eluted over night in RNA elution buffer. After recovery by ethanol precipitation, the RNA was cap-labelled with guanyltransferase in the presence of ^{32}P-GTP in GT buffer supplemented with 1,25% RiboLock RNase inhibitor (Fermentas, Burlington, Canada), 25 µM S-adenosyl methionine and 50 mM DTT for 3 h at 37°C. To purify the labeled RNA, it was separated from free nucleotides on an 8% denaturing polyacrylamide gel, detected by autoradiography on MR films (Kodak, Stuttgart, Germany), eluted over night in RNA elution buffer and precipitated with ethanol.

For the activity reaction AGO2 containing samples were preincubated in reaction buffer supplemented with 20 nM exogenous siRNA for 15 min at 30°C. When using the miR-19b target RNA this preincubation step was omitted. One Bq/cm^2 of labeled target RNA were then added to the samples and the reaction was incubated at 30°C for 1.5 h. The reaction was stopped by the addition of Protease K buffer. The RNA was isolated as described previously (see Section "RNA Isolation" on page 115) and analyzed on an 8% denaturing polyacrylamide sequencing gel. In order to be able to identify the specific cleavage product the labeled target RNA was digested with RNase T1 (Fermentas, Burlington, Canada) in T1 reaction buffer and used as a size marker in the gel electrophoresis. The detection of signals was realized with MS films and an intensifying screen at -80°C.

Dicer Activity Assay

Dicer activity was tested by using two different internally labeled RNAs. The template for pri-miR-27a RNA has been described previously [172, 220] and for the pre-miR-27a template the two DNA oligos 5'-TAATACGACTCACTATAGCTGAGGAGCAGGG CTTAGCTGCTTGTGAGCAGGGTCCACACCAGTCGTGTTCACAGTGGCTAAG TTCCGCCCCCCAGC-3' and 5'-GCTGGGGGGGCGGAACTTAGCCACTGTGAACA CGACTTGGTGTGGACCCTGCTCCAAGCAGCTAAGCCCTGCTCCTCAGCTAT AGTGAGTCGTATTAA-3' were annealed. RNA was produced by *in vitro* transcription of the DNA template with T7 RNA polymerase (Fermentas, Burlington, Canada) in transcription buffer supplemented with ^{32}P-UTP for 2 h at 37°C. The reaction was stopped by adding an equal volume of RNA sample buffer and incubation at 95°C for 5 min. For use as a size marker a mixture of 19, 21 and 24 nt or 21 nt only RNA oligos were labeled with ^{32}P-ATP by T4 Polynucleotide kinase (Fermentas, Burlington, Canada) for 5 min at 37°C. To purify labeled RNAs they were separated from free nucleotides on an 8% denaturing polyacrylamide gel, detected by autoradiography with MR film (Kodak, Stuttgart, Germany), eluted over night in RNA elution buffer and recovered by ethanol precipitation.

The activity reaction was carried out in reaction buffer supplemented with 10 U/ml RiboLock (Fermentas, Burlington, Canada) and 2 Bq/cm^2 RNA substrate for 1 h at 37°C. The addition of Protease K buffer stopped the reaction and RNA was isolated as described previously. Samples were analyzed on 15% denaturing polyacrylamide gels and signal detection was carried out with MS films and an intensifying screen at -80°C.

4.2.2 Cell Culture

Cultivation of Mammalian Cells

Mammalian cells were cultured in DMEM at 37°C and 5% CO_2. In order to split cells the medium was removed, the cells were washed once with PBS and were detached by treatment with Trypsin-EDTA (PAA, Pasching, Austria). Trypsin was inhibited by the addition of DMEM. Detached cells were pelleted by centrifugation at 200 g for 5 min and plated on fresh plates.

Calcium Phosphate Transfection

Cells were grown to 30% confluency and medium was changed 3-5 h prior to infection. For transfection of a 15 cm plate, 10-15 µg of plasmid DNA was diluted in 246 mM $CaCl_2$ and added to an equal volume of 2x HEPES buffer while vortexing. The mixure was incubated at room temperature for 30 min and added drop wise to the medium in the culture plate. Medium was exchanged only if required by the vitality of the cells. Cells were harvested 2 d after transfection, flash frozen and stored at -80°C.

Generation of Mouse Embryonic Fibroblasts Stably Expressing FLAG/HA-Tagged Murine AGO2

The MEF cell lines expressing F/H-tagged murine AGO2 were generated in collaboration with Elke Glasmacher from the Research Group Vigo Heissmeyer at the Helmholtz Center Munich. In short, retroviral supernatants were produced in HEK293T cells by calcium phosphate transfection of amphotropic packaging vectors expressing F/H-AGO2 and IRES-GFP or IRES-GFP alone. Supernatants were collected 72 h post transfection, filtered through 0.45 mm filters and used for spin-infections of Dicer -/- and Dicer +/+ MEF cells at 900 g for 1 hour at RT [254]. The media was replaced after 24 h. Dicer -/- and Dicer +/+ expressing F/H-AGO2 were grown in DMEM with 10% FCS, 1000 U/ml penicillin-streptomycin and 10 mM HEPES.

Stable Isotope Labeling with Amino Acids in Cell Culture (SILAC)

The Mann department kindly provided SILAC media containing amino acids with heavy or light isotopes. Cells were cultured in SILAC medium to 90% confluency, detached from the plate by trypsin digestion and pelleted by centrifugation (300 g, 5 min, RT). The medium was aspirated, the were cells resuspended in SILAC medium and cultured at 37°C and 5% CO_2. To ensure full incorporation of SILAC amino acids, the cells were grown in SILAC media for at least ten doublings.

To asses the incorporation rate and arginine-proline conversion total protein in whole cell lysate from heavy labeled cells was checked by LC-MS. The incorporation rate for every identified peptide was determined as follows:

$$1 - \frac{1}{(1 + Ratio\ H/L)} \tag{4.2.1}$$

The overall incorporation rate was calculated as the maximum of the density distribution of all quantified peptides.

Arginine to proline conversion would generate an additional peak for all proline containing peptides of +6 Da. In order to detect arginine to proline the 10 most intense proline containing peptides were manually inspected for this additional isotope cluster.

4.2.3 Antibody Generation

The monoclonal rat anti-AGO2(6F4) antibody was generated in collaboration with Elizabeth Kremmer at the Helmholtz Center Munich as described previously [20]. For immunization the N-terminal peptide H-APTTSPIPGYAFKP-OH of mouse Argonaute2 (Peptide Specialty Laboratories, Heidelberg, Germany) was used.

4.2.4 Purification of Protein Complexes for Electron Microscopy

Sucrose Density Centrifugation

Lysates were prepared as described previously (see "Whole Cell Lysate Preparation" on page 112). For the purification of the PRMT5/MEP50 untransfected HEK293T were lysed. The purification of the AGO2/Dicer complex was carried out from HEK293T cells transfected with pVP5–hAGO2 and pDest26-cmyc-hDicer. The lysates were loaded onto sucrose density gradients with 15-55 % (w/v) sucrose in the respective gradient buffer and separated by centrifugation (17 h, 4° C, 30000 rpm) in a SW32 T rotor.

Immunoprecipitation with anti-FLAG M2 Affinity Gel

Anti-FLAG M2 Affinity Gel (Sigma, St. Louis, USA) was used for the immunoprecipitation of FLAG/HA-tagged AGO2 or the PRMT5/MEP50 complex. The beads were washed twice with PBS and 500 µl beads were added directly to the combined sucrose gradient fractions 3-8 for AGO2 precipitation or 4-9 for precipitation of PRMT5. After incubation for 4 h at 4° C with light rotation the beads were washed three times with IP wash buffer and two times with elution buffer. Bound protein was eluted from the beads with 1 mg/ml 3x FLAG peptide (H-MDTKDHDGDYDHDlDYLDDDDL-OH) in

elution buffer for 1 h at 4° C with light rotation. The elution step was repeated twice and all three eluates were combined. The total volume was reduced to 300 μl by concentration in centrifugal filter units with a molecular weight cut off of 30 kDa (Vivaspin 500, Sartorius, Göttingen, Germany, or Microcon Ultracell YM-30, Millipore, Billerica, USA).

Glycerol Density Centrifugation (GraFix)

The concentrated sample was loaded onto a 10-30% glycerol gradient in gradient buffer. For GraFix gradients [150], 0.1% glutaraldehyde was added to the 30% glycerol solution prior to gradient mixing. The gradients were centrifuged with 42500 rpm at 4° C for 16 h in an SW 60 rotor and fractionated manually.

Electron Microscopy

The electron micrographs shown in Figure 2.1.2 were taken by Ilonka Bartozek at the Holger Stark Laboratory at the MPI for Biophysical Chemistry in Göttingen.
All further work was carried out by members of the Beckmann Group at the Ludwigs-Maximilians University Munich. Negative staining of the samples with uranyl acetate for electron microscopy was performed by Charlotte Ungewickell. Micrographs were recorded on a 120 kV Tecnai G2 Spirit (FEI, Oregon, USA) by Otto Berninghausen and Charlotte Ungewickell. Martin Turk performed all data analysis and 3D reconstructions. In short, about 6000 particles were picked automatically with a template based particle selection tool, manually adjusting the threshold values for each micrograph. Particles with positive staining or a flat appearance as well as particles not discernible from background were sorted out manually. The remaining 1700 particles were normalized, band pass filtered, centered and masked in IMAGIC. Class averages were generated by multi-variant statistical analysis and multi reference alignment in IMAGIC. Three class averages with obvious size differences were selected and particles were sub-classified into three groups based on the selected class averages. For each group 10 initial models were generated using common lines and the best initial model was submitted to 50 rounds of refinement by projection matching in EMAN2.

4.2.5 Purification of Protein Complexes for Mass Spectrometry Analysis

Preparation of Antibody Matrix by Direct Coupling

Antibodies against endogenous proteins were coupled to Protein G Sepharose beads as described previously (see Section "Antibody Matrix Preparation" on page 113) with

the alteration that beads were washed twice with 10 volumes of 0.2 mM sodium borate
pH 9.0 after incubation. The beads were then resuspended in 10 volumes of 200 mM
sodium borate and solid dimethylpimelimidate was added to reach a final concentration
of 20 mM. The reaction was incubated at RT for 30 min and stopped by washing the
beads once in 200 mM ethanolamine, pH 8.0 and followed by incubation in 200 mM
ethanolamine, pH 8.0 at RT for 2 h with gentle mixing. The beads were washed twice
with PBS and either used directly or stored in PBS with 0.01% sodium azide at 4°C for
up to 8 weeks.

Immunoprecipitation of Endogenous AGO2-Containing Complexes

Lysates from SILAC labeled cells were prepared as described previously (see Section
"Whole Cell Lysate Preparation" on page 112). Five mg of total lysate protein were
incubated with 50 µl antibody coupled beads for 4 h at 4°C with rotation. If necessary,
the lysate volume was equalized by adding lysis buffer. After protein binding, the beads
were washed three times with IP wash buffer followed by two washing steps with elution
buffer. The samples were combined and for IPs with the anti-AGO2(6F4) antibody
bound protein was eluted from the beads in elution buffer with 500 µg/ml AGO2 peptide
(H-APTTSPIPGYAFKP-OH) for 1 h at RT and shaking at 1000 rpm. In IPs using
the anti-AGO2(C43C6) antibody (Cell Signalling, Danvers, USA), bound protein was
eluted from the beads by adding an equal volume of 2x Novex Sample Buffer (Invitrogen,
Carlsbad, USA) with 20 mM DTT followed by an incubation at 75°C for 10 min.

Immunoprecipitation of FLAG/HA-tagged AGO2-Containing Complexes

SILAC labeled MEFs were lysed in lysis buffer as described earlier (see Section "Whole
Cell Lysate Preparation" on page 112). For immunoprecipitation, 3-4 mg total lysate
protein were incubated with 50 µl M2 anti-FLAG M2 affinity gel (Sigma, St. Louis, USA)
for 4 h at 4°C with rotation. In the cases where the experiments addressed the RNA
dependency of the interactions, 100 µg/ml RNase A (Fermentas, Burlington, Canada)
was added either at the beginning of the 4 h incubation or 20 min prior to the washing
steps. Beads were washed three times with IP wash buffer and twice with elution buffer.
Samples were combined and bound protein was eluted with 500 µg/ml 3x FLAG peptide
in elution buffer for 90 min at 4°C with shaking at 800 rpm.

Large RNA Binding Assay

Lysate preparation and immunoprecipitations were conducted as described above with
the alteration that 100 µg/ml RNase A (Fermentas, Burlington, Canada) was added

either at the beginning of the 4 h incubation or 20 min prior to the washing steps. RNAs were isolated by Protease K digest and phenol-chlorophorm extraction as described (see Section "RNA isolation" on page 115). Precipitated RNAs were resuspended in a formaldehyde containing, denaturing loading buffer and were either visualized with ethidium bromide staining after size separation in an 1% TBE buffered agarose gel or analyzed by Northern blotting as described previously (see Section "Northern Blotting" on page 115).

In Gel Trypsin Digest, Peptide Extraction and Stage Tipping

The protein samples were separated on NuPAGE Novex 4-12% Bis-Tris gels (Invitrogen, Carlsbad, USA) and stained with the Novex Colloidal Blue Stain Kit (Invitrogen, Carlsbad, USA) according to the manufacturers instruction. Each lane was cut into eight slices and each slice was cut into 1 mm x 1 mm cubes. Gel pieces were destained in 25 mM ammonium bicarbonate and 50% ethanol for 10 min at RT and 1200 rpm. This destaining step was repeated until no more coomassie was visible. The gel pieces were dehydrated by adding 100% acetonitrile and dried in a vacuum centrifuge. Disulfide bonds on cysteine were reduced with 1 mM DTT in 50 mM ammonium bicarbonate for 45 min at 56° C and shaking at 800 rpm followed by alkylation of cysteins by 5 mM iodacetamide 50 mM ammonium bicarbonate for 30 min at RT in the dark. Samples were washed twice with 50 mM ammonium bicarbonate, dehydrated twice with 100% acetonitrile and dried in a vacuum centrifuge. Proteins were digested with 13 ng/μl trypsin (sequencing grade, modified; Promega, Madison, USA) in 50 mM ammonium bicarbonate over night at 37° C. The digestion was stopped by the addition of 30% (v/v) acetronitrile and 3% (v/v) trifluoroacetic acid in 50 mM ammonium bicarbonate. Samples were incubated at RT for 30 min and the extract was collected in a fresh reaction tube. Extraction of proteins was continued with 100% acetonitrile at RT until the gel cubes were completely dehydrated. The volume of the extract was reduced to 1/5 of initial volume by vacuum centrifugation and the pH was lowered by addition of 40 μl buffer A*. Stage tips for desalting of the samples were prepared by assembling C18 material (3M, St. Paul, USA) in a pipette tip. The C18 material was activated with methanol and equilibrated with buffer A*. After protein sample loading stage tips were washed twice with buffer A. Loaded stage tips were stored at 4° C until mass spectrometry analysis.

4.2.6 Mass Spectrometry Analysis and Data Processing

Peptides were eluted from stage tips with 40 μl buffer B, evaporated to 4 μl in a vacuum centrifuge and 4 μl buffer A were added. Peptides were separated on line to the mass

spectrometer by using an easy nano-LC system (Proxeon Biosystems, Thermo Fisher Scientific, Waltham, USA). 4 µl sample were loaded with a constant flow of 700 nl/min onto a 15 cm fused silica emitter with an inner diameter of 75 µm (Proxeon Biosystems,Thermo Fisher Scientific, Waltham, USA) packed in-house with RP ReproSil-Pur C18-AQ 3 µm resin (Dr. Maisch, Ammerbuch-Entringen, Germany). Peptides were eluted with a segmented gradient of 5–60% solvent B over 105 min with a constant flow of 250 nl/min. The nano-LC system was coupled to a mass spectrometer (LTQ-Orbitrap or LTQ-Orbitrap Velos, Thermo Fisher Scientific, Waltham, USA) via a nanoscale LC interface (Proxeon Biosystems, Thermo Fisher Scientific, Waltham, USA). The spray voltage was set between 2.0 and 2.2 kV, and the temperature of the heated capillary was set to 200° C.

Survey full-scan MS spectra (m/z = 300–2000) were acquired in the Orbitrap with a resolution of 60,000 at the theoretical m/z = 400 after accumulation of 1 000 000 ions in the Orbitrap. The five most intense ions from the preview survey scan delivered by the Orbitrap were sequenced by centromere identifier (collision energy 35%) in the LTQ after accumulation of 5 000 ions concurrently to full scan acquisition in the Orbitrap. Maximal filling times were 1 000 ms for the full scans and 150 ms for the MS/MS. Precursor ion charge state screening was enabled and all unassigned charge states as well as singly charged peptides were rejected. The dynamic exclusion list was restricted to a maximum of 500 entries with a maximum retention period of 90 s and a relative mass window of 10 ppm. Orbitrap measurements were performed with the lock mass option enabled for survey scans to improve mass accuracy [242].

Raw MS data was analyzed using the in-house developed software MaxQuant (version 1.1.1.27, [48]). Data was searched against an IPI mouse database (version 3.68), supplemented with frequently observed contaminants, employing a reverse database search strategy for FDR estimation [260]. Carbamidomethylated cysteins were set as fixed, oxidation of methionine and N-terminal acetylation as variable modifications. Mass deviation of 0.5 D was set as maximum allowed for MS/MS peaks, and a maximum of two missed cleavages were allowed. Maximum false discovery rates were set to 0.01 both on peptide and protein levels. Minimum required peptide length was six amino acids. Corresponding forward and reverse experiments were analyzed together and specified as 'forward' and 'reverse' in the experimental design.

Raw MS data, unfilted proteingroups tables and peptides tables can be downloaded from https://proteomecommons.org/tranche using the following hash:

a6LrT+dbaF4jmWZcpYPJuvIzNTFmI0VhkHfqhh4SwQ8l68MSFv5dnfBw35h8RNo99y QZUIAhTvWHpL+xXo7dW25eigAAAAAAAABXfA==

All further analysis was done in a script based manner employing R (http://www.r-project.org). Proteingroups were further filtered requiring at least two unique peptides per protein identification, and 2 ratio counts (quantification events) in the forward as well as in the reverse experiment. For all analysis log2 transformed normalized ratios (as computed by MaxQuant) were used. To visualize the data, the logarithmized normalized ratios of the forward and reverse experiments are plotted against each other. For the hierarchical clustering proteins were considered that show a ratio of above 3.8 and below 0.3 in the forward and the reverse experiment, respectively, for the wt F/H-AGO2 vs wt GFP dataset and 3.0 and 0.3 for the ko F/H-AGO2 vs ko GFP dataset. The cut offs were derived manually from the ratio plots. In addition, quantification of the protein in at least 2 out of 3 experiments was required. The three separate experiments were combined using the Uniprot identifier, and proteins were clustered employing an euclidian distance matrix. Columns were not clustered.

Abbreviations

List of Figures

128

List of Tables

References

[1] R. Aebersold and M. Mann. Mass spectrometry-based proteomics. *Nature*, 422(6928):198–207, Mar 2003.

[2] A. S. Alvarado and P. A. Newmark. Double-stranded rna specifically disrupts gene expression during planarian regeneration. *Proc Natl Acad Sci U S A*, 96(9):5049–5054, Apr 1999.

[3] P. Anderson and N. Kedersha. Rna granules. *J Cell Biol*, 172(6):803–808, Mar 2006.

[4] T. Andl, E. P. Murchison, F. Liu, Y. Zhang, M. Yunta-Gonzalez, J. W. Tobias, C. D. Andl, J. T. Seykora, G. J. Hannon, and S. E. Millar. The mirna-processing enzyme dicer is essential for the morphogenesis and maintenance of hair follicles. *Curr Biol*, 16(10):1041–1049, May 2006.

[5] M. A. Andrei, D. Ingelfinger, R. Heintzmann, T. Achsel, R. Rivera-Pomar, and R. Lührmann. A role for eif4e and eif4e-transporter in targeting mrnps to mammalian processing bodies. *RNA*, 11(5):717–727, May 2005.

[6] J. Anne and B. M. Mechler. Valois, a component of the nuage and pole plasm, is involved in assembly of these structures, and binds to tudor and the methyltransferase capsuléen. *Development*, 132(9):2167–2177, May 2005.

[7] A. Aravin, D. Gaidatzis, S. Pfeffer, M. Lagos-Quintana, P. Landgraf, N. Iovino, P. Morris, M. J. Brownstein, S. Kuramochi-Miyagawa, T. Nakano, M. Chien, J. J. Russo, J. Ju, R. Sheridan, C. Sander, M. Zavolan, and T. Tuschl. A novel class of small rnas bind to mili protein in mouse testes. *Nature*, 442(7099):203–207, Jul 2006.

[8] A. A. Aravin, M. Lagos-Quintana, A. Yalcin, M. Zavolan, D. Marks, B. Snyder, T. Gaasterland, J. Meyer, and T. Tuschl. The small rna profile during drosophila melanogaster development. *Dev Cell*, 5(2):337–350, Aug 2003.

[9] A. A. Aravin, N. M. Naumova, A. V. Tulin, V. V. Vagin, Y. M. Rozovsky, and V. A. Gvozdev. Double-stranded rna-mediated silencing of genomic tandem repeats and transposable elements in the d. melanogaster germline. *Curr Biol*, 11(13):1017–1027, Jul 2001.

[10] A. A. Aravin, R. Sachidanandam, D. Bourc'his, C. Schaefer, D. Pezic, K. F. Toth, T. Bestor, and G. J. Hannon. A pirna pathway primed by individual transposons is linked to de novo dna methylation in mice. *Mol Cell*, 31(6):785–799, Sep 2008.

[11] A. A. Aravin, R. Sachidanandam, A. Girard, K. Fejes-Toth, and G. J. Hannon. Developmentally regulated pirna clusters implicate mili in transposon control. *Science*, 316(5825):744–747, May 2007.

[12] A. Azuma-Mukai, H. Oguri, T. Mituyama, Z. R. Qian, K. Asai, H. Siomi, and M. C. Siomi. Characterization of endogenous human argonautes and their mirna partners in rna silencing. *Proc Natl Acad Sci U S A*, 105(23):7964–7969, Jun 2008.

[13] J. E. Babiarz, J. G. Ruby, Y. Wang, D. P. Bartel, and R. Blelloch. Mouse es cells express endogenous shrnas, sirnas, and other microprocessor-independent, dicer-dependent small rnas. *Genes Dev*, 22(20):2773–2785, Oct 2008.

[14] D. Baek, J. Villén, C. Shin, F. D. Camargo, S. P. Gygi, and D. P. Bartel. The impact of micrornas on protein output. *Nature*, 455(7209):64–71, Sep 2008.

[15] S. Bagga, J. Bracht, S. Hunter, K. Massirer, J. Holtz, R. Eachus, and A. E. Pasquinelli. Regulation by let-7 and lin-4 mirnas results in target mrna degradation. *Cell*, 122(4):553–563, Aug 2005.

[16] M. B. Bahramian and H. Zarbl. Transcriptional and posttranscriptional silencing of rodent alpha1(i) collagen by a homologous transcriptionally self-silenced transgene. *Mol Cell Biol*, 19(1):274–283, Jan 1999.

[17] C. Barreau, L. Paillard, and H. B. Osborne. Au-rich elements and associated factors: are there unifying principles? *Nucleic Acids Res*, 33(22):7138–7150, 2005.

[18] D. P. Bartel. Micrornas: genomics, biogenesis, mechanism, and function. *Cell*, 116(2):281–297, Jan 2004.

[19] I. Behm-Ansmant, J. Rehwinkel, T. Doerks, A. Stark, P. Bork, and E. Izaurralde. mrna degradation by mirnas and gw182 requires both ccr4:not deadenylase and dcp1:dcp2 decapping complexes. *Genes Dev*, 20(14):1885–1898, Jul 2006.

134

[20] M. Beitzinger, L. Peters, J. Y. Zhu, E. Kremmer, and G. Meister. Identification of human microrna targets from isolated argonaute protein complexes. *RNA Biol*, 4(2):76–84, Jun 2007.

[21] A. Belisova, K. Semrad, O. Mayer, G. Kocian, E. Waigmann, R. Schroeder, and G. Steiner. Rna chaperone activity of protein components of human ro rnps. *RNA*, 11(7):1084–1094, Jul 2005.

[22] E. Bernstein, A. A. Caudy, S. M. Hammond, and G. J. Hannon. Role for a bidentate ribonuclease in the initiation step of rna interference. *Nature*, 409(6818):363–366, Jan 2001.

[23] S. N. Bhattacharyya, R. Habermacher, U. Martine, E. I. Closs, and W. Filipowicz. Relief of microrna-mediated translational repression in human cells subjected to stress. *Cell*, 125(6):1111–1124, Jun 2006.

[24] B. Blagoev, I. Kratchmarova, S.-E. Ong, M. Nielsen, L. J. Foster, and M. Mann. A proteomics strategy to elucidate functional protein-protein interactions applied to egf signaling. *Nat Biotechnol*, 21(3):315–318, Mar 2003.

[25] M. T. Bohnsack, K. Czaplinski, and D. Gorlich. Exportin 5 is a rangtp-dependent dsrna-binding protein that mediates nuclear export of pre-mirnas. *RNA*, 10(2):185–191, Feb 2004.

[26] A. Boland, E. Huntzinger, S. Schmidt, E. Izaurralde, and O. Weichenrieder. Crystal structure of the mid-piwi lobe of a eukaryotic argonaute protein. *Proc Natl Acad Sci U S A*, Jun 2011.

[27] A. Boland, F. Tritschler, S. Heimstädt, E. Izaurralde, and O. Weichenrieder. Crystal structure and ligand binding of the mid domain of a eukaryotic argonaute protein. *EMBO Rep*, 11(7):522–527, Jul 2010.

[28] H. M. Bond, M. Mesuraca, N. Amodio, T. Mega, V. Agosti, D. Fanello, D. Pelaggi, L. Bullinger, M. Grieco, M. A. S. Moore, S. Venuta, and G. Morrone. Early hematopoietic zinc finger protein-zinc finger protein 521: a candidate regulator of diverse immature cells. *Int J Biochem Cell Biol*, 40(5):848–854, 2008.

[29] G. M. Borchert, W. Lanier, and B. L. Davidson. Rna polymerase iii transcribes human micrornas. *Nat Struct Mol Biol*, 13(12):1097–1101, Dec 2006.

[30] T. L. Branscombe, A. Frankel, J. H. Lee, J. R. Cook, Z. Yang, S. Pestka, and S. Clarke. Prmt5 (janus kinase-binding protein 1) catalyzes the formation of symmetric dimethylarginine residues in proteins. *J Biol Chem*, 276(35):32971–32976, Aug 2001.

[31] M. Brengues, D. Teixeira, and R. Parker. Movement of eukaryotic mrnas between polysomes and cytoplasmic processing bodies. *Science*, 310(5747):486–489, Oct 2005.

[32] J. Brennecke, A. A. Aravin, A. Stark, M. Dus, M. Kellis, R. Sachidanandam, and G. J. Hannon. Discrete small rna-generating loci as master regulators of transposon activity in drosophila. *Cell*, 128(6):1089–1103, Mar 2007.

[33] J. Brennecke, C. D. Malone, A. A. Aravin, R. Sachidanandam, A. Stark, and G. J. Hannon. An epigenetic role for maternally inherited pirnas in transposon silencing. *Science*, 322(5906):1387–1392, Nov 2008.

[34] C. Burrows, N. A. Latip, S.-J. Lam, L. Carpenter, K. Sawicka, G. Tzolovsky, H. Gabra, M. Bushell, D. M. Glover, A. E. Willis, and S. P. Blagden. The rna binding protein larp1 regulates cell division, apoptosis and cell migration. *Nucleic Acids Res*, 38(16):5542–5553, Sep 2010.

[35] M. A. Carmell, A. Girard, H. J. G. van de Kant, D. Bourc'his, T. H. Bestor, D. G. de Rooij, and G. J. Hannon. Miwi2 is essential for spermatogenesis and repression of transposons in the mouse male germline. *Dev Cell*, 12(4):503–514, Apr 2007.

[36] R. W. Carthew and E. J. Sontheimer. Origins and mechanisms of mirnas and sirnas. *Cell*, 136(4):642–655, Feb 2009.

[37] A. A. Caudy, M. Myers, G. J. Hannon, and S. M. Hammond. Fragile x-related protein and vig associate with the rna interference machinery. *Genes Dev*, 16(19):2491–2496, Oct 2002.

[38] C. C. Chan, J. Dostie, M. D. Diem, W. Feng, M. Mann, J. Rappsilber, and G. Dreyfuss. eif4a3 is a novel component of the exon junction complex. *RNA*, 10(2):200–209, Feb 2004.

[39] N. Chang, J. Yi, G. Guo, X. Liu, Y. Shang, T. Tong, Q. Cui, M. Zhan, M. Gorospe, and W. Wang. Hur uses auf1 as a cofactor to promote p16ink4 mrna decay. *Mol Cell Biol*, 30(15):3875–3886, Aug 2010.

[40] S. Cheloufi, C. O. D. Santos, M. M. W. Chong, and G. J. Hannon. A dicer-independent mirna biogenesis pathway that requires ago catalysis. *Nature*, 465(7298):584–589, Jun 2010.

[41] C. Chen, J. Jin, D. A. James, M. A. Adams-Cioaba, J. G. Park, Y. Guo, E. Tenaglia, C. Xu, G. Gish, J. Min, and T. Pawson. Mouse piwi interactome identifies binding mechanism of tdrkh tudor domain to arginine methylated miwi. *Proc Natl Acad Sci U S A*, 106(48):20336–20341, Dec 2009.

[42] T. P. Chendrimada, K. J. Finn, X. Ji, D. Baillat, R. I. Gregory, S. A. Liebhaber, A. E. Pasquinelli, and R. Shiekhattar. Microrna silencing through risc recruitment of eif6. *Nature*, 447(7146):823–828, Jun 2007.

[43] T. P. Chendrimada, R. I. Gregory, E. Kumaraswamy, J. Norman, N. Cooch, K. Nishikura, and R. Shiekhattar. Trbp recruits the dicer complex to ago2 for microrna processing and gene silencing. *Nature*, 436(7051):740–744, Aug 2005.

[44] S. W. Chi, J. B. Zang, A. Mele, and R. B. Darnell. Argonaute hits-clip decodes microrna-mrna interaction maps. *Nature*, 460(7254):479–486, Jul 2009.

[45] D. Cifuentes, H. Xue, D. W. Taylor, H. Patnode, Y. Mishima, S. Cheloufi, E. Ma, S. Mane, G. J. Hannon, N. D. Lawson, S. A. Wolfe, and A. J. Giraldez. A novel mirna processing pathway independent of dicer requires argonaute2 catalytic activity. *Science*, 328(5986):1694–1698, Jun 2010.

[46] L. C. Cobbold, L. A. Wilson, K. Sawicka, H. A. King, A. V. Kondrashov, K. A. Spriggs, M. Bushell, and A. E. Willis. Upregulated c-myc expression in multiple myeloma by internal ribosome entry results from increased interactions with and expression of ptb-1 and yb-1. *Oncogene*, 29(19):2884–2891, May 2010.

[47] S. Covey, N. Al-Kaff, A. Lángara, and D. Turner. Plants combat infection by gene silencing. *Nature*, 385:781–782, 1997.

[48] J. Cox and M. Mann. Maxquant enables high peptide identification rates, individualized p.p.b.-range mass accuracies and proteome-wide protein quantification. *Nat Biotechnol*, 26(12):1367–1372, Dec 2008.

[49] J. Cox and M. Mann. Quantitative, high-resolution proteomics for data-driven systems biology. *Annu Rev Biochem*, 80:273–299, Jun 2011.

[50] B. Czech, C. D. Malone, R. Zhou, A. Stark, C. Schlingeheyde, M. Dus, N. Perrimon, M. Kellis, J. A. Wohlschlegel, R. Sachidanandam, G. J. Hannon, and

J. Brennecke. An endogenous small interfering rna pathway in drosophila. *Nature*, 453(7196):798–802, Jun 2008.

[51] T. Dalmay, A. Hamilton, S. Rudd, S. Angell, and D. C. Baulcombe. An rna-dependent rna polymerase gene in arabidopsis is required for posttranscriptional gene silencing mediated by a transgene but not by a virus. *Cell*, 101(5):543–553, May 2000.

[52] B. N. Davis, A. C. Hilyard, G. Lagna, and A. Hata. Smad proteins control drosha-mediated microrna maturation. *Nature*, 454(7200):56–61, Jul 2008.

[53] E. Davis, F. Caiment, X. Tordoir, J. Cavaillé, A. Ferguson-Smith, N. Cockett, M. Georges, and C. Charlier. Rnai-mediated allelic trans-interaction at the imprinted rtl1/peg11 locus. *Curr Biol*, 15(8):743–749, Apr 2005.

[54] A. M. Denli, B. B. J. Tops, R. H. A. Plasterk, R. F. Ketting, and G. J. Hannon. Processing of primary micrornas by the microprocessor complex. *Nature*, 432(7014):231–235, Nov 2004.

[55] S. Diederichs and D. A. Haber. Dual role for argonautes in microrna processing and posttranscriptional regulation of microrna expression. *Cell*, 131(6):1097–1108, Dec 2007.

[56] S. Djuranovic, M. K. Zinchenko, J. K. Hur, A. Nahvi, J. L. Brunelle, E. J. Rogers, and R. Green. Allosteric regulation of argonaute proteins by mirnas. *Nat Struct Mol Biol*, 17(2):144–150, Feb 2010.

[57] J. G. Doench, C. P. Petersen, and P. A. Sharp. sirnas can function as mirnas. *Genes Dev*, 17(4):438–442, Feb 2003.

[58] J. G. Doench and P. A. Sharp. Specificity of microrna target selection in translational repression. *Genes Dev*, 18(5):504–511, Mar 2004.

[59] Z. Du, J. K. Lee, R. Tjhen, R. M. Stroud, and T. L. James. Structural and biochemical insights into the dicing mechanism of mouse dicer: a conserved lysine is critical for dsrna cleavage. *Proc Natl Acad Sci U S A*, 105(7):2391–2396, Feb 2008.

[60] K. Duncan, M. Grskovic, C. Strein, K. Beckmann, R. Niggeweg, I. Abaza, F. Gebauer, M. Wilm, and M. W. Hentze. Sex-lethal imparts a sex-specific function to unr by recruiting it to the msl-2 mrna 3' utr: translational repression for dosage compensation. *Genes Dev*, 20(3):368–379, Feb 2006.

[61] K. E. Duncan, C. Strein, and M. W. Hentze. The sxl-unr corepressor complex uses a pabp-mediated mechanism to inhibit ribosome recruitment to msl-2 mrna. *Mol Cell*, 36(4):571–582, Nov 2009.

[62] A. M. Duursma, M. Kedde, M. Schrier, C. le Sage, and R. Agami. mir-148 targets human dnmt3b protein coding region. *RNA*, 14(5):872–877, May 2008.

[63] G. Easow, A. A. Teleman, and S. M. Cohen. Isolation of microrna targets by mirnp immunopurification. *RNA*, 13(8):1198–1204, Aug 2007.

[64] H. C. Eberl, M. Mann, and M. Vermeulen. Quantitative proteomics for epigenetics. *Chembiochem*, 12(2):224–234, Jan 2011.

[65] A. M. Eiring, J. G. Harb, P. Neviani, C. Garton, J. J. Oaks, R. Spizzo, S. Liu, S. Schwind, R. Santhanam, C. J. Hickey, H. Becker, J. C. Chandler, R. Andino, J. Cortes, P. Hokland, C. S. Huettner, R. Bhatia, D. C. Roy, S. A. Liebhaber, M. A. Caligiuri, G. Marcucci, R. Garzon, C. M. Croce, G. A. Calin, and D. Perrotti. mir-328 functions as an rna decoy to modulate hnrnp e2 regulation of mrna translation in leukemic blasts. *Cell*, 140(5):652–665, Mar 2010.

[66] S. M. Elbashir, J. Harborth, W. Lendeckel, A. Yalcin, K. Weber, and T. Tuschl. Duplexes of 21-nucleotide rnas mediate rna interference in cultured mammalian cells. *Nature*, 411(6836):494–498, May 2001.

[67] S. M. Elbashir, J. Martinez, A. Patkaniowska, W. Lendeckel, and T. Tuschl. Functional anatomy of sirnas for mediating efficient rnai in drosophila melanogaster embryo lysate. *EMBO J*, 20(23):6877–6888, Dec 2001.

[68] C. Ender, A. Krek, M. R. Friedländer, M. Beitzinger, L. Weinmann, W. Chen, S. Pfeffer, N. Rajewsky, and G. Meister. A human snorna with microrna-like functions. *Mol Cell*, 32(4):519–528, Nov 2008.

[69] C. Ender and G. Meister. Argonaute proteins at a glance. *J Cell Sci*, 123(Pt 11):1819–1823, Jun 2010.

[70] A. Eulalio, I. Behm-Ansmant, and E. Izaurralde. P bodies: at the crossroads of post-transcriptional pathways. *Nat Rev Mol Cell Biol*, 8(1):9–22, Jan 2007.

[71] A. Eulalio, I. Behm-Ansmant, D. Schweizer, and E. Izaurralde. P-body formation is a consequence, not the cause, of rna-mediated gene silencing. *Mol Cell Biol*, 27(11):3970–3981, Jun 2007.

[72] A. Eulalio, S. Helms, C. Fritzsch, M. Fauser, and E. Izaurralde. A c-terminal silencing domain in gw182 is essential for mirna function. *RNA*, 15(6):1067–1077, Jun 2009.

[73] A. Eulalio, E. Huntzinger, and E. Izaurralde. Gw182 interaction with argonaute is essential for mirna-mediated translational repression and mrna decay. *Nat Struct Mol Biol*, 15(4):346–353, Apr 2008.

[74] A. Eulalio, E. Huntzinger, T. Nishihara, J. Rehwinkel, M. Fauser, and E. Izaurralde. Deadenylation is a widespread effect of mirna regulation. *RNA*, 15(1):21–32, Jan 2009.

[75] A. Eulalio, J. Rehwinkel, M. Stricker, E. Huntzinger, S.-F. Yang, T. Doerks, S. Dorner, P. Bork, M. Boutros, and E. Izaurralde. Target-specific requirements for enhancers of decapping in mirna-mediated gene silencing. *Genes Dev*, 21(20):2558–2570, Oct 2007.

[76] A. Eulalio, F. Tritschler, and E. Izaurralde. The gw182 protein family in animal cells: new insights into domains required for mirna-mediated gene silencing. *RNA*, 15(8):1433–1442, Aug 2009.

[77] T. Eystathioy, E. K. L. Chan, S. A. Tenenbaum, J. D. Keene, K. Griffith, and M. J. Fritzler. A phosphorylated cytoplasmic autoantigen, gw182, associates with a unique population of human mrnas within novel cytoplasmic speckles. *Mol Biol Cell*, 13(4):1338–1351, Apr 2002.

[78] T. Eystathioy, A. Jakymiw, E. K. L. Chan, B. Séraphin, N. Cougot, and M. J. Fritzler. The gw182 protein colocalizes with mrna degradation associated proteins hdcp1 and hlsm4 in cytoplasmic gw bodies. *RNA*, 9(10):1171–1173, Oct 2003.

[79] M. R. Fabian, G. Mathonnet, T. Sundermeier, H. Mathys, J. T. Zipprich, Y. V. Svitkin, F. Rivas, M. Jinek, J. Wohlschlegel, J. A. Doudna, C.-Y. A. Chen, A.-B. Shyu, J. R. Yates, G. J. Hannon, W. Filipowicz, T. F. Duchaine, and N. Sonenberg. Mammalian mirna risc recruits caf1 and pabp to affect pabp-dependent deadenylation. *Mol Cell*, 35(6):868–880, Sep 2009.

[80] M. R. Fabian, N. Sonenberg, and W. Filipowicz. Regulation of mrna translation and stability by micrornas. *Annu Rev Biochem*, 79:351–379, 2010.

[81] S. Fields and R. Sternglanz. The two-hybrid system: an assay for protein-protein interactions. *Trends Genet*, 10(8):286–292, Aug 1994.

[82] W. Filipowicz, S. N. Bhattacharyya, and N. Sonenberg. Mechanisms of post-transcriptional regulation by micrornas: are the answers in sight? *Nat Rev Genet*, 9(2):102–114, Feb 2008.

[83] A. Fire, S. Xu, M. K. Montgomery, S. A. Kostas, S. E. Driver, and C. C. Mello. Potent and specific genetic interference by double-stranded rna in caenorhabditis elegans. *Nature*, 391(6669):806–811, Feb 1998.

[84] F. Frank, M. R. Fabian, J. Stepinski, J. Jemielity, E. Darzynkiewicz, N. Sonenberg, and B. Nagar. Structural analysis of 5'-mrna-cap interactions with the human ago2 mid domain. *EMBO Rep*, 12(5):415–420, May 2011.

[85] F. Frank, N. Sonenberg, and B. Nagar. Structural basis for 5'-nucleotide base-specific recognition of guide rna by human ago2. *Nature*, 465(7299):818–822, Jun 2010.

[86] T. M. Franks and J. Lykke-Andersen. Ttp and brf proteins nucleate processing body formation to silence mrnas with au-rich elements. *Genes Dev*, 21(6):719–735, Mar 2007.

[87] W. J. Friesen, S. Paushkin, A. Wyce, S. Massenet, G. S. Pesiridis, G. V. Duyne, J. Rappsilber, M. Mann, and G. Dreyfuss. The methylosome, a 20s complex containing jbp1 and picln, produces dimethylarginine-modified sm proteins. *Mol Cell Biol*, 21(24):8289–8300, Dec 2001.

[88] W. J. Friesen, A. Wyce, S. Paushkin, L. Abel, J. Rappsilber, M. Mann, and G. Dreyfuss. A novel wd repeat protein component of the methylosome binds sm proteins. *J Biol Chem*, 277(10):8243–8247, Mar 2002.

[89] K. Förstemann, M. D. Horwich, L. Wee, Y. Tomari, and P. D. Zamore. Drosophila micrornas are sorted into functionally distinct argonaute complexes after production by dicer-1. *Cell*, 130(2):287–297, Jul 2007.

[90] K. Förstemann, Y. Tomari, T. Du, V. V. Vagin, A. M. Denli, D. P. Bratu, C. Klattenhoff, W. E. Theurkauf, and P. D. Zamore. Normal microrna maturation and germ-line stem cell maintenance requires loquacious, a double-stranded rna-binding domain protein. *PLoS Biol*, 3(7):e236, Jul 2005.

[91] A. Galgano, M. Forrer, L. Jaskiewicz, A. Kanitz, M. Zavolan, and A. P. Gerber. Comparative analysis of mrna targets for human puf-family proteins suggests extensive interaction with the mirna regulatory system. *PLoS One*, 3(9):e3164, 2008.

[92] N. H. Gehring, J. B. Kunz, G. Neu-Yilik, S. Breit, M. H. Viegas, M. W. Hentze, and A. E. Kulozik. Exon-junction complex components specify distinct routes of nonsense-mediated mrna decay with differential cofactor requirements. *Mol Cell*, 20(1):65–75, Oct 2005.

[93] N. H. Gehring, S. Lamprinaki, M. W. Hentze, and A. E. Kulozik. The hierarchy of exon-junction complex assembly by the spliceosome explains key features of mammalian nonsense-mediated mrna decay. *PLoS Biol*, 7(5):e1000120, May 2009.

[94] A. D. George and S. A. Tenenbaum. Microrna modulation of rna-binding protein regulatory elements. *RNA Biol*, 3(2):57–59, Apr 2006.

[95] V. R. Gerbasi, D. E. Golden, S. B. Hurtado, and E. J. Sontheimer. Proteomics identification of drosophila small interfering rna-associated factors. *Mol Cell Proteomics*, 9(9):1866–1872, Sep 2010.

[96] M. Ghildiyal and P. D. Zamore. Small silencing rnas: an expanding universe. *Nat Rev Genet*, 10(2):94–108, Feb 2009.

[97] D. J. Gibbings, C. Ciaudo, M. Erhardt, and O. Voinnet. Multivesicular bodies associate with components of mirna effector complexes and modulate mirna activity. *Nat Cell Biol*, 11(9):1143–1149, Sep 2009.

[98] A.-C. Gingras, M. Gstaiger, B. Raught, and R. Aebersold. Analysis of protein complexes using mass spectrometry. *Nat Rev Mol Cell Biol*, 8(8):645–654, Aug 2007.

[99] A. J. Giraldez, Y. Mishima, J. Rihel, R. J. Grocock, S. V. Dongen, K. Inoue, A. J. Enright, and A. F. Schier. Zebrafish mir-430 promotes deadenylation and clearance of maternal mrnas. *Science*, 312(5770):75–79, Apr 2006.

[100] A. Girard, R. Sachidanandam, G. J. Hannon, and M. A. Carmell. A germline-specific class of small rnas binds mammalian piwi proteins. *Nature*, 442(7099):199–202, Jul 2006.

[101] E. Glasmacher, K. P. Hoefig, K. U. Vogel, N. Rath, L. Du, C. Wolf, E. Kremmer, X. Wang, and V. Heissmeyer. Roquin binds inducible costimulator mrna and effectors of mrna decay to induce microrna-independent post-transcriptional repression. *Nat Immunol*, 11(8):725–733, Aug 2010.

[102] R. I. Gregory, T. P. Chendrimada, N. Cooch, and R. Shiekhattar. Human risc couples microrna biogenesis and posttranscriptional gene silencing. *Cell*, 123(4):631–640, Nov 2005.

[103] R. I. Gregory, K.-P. Yan, G. Amuthan, T. Chendrimada, B. Doratotaj, N. Cooch, and R. Shiekhattar. The microprocessor complex mediates the genesis of micrornas. *Nature*, 432(7014):235–240, Nov 2004.

[104] M. Grimmler, S. Otter, C. Peter, F. Müller, A. Chari, and U. Fischer. Unrip, a factor implicated in cap-independent translation, associates with the cytosolic smn complex and influences its intracellular localization. *Hum Mol Genet*, 14(20):3099–3111, Oct 2005.

[105] A. Grimson, K. K.-H. Farh, W. K. Johnston, P. Garrett-Engele, L. P. Lim, and D. P. Bartel. Microrna targeting specificity in mammals: determinants beyond seed pairing. *Mol Cell*, 27(1):91–105, Jul 2007.

[106] A. Grishok, A. E. Pasquinelli, D. Conte, N. Li, S. Parrish, I. Ha, D. L. Baillie, A. Fire, G. Ruvkun, and C. C. Mello. Genes and mechanisms related to rna interference regulate expression of the small temporal rnas that control c. elegans developmental timing. *Cell*, 106(1):23–34, Jul 2001.

[107] S. Gu, L. Jin, F. Zhang, P. Sarnow, and M. A. Kay. Biological basis for restriction of microrna targets to the 3' untranslated region in mammalian mrnas. *Nat Struct Mol Biol*, 16(2):144–150, Feb 2009.

[108] G. Guderian, C. Peter, J. Wiesner, A. Sickmann, K. Schulze-Osthoff, U. Fischer, and M. Grimmler. Riok1, a new interactor of protein arginine methyltransferase 5 (prmt5), competes with picln for binding and modulates prmt5 complex composition and substrate specificity. *J Biol Chem*, 286(3):1976–1986, Jan 2011.

[109] S. Guil and J. F. Cáceres. The multifunctional rna-binding protein hnrnp a1 is required for processing of mir-18a. *Nat Struct Mol Biol*, 14(7):591–596, Jul 2007.

[110] L. S. Gunawardane, K. Saito, K. M. Nishida, K. Miyoshi, Y. Kawamura, T. Nagami, H. Siomi, and M. C. Siomi. A slicer-mediated mechanism for repeat-associated sirna 5' end formation in drosophila. *Science*, 315(5818):1587–1590, Mar 2007.

[111] H. Guo, N. T. Ingolia, J. S. Weissman, and D. P. Bartel. Mammalian micrornas predominantly act to decrease target mrna levels. *Nature*, 466(7308):835–840, Aug 2010.

[112] C. Gurkan and W. E. Balch. Recombinant production in baculovirus-infected insect cells and purification of the mammalian sec13/sec31 complex. *Methods Enzymol*, 404:58–66, 2005.

[113] S. P. Gygi, B. Rist, S. A. Gerber, F. Turecek, M. H. Gelb, and R. Aebersold. Quantitative analysis of complex protein mixtures using isotope-coded affinity tags. *Nat Biotechnol*, 17(10):994–999, Oct 1999.

[114] A. D. Haase, L. Jaskiewicz, H. Zhang, S. Lainé, R. Sack, A. Gatignol, and W. Filipowicz. Trbp, a regulator of cellular pkr and hiv-1 virus expression, interacts with dicer and functions in rna silencing. *EMBO Rep*, 6(10):961–967, Oct 2005.

[115] M. Hafner, M. Landthaler, L. Burger, M. Khorshid, J. Hausser, P. Berninger, A. Rothballer, M. Ascano, A.-C. Jungkamp, M. Munschauer, A. Ulrich, G. S. Wardle, S. Dewell, M. Zavolan, and T. Tuschl. Transcriptome-wide identification of rna-binding protein and microrna target sites by par-clip. *Cell*, 141(1):129–141, Apr 2010.

[116] A. J. Hamilton and D. C. Baulcombe. A species of small antisense rna in post-transcriptional gene silencing in plants. *Science*, 286(5441):950–952, Oct 1999.

[117] C. M. Hammell, I. Lubin, P. R. Boag, T. K. Blackwell, and V. Ambros. nhl-2 modulates microrna activity in caenorhabditis elegans. *Cell*, 136(5):926–938, Mar 2009.

[118] S. M. Hammond, E. Bernstein, D. Beach, and G. J. Hannon. An rna-directed nuclease mediates post-transcriptional gene silencing in drosophila cells. *Nature*, 404(6775):293–296, Mar 2000.

[119] S. M. Hammond, S. Boettcher, A. A. Caudy, R. Kobayashi, and G. J. Hannon. Argonaute2, a link between genetic and biochemical analyses of rnai. *Science*, 293(5532):1146–1150, Aug 2001.

[120] J. Han, Y. Lee, K.-H. Yeom, Y.-K. Kim, H. Jin, and V. N. Kim. The drosha-dgcr8 complex in primary microrna processing. *Genes Dev*, 18(24):3016–3027, Dec 2004.

[121] J. Han, Y. Lee, K.-H. Yeom, J.-W. Nam, I. Heo, J.-K. Rhee, S. Y. Sohn, Y. Cho, B.-T. Zhang, and V. N. Kim. Molecular basis for the recognition of primary micrornas by the drosha-dgcr8 complex. *Cell*, 125(5):887–901, Jun 2006.

[122] W. He, X. Ma, X. Yang, Y. Zhao, J. Qiu, and H. Hang. A role for the arginine methylation of rad9 in checkpoint control and cellular sensitivity to dna damage. *Nucleic Acids Res*, 39(11):4719–4727, Jun 2011.

[123] I. R. Henderson, X. Zhang, C. Lu, L. Johnson, B. C. Meyers, P. J. Green, and S. E. Jacobsen. Dissecting arabidopsis thaliana dicer function in small rna processing, gene silencing and dna methylation patterning. *Nat Genet*, 38(6):721–725, Jun 2006.

[124] D. G. Hendrickson, D. J. Hogan, H. L. McCullough, J. W. Myers, D. Herschlag, J. E. Ferrell, and P. O. Brown. Concordant regulation of translation and mrna abundance for hundreds of targets of a human microrna. *PLoS Biol*, 7(11):e1000238, Nov 2009.

[125] J. I. Henke, D. Goergen, J. Zheng, Y. Song, C. G. Schüttler, C. Fehr, C. Jünemann, and M. Niepmann. microrna-122 stimulates translation of hepatitis c virus rna. *EMBO J*, 27(24):3300–3310, Dec 2008.

[126] C. Himber, P. Dunoyer, G. Moissiard, C. Ritzenthaler, and O. Voinnet. Transitivity-dependent and -independent cell-to-cell movement of rna silencing. *EMBO J*, 22(17):4523–4533, Sep 2003.

[127] J. Hock, L. Weinmann, C. Ender, S. Rudel, E. Kremmer, M. Raabe, H. Urlaub, and G. Meister. Proteomic and functional analysis of argonaute-containing mrna-protein complexes in human cells. *EMBO Rep*, 8(11):1052–1060, Nov 2007.

[128] M. D. Horwich, C. Li, C. Matranga, V. Vagin, G. Farley, P. Wang, and P. D. Zamore. The drosophila rna methyltransferase, dmhen1, modifies germline pirnas and single-stranded sirnas in risc. *Curr Biol*, 17(14):1265–1272, Jul 2007.

[129] S. Houwing, L. M. Kamminga, E. Berezikov, D. Cronembold, A. Girard, H. van den Elst, D. V. Filippov, H. Blaser, E. Raz, C. B. Moens, R. H. A. Plasterk, G. J. Hannon, B. W. Draper, and R. F. Ketting. A role for piwi and pirnas in germ cell maintenance and transposon silencing in zebrafish. *Cell*, 129(1):69–82, Apr 2007.

[130] D. T. Humphreys, B. J. Westman, D. I. K. Martin, and T. Preiss. Micrornas control translation initiation by inhibiting eukaryotic initiation factor 4e/cap and poly(a) tail function. *Proc Natl Acad Sci U S A*, 102(47):16961–16966, Nov 2005.

[131] E. Huntzinger, J. E. Braun, S. Heimstädt, L. Zekri, and E. Izaurralde. Two pabpc1-binding sites in gw182 proteins promote mirna-mediated gene silencing. *EMBO J*, 29(24):4146–4160, Dec 2010.

[132] E. Huntzinger and E. Izaurralde. Gene silencing by micrornas: contributions of translational repression and mrna decay. *Nat Rev Genet*, 12(2):99–110, Feb 2011.

[133] G. Hutvágner, J. McLachlan, A. E. Pasquinelli, E. Bálint, T. Tuschl, and P. D. Zamore. A cellular function for the rna-interference enzyme dicer in the maturation of the let-7 small temporal rna. *Science*, 293(5531):834–838, Aug 2001.

[134] T. Iki, M. Yoshikawa, M. Nishikiori, M. C. Jaudal, E. Matsumoto-Yokoyama, I. Mitsuhara, T. Meshi, and M. Ishikawa. In vitro assembly of plant rna-induced silencing complexes facilitated by molecular chaperone hsp90. *Mol Cell*, 39(2):282–291, Jul 2010.

[135] Y. Ishihama, Y. Oda, T. Tabata, T. Sato, T. Nagasu, J. Rappsilber, and M. Mann. Exponentially modified protein abundance index (empai) for estimation of absolute protein amount in proteomics by the number of sequenced peptides per protein. *Mol Cell Proteomics*, 4(9):1265–1272, Sep 2005.

[136] A. Ishizuka, M. C. Siomi, and H. Siomi. A drosophila fragile x protein interacts with components of rnai and ribosomal proteins. *Genes Dev*, 16(19):2497–2508, Oct 2002.

[137] S. Iwasaki, T. Kawamata, and Y. Tomari. Drosophila argonaute1 and argonaute2 employ distinct mechanisms for translational repression. *Mol Cell*, 34(1):58–67, Apr 2009.

[138] S. Iwasaki, M. Kobayashi, M. Yoda, Y. Sakaguchi, S. Katsuma, T. Suzuki, and Y. Tomari. Hsc70/hsp90 chaperone machinery mediates atp-dependent risc loading of small rna duplexes. *Mol Cell*, 39(2):292–299, Jul 2010.

[139] A. L. Jackson and P. S. Linsley. Noise amidst the silence: off-target effects of sirnas? *Trends Genet*, 20(11):521–524, Nov 2004.

[140] R. J. Jackson, C. U. T. Hellen, and T. V. Pestova. The mechanism of eukaryotic translation initiation and principles of its regulation. *Nat Rev Mol Cell Biol*, 11(2):113–127, Feb 2010.

[141] B. A. Janowski, K. E. Huffman, J. C. Schwartz, R. Ram, R. Nordsell, D. S. Shames, J. D. Minna, and D. R. Corey. Involvement of ago1 and ago2 in mammalian transcriptional silencing. *Nat Struct Mol Biol*, 13(9):787–792, Sep 2006.

[142] B. A. Janowski, S. T. Younger, D. B. Hardy, R. Ram, K. E. Huffman, and D. R. Corey. Activating gene expression in mammalian cells with promoter-targeted duplex rnas. *Nat Chem Biol*, 3(3):166–173, Mar 2007.

[143] H. Jin, M. R. Suh, J. Han, K.-H. Yeom, Y. Lee, I. Heo, M. Ha, S. Hyun, and V. N. Kim. Human upf1 participates in small rna-induced mrna downregulation. *Mol Cell Biol*, 29(21):5789–5799, Nov 2009.

[144] P. Jin, D. C. Zarnescu, S. Ceman, M. Nakamoto, J. Mowrey, T. A. Jongens, D. L. Nelson, K. Moses, and S. T. Warren. Biochemical and genetic interaction between the fragile x mental retardation protein and the microrna pathway. *Nat Neurosci*, 7(2):113–117, Feb 2004.

[145] M. Jinek and J. A. Doudna. A three-dimensional view of the molecular machinery of rna interference. *Nature*, 457(7228):405–412, Jan 2009.

[146] M. Jinek, M. R. Fabian, S. M. Coyle, N. Sonenberg, and J. A. Doudna. Structural insights into the human gw182-pabc interaction in microrna-mediated deadenylation. *Nat Struct Mol Biol*, 17(2):238–240, Feb 2010.

[147] Q. Jing, S. Huang, S. Guth, T. Zarubin, A. Motoyama, J. Chen, F. D. Padova, S.-C. Lin, H. Gram, and J. Han. Involvement of microrna in au-rich element-mediated mrna instability. *Cell*, 120(5):623–634, Mar 2005.

[148] M. Johnston, M.-C. Geoffroy, A. Sobala, R. Hay, and G. Hutvagner. Hsp90 protein stabilizes unloaded argonaute complexes and microscopic p-bodies in human cells. *Mol Biol Cell*, 21(9):1462–1469, May 2010.

[149] C. L. Jopling, M. Yi, A. M. Lancaster, S. M. Lemon, and P. Sarnow. Modulation of hepatitis c virus rna abundance by a liver-specific microrna. *Science*, 309(5740):1577–1581, Sep 2005.

[150] B. Kastner, N. Fischer, M. M. Golas, B. Sander, P. Dube, D. Boehringer, K. Hartmuth, J. Deckert, F. Hauer, E. Wolf, H. Uchtenhagen, H. Urlaub, F. Herzog, J. M. Peters, D. Poerschke, R. Lührmann, and H. Stark. Grafix: sample preparation for single-particle electron cryomicroscopy. *Nat Methods*, 5(1):53–55, Jan 2008.

[151] T. Kawamata, H. Seitz, and Y. Tomari. Structural determinants of mirnas for risc loading and slicer-independent unwinding. *Nat Struct Mol Biol*, 16(9):953–960, Sep 2009.

[152] Y. Kawamura, K. Saito, T. Kin, Y. Ono, K. Asai, T. Sunohara, T. N. Okada, M. C. Siomi, and H. Siomi. Drosophila endogenous small rnas bind to argonaute 2 in somatic cells. *Nature*, 453(7196):793–797, Jun 2008.

[153] M. Kedde, M. J. Strasser, B. Boldajipour, J. A. F. O. Vrielink, K. Slanchev, C. le Sage, R. Nagel, P. M. Voorhoeve, J. van Duijse, U. A. Ørom, A. H. Lund, A. Perrakis, E. Raz, and R. Agami. Rna-binding protein dnd1 inhibits microrna access to target mrna. *Cell*, 131(7):1273–1286, Dec 2007.

[154] N. Kedersha, G. Stoecklin, M. Ayodele, P. Yacono, J. Lykke-Andersen, M. J. Fritzler, D. Scheuner, R. J. Kaufman, D. E. Golan, and P. Anderson. Stress granules and processing bodies are dynamically linked sites of mrnp remodeling. *J Cell Biol*, 169(6):871–884, Jun 2005.

[155] J. R. Kennerdell and R. W. Carthew. Use of dsrna-mediated genetic interference to demonstrate that frizzled and frizzled 2 act in the wingless pathway. *Cell*, 95(7):1017–1026, Dec 1998.

[156] A. Khvorova, A. Reynolds, and S. D. Jayasena. Functional sirnas and mirnas exhibit strand bias. *Cell*, 115(2):209–216, Oct 2003.

[157] D. H. Kim, P. Saetrom, O. Snøve, and J. J. Rossi. Microrna-directed transcriptional gene silencing in mammalian cells. *Proc Natl Acad Sci U S A*, 105(42):16230–16235, Oct 2008.

[158] D. H. Kim, L. M. Villeneuve, K. V. Morris, and J. J. Rossi. Argonaute-1 directs sirna-mediated transcriptional gene silencing in human cells. *Nat Struct Mol Biol*, 13(9):793–797, Sep 2006.

[159] H. H. Kim, Y. Kuwano, S. Srikantan, E. K. Lee, J. L. Martindale, and M. Gorospe. Hur recruits let-7/risc to repress c-myc expression. *Genes Dev*, 23(15):1743–1748, Aug 2009.

[160] K. Kim, Y. S. Lee, and R. W. Carthew. Conversion of pre-risc to holo-risc by ago2 during assembly of rnai complexes. *RNA*, 13(1):22–29, Jan 2007.

[161] V. N. Kim, J. Han, and M. C. Siomi. Biogenesis of small rnas in animals. *Nat Rev Mol Cell Biol*, 10(2):126–139, Feb 2009.

[162] L. N. Kinch and N. V. Grishin. The human ago2 mc region does not contain an eif4e-like mrna cap binding motif. *Biol Direct*, 4:2, 2009.

[163] M. Kiriakidou, G. S. Tan, S. Lamprinaki, M. D. Planell-Saguer, P. T. Nelson, and Z. Mourelatos. An mrna m7g cap binding-like motif within human ago2 represses translation. *Cell*, 129(6):1141–1151, Jun 2007.

[164] Y. Kirino, N. Kim, M. de Planell-Saguer, E. Khandros, S. Chiorean, P. S. Klein, I. Rigoutsos, T. A. Jongens, and Z. Mourelatos. Arginine methylation of piwi proteins catalysed by dprmt5 is required for ago3 and aub stability. *Nat Cell Biol*, 11(5):652–658, May 2009.

[165] Y. Kirino and Z. Mourelatos. Mouse piwi-interacting rnas are 2'-o-methylated at their 3' termini. *Nat Struct Mol Biol*, 14(4):347–348, Apr 2007.

[166] W. P. Kloosterman, E. Wienholds, R. F. Ketting, and R. H. A. Plasterk. Substrate requirements for let-7 function in the developing zebrafish embryo. *Nucleic Acids Res*, 32(21):6284–6291, 2004.

[167] K. H. Kok, M.-H. J. Ng, Y.-P. Ching, and D.-Y. Jin. Human trbp and pact directly interact with each other and associate with dicer to facilitate the production of small interfering rna. *J Biol Chem*, 282(24):17649–17657, Jun 2007.

[168] G. Kozlov, N. Safaee, A. Rosenauer, and K. Gehring. Structural basis of binding of p-body-associated proteins gw182 and ataxin-2 by the mlle domain of poly(a)-binding protein. *J Biol Chem*, 285(18):13599–13606, Apr 2010.

[169] S. Kuramochi-Miyagawa, T. Watanabe, K. Gotoh, Y. Totoki, A. Toyoda, M. Ikawa, N. Asada, K. Kojima, Y. Yamaguchi, T. W. Ijiri, K. Hata, E. Li, Y. Matsuda, T. Kimura, M. Okabe, Y. Sakaki, H. Sasaki, and T. Nakano. Dna methylation of retrotransposon genes is regulated by piwi family members mili and miwi2 in murine fetal testes. *Genes Dev*, 22(7):908–917, Apr 2008.

[170] P. Landgraf, M. Rusu, R. Sheridan, A. Sewer, N. Iovino, A. Aravin, S. Pfeffer, A. Rice, A. O. Kamphorst, M. Landthaler, C. Lin, N. D. Socci, L. Hermida, V. Fulci, S. Chiaretti, R. Foà, J. Schliwka, U. Fuchs, A. Novosel, R.-U. Müller, B. Schermer, U. Bissels, J. Inman, Q. Phan, M. Chien, D. B. Weir, R. Choksi, G. D. Vita, D. Frezzetti, H.-I. Trompeter, V. Hornung, G. Teng, G. Hartmann, M. Palkovits, R. D. Lauro, P. Wernet, G. Macino, C. E. Rogler, J. W. Nagle, J. Ju, F. N. Papavasiliou, T. Benzing, P. Lichter, W. Tam, M. J. Brownstein, A. Bosio, A. Borkhardt, J. J. Russo, C. Sander, M. Zavolan, and T. Tuschl. A mammalian microrna expression atlas based on small rna library sequencing. *Cell*, 129(7):1401–1414, Jun 2007.

[171] M. Landthaler, D. Gaidatzis, A. Rothballer, P. Y. Chen, S. J. Soll, L. Dinic, T. Ojo, M. Hafner, M. Zavolan, and T. Tuschl. Molecular characterization of human argonaute-containing ribonucleoprotein complexes and their bound target mrnas. *RNA*, 14(12):2580–2596, Dec 2008.

[172] M. Landthaler, A. Yalcin, and T. Tuschl. The human digeorge syndrome critical region gene 8 and its d. melanogaster homolog are required for mirna biogenesis. *Curr Biol*, 14(23):2162–2167, Dec 2004.

[173] P.-W. Lau, C. S. Potter, B. Carragher, and I. J. MacRae. Structure of the human dicer-trbp complex by electron microscopy. *Structure*, 17(10):1326–1332, Oct 2009.

[174] D. Lazzaretti, I. Tournier, and E. Izaurralde. The c-terminal domains of human tnrc6a, tnrc6b, and tnrc6c silence bound transcripts independently of argonaute proteins. *RNA*, 15(6):1059–1066, Jun 2009.

[175] S. Lebedeva, M. Jens, K. Theil, B. Schwanhäusser, M. Selbach, M. Landthaler, and N. Rajewsky. Transcriptome-wide analysis of regulatory interactions of the rna-binding protein hur. *Mol Cell*, 43(3):340–352, Aug 2011.

[176] R. C. Lee, R. L. Feinbaum, and V. Ambros. The c. elegans heterochronic gene lin-4 encodes small rnas with antisense complementarity to lin-14. *Cell*, 75(5):843–854, Dec 1993.

[177] Y. Lee, C. Ahn, J. Han, H. Choi, J. Kim, J. Yim, J. Lee, P. Provost, O. Rådmark, S. Kim, and V. N. Kim. The nuclear rnase iii drosha initiates microrna processing. *Nature*, 425(6956):415–419, Sep 2003.

[178] Y. Lee, I. Hur, S.-Y. Park, Y.-K. Kim, M. R. Suh, and V. N. Kim. The role of pact in the rna silencing pathway. *EMBO J*, 25(3):522–532, Feb 2006.

[179] Y. Lee, M. Kim, J. Han, K.-H. Yeom, S. Lee, S. H. Baek, and V. N. Kim. Microrna genes are transcribed by rna polymerase ii. *EMBO J*, 23(20):4051–4060, Oct 2004.

[180] Y. S. Lee, K. Nakahara, J. W. Pham, K. Kim, Z. He, E. J. Sontheimer, and R. W. Carthew. Distinct roles for drosophila dicer-1 and dicer-2 in the sirna/mirna silencing pathways. *Cell*, 117(1):69–81, Apr 2004.

[181] Y. S. Lee, S. Pressman, A. P. Andress, K. Kim, J. L. White, J. J. Cassidy, X. Li, K. Lubell, D. H. Lim, I. S. Cho, K. Nakahara, J. B. Preall, P. Bellare, E. J. Sontheimer, and R. W. Carthew. Silencing by small rnas is linked to endosomal trafficking. *Nat Cell Biol*, 11(9):1150–1156, Sep 2009.

[182] A. K. L. Leung, J. M. Calabrese, and P. A. Sharp. Quantitative analysis of argonaute protein reveals microrna-dependent localization to stress granules. *Proc Natl Acad Sci U S A*, 103(48):18125–18130, Nov 2006.

[183] A. K. L. Leung, A. G. Young, A. Bhutkar, G. X. Zheng, A. D. Bosson, C. B. Nielsen, and P. A. Sharp. Genome-wide identification of ago2 binding sites from mouse embryonic stem cells with and without mature micrornas. *Nat Struct Mol Biol*, 18(2):237–244, Feb 2011.

[184] P. J. F. Leuschner, S. L. Ameres, S. Kueng, and J. Martinez. Cleavage of the sirna passenger strand during risc assembly in human cells. *EMBO Rep*, 7(3):314–320, Mar 2006.

[185] B. P. Lewis, C. B. Burge, and D. P. Bartel. Conserved seed pairing, often flanked by adenosines, indicates that thousands of human genes are microrna targets. *Cell*, 120(1):15–20, Jan 2005.

[186] X. Li and R. W. Carthew. A microrna mediates egf receptor signaling and promotes photoreceptor differentiation in the drosophila eye. *Cell*, 123(7):1267–1277, Dec 2005.

[187] S. Lian, A. Jakymiw, T. Eystathioy, J. C. Hamel, M. J. Fritzler, and E. K. L. Chan. Gw bodies, micrornas and the cell cycle. *Cell Cycle*, 5(3):242–245, Feb 2006.

[188] S. L. Lian, S. Li, G. X. Abadal, B. A. Pauley, M. J. Fritzler, and E. K. L. Chan. The c-terminal half of human ago2 binds to multiple gw-rich regions of gw182 and requires gw182 to mediate silencing. *RNA*, 15(5):804–813, May 2009.

[189] L. P. Lim, N. C. Lau, P. Garrett-Engele, A. Grimson, J. M. Schelter, J. Castle, D. P. Bartel, P. S. Linsley, and J. M. Johnson. Microarray analysis shows that some micrornas downregulate large numbers of target mrnas. *Nature*, 433(7027):769–773, Feb 2005.

[190] J. A. Lindbo, L. Silva-Rosales, W. M. Proebsting, and W. G. Dougherty. Induction of a highly specific antiviral state in transgenic plants: Implications for regulation of gene expression and virus resistance. *Plant Cell*, 5(12):1749–1759, Dec 1993.

[191] A. Lingel, B. Simon, E. Izaurralde, and M. Sattler. Structure and nucleic-acid binding of the drosophila argonaute 2 paz domain. *Nature*, 426(6965):465–469, Nov 2003.

References

[192] Z. Lippman and R. Martienssen. The role of rna interference in heterochromatic silencing. *Nature*, 431(7006):364–370, Sep 2004.

[193] Z. Lippman, B. May, C. Yordan, T. Singer, and R. Martienssen. Distinct mechanisms determine transposon inheritance and methylation via small interfering rna and histone modification. *PLoS Biol*, 1(3):E67, Dec 2003.

[194] J. Liu, M. A. Carmell, F. V. Rivas, C. G. Marsden, J. M. Thomson, J.-J. Song, S. M. Hammond, L. Joshua-Tor, and G. J. Hannon. Argonaute2 is the catalytic engine of mammalian rnai. *Science*, 305(5689):1437–1441, Sep 2004.

[195] J. Liu, F. V. Rivas, J. Wohlschlegel, J. R. Yates, R. Parker, and G. J. Hannon. A role for the p-body component gw182 in microrna function. *Nat Cell Biol*, 7(12):1261–1266, Dec 2005.

[196] J. Liu, M. A. Valencia-Sanchez, G. J. Hannon, and R. Parker. Microrna-dependent localization of targeted mrnas to mammalian p-bodies. *Nat Cell Biol*, 7(7):719–723, Jul 2005.

[197] Q. Liu, T. A. Rand, S. Kalidas, F. Du, H.-E. Kim, D. P. Smith, and X. Wang. R2d2, a bridge between the initiation and effector steps of the drosophila rnai pathway. *Science*, 301(5641):1921–1925, Sep 2003.

[198] X. Liu, F. Jiang, S. Kalidas, D. Smith, and Q. Liu. Dicer-2 and r2d2 coordinately bind sirna to promote assembly of the sirisc complexes. *RNA*, 12(8):1514–1520, Aug 2006.

[199] Y. Liu, X. Ye, F. Jiang, C. Liang, D. Chen, J. Peng, L. N. Kinch, N. V. Grishin, and Q. Liu. C3po, an endoribonuclease that promotes rnai by facilitating risc activation. *Science*, 325(5941):750–753, Aug 2009.

[200] J. U. Lohmann, I. Endl, and T. C. Bosch. Silencing of developmental genes in hydra. *Dev Biol*, 214(1):211–214, Oct 1999.

[201] Z. H. Lu, J. T. Books, and T. J. Ley. Cold shock domain family members yb-1 and msy4 share essential functions during murine embryogenesis. *Mol Cell Biol*, 26(22):8410–8417, Nov 2006.

[202] E. Lund, S. Güttinger, A. Calado, J. E. Dahlberg, and U. Kutay. Nuclear export of microrna precursors. *Science*, 303(5654):95–98, Jan 2004.

[203] J. Lykke-Andersen. Identification of a human decapping complex associated with hupf proteins in nonsense-mediated decay. *Mol Cell Biol*, 22(23):8114–8121, Dec 2002.

[204] J. R. Lytle, T. A. Yario, and J. A. Steitz. Target mrnas are repressed as efficiently by microrna-binding sites in the 5' utr as in the 3' utr. *Proc Natl Acad Sci U S A*, 104(23):9667–9672, Jun 2007.

[205] E. Ma, I. J. MacRae, J. F. Kirsch, and J. A. Doudna. Autoinhibition of human dicer by its internal helicase domain. *J Mol Biol*, 380(1):237–243, Jun 2008.

[206] J.-B. Ma, K. Ye, and D. J. Patel. Structural basis for overhang-specific small interfering rna recognition by the paz domain. *Nature*, 429(6989):318–322, May 2004.

[207] J.-B. Ma, Y.-R. Yuan, G. Meister, Y. Pei, T. Tuschl, and D. J. Patel. Structural basis for 5'-end-specific recognition of guide rna by the a. fulgidus piwi protein. *Nature*, 434(7033):666–670, Mar 2005.

[208] I. J. MacRae, E. Ma, M. Zhou, C. V. Robinson, and J. A. Doudna. In vitro reconstitution of the human risc-loading complex. *Proc Natl Acad Sci U S A*, 105(2):512–517, Jan 2008.

[209] I. J. MacRae, K. Zhou, and J. A. Doudna. Structural determinants of rna recognition and cleavage by dicer. *Nat Struct Mol Biol*, 14(10):934–940, Oct 2007.

[210] I. J. Macrae, K. Zhou, F. Li, A. Repic, A. N. Brooks, W. Z. Cande, P. D. Adams, and J. A. Doudna. Structural basis for double-stranded rna processing by dicer. *Science*, 311(5758):195–198, Jan 2006.

[211] C. D. Malone and G. J. Hannon. Small rnas as guardians of the genome. *Cell*, 136(4):656–668, Feb 2009.

[212] E. Maniataki and Z. Mourelatos. A human, atp-independent, risc assembly machine fueled by pre-mirna. *Genes Dev*, 19(24):2979–2990, Dec 2005.

[213] P. A. Maroney, Y. Yu, J. Fisher, and T. W. Nilsen. Evidence that micrornas are associated with translating messenger rnas in human cells. *Nat Struct Mol Biol*, 13(12):1102–1107, Dec 2006.

[214] J. Martinez, A. Patkaniowska, H. Urlaub, R. Lührmann, and T. Tuschl. Single-stranded antisense sirnas guide target rna cleavage in rnai. *Cell*, 110(5):563–574, Sep 2002.

[215] J. Martinez and T. Tuschl. Risc is a 5' phosphomonoester-producing rna endonuclease. *Genes Dev*, 18(9):975–980, May 2004.

[216] G. Mathonnet, M. R. Fabian, Y. V. Svitkin, A. Parsyan, L. Huck, T. Murata, S. Biffo, W. C. Merrick, E. Darzynkiewicz, R. S. Pillai, W. Filipowicz, T. F. Duchaine, and N. Sonenberg. Microrna inhibition of translation initiation in vitro by targeting the cap-binding complex eif4f. *Science*, 317(5845):1764–1767, Sep 2007.

[217] C. Matranga, Y. Tomari, C. Shin, D. P. Bartel, and P. D. Zamore. Passenger-strand cleavage facilitates assembly of sirna into ago2-containing rnai enzyme complexes. *Cell*, 123(4):607–620, Nov 2005.

[218] G. Meister, C. Eggert, D. Bühler, H. Brahms, C. Kambach, and U. Fischer. Methylation of sm proteins by a complex containing prmt5 and the putative u snrnp assembly factor picln. *Curr Biol*, 11(24):1990–1994, Dec 2001.

[219] G. Meister, C. Eggert, and U. Fischer. Smn-mediated assembly of rnps: a complex story. *Trends Cell Biol*, 12(10):472–478, Oct 2002.

[220] G. Meister, M. Landthaler, A. Patkaniowska, Y. Dorsett, G. Teng, and T. Tuschl. Human argonaute2 mediates rna cleavage targeted by mirnas and sirnas. *Mol Cell*, 15(2):185–197, Jul 2004.

[221] G. Meister, M. Landthaler, L. Peters, P. Y. Chen, H. Urlaub, R. Lührmann, and T. Tuschl. Identification of novel argonaute-associated proteins. *Curr Biol*, 15(23):2149–2155, Dec 2005.

[222] C. W. Melnyk, A. Molnar, and D. C. Baulcombe. Intercellular and systemic movement of rna silencing signals. *EMBO J*, 30(17):3553–3563, 2011.

[223] M. F. Mette, W. Aufsatz, J. van der Winden, M. A. Matzke, and A. J. Matzke. Transcriptional silencing and promoter methylation triggered by double-stranded rna. *EMBO J*, 19(19):5194–5201, Oct 2000.

[224] Y. Mishima, A. J. Giraldez, Y. Takeda, T. Fujiwara, H. Sakamoto, A. F. Schier, and K. Inoue. Differential regulation of germline mrnas in soma and germ cells by zebrafish mir-430. *Curr Biol*, 16(21):2135–2142, Nov 2006.

[225] K. Miyoshi, H. Tsukumo, T. Nagami, H. Siomi, and M. C. Siomi. Slicer function of drosophila argonautes and its involvement in risc formation. *Genes Dev*, 19(23):2837–2848, Dec 2005.

[226] T. Miyoshi, A. Takeuchi, H. Siomi, and M. C. Siomi. A direct role for hsp90 in pre-risc formation in drosophila. *Nat Struct Mol Biol*, 17(8):1024–1026, Aug 2010.

[227] D. Moazed. Small rnas in transcriptional gene silencing and genome defence. *Nature*, 457(7228):413–420, Jan 2009.

[228] M. R. Motamedi, A. Verdel, S. U. Colmenares, S. A. Gerber, S. P. Gygi, and D. Moazed. Two rnai complexes, rits and rdrc, physically interact and localize to noncoding centromeric rnas. *Cell*, 119(6):789–802, Dec 2004.

[229] Z. Mourelatos, J. Dostie, S. Paushkin, A. Sharma, B. Charroux, L. Abel, J. Rapp-silber, M. Mann, and G. Dreyfuss. mirnps: a novel class of ribonucleoproteins containing numerous micrornas. *Genes Dev*, 16(6):720–728, Mar 2002.

[230] P. Mourrain, C. Béclin, T. Elmayan, F. Feuerbach, C. Godon, J. B. Morel, D. Jou-ette, A. M. Lacombe, S. Nikic, N. Picault, K. Rémoué, M. Sanial, T. A. Vo, and H. Vaucheret. Arabidopsis sgs2 and sgs3 genes are required for posttranscriptional gene silencing and natural virus resistance. *Cell*, 101(5):533–542, May 2000.

[231] F. Mousson, A. Kolkman, W. W. M. P. Pijnappel, H. T. M. Timmers, and A. J. R. Heck. Quantitative proteomics reveals regulation of dynamic components within tata-binding protein (tbp) transcription complexes. *Mol Cell Proteomics*, 7(5):845–852, May 2008.

[232] E. P. Murchison, J. F. Partridge, O. H. Tam, S. Cheloufi, and G. J. Hannon. Characterization of dicer-deficient murine embryonic stem cells. *Proc Natl Acad Sci U S A*, 102(34):12135–12140, Aug 2005.

[233] C. Napoli, C. Lemieux, and R. Jorgensen. Introduction of a chimeric chalcone synthase gene into petunia results in reversible co-suppression of homologous genes in trans. *Plant Cell*, 2(4):279–289, Apr 1990.

[234] C. B. Nielsen, N. Shomron, R. Sandberg, E. Hornstein, J. Kitzman, and C. B. Burge. Determinants of targeting by endogenous and exogenous micrornas and sirnas. *RNA*, 13(11):1894–1910, Nov 2007.

[235] K. M. Nishida, T. N. Okada, T. Kawamura, T. Mituyama, Y. Kawamura, S. In-agaki, H. Huang, D. Chen, T. Kodama, H. Siomi, and M. C. Siomi. Functional involvement of tudor and dprmt5 in the pirna processing pathway in drosophila germlines. *EMBO J*, 28(24):3820–3831, Dec 2009.

[236] K. M. Nishida, K. Saito, T. Mori, Y. Kawamura, T. Nagami-Okada, S. Inagaki, H. Siomi, and M. C. Siomi. Gene silencing mechanisms mediated by aubergine pirna complexes in drosophila male gonad. *RNA*, 13(11):1911–1922, Nov 2007.

[237] C. L. Noland, E. Ma, and J. A. Doudna. sirna repositioning for guide strand selection by human dicer complexes. *Mol Cell*, 43(1):110–121, Jul 2011.

[238] S. Nottrott, M. J. Simard, and J. D. Richter. Human let-7a mirna blocks protein production on actively translating polyribosomes. *Nat Struct Mol Biol*, 13(12):1108–1114, Dec 2006.

[239] A. Nykänen, B. Haley, and P. D. Zamore. Atp requirements and small interfering rna structure in the rna interference pathway. *Cell*, 107(3):309–321, Nov 2001.

[240] T. Ohara, Y. Sakaguchi, T. Suzuki, H. Ueda, K. Miyauchi, and T. Suzuki. The 3' termini of mouse piwi-interacting rnas are 2'-o-methylated. *Nat Struct Mol Biol*, 14(4):349–350, Apr 2007.

[241] K. Okamura, J. W. Hagen, H. Duan, D. M. Tyler, and E. C. Lai. The mirtron pathway generates microrna-class regulatory rnas in drosophila. *Cell*, 130(1):89–100, Jul 2007.

[242] J. V. Olsen, L. M. F. de Godoy, G. Li, B. Macek, P. Mortensen, R. Pesch, A. Makarov, O. Lange, S. Horning, and M. Mann. Parts per million mass accuracy on an orbitrap mass spectrometer via lock mass injection into a c-trap. *Mol Cell Proteomics*, 4(12):2010–2021, Dec 2005.

[243] P. H. Olsen and V. Ambros. The lin-4 regulatory rna controls developmental timing in caenorhabditis elegans by blocking lin-14 protein synthesis after the initiation of translation. *Dev Biol*, 216(2):671–680, Dec 1999.

[244] S.-E. Ong, B. Blagoev, I. Kratchmarova, D. B. Kristensen, H. Steen, A. Pandey, and M. Mann. Stable isotope labeling by amino acids in cell culture, silac, as a simple and accurate approach to expression proteomics. *Mol Cell Proteomics*, 1(5):376–386, May 2002.

[245] S.-E. Ong and M. Mann. A practical recipe for stable isotope labeling by amino acids in cell culture (silac). *Nat Protoc*, 1(6):2650–2660, 2006.

[246] T. I. Orban and E. Izaurralde. Decay of mrnas targeted by risc requires xrn1, the ski complex, and the exosome. *RNA*, 11(4):459–469, Apr 2005.

156

[247] A. N. Packer, Y. Xing, S. Q. Harper, L. Jones, and B. L. Davidson. The bifunctional microrna mir-9/mir-9* regulates rest and corest and is downregulated in huntington's disease. *J Neurosci*, 28(53):14341–14346, Dec 2008.

[248] A. Pagano, F. Letourneur, D. Garcia-Estefania, J. L. Carpentier, L. Orci, and J. P. Paccaud. Sec24 proteins and sorting at the endoplasmic reticulum. *J Biol Chem*, 274(12):7833–7840, Mar 1999.

[249] J. Pak and A. Fire. Distinct populations of primary and secondary effectors during rnai in c. elegans. *Science*, 315(5809):241–244, Jan 2007.

[250] M. Pal-Bhadra, U. Bhadra, and J. A. Birchler. Cosuppression in drosophila: gene silencing of alcohol dehydrogenase by white-adh transgenes is polycomb dependent. *Cell*, 90(3):479–490, Aug 1997.

[251] J. C. Palauqui, T. Elmayan, F. D. D. Borne, P. Crete, C. Charles, and H. Vaucheret. Frequencies, timing, and spatial patterns of co-suppression of nitrate reductase and nitrite reductase in transgenic tobacco plants. *Plant Physiol*, 112(4):1447–1456, Dec 1996.

[252] G. S. Pall and A. J. Hamilton. Improved northern blot method for enhanced detection of small rna. *Nat Protoc*, 3(6):1077–1084, 2008.

[253] D. Palliser, D. Chowdhury, Q.-Y. Wang, S. J. Lee, R. T. Bronson, D. M. Knipe, and J. Lieberman. An sirna-based microbicide protects mice from lethal herpes simplex virus 2 infection. *Nature*, 439(7072):89–94, Jan 2006.

[254] P. Parameswaran, E. Sklan, C. Wilkins, T. Burgon, M. A. Samuel, R. Lu, K. M. Ansel, V. Heissmeyer, S. Einav, W. Jackson, T. Doukas, S. Paranjape, C. Polacek, F. B. dos Santos, R. Jalili, F. Babrzadeh, B. Gharizadeh, D. Grimm, M. Kay, S. Koike, P. Sarnow, M. Ronaghi, S.-W. Ding, E. Harris, M. Chow, M. S. Diamond, K. Kirkegaard, J. S. Glenn, and A. Z. Fire. Six rna viruses and forty-one hosts: viral small rnas and modulation of small rna repertoires in vertebrate and invertebrate systems. *PLoS Pathog*, 6(2):e1000764, Feb 2010.

[255] J. M. Pare, N. Tahbaz, J. López-Orozco, P. LaPointe, P. Lasko, and T. C. Hobman. Hsp90 regulates the function of argonaute 2 and its recruitment to stress granules and p-bodies. *Mol Biol Cell*, 20(14):3273–3284, Jul 2009.

[256] J.-E. Park, I. Heo, Y. Tian, D. K. Simanshu, H. Chang, D. Jee, D. J. Patel, and V. N. Kim. Dicer recognizes the 5' end of rna for efficient and accurate processing. *Nature*, 475(7355):201–205, Jul 2011.

[257] J. S. Parker, S. M. Roe, and D. Barford. Crystal structure of a piwi protein suggests mechanisms for sirna recognition and slicer activity. *EMBO J*, 23(24):4727–4737, Dec 2004.

[258] J. S. Parker, S. M. Roe, and D. Barford. Structural insights into mrna recognition from a piwi domain-sirna guide complex. *Nature*, 434(7033):663–666, Mar 2005.

[259] K. M. Pauley, T. Eystathioy, A. Jakymiw, J. C. Hamel, M. J. Fritzler, and E. K. L. Chan. Formation of gw bodies is a consequence of microrna genesis. *EMBO Rep*, 7(9):904–910, Sep 2006.

[260] J. Peng, J. E. Elias, C. C. Thoreen, L. J. Licklider, and S. P. Gygi. Evaluation of multidimensional chromatography coupled with tandem mass spectrometry (lc/lc-ms/ms) for large-scale protein analysis: the yeast proteome. *J Proteome Res*, 2(1):43–50, 2003.

[261] G. S. Pesiridis, E. Diamond, and G. D. V. Duyne. Role of picln in methylation of sm proteins by prmt5. *J Biol Chem*, 284(32):21347–21359, Aug 2009.

[262] C. P. Petersen, M.-E. Bordeleau, J. Pelletier, and P. A. Sharp. Short rnas repress translation after initiation in mammalian cells. *Mol Cell*, 21(4):533–542, Feb 2006.

[263] J. W. Pham, J. L. Pellino, Y. S. Lee, R. W. Carthew, and E. J. Sontheimer. A dicer-2-dependent 80s complex cleaves targeted mrnas during rnai in drosophila. *Cell*, 117(1):83–94, Apr 2004.

[264] X. Piao, X. Zhang, L. Wu, and J. G. Belasco. Ccr4-not deadenylates mrna associated with rna-induced silencing complexes in human cells. *Mol Cell Biol*, 30(6):1486–1494, Mar 2010.

[265] R. S. Pillai, S. N. Bhattacharyya, C. G. Artus, T. Zoller, N. Cougot, E. Basyuk, E. Bertrand, and W. Filipowicz. Inhibition of translational initiation by let-7 microrna in human cells. *Science*, 309(5740):1573–1576, Sep 2005.

[266] I. Plante, L. Davidovic, D. L. Ouellet, L.-A. Gobeil, S. Tremblay, E. W. Khandjian, and P. Provost. Dicer-derived micrornas are utilized by the fragile x mental retardation protein for assembly on target rnas. *J Biomed Biotechnol*, 2006(4):64347, 2006.

[267] B. P. Pollack, S. V. Kotenko, W. He, L. S. Izotova, B. L. Barnoski, and S. Pestka. The human homologue of the yeast proteins skb1 and hsl7p interacts with jak ki-

nases and contains protein methyltransferase activity. *J Biol Chem*, 274(44):31531–31542, Oct 1999.

[268] M. A. Powers, M. M. Fay, R. E. Factor, A. L. Welm, and K. S. Ullman. Protein arginine methyltransferase 5 accelerates tumor growth by arginine methylation of the tumor suppressor programmed cell death 4. *Cancer Res*, Jun 2011.

[269] H. H. Qi, P. P. Ongusaha, J. Myllyharju, D. Cheng, O. Pakkanen, Y. Shi, S. W. Lee, J. Peng, and Y. Shi. Prolyl 4-hydroxylation regulates argonaute 2 stability. *Nature*, 455(7211):421–424, Sep 2008.

[270] N. Rajewsky. microrna target predictions in animals. *Nat Genet*, 38 Suppl:S8–13, Jun 2006.

[271] T. A. Rand, S. Petersen, F. Du, and X. Wang. Argonaute2 cleaves the anti-guide strand of sirna during risc activation. *Cell*, 123(4):621–629, Nov 2005.

[272] J. A. Ranish, E. C. Yi, D. M. Leslie, S. O. Purvine, D. R. Goodlett, J. Eng, and R. Aebersold. The study of macromolecular complexes by quantitative proteomics. *Nat Genet*, 33(3):349–355, Mar 2003.

[273] J. Rehwinkel, I. Behm-Ansmant, D. Gatfield, and E. Izaurralde. A crucial role for gw182 and the dcp1:dcp2 decapping complex in mirna-mediated gene silencing. *RNA*, 11(11):1640–1647, Nov 2005.

[274] M. Reuter, S. Chuma, T. Tanaka, T. Franz, A. Stark, and R. S. Pillai. Loss of the mili-interacting tudor domain-containing protein-1 activates transposons and alters the mili-associated small rna profile. *Nat Struct Mol Biol*, 16(6):639–646, Jun 2009.

[275] J. Rho, S. Choi, Y. R. Seong, W. K. Cho, S. H. Kim, and D. S. Im. Prmt5, which forms distinct homo-oligomers, is a member of the protein-arginine methyltransferase family. *J Biol Chem*, 276(14):11393–11401, Apr 2001.

[276] F. V. Rivas, N. H. Tolia, J.-J. Song, J. P. Aragon, J. Liu, G. J. Hannon, and L. Joshua-Tor. Purified argonaute2 and an sirna form recombinant human risc. *Nat Struct Mol Biol*, 12(4):340–349, Apr 2005.

[277] G. B. Robb, K. M. Brown, J. Khurana, and T. M. Rana. Specific and potent rnai in the nucleus of human cells. *Nat Struct Mol Biol*, 12(2):133–137, Feb 2005.

[278] G. B. Robb and T. M. Rana. Rna helicase a interacts with risc in human cells and functions in risc loading. *Mol Cell*, 26(4):523–537, May 2007.

[279] N. Romano and G. Macino. Quelling: transient inactivation of gene expression in neurospora crassa by transformation with homologous sequences. *Mol Microbiol*, 6(22):3343–3353, Nov 1992.

[280] P. L. Ross, Y. N. Huang, J. N. Marchese, B. Williamson, K. Parker, S. Hattan, N. Khainovski, S. Pillai, S. Dey, S. Daniels, S. Purkayastha, P. Juhasz, S. Martin, M. Bartlet-Jones, F. He, A. Jacobson, and D. J. Pappin. Multiplexed protein quantitation in saccharomyces cerevisiae using amine-reactive isobaric tagging reagents. *Mol Cell Proteomics*, 3(12):1154–1169, Dec 2004.

[281] J. G. Ruby, C. H. Jan, and D. P. Bartel. Intronic microrna precursors that bypass drosha processing. *Nature*, 448(7149):83–86, Jul 2007.

[282] S. Rudel, A. Flatley, L. Weinmann, E. Kremmer, and G. Meister. A multifunctional human argonaute2-specific monoclonal antibody. *RNA*, 14(6):1244–1253, Jun 2008.

[283] A. Rybak, H. Fuchs, K. Hadian, L. Smirnova, E. A. Wulczyn, G. Michel, R. Nitsch, D. Krappmann, and F. G. Wulczyn. The let-7 target gene mouse lin-41 is a stem cell specific e3 ubiquitin ligase for the mirna pathway protein ago2. *Nat Cell Biol*, 11(12):1411–1420, Dec 2009.

[284] S. Rüdel, Y. Wang, R. Lenobel, R. Körner, H.-H. Hsiao, H. Urlaub, D. Patel, and G. Meister. Phosphorylation of human argonaute proteins affects small rna binding. *Nucleic Acids Res*, 39(6):2330–2343, Mar 2011.

[285] K. Saito, A. Ishizuka, H. Siomi, and M. C. Siomi. Processing of pre-micrornas by the dicer-1-loquacious complex in drosophila cells. *PLoS Biol*, 3(7):e235, Jul 2005.

[286] K. Saito, K. M. Nishida, T. Mori, Y. Kawamura, K. Miyoshi, T. Nagami, H. Siomi, and M. C. Siomi. Specific association of piwi with rasirnas derived from retrotransposon and heterochromatic regions in the drosophila genome. *Genes Dev*, 20(16):2214–2222, Aug 2006.

[287] K. Saito, Y. Sakaguchi, T. Suzuki, T. Suzuki, H. Siomi, and M. C. Siomi. Pimet, the drosophila homolog of hen1, mediates 2'-o-methylation of piwi- interacting rnas at their 3' ends. *Genes Dev*, 21(13):1603–1608, Jul 2007.

[288] J. Sambrook, E. Fritsch, and F. Maniatis. *Molecular cloning: A Laboratory Manual.* Cold Spring Harbour, N.Y., Cold Spring Laboratory Press, 1989.

[289] T. Sasaki and N. Shimizu. Evolutionary conservation of a unique amino acid sequence in human dicer protein essential for binding to argonaute family proteins. *Gene*, 396(2):312–320, Jul 2007.

[290] G. M. Schratt, F. Tuebing, E. A. Nigh, C. G. Kane, M. E. Sabatini, M. Kiebler, and M. E. Greenberg. A brain-specific microrna regulates dendritic spine development. *Nature*, 439(7074):283–289, Jan 2006.

[291] J. C. Schwamborn, E. Berezikov, and J. A. Knoblich. The trim-nhl protein trim32 activates micrornas and prevents self-renewal in mouse neural progenitors. *Cell*, 136(5):913–925, Mar 2009.

[292] B. Schwanhäusser, M. Gossen, G. Dittmar, and M. Selbach. Global analysis of cellular protein translation by pulsed silac. *Proteomics*, 9(1):205–209, Jan 2009.

[293] J. C. Schwartz, S. T. Younger, N.-B. Nguyen, D. B. Hardy, B. P. Monia, D. R. Corey, and B. A. Janowski. Antisense transcripts are targets for activating small rnas. *Nat Struct Mol Biol*, 15(8):842–848, Aug 2008.

[294] D. S. Schwarz, G. Hutvágner, T. Du, Z. Xu, N. Aronin, and P. D. Zamore. Asymmetry in the assembly of the rnai enzyme complex. *Cell*, 115(2):199–208, Oct 2003.

[295] K. Seggerson, L. Tang, and E. G. Moss. Two genetic circuits repress the caenorhabditis elegans heterochronic gene lin-28 after translation initiation. *Dev Biol*, 243(2):215–225, Mar 2002.

[296] M. Selbach and M. Mann. Protein interaction screening by quantitative immunoprecipitation combined with knockdown (quick). *Nat Methods*, 3(12):981–983, Dec 2006.

[297] M. Selbach, B. Schwanhäusser, N. Thierfelder, Z. Fang, R. Khanin, and N. Rajewsky. Widespread changes in protein synthesis induced by micrornas. *Nature*, 455(7209):58–63, Sep 2008.

[298] G. L. Sen and H. M. Blau. Argonaute 2/risc resides in sites of mammalian mrna decay known as cytoplasmic bodies. *Nat Cell Biol*, 7(6):633–636, Jun 2005.

[299] B. Shen and H. M. Goodman. Uridine addition after microrna-directed cleavage. *Science*, 306(5698):997, Nov 2004.

[300] U. Sheth and R. Parker. Decapping and decay of messenger rna occur in cytoplasmic processing bodies. *Science*, 300(5620):805–808, May 2003.

[301] T. Sijen, J. Fleenor, F. Simmer, K. L. Thijssen, S. Parrish, L. Timmons, R. H. Plasterk, and A. Fire. On the role of rna amplification in dsrna-triggered gene silencing. *Cell*, 107(4):465–476, Nov 2001.

[302] T. Sijen, F. A. Steiner, K. L. Thijssen, and R. H. A. Plasterk. Secondary sirnas result from unprimed rna synthesis and form a distinct class. *Science*, 315(5809):244–247, Jan 2007.

[303] H. Siomi and M. C. Siomi. On the road to reading the rna-interference code. *Nature*, 457(7228):396–404, Jan 2009.

[304] M. C. Siomi, T. Mannen, and H. Siomi. How does the royal family of tudor rule the piwi-interacting rna pathway? *Genes Dev*, 24(7):636–646, Apr 2010.

[305] J.-J. Song, J. Liu, N. H. Tolia, J. Schneiderman, S. K. Smith, R. A. Martienssen, G. J. Hannon, and L. Joshua-Tor. The crystal structure of the argonaute2 paz domain reveals an rna binding motif in rnai effector complexes. *Nat Struct Biol*, 10(12):1026–1032, Dec 2003.

[306] J.-J. Song, S. K. Smith, G. J. Hannon, and L. Joshua-Tor. Crystal structure of argonaute and its implications for risc slicer activity. *Science*, 305(5689):1434–1437, Sep 2004.

[307] J. Soutschek, A. Akinc, B. Bramlage, K. Charisse, R. Constien, M. Donoghue, S. Elbashir, A. Geick, P. Hadwiger, J. Harborth, M. John, V. Kesavan, G. Lavine, R. K. Pandey, T. Racie, K. G. Rajeev, I. Röhl, I. Toudjarska, G. Wang, S. Wuschko, D. Bumcrot, V. Koteliansky, S. Limmer, M. Manoharan, and H.-P. Vornlocher. Therapeutic silencing of an endogenous gene by systemic administration of modified sirnas. *Nature*, 432(7014):173–178, Nov 2004.

[308] G. R. Stark, I. M. Kerr, B. R. Williams, R. H. Silverman, and R. D. Schreiber. How cells respond to interferons. *Annu Rev Biochem*, 67:227–264, 1998.

[309] G. Stoecklin, T. Stubbs, N. Kedersha, S. Wax, W. F. C. Rigby, T. K. Blackwell, and P. Anderson. Mk2-induced tristetraprolin:14-3-3 complexes prevent stress granule association and are-mrna decay. *EMBO J*, 23(6):1313–1324, Mar 2004.

[310] T. Sugiyama, H. Cam, A. Verdel, D. Moazed, and S. I. S. Grewal. Rna-dependent rna polymerase is an essential component of a self-enforcing loop coupling heterochromatin assembly to sirna production. *Proc Natl Acad Sci U S A*, 102(1):152–157, Jan 2005.

[311] N. Tahbaz, F. A. Kolb, H. Zhang, K. Jaronczyk, W. Filipowicz, and T. C. Hobman. Characterization of the interactions between mammalian paz piwi domain proteins and dicer. *EMBO Rep*, 5(2):189–194, Feb 2004.

[312] D. Takeshita, S. Zenno, W. C. Lee, K. Nagata, K. Saigo, and M. Tanokura. Homodimeric structure and double-stranded rna cleavage activity of the c-terminal rnase iii domain of human dicer. *J Mol Biol*, 374(1):106–120, Nov 2007.

[313] K. Takimoto, M. Wakiyama, and S. Yokoyama. Mammalian gw182 contains multiple argonaute-binding sites and functions in microrna-mediated translational repression. *RNA*, 15(6):1078–1089, Jun 2009.

[314] W.-W. Tee, M. Pardo, T. W. Theunissen, L. Yu, J. S. Choudhary, P. Hajkova, and M. A. Surani. Prmt5 is essential for early mouse development and acts in the cytoplasm to maintain es cell pluripotency. *Genes Dev*, 24(24):2772–2777, Dec 2010.

[315] D. Teixeira, U. Sheth, M. A. Valencia-Sanchez, M. Brengues, and R. Parker. Processing bodies require rna for assembly and contain nontranslating mrnas. *RNA*, 11(4):371–382, Apr 2005.

[316] R. Thermann and M. W. Hentze. Drosophila mir2 induces pseudo-polysomes and inhibits translation initiation. *Nature*, 447(7146):875–878, Jun 2007.

[317] S. Till, E. Lejeune, R. Thermann, M. Bortfeld, M. Hothorn, D. Enderle, C. Heinrich, M. W. Hentze, and A. G. Ladurner. A conserved motif in argonaute-interacting proteins mediates functional interactions through the argonaute piwi domain. *Nat Struct Mol Biol*, 14(10):897–903, Oct 2007.

[318] Y. Tomari, T. Du, B. Haley, D. S. Schwarz, R. Bennett, H. A. Cook, B. S. Koppetsch, W. E. Theurkauf, and P. D. Zamore. Risc assembly defects in the drosophila rnai mutant armitage. *Cell*, 116(6):831–841, Mar 2004.

[319] Y. Tomari, T. Du, and P. D. Zamore. Sorting of drosophila small silencing rnas. *Cell*, 130(2):299–308, Jul 2007.

[320] Y. Tomari, C. Matranga, B. Haley, N. Martinez, and P. D. Zamore. A protein sensor for sirna asymmetry. *Science*, 306(5700):1377–1380, Nov 2004.

[321] Y. Tomari and P. D. Zamore. Perspective: machines for rnai. *Genes Dev*, 19(5):517–529, Mar 2005.

[322] L. Trinkle-Mulcahy, J. Andersen, Y. W. Lam, G. Moorhead, M. Mann, and A. I. Lamond. Repo-man recruits pp1 gamma to chromatin and is essential for cell viability. *J Cell Biol*, 172(5):679–692, Feb 2006.

[323] L. Trinkle-Mulcahy, S. Boulon, Y. W. Lam, R. Urcia, F.-M. Boisvert, F. Vander-moere, N. A. Morrice, S. Swift, U. Rothbauer, H. Leonhardt, and A. Lamond. Identifying specific protein interaction partners using quantitative mass spectrom-etry and bead proteomes. *J Cell Biol*, 183(2):223–239, Oct 2008.

[324] F. Tritschler, E. Huntzinger, and E. Izaurralde. Role of gw182 proteins and pabpc1 in the mirna pathway: a sense of déjà vu. *Nat Rev Mol Cell Biol*, 11(5):379–384, May 2010.

[325] L. Unterholzner and E. Izaurralde. Smg7 acts as a molecular link between mrna surveillance and mrna decay. *Mol Cell*, 16(4):587–596, Nov 2004.

[326] V. V. Vagin, G. J. Hannon, and A. A. Aravin. Arginine methylation as a molecular signature of the piwi small rna pathway. *Cell Cycle*, 8(24):4003–4004, Dec 2009.

[327] V. V. Vagin, A. Sigova, C. Li, H. Seitz, V. Gvozdev, and P. D. Zamore. A dis-tinct small rna pathway silences selfish genetic elements in the germline. *Science*, 313(5785):320–324, Jul 2006.

[328] V. V. Vagin, J. Wohlschlegel, J. Qu, Z. Jonsson, X. Huang, S. Chuma, A. Girard, R. Sachidanandam, G. J. Hannon, and A. A. Aravin. Proteomic analysis of murine piwi proteins reveals a role for arginine methylation in specifying interaction with tudor family members. *Genes Dev*, 23(15):1749–1762, Aug 2009.

[329] F. E. Vaistij, L. Jones, and D. C. Baulcombe. Spreading of rna targeting and dna methylation in rna silencing requires transcription of the target gene and a putative rna-dependent rna polymerase. *Plant Cell*, 14(4):857–867, Apr 2002.

[330] H. Valadi, K. Ekström, A. Bossios, M. Sjöstrand, J. J. Lee, and J. O. Lötvall. Exosome-mediated transfer of mrnas and micrornas is a novel mechanism of genetic exchange between cells. *Nat Cell Biol*, 9(6):654–659, Jun 2007.

[331] S. Vasudevan and J. A. Steitz. Au-rich-element-mediated upregulation of translation by fxr1 and argonaute 2. *Cell*, 128(6):1105–1118, Mar 2007.

[332] S. Vasudevan, Y. Tong, and J. A. Steitz. Switching from repression to activation: micrornas can up-regulate translation. *Science*, 318(5858):1931–1934, Dec 2007.

[333] A. Verdel, S. Jia, S. Gerber, T. Sugiyama, S. Gygi, S. I. S. Grewal, and D. Moazed. Rnai-mediated targeting of heterochromatin by the rits complex. *Science*, 303(5658):672–676, Jan 2004.

[334] M. Vermeulen, N. C. Hubner, and M. Mann. High confidence determination of specific protein-protein interactions using quantitative mass spectrometry. *Curr Opin Biotechnol*, 19(4):331–337, Aug 2008.

[335] O. Voinnet and D. C. Baulcombe. Systemic signalling in gene silencing. *Nature*, 389(6651):553, Oct 1997.

[336] T. A. Volpe, C. Kidner, I. M. Hall, G. Teng, S. I. S. Grewal, and R. A. Martienssen. Regulation of heterochromatic silencing and histone h3 lysine-9 methylation by rnai. *Science*, 297(5588):1833–1837, Sep 2002.

[337] C. von Roretz and I.-E. Gallouzi. Decoding are-mediated decay: is microrna part of the equation? *J Cell Biol*, 181(2):189–194, Apr 2008.

[338] M. Wakiyama, K. Takimoto, O. Ohara, and S. Yokoyama. Let-7 microrna-mediated mrna deadenylation and translational repression in a mammalian cell-free system. *Genes Dev*, 21(15):1857–1862, Aug 2007.

[339] R. W. Walters, S. S. Bradrick, and M. Gromeier. Poly(a)-binding protein modulates mrna susceptibility to cap-dependent mirna-mediated repression. *RNA*, 16(1):239–250, Jan 2010.

[340] B. Wang, T. M. Love, M. E. Call, J. G. Doench, and C. D. Novina. Recapitulation of short rna-directed translational gene silencing in vitro. *Mol Cell*, 22(4):553–560, May 2006.

[341] B. Wang, A. Yanez, and C. D. Novina. Microrna-repressed mrnas contain 40s but not 60s components. *Proc Natl Acad Sci U S A*, 105(14):5343–5348, Apr 2008.

[342] H.-W. Wang, C. Noland, B. Siridechadilok, D. W. Taylor, E. Ma, K. Felderer, J. A. Doudna, and E. Nogales. Structural insights into rna processing by the human risc-loading complex. *Nat Struct Mol Biol*, 16(11):1148–1153, Nov 2009.

[343] J. Wang, J. P. Saxe, T. Tanaka, S. Chuma, and H. Lin. Mili interacts with tudor domain-containing protein 1 in regulating spermatogenesis. *Curr Biol*, 19(8):640–644, Apr 2009.

[344] Y. Wang, S. Juranek, H. Li, G. Sheng, T. Tuschl, and D. J. Patel. Structure of an argonaute silencing complex with a seed-containing guide dna and target rna duplex. *Nature*, 456(7224):921–926, Dec 2008.

[345] Y. Wang, G. Sheng, S. Juranek, T. Tuschl, and D. J. Patel. Structure of the guide-strand-containing argonaute silencing complex. *Nature*, 456(7219):209–213, Nov 2008.

[346] A. Wargelius, S. Ellingsen, and A. Fjose. Double-stranded rna induces specific developmental defects in zebrafish embryos. *Biochem Biophys Res Commun*, 263(1):156–161, Sep 1999.

[347] M. Wassenegger, S. Heimes, L. Riedel, and H. L. Sänger. Rna-directed de novo methylation of genomic sequences in plants. *Cell*, 76(3):567–576, Feb 1994.

[348] P. M. Waterhouse, M. W. Graham, and M. B. Wang. Virus resistance and gene silencing in plants can be induced by simultaneous expression of sense and antisense rna. *Proc Natl Acad Sci U S A*, 95(23):13959–13964, Nov 1998.

[349] L. Weinmann, J. Hock, T. Ivacevic, T. Ohrt, J. Mütze, P. Schwille, E. Kremmer, V. Benes, H. Urlaub, and G. Meister. Importin 8 is a gene silencing factor that targets argonaute proteins to distinct mrnas. *Cell*, 136(3):496–507, Feb 2009.

[350] B. Wightman, I. Ha, and G. Ruvkun. Posttranscriptional regulation of the heterochronic gene lin-14 by lin-4 mediates temporal pattern formation in c. elegans. *Cell*, 75(5):855–862, Dec 1993.

[351] J. J. Y. Wong, Y. F. Pung, N. S.-K. Sze, and K.-C. Chin. Herc5 is an ifn-induced hect-type e3 protein ligase that mediates type i ifn-induced isgylation of protein targets. *Proc Natl Acad Sci U S A*, 103(28):10735–10740, Jul 2006.

[352] L. Wu and J. G. Belasco. Micro-rna regulation of the mammalian lin-28 gene during neuronal differentiation of embryonal carcinoma cells. *Mol Cell Biol*, 25(21):9198–9208, Nov 2005.

[353] L. Wu, J. Fan, and J. G. Belasco. Micrornas direct rapid deadenylation of mrna. *Proc Natl Acad Sci U S A*, 103(11):4034–4039, Mar 2006.

[354] K. S. Yan, S. Yan, A. Farooq, A. Han, L. Zeng, and M.-M. Zhou. Structure and conserved rna binding of the paz domain. *Nature*, 426(6965):468–474, Nov 2003.

[355] Z. Yang, A. Jakymiw, M. R. Wood, T. Eystathioy, R. L. Rubin, M. J. Fritzler, and E. K. L. Chan. Gw182 is critical for the stability of gw bodies expressed during the cell cycle and cell proliferation. *J Cell Sci*, 117(Pt 23):5567–5578, Nov 2004.

[356] X. Ye, N. Huang, Y. Liu, Z. Paroo, C. Huerta, P. Li, S. Chen, Q. Liu, and H. Zhang. Structure of c3po and mechanism of human risc activation. *Nat Struct Mol Biol*, 18(6):650–657, Jun 2011.

[357] S. Yekta, I.-H. Shih, and D. P. Bartel. Microrna-directed cleavage of hoxb8 mrna. *Science*, 304(5670):594–596, Apr 2004.

[358] R. Yi, Y. Qin, I. G. Macara, and B. R. Cullen. Exportin-5 mediates the nuclear export of pre-micrornas and short hairpin rnas. *Genes Dev*, 17(24):3011–3016, Dec 2003.

[359] C. ying Chu and T. M. Rana. Translation repression in human cells by microrna-induced gene silencing requires rck/p54. *PLoS Biol*, 4(7):e210, Jul 2006.

[360] M. Yoda, T. Kawamata, Z. Paroo, X. Ye, S. Iwasaki, Q. Liu, and Y. Tomari. Atp-dependent human risc assembly pathways. *Nat Struct Mol Biol*, 17(1):17–23, Jan 2010.

[361] Y.-R. Yuan, Y. Pei, J.-B. Ma, V. Kuryavyi, M. Zhadina, G. Meister, H.-Y. Chen, Z. Dauter, T. Tuschl, and D. J. Patel. Crystal structure of a. aeolicus argonaute, a site-specific dna-guided endoribonuclease, provides insights into risc-mediated mrna cleavage. *Mol Cell*, 19(3):405–419, Aug 2005.

[362] P. D. Zamore, T. Tuschl, P. A. Sharp, and D. P. Bartel. Rnai: double-stranded rna directs the atp-dependent cleavage of mrna at 21 to 23 nucleotide intervals. *Cell*, 101(1):25–33, Mar 2000.

[363] L. Zekri, E. Huntzinger, S. Heimstädt, and E. Izaurralde. The silencing domain of gw182 interacts with pabpc1 to promote translational repression and degradation of microrna targets and is required for target release. *Mol Cell Biol*, 29(23):6220–6231, Dec 2009.

[364] Y. Zeng, H. Sankala, X. Zhang, and P. R. Graves. Phosphorylation of argonaute 2 at serine-387 facilitates its localization to processing bodies. *Biochem J*, 413(3):429–436, Aug 2008.

[365] J. Y. Zhu, M. Strehle, A. Frohn, E. Kremmer, K. P. Höfig, G. Meister, and H. Adler. Identification and analysis of expression of novel micrornas of murine gammaherpesvirus 68. *J Virol*, 84(19):10266–10275, Oct 2010.

[366] D. Zilberman, X. Cao, and S. E. Jacobsen. Argonaute4 control of locus-specific sirna accumulation and dna and histone methylation. *Science*, 299(5607):716–719, Jan 2003.

[367] T. S. Zimmermann, A. C. H. Lee, A. Akinc, B. Bramlage, D. Bumcrot, M. N. Fedoruk, J. Harborth, J. A. Heyes, L. B. Jeffs, M. John, A. D. Judge, K. Lam, K. McClintock, L. V. Nechev, L. R. Palmer, T. Racie, I. Röhl, S. Seiffert, S. Shanmugam, V. Sood, J. Soutschek, I. Toudjarska, A. J. Wheat, E. Yaworski, W. Zedalis, V. Koteliansky, M. Manoharan, H.-P. Vornlocher, and I. MacLachlan. Rnai-mediated gene silencing in non-human primates. *Nature*, 441(7089):111–114, May 2006.

[368] J. T. Zipprich, S. Bhattacharyya, H. Mathys, and W. Filipowicz. Importance of the c-terminal domain of the human gw182 protein tnrc6c for translational repression. *RNA*, 15(5):781–793, May 2009.

[369] U. A. Ørom, F. C. Nielsen, and A. H. Lund. Microrna-10a binds the 5'utr of ribosomal protein mrnas and enhances their translation. *Mol Cell*, 30(4):460–471, May 2008.

Acknowledgements

Curriculum Vitae

Personal details

Name   Anne Frohn

Place of birth   Düsseldorf, Germany

Publications

A. Frohn, H.C. Eberl, J. Stöhr, E. Glasmacher, S. Rüdel, V. Heissmeier, M. Mann and G. Meister. RNA-dependent and -independent Argonaute2 protein interaction networks in mammalian cells. submitted.

Y. Zhu, M. Strehle, **A. Frohn**, E. Kremmer, K. P. Höfig, G. Meister, and H. Adler. Identification and analysis of expression of novel micrornas of murine gammaherpesvirus 68. *J Virol*, 84(19):10266–10275, Oct 2010.

M. J. Hartl, B. Kretzschmar, **A. Frohn**, A. Nowrouzi, A. Rethwilm, and B. M. Wöhrl. Azt resistance of simian foamy virus reverse transcriptase is based on the excision of aztmp in the presence of atp. *Nucleic Acids Res*, 36(3):1009–1016, Feb 2008.

K. A. Johnson, S. Bhushan, A. Ståhl, B. M. Hallberg, **A. Frohn**, E. Glaser, and T. Eneqvist. The closed structure of presequence protease prep forms a unique 10,000 Å^3 chamber for proteolysis. *EMBO J*, 25(9):1977–1986, May 2006.